In vitro adipose-derived stromal cell myogenic differentiation

By

Simoné Grobbelaar

29051739

Submitted in fulfilment of the requirements for the degree

Master of Science (Human Physiology)

In the Faculty of Health Sciences

Department of Physiology in collaboration with the Department of Immunology

University of Pretoria

2021

Supervisor: Prof. Michael S. Pepper

Co-Supervisor: Prof. Anne E. Mercier

Contact information

MSc Candidate

Simoné Grobbelaar

Student number: 29051739

E-mail: *simonegrow@gmail.com*

Supervisor

Prof. MS Pepper

Institute for Cellular and Molecular Medicine

Department of Immunology

Faculty of Health Sciences

University of Pretoria

E-mail: *michael.pepper@up.ac.za*

Co-Supervisor

Prof. AE Mercier

Department of Physiology

Faculty of Health Sciences

University of Pretoria

E-mail: joji.mercier@up.ac.za

Dei Gratia

Declaration of originality

I, ***Simoné Grobbelaar***, hereby declare that this dissertation entitled:

In vitro adipose derived stromal cell myogenic differentiation

which I herewith submit to the University of Pretoria for the Degree of Master of Science in Human Physiology, is my own original work and has never been submitted for any academic award to any other tertiary institution for any degree.

Date: 08/10/21

Signature: 

S Grobbelaar

Acknowledgements

I would like to thank my Supervisor Prof. Michael Pepper for the opportunity to complete this MSc degree at the Institute for Cellular and Molecular Medicine, and for his continuous and generous support, guidance and input in this project. It was an incredibly hard experience, but it was worth it.

I would like to thank my Co-Supervisor Prof. Anne E Mercier for her continuous support and guidance in this project.

Dr. Chrisna Durandt, for all the time she did not have to give, but gave anyway. I would not have been able to do this without her help and encouragement.

Dr. Iman van den Bout and Mr. Andy Ellero, for their incredible help and support with the confocal microscope and my immunocytochemistry experiments.

Prof. Kathy Myburgh (Department of Physiology, University of Stellenbosch) and her laboratory, for kindly providing the cells I needed and for her advice on all things myogenesis.

Mrs. Candice Murdoch, for teaching me cell culture and for providing support in the laboratory. She is absolutely an amazing laboratory manager.

Mrs. Sumari Marais, for her help with calculations and advice on cell culture and microscopy.

Ms. Candice Herd, for helping me at every stage during this degree, as a senior colleague and as a friend. Thank you for going through every single chapter, for encouragement and for helping me make sense of it all.

Ms. Aurona Gerber… We started together, and submitted together. We faced the same challenges together, overcame them together and then repeated that process multiple times. Thank you for being in my boat, and for navigating these waters with me… It took a while, but we did it.

I thank my incredibly precious friends. I would not have made it here without any of you. To Sibyl Cooke and Carita van Rooyen, for continuously encouraging me and believing in me. For pushing me to not give up when I desperately wanted to quit and run away to another corner of the planet. For coffees and lunches and hugs and conversations and patience and love. To Roxy Rule and Lauren van Niekerk, for their support, kindness and constant encouragement. To Floris Bonafede, for copious amounts of wine, spoils, support and encouragement.

To my parents Reinier and Marli Grobbelaar, and my brother Reinhardt for support, patience and love.

Finally, my Abba in Heaven. I am here only by the Grace and Miracle of God, who started me on this journey and brought it to completion.

Therefore, do not cast away your confidence, which has great reward. For you have need of endurance, so that after you have done the will of God, you may receive the promise. - Hebrews 10:35 - 36

Table of Contents

List of Figures

Chapter 2

Chapter 4

Chapter 5

List of Tables

Chapter 2

Chapter 4

Chapter 5

Table of Abbreviations, symbols and units

Abbreviation	Definition
Oct-4	Octamer binding transcription factor-4
5-Aza	5-Azacytidine
7-AAD	7-aminoactinomycin D
ACTB	Beta-actin
AF	Alexa Fluor
AmB	Amphotericin B
APC	Allophycocyanin
APC Cy7	Allophycocyanin cayanin dye -7 tandem conjugate
ASC	Adipose-derived stromal cell
ASC-CGM	DMEM, 5% pHPL, 2% pen/strep, 0.2% amphotericin B
ASC-Cryo	90% ASC-CGM and 10% DMSO
ASC-NI	DMEM, 10% FBS, 2% p/s and 0.2% AmB; 0.1 mm
b-FGF	Basic fibroblast growth factor
β-ME	Beta-mercaptoethanol
bHLH	Basic-helix-loop-helix
BM-MSC	Bone marrow derived-MSCs
BMP	Bone morphogenetic protein
BP	Band-pass
BV421	Brilliant violet 421
C/EBP	CCAAT/enhancer-binding protein
C2C12-CGM	DMEM with 20% FBS, 2% pen/strep, 0.2% amphotericin B
C2C12-Cryo	20% C2C12-CGM, 70% FBS and 10% DMSO
C2C12-MIM	DMEM with 2% FBS, 2% p/s, 0.2% AmB
CD	Cluster of differentiation
CDK	Cyclin-dependent kinases
CGM	Complete growth medium
C_P	Crossing point
CpG	Cytosine-guanine
Cryo	Cryopreservation medium
C_T	Threshold cycle
DAPI	4′,6-Diamidino-2-phenylindole
dd	Double distilled
DMD	Duchenne muscular dystrophy
DMEM	Dulbecco’s Modified Eagle’s Medium
DMSO	Dimethyl sulfoxide
DNMT3B	Deoxyribonucleic acid methyl transferase 3B
dNTP	Deoxynucleoside triphosphates
ECM	Extracellular matrix

EDTA	Ethylenediaminetetraacetic acid
Eya	Eyes absent homolog
FBS	Fetal bovine serum
FDA	Food and Drug Administration
FGF	Fibroblast growth factor
FITC	Fluorescein Isothiocyanate
FL	Fluorescence channel
FS	Forward scatter
GC	Glucocorticoids
gDNA	Genomic DNA
GMP	Good Manufacturing Practice
GR	Glucocorticoid receptors
HLA	Human leukocyte antigen
HrS	Horse serum
ICC	Immunocytochemistry
ICMM	Institute for Cellular and Molecular Medicine
IgG	Immunoglobulin G
IHC	Immunohistochemistry
IL	Interleukin
ISCT	International Society for Cellular Therapy
ISHAGE	The International Society for Hematotherapy and Graft Engineering
KO	Krome Orange
LED	Light emitting diode
LSM	Laser scanning microscope
mAb	Monoclonal antibodies
MD	Muscle-derived
MEF 2	Myocyte enhancer factor 2
MHC	Myosin heavy chain
MIM	Muscle induction medium
MIM 1	DMEM, 10% FBS, 5% HrS, 2% p/s and 0.2% AmB; 0.1 mm dexamethasone, 50 mm hydrocortisone
MIM 2	Low glucose DMEM, 10% FBS, 2% p/s, 0.2% AmB
Mim 2-m	Low glucose DMEM, 10% FBS, 2% p/s, 0.2% AmB, 1 ng/mL b-FGF
Min	Minutes
MIQE	Minimum information for publication of quantitative real-time PCR experiments
ml	Millilitre
Mrf 4	Myogenic regulatory factor 4
mRNA	Messenger RNA
MSC	Mesenchymal stromal/stem cell

Myf 5	Myogenic factor 5
MyoD	Myogenic differentiation
MyoG	Myogenin
nm	Nanometer
NRT	No reverse transcriptase
NTC	No template control
Oct	Octamer binding transcription factor-4
P/s	Penicillin/streptomycin
Pax	Paired box gene
PC	Platelet concentrate
PC5	Phycoerythrin-Cyanin 5
PDGF-beta	Platelet derived growth factor b
PDT	Population doubling time
PE	Phycoerythrin
PFA	Paraformaldehyde
PHM	Primary human myoblast
PHM-CGM	DMEM, 10% FBS, 2% pen/strep and 0.2% amphotericin B
PHM-Cryo	90% FBS and 10% DMSO
PHM-MIM	DMEM, 2% FBS, 2% pen/strep and 0.2% AmB
pHPL	Pooled human platelet lysates
PODXL	Podocalyxin-like protein 1
Pol	Polymerase
POU5F1	POU class 5 homeobox 1
PPARγ	Peroxisome proliferator-activated receptor gamma
q	Real-time
RA	Retinoic acid
Rin	RNA integrity number
RNA	Ribonucleic acid
RPM	Rotations per minute
RT-qPCR	Reverse-transcriptase real-time polymerase chain reaction
Runx2	Runt-related transcription factor 2
s	Seconds
SANBS	South African National Blood Service
SD	Standard deviation
SEM	Standard error of the mean
SHH	Sonic hedgehog homolog
Six	Sineoculis homeobox homolog
Sox 2	Sex determining region Y-box transcription factor 2
SS	Side scatter
SVF	Stromal vascular fraction
TBP	Tata binding protein

Tbx18	T-box transcription factor 18
TE	Tris-ethylenediaminetetraacetic acid
TF	Transcription factor
TGF-β	Tumour growth factor b
Tm	Primer melting temperature
TNF-α	Tumour necrosis factor-alpha
TRITC	Tetramethylrhodamine
UC-MSCs	Umbilical cord-derived MSCs
USA	United states of America
v/v	Volume/volume
VDC	Vybrant® DyeCycle™
vs	Versus
w/v	Weight/volume
YWHAZ	Tyrosine 3-monooxygenase/tryptophan 5-monooxygenase activation protein, zeta
Greek symbol	**Definition**
α	alpha
β	beta
γ	gamma
μ	micro

Chapter 1: Executive summary

Adipose-derived stromal cells (ASCs) are multipotent cells obtained from adipose tissue. ASCs are able to differentiate into multiple cell lineages including adipose, cartilage, bone and muscle with the appropriate stimulus. The multipotency of ASCs has brought attention to these cells as possible therapeutic agents in regenerative medicine. The aim of this study was to optimise the methods involved in differentiating ASCs isolated from lipoaspirates into a myogenic lineage for the Institute for Cellular and Molecular Medicine (ICMM, University of Pretoria, Department of Immunology) using two previously published induction methods. ASCs, isolated from lipoaspirates, were immunophenotyped by flow cytometry, and myogenesis evaluated at the protein level using immunocytochemistry (ICC) and the transcriptomic level using reverse transcriptase quantitative real time polymerase chain reaction (RT-qPCR). ASC myogenesis was induced using either dexamethasone/ hydrocortisone (DH)- or 5-Azacytidine (5-Aza)-based induction media over 42- and 24-days respectively. Relative gene expression of myogenic targets desmin, myogenic differentiation (MyoD) and myogenin (MyoG) was determined using RT-qPCR. The presence of myogenic target proteins paired box proteins (Pax) 3/7, MyoD, MyoG and desmin was qualitatively determined by ICC and visualised using a confocal microscope. In ASCs induced to differentiate, neither MyoD nor MyoG mRNA were amplified in any condition, at any time-point. The expression of desmin was confirmed; however, there was no statistically significant change in desmin expression using either the DH or 5-Aza-based methods. The fold-increase in the expression of desmin mRNA was the highest on day twelve post-induction for the 5-Aza-based method relative to the non-induced control sample. Interestingly, when comparing the induced and non-induced samples relative to day zero, the non-induced samples showed the highest fold-increase in the expression of desmin on day six, whilst all three conditions indicated an increase in the expression on desmin on day twelve. ICC confirmed the presence of desmin from as early as day three and at every subsequent time-point, and the expression of Pax 3/7 from day six in both the DH-based induction methods. According to recent ASC myogenic modelling, where ASC differentiation is described in terms of 6 stages based on the presence of myogenic markers Pax 3/7 and desmin, ASCs in

this study only achieved stage two myogenic differentiation, based on the presence of desmin and pax 3/7. Based on the data collected in this study, no conclusion could be made as to which induction medium most efficiently induced myogenesis. As the aim of this study was to optimise the differentiation of ASCs into a myogenic lineage, it could be concluded that the assays involved were optimised. However, taking into consideration limitations that were identified through the course of this study, suggestions for future experimental endeavours have been made in order to further optimise the myogenic process and accompanying assays. These include the further optimisation of primer melting temperatures, using a fluorescent signal amplification system in ICC, methods that could potentially be used to obtain quantitative data from fluorescent images and the concept of differentiating ASCs into a myogenic lineage using both chemical and mechanical stimuli under dynamic conditions.

Key words: Adipose-derived stromal cells; ASCs; myogenesis; muscle; differentiation; mesenchymal stromal cells; MSCs.

Chapter 2: Literature Review

This chapter provides an overview of the current literature as it relates to mesenchymal stromal/stem cells, adipose-derived stromal cells and myogenesis. Discussed below are definitions of stem cells, mesenchymal stromal/stem cell nomenclature, definitions and characterisations, concepts related to adipose-derived stromal cells, myogenesis and myogenic induction. This chapter concludes with the rationale of the proposed study.

2.1. Defining stem cells and lineage differentiation

The term ‘stem cell’, derived from the word ‘*stammzelle*’ has been present in the literature since 1868 when it was first described by German biologist Ernst Haeckel. Haeckel drew a series of phylogenetic trees he called ‘*stammbäume*’ or “stem trees” to theorise how unicellular ancestor organisms ‘*stammzelle*’ evolved to form multicellular organisms (Figure 2.1).[1,2] Furthermore, he proposed that the fertilised embryo also be referred to as a stem cell and that the stem cell itself had both paternal and maternal origins. To Haeckel, the fertilised embryo represented an entire future organism.[3]

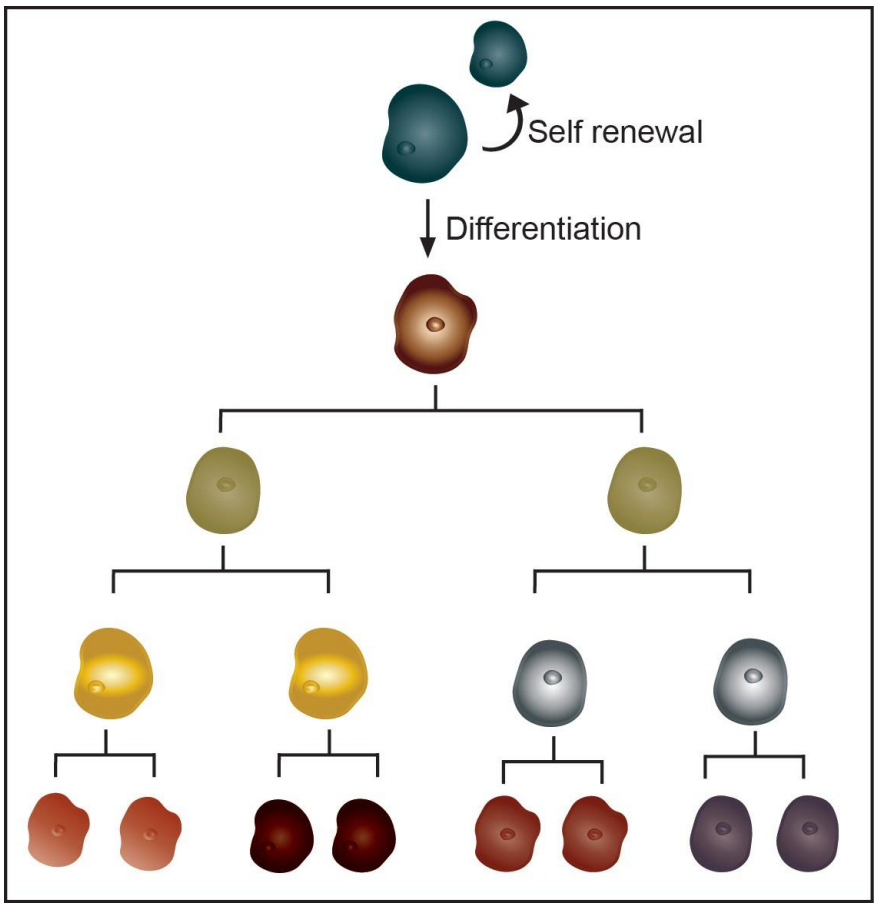

Figure 2.1. The stem tree concept to illustrate differentiation as described by Ernst Haeckel.
Ernst Haeckel attempted to illustrate the process of differentiation using 'stem trees', and hypothesised that one common progenitor (capable of self-renewal) could give rise to multiple cellular lineages.[1,2]

Definitions of a stem cell have expanded over the last century as research has expanded our understanding to include specific molecular characteristics and differentiation potency. It is now accepted that a 'stem cell' is a cell with the ability to self-renew through asymmetric cell division, and has the capacity to generate multiple cell lineages.[4] Stem cell potency describes a stem cell's inherent capacity to differentiate into either all, multiple or single germ layer lineages (Figure 2.2). The morula of a developing embryo is comprised of totipotent cells, prior to the formation of the blastocyst, which is capable of differentiating into all embryonic and extra-embryonic tissues.[5] Pluripotent stem cells are found in the inner cell mass of the blastocyst and differentiate into the endodermal, mesodermal and ectodermal

embryonic germ layers.[6] The endoderm (forming internal linings and organs), mesoderm (forming musculoskeletal system, adipose tissue) and ectoderm (forming external linings such as the skin) are comprised of multipotent stem cells. Cells that derive from the individual germ layers persist into adulthood where multipotent stem cells replenish particular cell populations over a lifetime. As examples, haematopoietic stem cells derive from the mesoderm and reconstitute cells of the blood and immune systems. Mesenchymal stromal/stem cells (MSC) are multipotent stem cells which have been suggested to play a role in local wound healing and repair.[7] Other adult stem cells include hepatic stem cells which regenerate the liver and originate from the endoderm, and neural stem cells originating from the ectoderm which replace neuronal cells.[4,8,9]

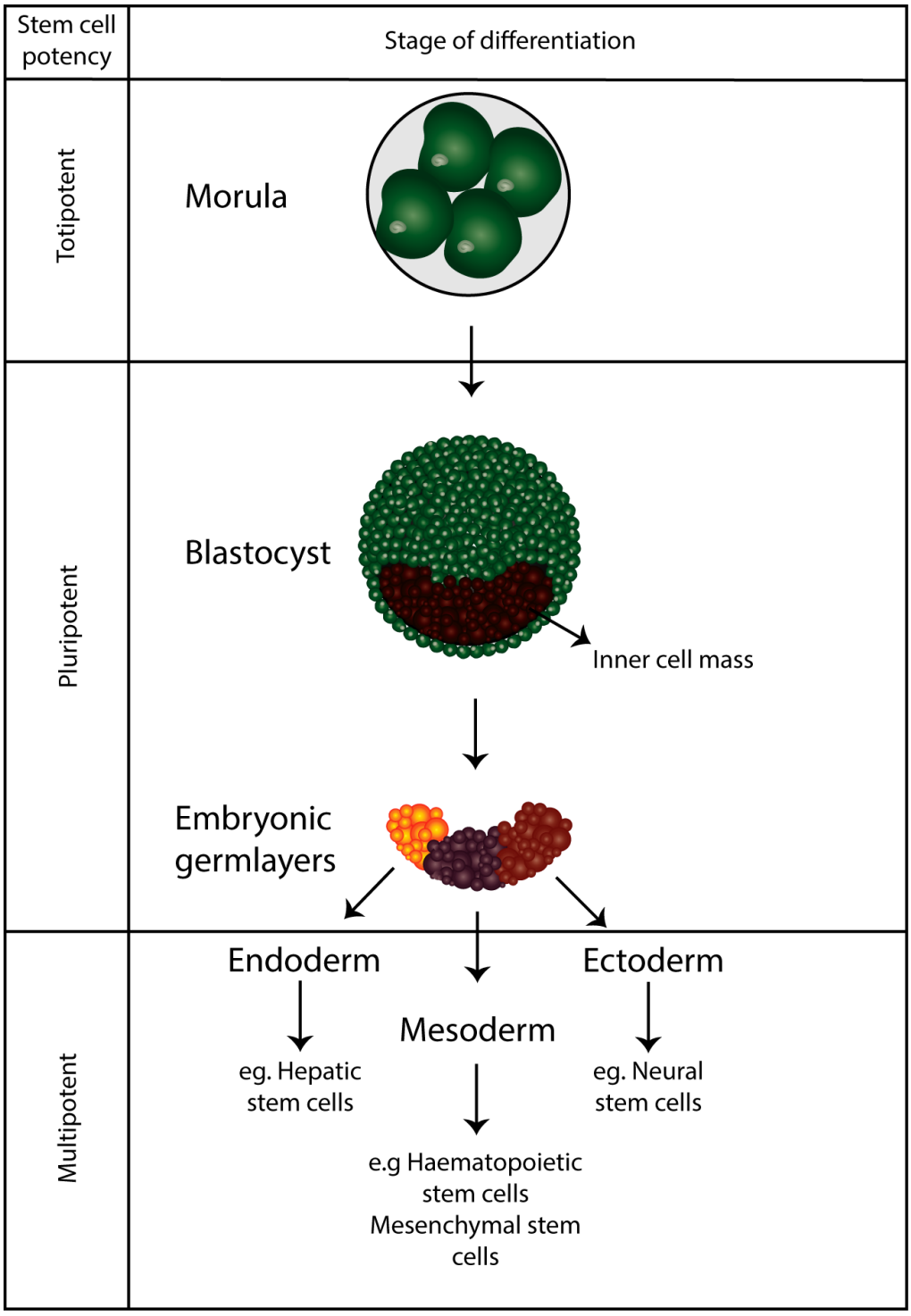

Figure 2.2. Defining stem cells according to their potency and ability to differentiate. Stem cells may be classified as either totipotent, pluripotent or multipotent. Totipotent stem cells are found prior to the formation of the blastocyst. The inner cell mass of the blastocyst is comprised of pluripotent stem cells, and forms the three embryonic germ layers (endoderm, mesoderm, ectoderm). Stem cells that derive from the individual germ layers are labelled as multipotent stem cells, as they have the ability to form multiple cellular lineages.[4-7]

Differentiation is a term used to describe the process by which a stem or progenitor cell transforms or evolves into one or multiple cellular lineages. Using a tree to illustrate differentiation is misleading, as it suggests differentiation is a unilateral process. In reality, the process is more complicated. Cell fate decisions are governed by transcriptional cues, guiding primitive cells through lineage specification in a sequential manner.[4] Stem cells possess plasticity in this regard and may dedifferentiate through transcription factor-mediated reprogramming. The concept of dedifferentiation is clearly demonstrated with induced pluripotent stem cells, where a cell in a terminal state of differentiation re-acquires it's pluripotency *in vitro* after the introduction of transcription factors associated with pluripotency.[10] Cells may also transdifferentiate from lineages of one germ layer to those of another, clearly illustrated by Waddington's 'epigenetic landscape' (Figure 2.3).[11,12] Waddington first presented the illustration to explain stable pathways in epigenetic development but it has been adopted to a more accurate visual model for stem cell differentiation.[13]

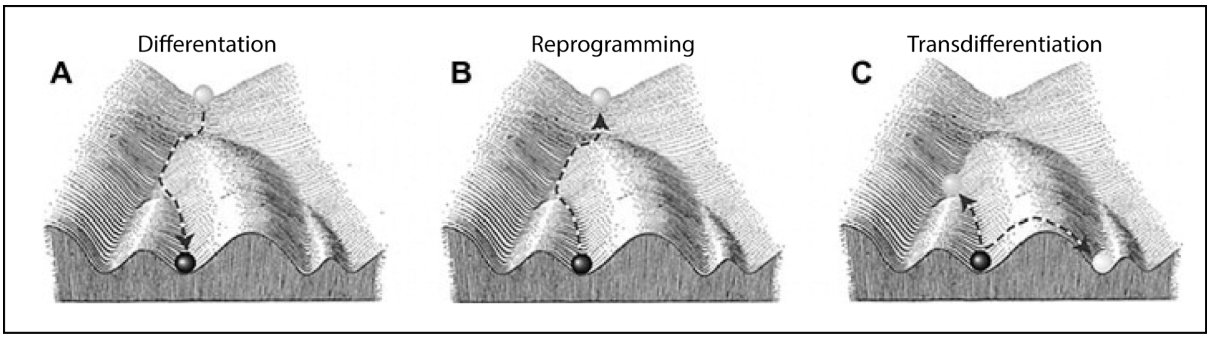

Figure 2.3. Waddington landscapes to illustrate stem cell differentiation.
A. Differentiation. The process through which a stem cell becomes committed to specified cell lineages, resulting in terminally differentiated cells. B. Reprogramming. The process through which somatic cells are dedifferentiated to a pluripotent state by the mediation of transcription factors. C. Transdifferentiation. Cells committed to one lineage may transdifferentiate into cells of another lineage.[13] *Reprinted from 'The epigenetic landscape in the course of time: Conrad Hal Waddington's methodological impact on the life sciences. Studies in History and Philosophy of Science Part C: Studies in History and Philosophy of Biological and Biomedical Sciences'. Baedke, J. 2013;44(4, Part B):756-773., with permission from Elsevier.*

2.2. Defining mesenchymal stem/stromal cells

MSCs are stromal cells with immunomodulatory and multipotent differentiating capabilities. These properties make MSCs potentially useful as therapeutic options in cell-based and regenerative medicine. The clinical promise of these cells is evidenced by more than 1000 listed MSC-based clinical trials and over 60 000 publications available on PubMed.gov to date.[14,15] Clinical trials include the evaluation of MSCs for the treatment of haematological pathologies, autoimmune disorders, liver-, kidney- and lung diseases, diabetes, graft-versus-host disease, neurological diseases and spinal cord injuries, amongst others.[16] MSCs have been reported as safe to use clinically, with minimal to no adverse effects.[17] Various MSC-based preparations have been approved for clinical use by international regulatory bodies. Prochymal® (Remestemcel-L; Osiris Therapeutics Inc;), a formulation of allogeneic (cells obtained from a donor) MSCs given intravenously, has been approved for the treatment of acute graft versus host disease in children.[18] Alofisel® (Darvadstrocel; Cx601; TriGenix and Takeda) is the first allogeneic adipose-derived mesenchymal stem cell therapy to treat perianal fistulas in Crohn's disease.[19] MSCs are clinically relevant because of their multipotent capabilities, ability to home to sites of tissue damage or injury, secrete bioactive factors and exert immunomodulatory effects to promote tissue regeneration *in vivo.*[20] Whilst MSCs appear indeed to be promising tools for cell-based therapies and are currently being utilised in clinical practice, there is some disparity surrounding how they are defined.

The term 'mesenchymal stem cell' was first coined in 1991 by Al Caplan, referring to cells isolated from the bone marrow as 'stromal precursors'.[21-23] Today, we know that MSCs can differentiate into multiple mesodermal lineages *in vitro*, and have since been isolated from many tissues, including umbilical cord blood and Wharton's jelly, peripheral blood, adipose tissue, dental pulp and synovial fluid.[21-27]

The International Society for Cellular Therapy (ISCT), previously known as the International Society for Hematotherapy and Graft Engineering (ISHAGE), was founded in 1992, and is the primary regulatory body for cell therapies. In addition, the ISCT is instrumental in the establishment of standardised guidelines and protocols regarding the use of cell therapies.[22,23,28] According to the ISCT, the term 'MSCs' is applied to plastic-adherent cells (when cultured *in vitro*) with adipogenic, osteogenic and chondrogenic differentiating potential *in vitro.*[29] Caplan, supported by various research groups, recently suggested that MSCs be renamed to 'medicinal signalling cells'.[20,30] No single cell surface marker currently exists to define the MSC population. Thus, a panel of markers that are either positively or negatively expressed on the cell surface are used to identify and isolate these cells.

Guidelines for the identification of human MSCs considered for laboratory and pre-clinical studies were recommended in 2006 by Dominici *et al*. (2006).[31] Firstly, MSCs must be plastic-adherent. Secondly, MSCs may be identified by the positive expression of cell surface proteins that have various cellular functions. These proteins are identified based on their function and presence on the surface of certain cell populations and are called cluster of differentiation (CD). MSCs are defined by the positive expression of CD 73 (ecto 5' nucleotidase; SH3; SH4), CD90 (Thy-1) and CD105 (endoglin; SH2) in the absence of CD11b and CD14, CD79α, CD19, CD34 and CD45. Additionally, MSCs should be negative for human leukocyte antigen (HLA) class II surface antigen receptor, HLA-antigen D Related (HLA-DR).[31] MSCs are known to have limited immunogenicity due to the limited to no expression of the self-identifying HLA molecules.[31] CD11b and CD14 are primarily expressed on macrophages and monocytes. CD79α and CD19 are expressed on B-lymphocytes that may adhere to plastic and survive in culture, contaminating the MSC population. CD34 is expressed on haematopoietic progenitors and CD45 is a pan-leukocyte antigen. HLA-DR is only expressed on MSCs in the presence of interferon-γ. Thirdly, MSCs must exhibit *in vitro* trilineage differentiation potential (Table 2.1).[31]

Table 2.1. Characterisation of mesenchymal stromal/stem cells *in vitro*
Mesenchymal stromal/stem cells are identified based on guidelines that include their behaviour in vitro, the expression of various cluster of differentiation cell surface markers and multipotent differentiating capability.[31]

	Recommendation
I	MSCs must be plastic adherent
II	MSC phenotype Positive surface protein expression: CD73, CD90 and CD105 Absent surface proteins (negative): CD11b and CD14, CD79α, CD19, CD34, CD45 and HLA-DR
III	MSCs must exhibit multipotent differentiating potential into adipogenic, chondrogenic and osteogenic lineages
MSC: mesenchymal stromal/stem cell; CD: cluster of differentiation; HLA: human leukocyte antigen; HLA-DR: HLA class II surface antigen receptor HLA-antigen D Related	

As the interest in MSCs has increased, many established laboratories have been researching these cells and, in doing so, introduced multiple inconsistencies into MSC characterization. It was suggested that the criteria defined by Dominici *et al*. (2006)[31] should be adopted to standardise MSC characterization. Additional markers have been used in some studies to identify MSCs in combination with those of the standard criteria (Table 2.1), and include STRO-1, CD106, CD146, stage-specific embryonic antigen-4, CD56 and mesenchymal stem cell antigen-1.[32-35] Markers may also identify specific subsets of MSCs derived from different tissue sites. MSCs derived from dental pulp positively express CD29 (β-1 integrin) at higher intensities than bone marrow derived-MSCs (BM-MSC), whereas BM-MSCs express CD105 at higher intensities than those from dental pulp.[36] The low-affinity nerve growth receptor, or CD271, has been used to isolate BM-MSCs.[37,38] There is increased expression of CD10 on MSCs derived from subcutaneous adipose tissue, while CD200 is associated more with MSCs from visceral adipose deposits.[39] *In vitro* culturing may also influence MSC marker expression. CD44, an adhesion molecule, is generally not expressed on freshly isolated MSCs. However, *in vitro* culturing results in the upregulation of the CD44 gene and its subsequent positive expression.[40] According to the criteria in Table 2.1, MSCs must be negative for CD34, although it has been reported that expression may be variable.[41]

MSCs may be isolated from nearly any vascularized anatomical site because they assist in tissue homeostasis and repair. This formed the controversial hypothesis that MSCs may either be, or are derived from, pericytes.[42] Pericytes are found along the walls of smaller blood vessels such as arterioles, capillaries and venules. *In vivo*, pericytes contribute to the development, remodeling and stabilization of vascular structures. Pericytes play key roles in regulating blood flow, immune cell trafficking and, together with astrocytes, form the blood-brain barrier.[43,44] The idea that MSCs may have a perivascular origin was introduced by Crisan *et al*. (2008).[45] Perivascular cells were isolated from multiple organs and differentiated into adipogenic, osteogenic, chondrogenic and myogenic lineages *in vitro*. Pericytes isolated from human skeletal muscle were also found to regenerate myofibers in mouse models several weeks after an intramuscular injection directly into damaged sites. Furthermore, the cells isolated in this study all expressed the recognised MSC markers CD44, CD73, CD90 and CD105, suggesting that MSCs may potentially be derived from pericytes.[45]

Studies by Dellavalle *et al.* (2007)[46], Chen *et al*. (2015)[47] and Krautler *et al*. (2012)[48] supported this suggestion by showing that *in vivo* transplanted perivascular cells displayed the ability to differentiate into tissue-specific lineages. However, a study by Guimarães-Camboa *et al*. (2017)[49] contradicted this concept. The researchers utilised a gene, T-box transcription factor 18 (Tbx18), expressed in all murine perivascular cells, to conduct a tissue-wide lineage-tracing study on perivascular cell progeny in mice. They found that while $Tbx18^{+}$ cells displayed MSC-like behavior *in vitro*, the progeny of these cells *in vivo* retained their perivascular phenotype in multiple organs for over two years. Furthermore, the researchers investigated the effects of $Tbx18^{+}$ cells post-injury through genetic tracing and found that labelled pericytes did not contribute to tissue-specific lineage differentiation *in vivo*. The results further strengthened the conclusion that pericytes do not behave as MSCs *in vivo*. Furthermore, Guimarães-Camboa and colleagues showed the platelet derived growth factor β (PDGFβ)-Cre lineage tracing method employed by Krautler *et al*. (2012)[48] was not suitable for *in vivo* tracing of perivascular cells. PDGFβ is expressed in both mural and non-mural cell types during embryogenesis and in adult organs, and thus is not a

suitable marker for tracing pericytes *in vitro*. The differences reported in these studies might suggest that perivascular cells can behave as MSCs, but that this is dependent on their developmental stage and anatomical location.[42]

2.3. Mesenchymal stromal/stem cells are heterogeneous

The consensus remains that MSCs are a highly heterogenous population of cells. This heterogeneity is evident between donors, tissues of origin and clonal sub-populations.[50]

Heterogeneity among donors and tissues of origin

Donor health and age have a significant impact on MSC viability, proliferation, and differentiation capability. Advanced age is associated with cell senescence and is negatively associated with viability, proliferation, and differentiation capabilities, possibly due to the age-related shortening of telomeres.[51,52] Ferrer-Lorente *et al.* (2014)[53] investigated the effects of diabetes on adipose-derived stromal cells (ASC) in rat models. They reported significant alterations to signalling pathways related to stem cell maintenance including Notch, Wnt ('Wnt' is an amalgamation of 'wingless' and 'integration' or 'Int-1') and Hedgehog signalling. Deoxyribonucleic acid methyl transferase 3B (DNMT3B), sex determining region Y-box transcription factor 2 (Sox 2), fibroblast growth factor (FGF) 2, FGF4, podocalyxin-like protein 1 (PODXL) and POU class 5 homeobox 1 (POU5F1; also known as octamer binding transcription factor-4; Oct-4), genes associated with stemness and self-renewal, were found to be significantly downregulated in ASCs from diabetic rats. The expression of standard MSC markers (CD44, CD73, CD90 and CD105) was also found to be downregulated. Furthermore, the *in vitro* viability and differentiation capabilities of ASCs isolated from diabetic rats were diminished.[54]

MSC differentiation capacity may be influenced by the tissue of origin. Results from a study by Xu *et al.* (2017)[55] showed that BM-MSCs exhibited stronger osteogenic and lower adipogenic differentiation potential than ASCs. The proliferation of MSCs also differs between sources. Umbilical cord-derived MSCs (UC-MSCs) are reported to have higher population doubling times than BM-MSCs.[56] Furthermore, UC-MSCs can continue to propagate by multi-layering as opposed to BM-MSCs that exhibit contact inhibition. Peng *et al.* (2008)[57] showed that ASCs have a higher proliferation capacity than BM-MSCs, with a population doubling time of 45.2 hours for ASCs and 61.2 hours for BM-MSCs. The researchers also found that BM-MSCs were morphologically larger than ASCs, even though the cells expressed a similar molecular phenotype.

Heterogeneity between clonal sub-populations

Proliferating cells in culture may cause certain cellular clones (sub-populations of cells that stem from the original seeded population) to become dominant over multiple passages (Figure 2.4). Clonal sub-populations differ from each other with regard to proliferation dynamics, morphology and functionality. These differences become evident during *in vitro* culture and expansion.

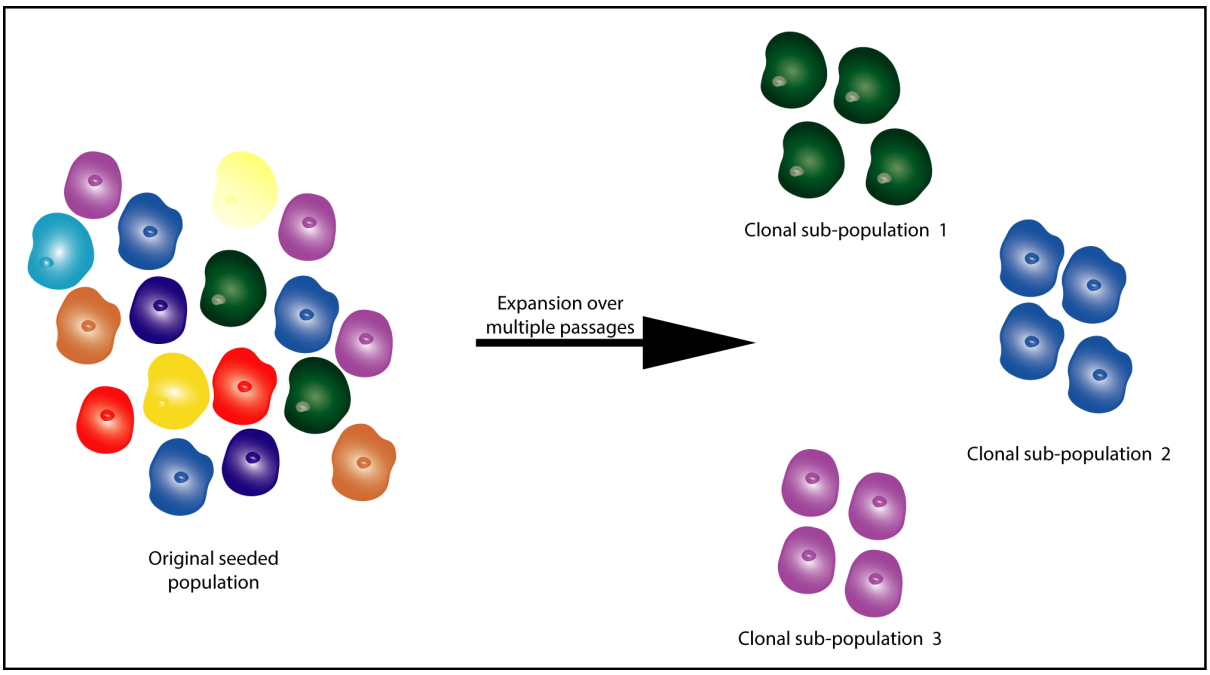

Figure 2.4. Illustration depicting clonal sub-populations.
Clonal sub-populations are formed from the original seeding population over multiple passages, and have varied morphology, proliferation dynamics and differentiation profiles.

Selich *et al.* (2016)[58] demonstrated the existence of these properties using multi-coloured lentiviral barcode labelling in order to follow clonal dynamics during *in vitro* expansion of UC-MSCs (Figure 2.5). The authors observed highly heterogeneous clonal sub-populations at the start of expansion and a subsequent time-dependent reduction in clonal diversity. The researchers further noted the appearance of transiently dominating populations and selection of single clones through multiple passages. The first reduction of clonal sub-populations started occurring as early as passage three. After twleve passages, only three dominant clones remained. Furthermore, they reported changes in proliferation rates at each stage of clonal reduction. Seeding MSCs on Matrigel® resulted in the formation of cell cords. This assay, known as the Matrigel® assay, can be used to assess the functionality of MSCs in culture.[59,60]

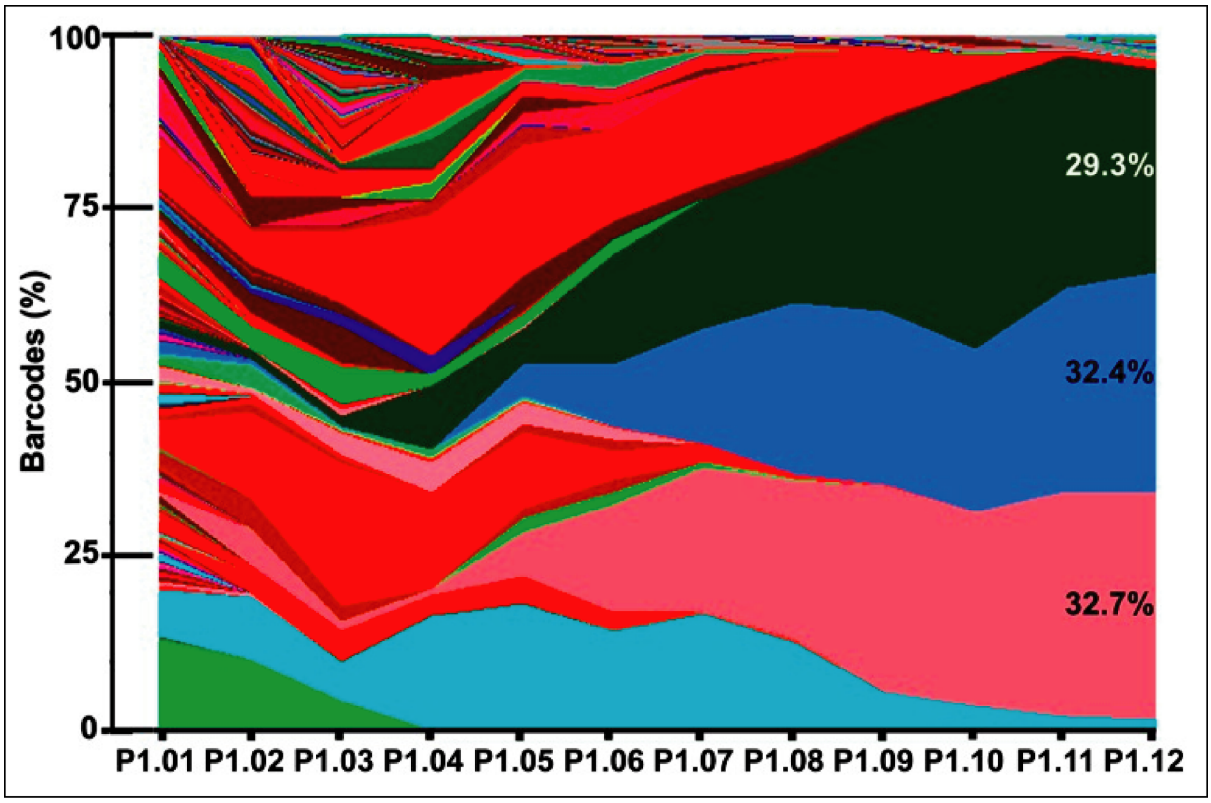

Figure 2.5. Mesenchymal stromal cell heterogeneity and clonal dominance.
The number of clonal sub-populations becomes more restricted over multiple passages as dominant clones emerge. *Reprinted from Selich A, Daudert J, Hass R, et al., Massive Clonal Selection and Transiently Contributing Clones During Expansion of Mesenchymal Stem Cell Cultures Revealed by Lentiviral RGB-Barcode Technology. Stem Cells Transl Med. 2016, 5(5): 591–601., with permission from John Wiley and Sons.*[58]

Selich *et al.* (2016)[58] demonstrated that whilst bulk sorted, non-labelled MSCs formed cord-like structures when seeded on Matrigel®, some labelled and sorted clonal-subpopulations exhibited significantly reduced cord-forming potential. The results indicate that mass MSC cultures are composed of multiple different clonal populations with varying functional properties. Some studies have reported on the differentiation efficiency of MSC clones. MSC clones may also possess varied differentiation potentials, where one clone may possess stronger osteogenic potential and another clone stronger adipogenic potential.[61] Colony forming studies by Kuci *et al.* (2013)[62] and Okamoto *et al.* (2002)[63] demonstrated that MSC cultures possess clones that exhibit either tri- (adipogenic, chondrogenic and osteogenic), bi- or uni-directional differentiation potentials. Research from Russel *et al.* (2010)[64] suggests that at least 50% of colony forming MSCs maintain trilineage potential. Results from these studies

not only highlight the heterogeneity of MSC cultures, but also how understanding clonal diversity, functionality and differentiation dynamics may lead to better selection of cells for clinical applications. Selich *et al.* (2019)[65] showed that clonal selection of MSCs *in vitro* can be controlled by supplementing growth medium with cytokines. In this study, introducing the cytokines FGF2 and epidermal growth factor increased the proliferation potential of MSCs without significant changes to the MSC secretome. Supplementation with transforming growth factor β (TGF-β) enabled the selection and expansion of only a few clones and significantly reduced the secretion of cytokines from the selected MSC clones.[65]

MSCs are highly heterogeneous and cannot be defined as a single cell type limited to specific functions. In most publications discussing heterogeneity however, MSCs exhibit a similar molecular phenotype and standard characteristics (Table 2.1). For the purpose of the present study, MSCs are thus defined as a heterogenous population of cells with varying self-renewal and differentiation capabilities characterised according to standard guidelines (Table 2.1). Heterogeneity in itself may be a limitation to the application of MSCs in the clinical setting. Standardization of culture and differentiation protocols as well as reproducibility of results are key components that allow cells to be used as a therapy. Understanding the heterogeneity present in MSC populations and how this affects their molecular functions, may provide the insight needed to more accurately characterise them. More definitive characterisation of MSCs may identify donor suitability as well as which molecular phenotypes are better-suited for specific experimental and clinical applications. This in turn may lead to experimental and treatment consistency, as well as reproducibility of results.

2.4. Adipose-derived stromal cells and myogenesis

Isolation of mesenchymal stromal/stem cells from adipose tissue

The therapeutic effect of MSCs is dose-dependent, and therefore harvesting therapeutic numbers of cells from a particular source is an important consideration in determining the harvesting site.[66] The invasive nature of certain of these procedures, such as bone marrow aspiration, is an additional point of consideration.[66] Thus, adipose tissue is becoming a preferred source, as it yields higher numbers of MSCs that are extracted through a less invasive aspiration procedure.[67,68]

MSCs harvested from adipose tissue are referred to as adipose-derived stromal cells.[69] ASCs are isolated from lipoaspirates or resected fat from consenting donors in the form of the stromal vascular fraction (SVF), a heterogeneous collection of cells that includes ASCs, haematopoietic stem cells, endothelial cells, erythrocytes, fibroblasts, pericytes, granulocytes, lymphocytes, monocytes and macrophages.[69] After isolation, the SVF is plated and ASCs are defined according to the criteria set out in Table 2.1. The greatest advantages of harvesting ASCs from adipose tissue is that this may be done autologously thereby eliminating the risk of an immune response. Cells may also be harvested in large quantities (although no clear range of cell quantities exist as it depends on therapeutic application).[68] The inherent multipotency of ASCs not only extends to adipogenic, chondrogenic and osteogenic lineages but also to the myogenic lineage. Differentiating ASCs into a myogenic lineage was the focus of this study.

2.5. Skeletal muscle structure, differentiation and lineage specification

Skeletal muscle structure

Striated skeletal muscle architecture is highly organised and is the primary determinant of muscle function.[70] Muscle structure is characterised by a specific arrangement of muscle fibers and associated connective tissue (Figure 2.6). Briefly, several myofibrils bundle together as myofibers.[71] Each myofiber represents a muscle cell with the functional unit known as the sarcomere. Several myofibers are bundled together by the endomysium as fascicles, and fascicles are bundled together by the perimysium to form muscle tissue. Muscle tissue is encapsulated by the epimysium.[71]

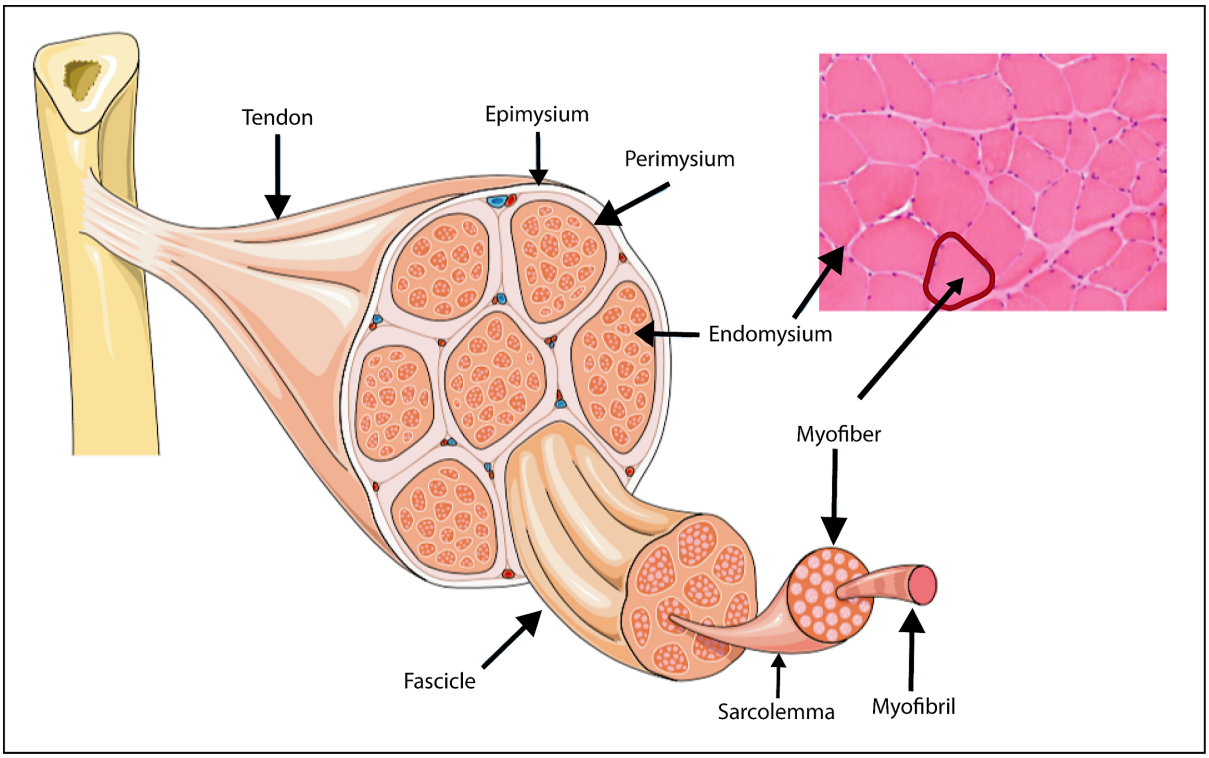

Figure 2.6. The complex structural organisation of skeletal muscle.
Myofibrils fuse to form myofibers that is surrounded by the sarcolemma. A group of muscle fibers is encased by the endomysium. Bundled together as a fascicle, it is surrounded by the perimysium. Muscle tissue is then surrounded by a membrane known as the epimysium.[72] *Reproduced from Le Verche V et al., Skeletal Muscle in Spinal Muscular Atrophy as an opportunity for therapeutic intervention. Spinal Muscular Atrophy: Academic Press; 2017. Ch21: p341-356., with permission from Elsevier.*

Contraction of the sarcomere generates force and rapid movement in skeletal muscle. The complex structure of the sarcomere consists of two distinct protein filaments, namely thin and thick filaments. Thin filaments are formed from polymerized actin isoforms and thick filaments are mainly comprised of myosin proteins.[73] The actin filaments are associated with proteins that facilitate contraction, including tropomyosin and troponin-I, -C and -T. Troponin-I is an inhibitory subunit that binds to α-actin and troponin-C is the subunit that binds calcium.[73] Troponin-T binds tropomyosin. Tropomyosin stabilises actin fibers and provides the scaffold necessary for the proper positioning of calcium-sensitive troponin molecules on the filament. Tropomodulin maintains adequate filament lengths necessary for contraction by capping the sharp ends of actin to prevent depolymerization of the actin filaments.[73]

The thick filament myosin acts as both a structural 'tail' protein as well as an enzyme 'head' that hydrolyses adenosine triphosphate. Myosin is associated with other structural proteins that include myosin binding proteins C and H, to regulate force generation at the actin-myosin complex.[73] Myosin binding proteins associate with titin, a large elastic protein that regulates force development.[74] Muscle fibers characteristically display a series of light and dark bands when viewed under the transmission electron microscope due to the arrangement of the myosin and actin filaments in the sarcomere (Figure 2.7).[75]

A single sarcomere is arranged between two dark Z-lines (also referred to as Z-discs). Z-Lines anchor and cross-link actin fibers while also connecting sarcomeres within the myofibril.[75] α-Actinin is a structural protein responsible for cross-linking actin fibers of neighbouring sarcomeres and connecting titin molecules within sarcomeres.[75] Each Z-line divides a lighter I-band which is shared between two adjacent sarcomeres. Thick filaments make up the A-band at the centre of the sarcomere and contain the lighter H-zone. The M-line divides the H-band, and interconnects the thick filaments. [73,75] Nebulin is a protein that forms part of the thin filaments and regulates thin filament length during muscle contraction. Nebulin interacts with desmin on the peripheral end

of the Z-line, suggesting it may also contribute to myofibril alignment.[76] Desmin is a structural protein located specifically in the sarcomere.[77] It is found around the Z-lines, in the periphery of cell nuclei as well as around the mitochondria. Desmin maintains cell integrity and facilitates efficient transmission of force.[77]

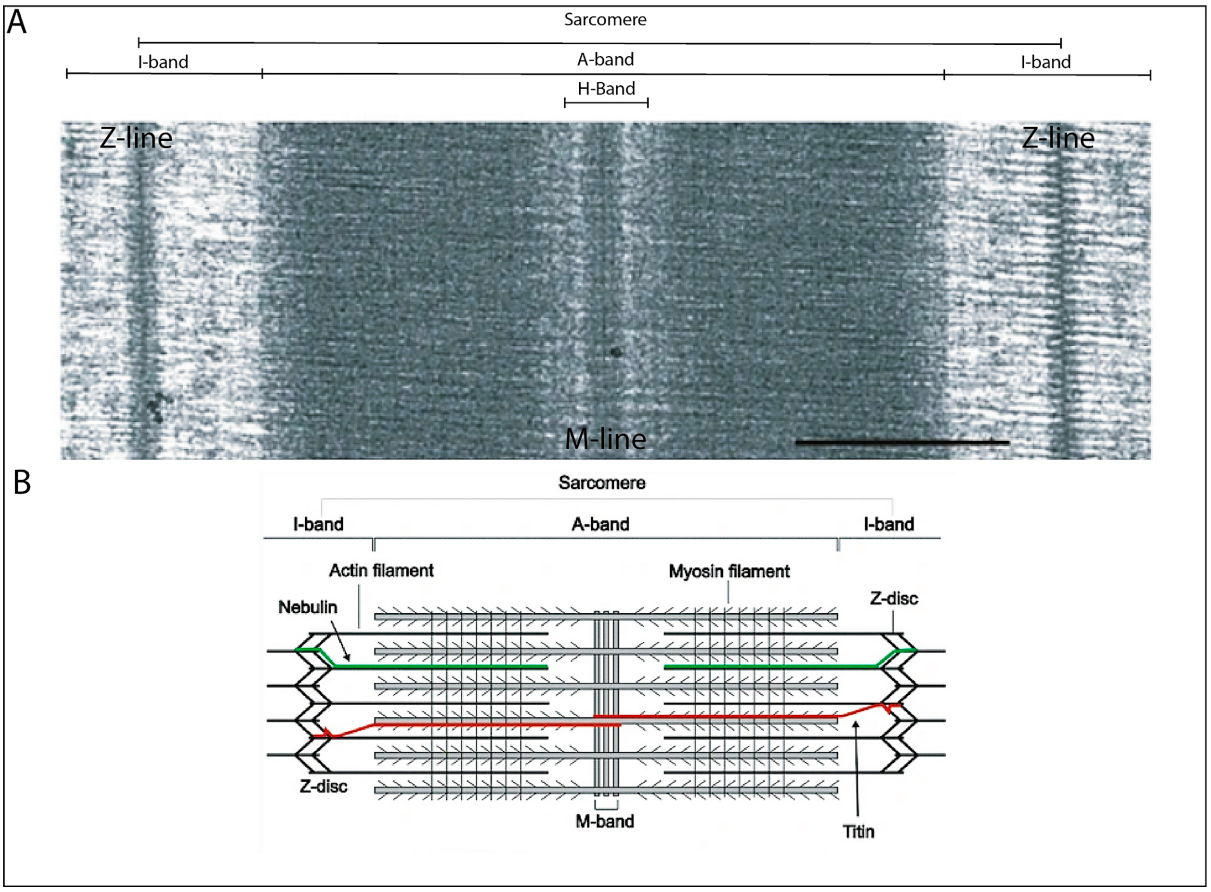

Figure 2.7. Microscopic image and schematic representation of the sarcomere ultrastructure.
A. The sarcomere as captured by electron microscopy. The sarcomere is bordered by darker Z-lines/discs. The Z-lines/discs bisect lighter I-bands which identify bordering sarcomeres. The A-band in the centre of the sarcomere contains thick filaments and the lighter H-band, which is bisected by the M-line. B. Line schematic of sarcomere ultrastructure. The M-line interconnects the thick and thin filaments. Titin and nebulin contribute to sarcomere structure around the Z-lines/discs. Titin is found between the Z- and M-lines and nebulin is found along the actin filaments, overlapping at the Z-line/discs.[75] *Reproduced from Luther PK. The vertebrate muscle z-disc: Sarcomere anchor for structure and signalling. J Muscle Res Cell Motil., 2009; 30(5):171-185 (no permission needed for reprint in a thesis/dissertation).*

2.6. Skeletal muscle differentiation and lineage specification

Myogenesis is the complex process through which new terminally differentiated myocytes form from satellite cells (the local adult stem cells found in muscles).[78] Muscle satellite cells are activated in response to specific transcription activators, and differentiate to form myoblasts. Myoblasts then differentiate into myocytes and fuse together to form myotubules and myofibers (Figure 2.8).[78]

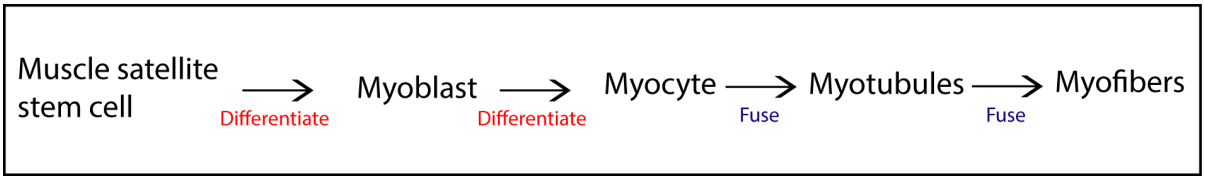

Figure 2.8. Skeletal myogenesis.
Muscle satellite stem cells are activated in response to transcription activators and differentiate into myoblasts, which differentiate into myocytes. Myocytes fuse into myotubules and then myofibers.

Skeletal muscle differentiation is a highly regulated process.[79,80] Signalling pathways involving bone morphogenetic protein (BMP), Wnt, FGF, sonic hedgehog homolog (SHH) and retinoic acid (RA) govern the activation of regulatory transcription factors which in turn activate the basic-helix-loop-helix (bHLH) transcription factor (TF) family.[81] The bHLH TFs are implicated in myogenic lineage commitment and differentiation. Over-expression of bHLH-transcription factors in non-muscle cells results in myogenic differentiation.[82] Lineage specification occurs through the expression of four main bHLH myogenic proteins, namely myogenic factor 5 (Myf 5), myogenic differentiation (MyoD), myogenin (MyoG), and myogenic regulatory factor 4 (Mrf 4) (Figure 2.9).[83] The paired box protein (Pax) family of transcription factors play key roles during skeletal muscle tissue specification. Embryonically, the loss of the Pax 3 lineage is lethal, and simultaneously inhibits the formation of Pax 7^{+} cells.[84] Moreover, replacing a knocked-out Pax 3 with Pax 7 results in the restoration of the functions of Pax 3.[84] While Pax 3 is necessary for myogenic lineage specification, Pax 7 appears to be dispensible.[80] It is postulated that during development Pax 3^{+} cells act

as founder cells to form the template for initial fiber formation. Pax 7^{+} cells then contribute to the formation of secondary fibers and established the satellite stem cell pool.[85]

Sineoculis homeobox homolog (Six) 1 and 4 are considered to be at the apex of the regulatory cascade that directs the myogenic lineage.[78] The Six-family of transcription factors have two conserved domains: one that binds to DNA and a second that binds myogenic transcription co-factors.[86] Six proteins translocate into the nucleus bound to eyes absent homolog (Eya) 1 and 2, where they act as cofactors to upregulate Pax 3, MyoD, Mrf 4 and MyoG expression.[87] Six 1 and 4, along with co-factors Eya 1 and 2, directly bind to the promoter of Pax 3 to activate its expression.[87] Pax 3 and Pax 7 are upstream regulators of myogenesis and control enhancer elements of Myf 5.[88] Figure 2.9 illustrates sequential gene expression relative to myogenic differentiation.

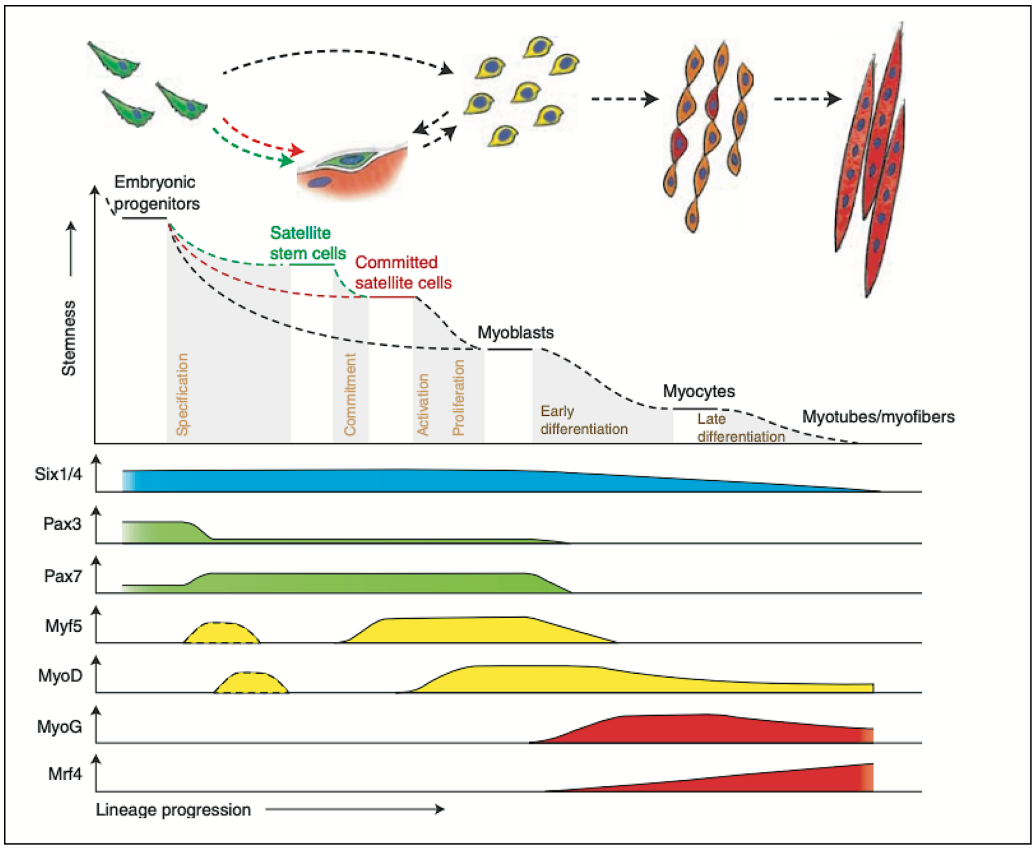

Figure 2.9. Overview of myogenic regulatory factors.
Sineoculis homeobox homolog (Six) 1 and 4 along with their co-factors eyes absent homolog (eya) 1 and 2 activate the expression of paired box gene (Pax) 3 and 7. Pax 3 and 7 binds to enhancer elements to induce the expression of myogenic factor 5. Myogenic differentiation (MyoD) becomes upregulated after myogenic factor 5 (Myf 5), where the two proteins function together to unwind deoxyribonucleic acid (DNA) and recruit ribonucleic acid (RNA) polymerase II to activate transcription of myogenic genes. MyoD induces the expression of myogenin (MyoG) after which Myf 5 becomes downregulated. MyoD and MyoG then cause Mrf 4 to become upregulated, where it persists into terminally differentiated myotubes. Following the expression of Mrf 4, MyoD and MyoG are subsequently downregulated.[78] Reprinted from Bentzinger CF, Wang YX, Rudnicki MA. Building muscle: Molecular regulation of myogenesis. Cold Spring Harb Perspect Biol., 2012;4(2):a008342., with permission from Cold Spring Harbour Perspectives in Biology.

The enhancer element of Myf 5 contains binding sites for Six-factors and Pax 3, indicating that these two factors have similar functions leading to the expression of Myf 5.[89] Pax 3 also regulates the expression of Myf 5 and MyoD, as well as MyoG.[90] Myf 5 has been shown to operate with MyoD and MyoG to upregulate myogenic factors, by co-localizing with MyoD or MyoG on the promoters of myogenic factors.[91]

The expression of MyoD is induced by the transcription factors Six 1 and 4, and Pax 3 and 7.[87,92] Nuclear localization appears to impact the transcriptional activity of MyoD. When MyoD is located near the periphery of the nucleus, low-level MyoD transcription is induced through the action of transcription factor II D (a general transcription factor that forms part of the ribonucleic acid (RNA) Polymerase (Pol) II pre-initiation complex).[93] As differentiation progresses, MyoD is shuttled to the nuclear lumen, where TATA-Box Binding Protein Associated Factor 3 and Topoisomerase 1-related protein 4 promote the expression of MyoD.[93] Additionally, the expression of MyoD, has been closely linked to regulation of the cell cycle.[94] MyoD recruits cyclin-dependent kinase (Cdk)9/CyclinT2) to the transcription complex, where the cdk9 complex then phosphorylates the carboxyl terminal domain of RNA Pol II to promote transcription elongation.[95] The upregulation of MyoD arrests G_1/S progression, and enhances the transcription of p21 which ultimately leads to the downregulation of cdk and thus blocks cell cycle progression. Furthermore, advancing to a differentiation state may depend on cross talk between MyoD and cell cycle signalling pathways.[96]

The bHLH family of transcription factors bind to DNA motifs containing core E-box consensus sequences. Interestingly, E-boxes are frequently found in the genome and another bHLH transcription factor, NeuroD can bind to E-boxes to initiate transcription and promote neuronal differentiation.[83] It appears however, that while both bHLH transcription factors bind to a shared E-box sequence (CAGCTG (cytosine(C), adenine (A), guanine (G), thymine (T)), they also bind to distinct E-box sequences that are lineage-specific. In the case of Myf 5 and MyoD, the E-box sequence is CANNTG while the E-box sequence for NeuroD is CAGATG.[83] To activate transcription, MyoD forms heterodimers with E-proteins. High dissociation rates have been reported when MyoD binds to only one. This indicates that inter-protein interactions are needed to stabilise DNA binding.[97] Binding sites in proteins such as myocyte enhancer factor 2 (MEF 2) may act as a functional substitute for a second E-box.[97] This suggests that cooperative interactions with factors in the immediate vicinity are imperative for the formation of functional transcriptional complexes. E-boxes are found in the regulatory regions of many skeletal muscle genes.[97] Myf 5 and MyoD have distinct functional

molecular properties. Myf 5 and MyoD both induce chromatin remodelling and histone acetylation around their binding sites.[83] However, only MyoD recruits RNA Pol II to activate transcription of myogenic factors.[83]

MyoD induces the expression of MyoG, resulting in the downregulation of Myf 5.[98] This process coincides with cell-cycle exit and indicates that a cell is committed to differentiation.[99] MyoG signals terminal differentiation and myoblast fusion into multinucleated myofibers.[88,100] MyoD in combination with MyoG leads to the expression of Mrf 4 and other late myogenic genes. In terminal muscle fibers the expression of MyoD and MyoG then becomes downregulated, whilst the expression of Mrf 4 persists.[101] Mrf 4, unlike the other members of the bHLH-family, displays a biphasic pattern of expression during mouse myogenesis. Mrf 4 is expressed during foetal development and the expression continues postnatally.[102] The regulation of myogenesis is carried out by multiple overlapping factors (as described above) as well as by Mrf 4, which may also specify myogenic lineage. Moretti *et al.* (2016)[102] demonstrated that some myogenesis still occurs in Myf 5/MyoD double mutant mouse models where Mrf 4 is still expressed.[103] The role of Mrf4 in adult tissues is unclear. Moretti *et al.* (2016)[102] found that knocking out Mrf4 through RNA interference in adult skeletal muscle causes a significant increase in the size of muscle fibers. Additionally, they demonstrated that muscle hypertrophy was induced by active MEF 2. The hypertrophic effect was abolished when MEF 2 was not expressed. These results suggest that Mrf 4 is a negative regulator of muscle growth.[102] Unlike Myf 5, MyoD and Mrf 4 which display an overlap in directing myogenesis, MyoG is indispensable for skeletal muscle development. MyoG-null mice display a deficiency of differentiated skeletal muscle fibers and die at birth.[100] The expression of MyoG has been associated with full and irreversible commitment to the myogenic program.[104]

The sarcomere protein desmin is the earliest detectable marker of muscle cell differentiation. It is diffusely expressed in committed and differentiating myoblasts and its expression increases over time.[105] In committed and differentiating myoblasts,

desmin is expressed before and then concurrently with Myf 5 and MyoD.[106] The expression of desmin appears to be regulated by two distinct E- box sites that serve as transcription initiation sites. The first E-box is found upstream of the desmin promoter and only confers low levels of expression.[107] A second E-box is found downstream of the promoter, along with a binding site for MEF 2, and is responsible for maximal transcriptional activity. Myf 5 and MyoD binds to both of the E-box sequences in the desmin gene to activate transcription.[107]

The myosin heavy chain (MHC) contractile proteins are late markers for skeletal muscle differentiation, and exist as multiple isoforms (types I, IIa, IIx and IIb).[108] The composition of the MHC isoforms depends on their activation state, functional history and the loading state of a particular muscle, and its expression in turn influences its contractile properties.[108] The MHC promoter appears to be regulated by MEF 2, MyoD and MyoG, with E-box sequences found in the regulatory region.[109] Mutations in the E-box sequence of the MHC promoter have been shown to block the binding of MyoD and MyoG, indicating their involvement in the transcription of MHC.[109] The expression of MHC has been associated with changes in cell cycle events. While the upregulation of MyoG indicates cell fusion, it is not sufficient on its own to bring the cell cycle to arrest.[104] p21 is upregulated after MyoG, and the proliferating myoblasts become quiescent. Following cell cycle exit, the expression of contractile proteins such as the MHC is initiated and the cells fuse into multinucleated myotubes.[104]

2.7. The clinical relevance of adipose-derived stromal cells for muscle regeneration

Skeletal muscle is fundamental to movement, posture, breathing and blood glucose homeostasis.[110] Although skeletal muscle retains a remarkable ability to regenerate from the native pool of muscle satellite stem cells, muscular injuries beyond a certain threshold result in fatty degeneration and fibrous scar tissue formation that subsequently compromises structural and functional integrity.[111] Additionally, genetic

disorders such as muscular dystrophies (the prevalence of dystrophies vary depending on the type, and is considered rare with a few cases per 100 000), and the progressive loss of muscle strength, mass and function associated with aging (sarcopenia; prevalent in approximately 10% of the aging population), represent a potential clinical target for ASC therapeutics.[111,112] Rare genetic diseases such as muscular dystrophies and, age-related muscle wasting are simply two areas highlighted because treatment regimens in both cases are not curative but focuses on delaying symptoms or progression. As curative therapies have not been identified for many diseases of genetic origin, it justifies the need to investigate the therapeutic potential that ASC have for the aforementioned and other similar diseases. Peçanha *et al.* (2012)[113] demonstrated that ASCs injected into a surgically damaged soleus muscle in a rat model improved muscle regeneration and contractile force two weeks post-transplantation. Additionally, research by Merritt *et al*. (2010)[114] demonstrated that BM-MSCs promoted restoration of muscle functionality. Merrit and colleagues implanted an extracellular matrix scaffold into the damaged gastrocnemius muscles of rats. Scaffolds seeded with BM-MSCs were compared to scaffolds not seeded with cells. The MSC-seeded scaffolds displayed more surrounding blood vessels, regenerating myotubes and partially restored muscle function and contractile ability after 42 days. The extracellular matrix scaffolds without MSCs displayed morphological but not functional recovery, indicating that MSCs could improve both morphological and functional recovery of skeletal muscle defects.[114] The study by Merritt *et al*. (2010)[114] did not specify whether the improved differentiation and functional capacity was due to the BM-MSCs directly differentiating into a myogenic lineage or whether it was due to paracrine signalling ability. This is important to note, as MSCs are thought by some to achieve regeneration by recruiting factors necessary for wound healing and generation because of their paracrine abilities as shown by the recent attempt to reclassify MSCs as ‘medicinal signalling cells’ by multiple researchers.[20,30]

Duchenne muscular dystrophy (DMD) is an X-linked recessive disorder and the most common lethal paediatric genetic disorder for which there is currently no cure.[115] DMD

is characterised by a lack of dystrophin at the sarcolemma of muscle fibers. The lack of dystrophin destabilises the cytoskeletal architecture between the extracellular matrix and sarcolemma.[115] Muscle fibers become susceptible to mechanical stress and degradation, depleting the satellite cells early in childhood. The degeneration is progressive and irreversible as the skeletal muscle is replaced by fibrotic tissue.[115] A proof-of-concept study by De Bari *et al.* (2003)[116] provided evidence to support the potential use of synovial membrane derived MSCs for DMD, where MSCs transplanted into immunosuppressed DMD mouse models restored the expression of dystrophin in the sarcolemma. Additionally, this restored the expression of mouse mechano growth factor, a molecule crucial in the maintenance and repair of skeletal muscle.[116] Results from a recent case report by Klimczak *et al.* (2020)[117] suggest that co-transplantation of allogeneic BM-MSCs and satellite cells (muscle adult stem cells) improve muscle function in patients diagnosed with DMD.

In the case of muscle pathologies that has a genetic origin (muscular dystrophies such as Duchenne and Limb-girdle), the application of any stem cell therapy might only serve to alleviate symptoms rather than cure the genetic origin of a particular pathology. Bouglé *et al*. (2019)[118] demonstrated an improvement in the symptoms associated with DMD in a murine model. Transplantation of ASCs resulted in an improved muscle phenotype, decreased necrosis, fibrosis and inflammatory cytokines and increased muscle strength. Qiu *et al.* (2018)[119] demonstrated that MSCs seeded on an extracellular matrix scaffold promote skeletal muscle regeneration in a rat model. ASCs are therefore potentially applicable to three mechanisms of clinical skeletal muscle regeneration, namely (i) wound healing and immunomodulation at sites of injury; (ii) replacement of muscle cells by differentiation of ASCs; and (iii) in combination with bio-scaffolds to repair muscle trauma.[120]

2.8. Adipose-derived stromal cell differentiation

ASCs have been differentiated into adipogenic, chondrogenic, osteogenic and myogenic lineages using induction media containing chemical compounds that have been tailored to each lineage.

Adipogenic, chondrogenic and osteogenic differentiation

ASC differentiation *in vitro* is achieved through biochemical stimuli that upregulate specific genetic factors committing ASCs to a particular lineage (Table 2.2). ASCs are expanded in growth medium such as Dulbecco's Modified Eagle's Medium (DMEM) supplemented with 10% fetal bovine serum (FBS) and an antibacterial/antimycotic agent. ASC adipogenesis may be achieved by the addition of insulin (10 µg/mL), dexamethasone (1 µM), isobutylmethylxanthine (0.5 M) and indomethacin (200 µM).[121] The adipogenic induction components function to increase the expression of the adipogenic master regulator peroxisome proliferator-activated receptor gamma (PPARγ) and other adipogenic factors that include CCAAT/enhancer-binding protein (C/EBP) α and β.[122]

Chondrogenesis has been achieved using a combination of many growth factors and supplements, but the most commonly used protocols include dexamethasone (0.1 µM), ascorbate-2-phosphate (50 nM), TGF-β1 (10 ng/mL), and insulin (6.25 µg/mL).[123] Chondrogenic differentiation is achieved through the addition of TGF-β1 particularly, as it upregulates lineage specific proteins such as aggrecan and type II collagen.[124] Osteogenesis is induced through the addition of 100 mg/mL ascorbic acid and 10 mM β-glycerophosphate to standard growth medium. This same induction cocktail has been used with added dexamethasone at varied concentrations.[125] Dexamethasone and β-glycerophosphate have been reported as the main chemical inducers for osteogenesis by increasing the expression and activity of alkaline phosphatase, while ascorbic acid increases the production of collagen during early osteogenesis.[126-128]

Dexamethasone reportedly increases the expression of the main regulator for osteogenic differentiation, runt-related transcription factor 2 (Runx2).[129]

Table 2.2. Composition of adipose-derived stromal cell differentiation media and gene expression required for lineage specification
ASC differentiation media contain combinations of induction components tailored to enhance commitment of ASCs into the different lineages regulating genes that govern lineage specification

Differentiation process	Differentiation medium	Genes	Reference
Adipogenesis	DMEM, 10% FBS, insulin (10 µg/mL), dexamethasone (1 µM), isobutylmethylxanthine (0.5 M) and indomethacin (200 µM)	Adiponectin, C/EBPα, FABP4, Leptin, PPARγ	Bourin *et al.* (2013)[69] Ambele *et al.* (2016)[121]
Chondrogenesis	DMEM, 10% FBS, dexamethasone (0.1 µM), ascorbate-2-phosphate (50 nM), TGF-β1 (10 ng/mL), and insulin (6.25 µg/mL)	Aggrecan, collagen type II, sox 9	Bourin *et al.* (2013)[69] Stromps *et al.* (2014)[123]
Osteogenesis	DMEM, 10% FBS, 100 mg/mL ascorbic acid and 10 mM β-glycerophosphate	Alkaline Phosphatase, Bone sialoprotein, Osteocalcin, Osterix, Runx2	Bourin *et al.* (2013)[69] Marshall *et al.* (2019)[125]
DMEM: Dulbecco's Modified Eagle's Medium; FBS: fetal bovine serum; TGF-β1: transforming growth factor beta-1; C/EBP: CCAAT/enhancer-binding protein; FABP4: fatty Acid-Binding Protein 4; PPARγ: peroxisome proliferator-activated receptor gamma; Runx2: runt-related transcription factor 2; Sox9: SRY-box 9			

Myogenic differentiation

ASC myogenesis has been achieved using various induction media (Table 2.3) and was first demonstrated by Zuk *et al.* (2001)[130] through the addition of 0.1 µM dexamethasone and 50 µM hydrocortisone to ASCs in culture. ASC myogenesis has also been demonstrated using hydrocortisone alone by Mizuno *et al.* (2002)[131]. Myogenesis was attained with varying success, with the original report from Zuk *et al*. (2001)[130] achieving 12% myogenic differentiation and Mizuno *et al.* (2002)[131] 15% after 6 weeks in culture. ASC myogenesis has been demonstrated by supplementing bioengineered forms of MyoD and through the use of serum free, chemically defined media.[132] More recently, commitment of ASCs to myogenesis has been accomplished by using the demethylating agent 5-Azacytidine (5-Aza).[133-135]

Table 2.3. Adipose-derived stromal cell myogenic chemical induction recipes. ASC commitment to myogenesis has successfully been achieved using multiple induction methods.

Reference	Medium	Serum supplementation	Chemical induction components
Zuk *et al.* (2001)[130]	DMEM	10% FBS 5% HrS	Dexamethasone (0.1 µM) Hydrocortisone (50 µM)
Mizuno *et al* (2002)[131]	DMEM	5% HrS	Hydrocortisone (50 µM)
Gang *et al.* (2004)[136]	Low glucose DMEM	15% FBS 5% HrS	Dexamethasone (0.1 µM) Hydrocortisone (50 µM)
Huri *et al* (2013)[133]	Low glucose DMEM	1% FBS 5% HrS	5-Azacytidine (10 µM)
Sung *et al.* (2013)[137]	DMEM	2% HrS	Myogenic differentiation (MyoD) and MyoD-IT (bioengineered MyoD) (0.2-10 µg/mL)
Meligy *et al.* (2012)[134]	DMEM	10% FBS 5% Hrs	5-Azacytidine (10 µM)
Drost et al (2009)[135]	α-MEM	10% FBS	5-Azacytidine (10 µM)
DMEM: Dulbecco's Modified Eagle's Medium; α-MEM: alpha-minimum essential medium; FBS: fetal bovine serum; HrS: horse serum			

2.9. Functional mechanisms of the chemical components in myogenic induction medium

Induction media compositions in ASC myogenesis generally include either dexamethasone and hydrocortisone and 5-Azacytidine. Myogenic media are often supplemented with horse serum (HrS). The passages below attempt to provide information from the currently available literature how these supplements might induce or enhance myogenesis.

Horse serum

HrS is frequently added to myogenic induction media. In media containing higher FBS concentrations (10% - 20%), myocytes proliferate even after confluency has been reached. Myogenic differentiation is achieved through serum starvation by switching expansion medium supplemented with 10% - 20% FBS with medium containing 1% to 2% FBS or HrS.[138,139] Yaffe *et al.* (1977)[140] demonstrated that, compared to FBS, HrS enhances myotube formation in murine myocytes. Franke *et al.* (2014)[141] demonstrated that equine bronchial fibroblasts (EBF) expanded in HrS-containing

medium displayed altered morphology to those expanded in FBS. EBFs cultured in the HrS-containing medium had slower doubling times, were smaller, and were more closely packed than cells expanded in FBS.[141] There is a paucity of literature which adequately describes the mechanism of action of the different sera in ASC or myocyte differentiation. Serum contains more than a thousand molecular components that include proteins, enzymes, lipids and hormones. Molecular factors in the various sera that direct cells to either proliferate or differentiate are difficult to determine.[142,143]

Glucocorticoids

The use of the glucocorticoids (GC) dexamethasone and hydrocortisone in *in vitro* ASC myogenesis is well-documented although their function in the differentiation process is not clear. GCs bind to glucocorticoid receptors (GRs) in the cytosol, which are ligand-dependent transcription factors and type I nuclear hormone receptors.[144] GC-GR complexes translocate into the nucleus and associate with GC response elements to induce or repress transcription. GR functions also include binding to other transcription regulatory factors (tethering), or binding to and removing transcriptional regulatory factors (squelching).[145] Clinically, GCs are used for their anti-inflammatory and immunosuppressive properties.

GCs regulate protein and glucose metabolism in skeletal muscle and are released under conditions of stress. Increased GC levels increase proteolysis in order to generate amino acids that serve as precursors for gluconeogenesis.[146] This GC-mediated protein degradation is responsible for muscle atrophy and weakness seen in patients treated with GCs over prolonged periods of time.[147] This atrophy is caused by the upregulation of myostatin (a negative regulator in myogenic differentiation).[148] A recent study by Larson *et al.* (2018)[148] showed that using dexamethasone at 10 nM on engineered skeletal muscle units yielded advanced sarcomeric structures with the ability to produce force.[148] Belanto *et al.* (2010)[149] found that dexamethasone may induce the early messenger RNA (mRNA) expression of MyoD, MyoG and dysferlin, a transmembrane protein that functions in skeletal muscle repair. Dexamethasone has

been reported to enhance myotube fusion of murine cells *in vitro* at low concentrations (5-25 nM). Using dexamethasone as a myogenic inducer *in vitro* may also either promote or inhibit the process depending on the stage of differentiation. Han *et al.* (2017)[150] showed that treating C2C12 myoblasts with dexamethasone at the myotube stage has been associated with myotube atrophy. However, when the cells were treated at the myoblast stage, before the onset of differentiation, an increase in MHC expression and in myotube diameter was observed.[150] Hydrocortisone has been reported to stimulate the proliferation of human myoblasts prior to myotube fusion.[151] The exact mechanisms and signalling pathways through which the glucocorticoids dexamethasone and hydrocortisone promote myogenesis *in vitro* are not clearly defined in the literature.

5-Azacytidine

5-Aza is a universal demethylating agent that acts by inhibiting DNA via irreversible covalent binding between DNA-cytosine methyltransferase and DNA.[152] It may be used as a component for ASC myogenic induction.[133-135]

The role of methylation status on gene expression is well described. Hypermethylation around cytosine-guanine (CpG) islands of promoters is associated with gene repression whereas hypomethylation is associated with the promoters of active genes.[153] Methylation status is an epigenetic trait that may be inherited or influenced by the environment. Xu *et al.* (2017)[55] attribute differences in osteogenic and adipogenic differentiation potential to methylation status, thereby influencing differentiation potential. They observed that CpG sites around the Runx2 promoter in BM-MSCs were hypomethylated while the same promoter in ASCs was hypermethylated, and therefore inactive. Furthermore, the CpG sites around the PPARγ promoter in ASCs was hypomethylated (actively available for transcription) as opposed to those of BM-MSCs that were hypermethylated.[55] A study by Nour *et al*. (2006)[154] revealed that the MyoG gene is methylated in uncultured ASCs and maintains this status when undifferentiated and after adipogenic induction. These

results were verified by Vera-Pérez *et al.* (2019)[155] who, in addition to MyoG, reported that 15 other genes associated with myogenesis were also methylated in ASCs.[155]

Montesano *et al.* (2013)[156] investigated the effects of 5-Aza on C2C12 murine myoblasts. Their results suggest that 5-Aza upregulates Myf 5 and MyoD while promoting cell cycle arrest by significantly upregulating the expression of p21. The researchers postulated that this may promote the shift from cell proliferation to differentiation. They concluded that 5-Aza treatment enhanced C2C12 maturity by acting on the cell cycle and upregulating muscle-specific determinants.[156] A study by Kaur *et al*. (2014)[157] further demonstrated the ability of 5-Aza to induce skeletal myogenesis. Treating cardiomyocytes with 5-Aza resulted in the upregulation of key skeletal muscle nuclear transcription factors such as MyoD and MyoG. Subsequently, the cardiomyocytes transdifferentiated into skeletal muscle cells.[157] In summary, 5-Aza is not used in the differentiation of other ASC lineages, and has consistently been shown to promote myogenic differentiation, and not adipogenesis, chondrogenesis or osteogenesis. The mechanism through which 5-Aza could achieve myogenesis in ASCs is by demethylating myogenic promoters, upregulating myogenic genes and by regulating cell cycle progression to promote the transition of cells from proliferation to differentiation.

2.9. Methods used to investigate MSC myogenesis

MSC myogenic differentiation from multiple tissue sources has been investigated using a variety of techniques (Table 2.4). Both phase-contrast light- and fluorescent microscopy have frequently been employed to investigate cell morphology. The actin cytoskeleton of cells can be viewed by staining with phalloidin (a fluorescent stain) to evaluate the formation of tube-like structures which indicate the formation of myotubes. 4′,6-Diamidino-2-phenylindole (DAPI) is a frequently used nuclear stain. Immunocytochemistry (ICC) is used to study myogenesis using antibodies targeted to myogenic proteins including Pax 3/7, desmin, MyoD, MyoG and MHC. These same targets have also been investigated using reverse-transcriptase real-time polymerase chain reaction (RT-qPCR). Other protein detection techniques include Western blot analysis to investigate the presence of MyoD and MHC, immunohistochemistry (IHC)

using antibodies directed at MyoD and MHC, flow cytometry to investigate cell cycle progression and desmin, MyoD, MyoG and MHC expression. Flow cytometry is most frequently used to immunophenotype ASCs according to standard criteria (Table 2.1). The timelines vary between experiments. Studies that involved 5-Aza lasted for up to twenty-one days and dexamethasone/hydrocortisone up to 42 days.

Table 2.4. Methods used to investigate mesenchymal stromal/stem cell myogenesis.
Summary of the methods and their associated target genes and/or proteins most frequently used to confirm successful myogenic differentiation.

Reference	MSC Source	Feature investigated	Technique	Detection method	Target proteins/genes investigated
Zuk *et al.* (2001)[130]	Human adipose tissue	Morphology	Light microscopy		
		Protein expression	Immunocytochemistry (colour)	Antibody	MyoD and MHC
Mizuno *et al* (2002)[131]	Human adipose tissue	Morphology	Light microscopy		
		Protein expression	Immunocytochemistry (colour)	Antibody	MyoD and MHC
Gang *et al.* (2004)[136]	Human umbilical cord	Morphology	Light microscopy		
		Protein expression	Immunocytochemistry (colour)	Antibody	MyoD and MyoG
				Haematoxilin	Nuclei
			Western blot	Antibody	MyoD, MyoG, MHC
			Flow cytometry - immunophenotyping	Antibody	CD 105, CD73, CD44, CD49e, CD54, CD90, CD14, CD34, CD45, CD31, CD49d, CD106, HLA-ABC and HLA-DR.
			Flow cytometry - myogenic targets	Antibody	MyoD, MyoG and MHC
		Gene expression	RT-qPCR	Primers	MyoD, MyoG and MHC
Huri *et al.* (2013)[133]	Human adipose tissue	Morphology	Phase contrast light microscopy		
			Fluorescent microscopy		
		Protein expression	Immunocytochemistry (fluorescent)	Antibody	MyoD, desmin, MHC

				Phalloidin	Actin filaments
				DAPI	Nuclei
Huri *et al.* (2014)[158]	Human adipose tissue	Morphology	Fluorescent microscopy		
		Protein expression	Immunocytochemistry (fluorescent)	Antibody	Pax3/7, MyoD, desmin and MHC
				DAPI	Nuclei
Huri *et al* (2018)[159]	Human adipose tissue	Morphology	Light microscopy		
			Fluorescent microscopy		
		Protein expression	Immunocytochemistry (fluorescent)	Antibody	Pax3/7, MyoD, desmin and MHC
				Phalloidin	Actin filaments
				DAPI	Nuclei
			Flow cytometry - immunophenotyping	Antibody	CD 73, CD90 and CD105
Sung *et al.* (2013)[137]	Human adipose tissue	Morphology	Fluorescent microscopy		
		Protein expression	Immunocytochemistry (fluorescent)	Antibody	MHC
				DAPI	Nuclei
			Westernblot	Antibody	MyoD
Drost et al (2009)[135]	Human bone marrow	Protein expression	Flow cytometry - immunophenotyping	Antibody	CD31, CD34, CD45, CD73, CD90, and CD105
		Gene expression	RT-qPCR	Primers	MyoD and MHC
Meligy *et al.* (2012)[134]	Rat adipose tissue, bone marrow, umbilical cord and skeletal muscle tissue	Morphology	Phase contrast light microscopy		
			Fluorescent microscopy		
		Protein expression	Immunocytochemistry (fluorescent)	Antibody	desmin
				DAPI	Nuclei
			Immunocytochemistry - immunophenotyping	Antibody	CD90, CD44, CD45, and CD34, CD31

			Flow cytometry - immunophenotyping	Antibody	CD90, CD45, CD44, CD31, and CD34
			Flow cytometry - myogenic targets	Antibody	MyoG
		Gene expression	RT-qPCR	Primers	desmin
DAPI: 4′,6-diamidino-2-phenylindole; CD: Cluster of differentiation; ICC: immunocytochemistry; IHC: immunohistochemistry; MHC: myosin heavy chain; MSC: mesenchymal stem/stromal cell; MyoD: myogenic differentiation; MyoG: myogenin; Pax3/7: paired box gene 3/7; RT-qPCR: reverse transcriptase real-time polymerase chain reaction.					

2.10. A modelling insight into adipose-derived stromal cell myogenic differentiation

The mechanisms and kinetics involved in cell fate determination are crucial in the understanding of normal development and disease. Gene expression or protein data generated in differentiation studies have been used to model how these myogenic determinants may initiate differentiation.

Huri *et al*. (2014)[158] were the first to model gene expression kinetics in ASCs using 5-Aza for induction of myogenesis. The researchers found that the expression of key myogenic factors in ASCs is temporal and mimics those of *in vivo* muscle satellite cell differentiation. They further showed that the expression of myogenic targets is sequential and that ASCs sequentially change to assume the myogenic cell morphology (eg. elongated, multinucleated).[158] The researchers used a mathematical kinetic stage-transition model to identify five stages of the ASC myogenic differentiation process. These stages may be identified by the expression of the key myogenic determinants Pax 3/7, desmin, MyoD and MHC (Figure 2.10. Model A).

Stage zero describes undifferentiated ASCs which are characterised by the negative expression of all myogenic targets. Stage one is characterised by the expression of Pax 3/7 in differentiating ASCs. Stage two is identified by the expression of Pax 3/7 and desmin, while the expression of MyoD and MHC remains negative. Stage three sees the differentiating ASCs express Pax 3/7, desmin and MyoD, whilst remaining negative for MHC. Stage four is characterised by the presence of mature muscle cells with positive expression of Pax 3/7, desmin, MyoD and MHC.[158]

A more recent model established by Deshpande and Spector[160] based on the work of Huri *et al*. (2014)[158] identified six stages of ASC myogenic differentiation. They also reported differences in the expression of Pax 3/7. In their model, stage zero

encompassed undifferentiated ASCs that negatively express Pax 3/7, desmin, MyoD, MyoG and MHC. Stage one was characterised by the positive expression of Pax3/7.[160] Stage two was positive for desmin only. Stage three was defined as cells negative for Pax 3/7, MyoG and MHC, but positively expressing desmin and MyoD. Stage four cells were negative for Pax 3/7 and MHC and positive for desmin, MyoD and MyoG. The fifth and final stage in their model described mature myocytes by the negative expression of Pax 3/7 and the positive expression for desmin, MyoD, MyoG and MHC (Figure 2.10. Model B).[160]

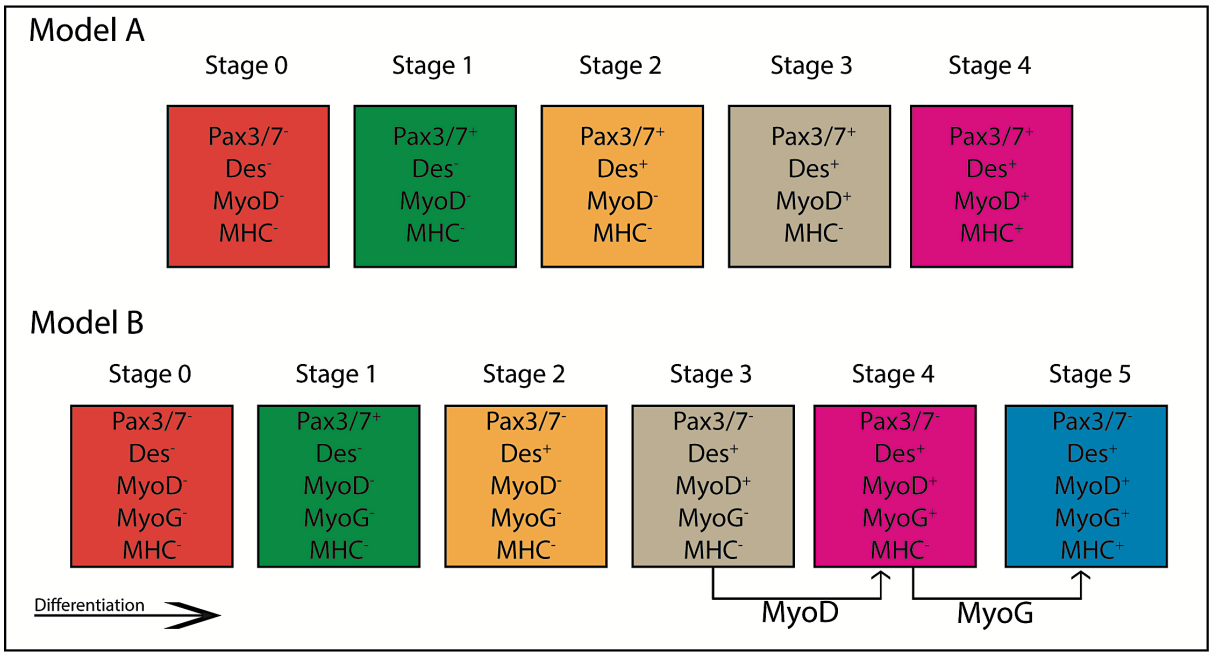

Figure 2.10. Theoretical models depicting the adipose-derived stromal cell myogenic differentiation pathway.
A. The first model depicts adipose-derived stromal cell (ASC) myogenesis as established by Huri et al. (2014)[158]. Five Stages of differentiation are depicted based on the expression of paired box gene 3, desmin (Des), myogenic differentiation (MyoD) and myosin heavy chain (MHC). B. The most recently published model as conceptualised by Deshpande and Spector.[160] In this model there are six stages based on the expression of the above-mentioned myogenic targets, as well as myogenin (MyoG). Stage zero is defined as undifferentiated ASCs and stage five as mature muscle cells. MyoD facilitates the transition from stage three to four and MyoG the transition from stage four to five.

Differentiation as illustrated by these models is thus a temporal process, with ASCs maintaining the capacity for self-renewal until stage three of differentiation.[158,160] The expression of myogenic targets seem to be subject to feedback inhibition exerted by

transcription factors, signals from the extracellular matrix and from cell density.[160] Pax 3/7 peaks on day three post-induction after which it steadily decreases. This is attributed to possible feedback inhibition by MyoD (stage three) on Pax 3/7 (stage one). The expression of desmin is observed after Pax 3/7 and before that of MyoD and MHC.[158] The model presented by Deshpande and Spector[160] further suggests that the activation of MyoG occurs during stage three and facilitates the transition into stage four, where MyoG in turn causes MHC to be upregulated and thus drives the transition to stage five. The results of both the aforementioned publications further suggest that the expression of key drivers of myogenic cell fate, such as MyoD and MyoG, must reach a certain threshold *in vitro* in order to progress along the differentiation pathway.[158,160]

2.11. Rationale for the study

The field of regenerative medicine has grown substantially in the past decade and involves the use of stem and progenitor cells, sought specifically for their incredible plasticity, as therapeutic agents. Regeneration is a process that aims to use these cells for restoration of both the structure and function of tissues and organs.[161]

Cell-mediated therapeutic protocols involving cell culture and differentiation must first be standardised *in vitro* and should adhere to certain criteria before they are applied in clinical practice. These criteria were put forth by Gimble *et al.* (2007)[162] and state: (i) MSCs must be harvestable in volumes large enough to be therapeutically relevant; (ii) the harvest procedure should be minimally invasive; (iii) the cells must display multipotent plasticity; (iv) clinical use of the cells must be safe in both autologous and allogeneic contexts; and (v) the cell product can be manufactured according to current Good Manufacturing Practice (GMP) guidelines.[162] GMP guidelines require that the 'active component' (the MSCs) is clearly defined in terms of its genotypic and phenotypic profiles; is free of any bacterial, fungal or viral pathogens or any other components that may otherwise harm a patient; are present as pure, highly

concentrated product free from other cell populations that may potentially impede their therapeutic potential; and that the therapy is competent in its potency to achieve a specified clinical effect.[163] Shortcomings to many cell-based protocols include a lack of standardization, batch-to-batch variation (particularly in primary cells), and the inclusion of xeno-derived products such as FBS and HrS to aid with proliferation and differentiation.[163] Expanding cells *in vitro* to attain therapeutic quantities should ideally involve culture methods that do not rely on xeno-derived supplementation to avoid cross-contamination of animal pathogens and immunogenic interactions. To this end, ongoing research into human alternatives aims to develop culture methods that eliminate the need for animal-derived supplements and produce a product that might be transplanted safely into humans in need of cell-based therapy.

ASCs are clinically relevant adult stem cells with adipogenic, chondrogenic, osteogenic and myogenic differentiation potential. There is a global need for the standardization of harvesting and expansion protocols to adhere to GMP guidelines to enhance the availability of these cells in clinical applications. Furthermore, understanding the mechanisms through which ASCs either directly differentiate into different cell lineages, or sequester factors and other adult stem cells required to potentiate tissue regeneration, will influence the extent to which they can be used clinically (either as differentiated or undifferentiated cells).

To work towards the aim of initiating a GMP-compliant protocol, FBS was substituted with pooled human platelet lysates (pHPL) during the ASC expansion phase of this study. pHPL has been described as a clinically acceptable alternative to FBS, which adheres to GMP guidelines.[164,165] Studies conducted at the Institute for Cellular and Molecular Medicine (ICMM; University of Pretoria, Department of Immunology) showed that ASCs expanded in media supplemented with pHPL have higher proliferation rates and increased cell viability.[166] pHPL has also been used to expand ASCs used in clinical trials.[167] pHPL is obtained from donated whole blood that is processed via high speed centrifugation, separating the blood components into

plasma, buffy coat and red blood cell layers.[168] The buffy coat layer is isolated and further processed by low speed centrifugation and the top layer of the processed product is isolated as a platelet concentrate (PC).[168] The PC is depleted of leukocytes via low speed centrifugation and pHPL is collected by pooling PCs. The pooled product is exposed to freeze-thaw cycles, resulting in disruption of platelet membranes and subsequent release of bioactive factors into the supernatant.[164,169] Studies have previously reported that pHPL does not adversely affect ASC differentiation and that it is comparable to the differentiation observed in FBS protocols.[170-172]

Scientists at the ICMM have previously studied and published extensively on the adipogenic differentiating potential of ASCs, optimizing the protocols.[121,164,173-176] The osteogenic and chondrogenic potential of ASCs have also been demonstrated and published by this group.[177,178]

The aim of this research study was to optimise the differentiation of ASCs into a myogenic lineage using previously published protocols. The rationale behind this aim was to establish a standardised and optimised ASC myogenic differentiation protocol to enable future investigation into the drivers of ASC myogenesis and ASC cell fate. Secondly, this study aimed to initiate a GMP-compliant culture protocol, by substituting FBS with pHPL during the ASC expansion phase, availing ASC myogenesis as a potential cell-based therapeutic avenue.

This concludes Chapter 2. The following, Chapter 3, summarises the aims, objectives, purpose of the study, an overview of the method of investigation and statistical considerations.

Chapter 3: Aim, objectives, ethics and statistics

This chapter provides an overview of the purpose, aim, ethics and a general outline of the statistics used in the dissertation.

3.1. Purpose of research

The purpose of this study was to investigate two previously published myogenic differentiation media, and to establish which induced effective myogenic differentiation of adipose-derived stromal cells *in vitro*. As the ICMM has previously not conducted any research pertaining to ASC myogenesis, the purpose of this study was also to optimise assays that may be used to assess myogenic differentiation *in vitro*.

3.2. Method of investigation

ASCs were isolated from fresh adipose tissue (lipoaspirate or resected fat) or thawed from a cryopreserved stock from previous isolations and characterised (Chapter 4). ASCs were differentiated into a myogenic lineage using two separate published methods of induction. The first protocol entailed the addition of dexamethasone and hydrocortisone, while the second used 5-Aza. The efficacy of these methods on ASC differentiation was investigated over time, focusing on myogenic morphological characteristics such as multinucleation and myotube formation, as well as expression of myogenic marker genes and proteins. Primary human myoblast (PHM) cells were used as positive controls for myogenesis. PHMs were used to optimise methods, including the fluorescent labelling of myogenic target proteins and protocols pertaining to relevant gene and protein expression. The protein markers used to investigate myogenesis using ICC included Pax 3/7, MyoD, MyoG and desmin. Relative gene expression of myogenic targets MyoD, MyoG and desmin was investigated using RT-

qPCR. The particulars of each assay (ICC and RT-qPCR) is summarised in Chapter 5.

3.3. Aim and objectives

The main aim of this study was to establish and optimise a method of controlled myogenic differentiation of ASCs *in vitro*, with the introduction of components to make the process GMP-compliant. In order to achieve this, the following objectives were defined:

- To determine whether the surface markers expressed on the adipose-derived cells were characteristic of ASCs using flow cytometry
- To initiate a GMP-compliant culture protocol by expanding ASCs in medium supplemented with pHPL
- To determine the optimal ASC differentiation medium by comparing the addition of dexamethasone/hydrocortisone and 5-Aza based on the expression of myogenic genes and proteins, and by observing changes in cell morphology
- To determine a myogenic differentiation time-line
- To document the effect of ASC myogenic induction on cell morphology using light and fluorescence microscopy to identify cell fusion, multinucleation and myotube formation
- To determine the efficacy of the induction media on ASC myogenesis by demonstrating the temporal expression of early and late myogenic proteins using immunocytochemistry
- To investigate the efficacy of the induction media on ASC myogenesis by quantifying the expression of early and late myogenic genes using RT-qPCR.

3.4. Ethical approval

Ethics approval for this project was obtained at the University of Pretoria Faculty of Health Sciences Research Ethics Committee (Appendix A; ethics reference number:

468/2018). To ensure that ASCs adhered to culture plates after myogenic induction, culture plates was coated with collagen type I (see sections 5.3.5 and Appendix G, section G5). The collagen type I was directly isolated from rat tails. In order to isolate type I collagen for cell culture purposes directly from rat tails, ethical approval was obtained from the Animal Ethics Committee (Appendix B; ethics reference number: REC107-19). Ethical clearance to procure and use pHPL was also obtained from SANBS (SANBS ethics reference number 2013/17; Appendix C). The use of freshly isolated ASCs was granted to the ICMM by the University of Pretoria under the MSc study conducted by Miss A. Gerber (ethics reference number: 424/2018; Appendix D). The current study was listed as part of the amendment. The immortalised murine C2C12 myoblast cell line and primary human myoblasts were obtained from Prof. Kathy Myburgh (University of Stellenbosch, Department of Physiology; ethics nr: S17/10/240).

3.5. Statistical considerations

3.5.1. Data analysis, plots and graphs

Data analysis was performed using GraphPad Prism version 9 for Macintosh (GraphPad Software, San Diego, California, United States). Plots and graphs were generated using GraphPad Prism version 9 for Macintosh.

3.5.2. Descriptive statistics

Descriptive statistics were included where applicable. Means were reported with standard deviations (SD) or the standard error of the mean (SEM). As biological samples are inherently highly variable, some descriptive data were reported as a median with corresponding minimum and maximum ranges.

3.5.3. Statistical comparisons

The sample size used in this study was n=3 and therefore the data was considered to be non-parametric. To compare the means between two culture conditions, a Mann-Whitney U test was employed. A Kruskal-Wallis test followed by a Dunn's post hoc multiple comparisons test was used to compare the means between three culture conditions or between days for each condition. The significance level was set as $\alpha = 0.05$, and a p-value < 0.05 was considered statistically significant. Further details pertaining to the statistical considerations for each chapter have been described within each chapter where relevant.

This concludes Chapter 3. Chapter 4 contains all the relevant information, methods, results, discussion and conclusions pertaining to ASC isolation and characterisation.

Chapter 4: Adipose-derived stromal cell isolation and characterisation

Chapter 4 summarises information pertaining to the isolation and characterisation of ASCs used throughout this study, and concludes with a short discussion of the findings which are elaborated on in the final discussion Chapter 6.

4.1. Introduction

ASCs refer to MSCs isolated from adipose tissue. Although minimum guidelines (Chapter 2, Table 2.1) have been recommended to characterise ASCs *in vitro,* standardised guidelines still do not exist for isolation procedures.[31,69] Several methods have been used successfully to isolate the SVF from adipose tissue.

Adipose-derived stromal cell isolation procedures

ASCs are isolated using manual or mechanical methods, and these may either be enzymatic or non-enzymatic (Figure 4.1). Non-enzymatic methods have been developed in order to create protocols that adhere to a GMP guideline related to 'cell manufacturing'. This particular guideline requires cells that are to be used for clinical purposes to be 'minimally manipulated'.[179] The United States Food and Drug Administration (FDA) considers enzymatic treatment 'more than minimally manipulated,' as enzyme digested tissue may alter the membrane receptor profile of cells, resulting in alterations in biological activity. The use of collagenase to obtain the SVF is thus considered a substantial manipulation and is therefore excluded as a GMP compliant method. However, enzymatic digestion is still acceptable when isolating cells for research purposes.[179] Non-enzymatic isolation of ASCs involves explant culture, where tissue sections are butterflied onto a tissue culture surface, or adipose tissue is emulsified mechanically.[180,181] The most well-described enzymatic digestion method involves the use of the enzyme collagenase to digest cellular tight junctions

and components of the extracellular matrix (ECM). This method was first published by Zuk *et al.* (2001)[130] and has been used predominantly for research purposes. Other enzymes that have been used include trypsin and dispase. There is some consensus when using enzyme-based isolation with respect to temperature (37°C) and digestion duration (30min to 1 hour). Most laboratories who use the method developed by Zuk and colleagues do so with minor adjustments tailored to their laboratory needs and reagent inventory.[69]

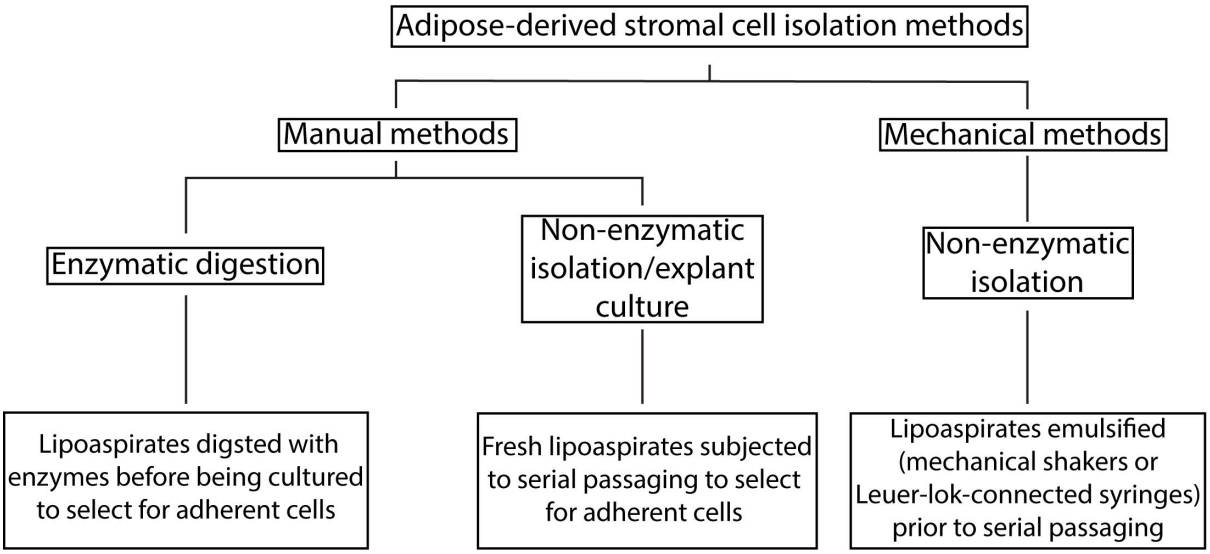

Figure 4.1. Methods used to isolate adipose-derived stromal cells.
Different methods are used to isolate adipose-derived stromal cells and selecting a method depends on the application. Enzymatic digestion is a popular isolation method for research purposes, while non-enzymatic methods are more suited to clinical applications.[69,179-182]

Factors that affect adipose-derived stromal cell expansion and immunophenotype

Multiple factors including adipose tissue acquisition techniques, SVF isolation methods and expansion modalities affect ASC immunophenotypic profiles and proliferation capabilities. Bajek *et al.* (2015)[182] found that using different liposuction techniques had no significant effect on the defining surface markers expressed on ASCs. However, they reported significant variations in the expression of 58 out of 242 non-defining surface antigens studied in ASCs obtained either from mechanical- or

ultrasound-assisted liposuction. Bussar *et al.* (2015)[183] demonstrated that CD34 was expressed at significantly lower levels in ASCs obtained using a non-enzymatic isolation method (3.16% after two passages) when compared to ASCs isolated using the collagenase-based method (8.06% after two passages).

Serum supplementation has also been reported to influence ASC proliferation, with a particular focus on FBS compared to human alternatives such as pHPL. Fuoco *et al*. (2020)[184] reported population doubling times (PDT) that differed significantly with both isolation methods and serum supplementation. ASCs isolated by enzymatic digestion and expanded in medium supplemented with 10% FBS had a PDT of 59.59 hours as opposed to 10% pHPL-supplementation, with a PDT of 39.96 hours. Furthermore, ASCs obtained by mechanical isolation and expanded in 10% FBS had a PDT of 49.75 hours and 20.69 hours when expanded in 10% pHPL.

Immunophenotyping of the adipose-derived stromal cells

Dominici *et al*. (2006)[1] published the first guidelines (Chapter 2, Table 2.1) with the aim to standardise the characterization of MSCs, while Bourin *et al.* (2013)[2] aimed to tailor these guidelines to ASCs specifically. Bourin and colleagues suggested that immunophenotyping be done using flow cytometry.

Flow cytometry is uniquely suited to the objective of immunophenotyping, as it allows for high-throughput analysis on a single-cell level to identify cell populations with similar immunophenotypic profiles. Briefly, flow cytometry uses the principles of immunofluorescence and light scatter, which allows extra- and intra-cellular features and molecular targets linked to specific fluorochromes to be visualised. This is achieved by exciting fluorochromes conjugated to antibodies against specific cell surface proteins, and detecting the resultant emission of light.[185] Each fluorochrome has an optimum wavelength at which it is excited, and emits light at a different wavelength which is measured by the instrument and recorded using corresponding

software. Within the flow cytometer, the optical system is comprised of a light source (laser), lens and mirrors designed to focus and direct light to a point where individual cells flow through.[185] The second component of the optical system involves sets of mirrors and filters that absorb and measure emitted light at different wavelengths. The fluidics system collects cells in a stream where they flow past a specific point, one at a time, to intersect with the laser and optical path for detectors.[185] The electronic system converts the captured emission information into readable data while the computer system is used for visualisation and analysis.[185]

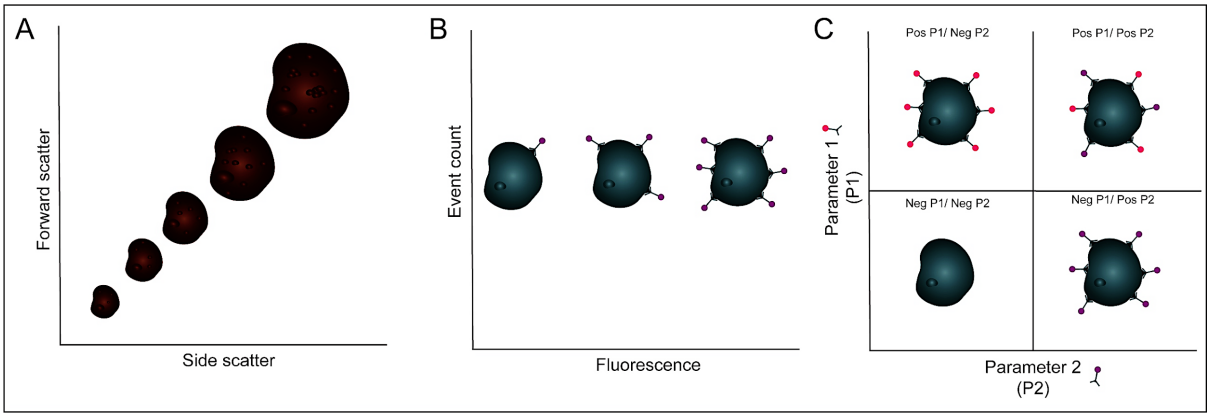

Figure 4.2. Principles of light scatter and fluorescence intensity.
Plot A demonstrates a simple two-parameter plot (side scatter versus forward scatter). Plot B represents a one-parameter plot to measure relative fluorescence intensity. More antibody binding results in an increase in fluorescence, and a signal shift to the right of the x-axis. More bound antibodies result in a greater fluorescence signal (measured signal shifts to the right). Plot C demonstrates a two-parameter plot, where two variables are measured in four quadrants.[186,187]

Light scatter is the measurable phenomenon that occurs when light bounces off the target (single cell) to be analysed. Forward and side scattered (FS and SS) light are parameters that can be used to measure cell granularity and size. Conventionally, forward scatter is indicative of size while side scatter indicates internal complexity and may be visualised on a FS versus SS two-parameter plot (Figure 4.2A).[186] Single-parameter plots may be used to analyse fluorescence intensity, where bound antibodies conjugated to fluorochromes cause the measured signal to shift to the right of the plot (Figure 4.2B).[187] As bound antibody conjugates increase, higher fluorescence intensities are measured, and a larger shift to the right of the x-axis is

observed. Two-parameter plots also yield results in four quadrants, identifying cell populations that are positive or negative for both parameters or positive for one only (Figure 4.2C).[187] The ASC immunophenotype investigated at the ICMM was $CD44^{+}CD73^{+}CD90^{+}CD105^{+}CD36^{+}CD34^{variable}CD45^{-}$. The functions and recommended expression of these surface markers have been summarised in Table 4.1.

Table 4.1. Defining surface markers used to immunophenotype adipose-derived stromal cells.
A summary of the surface antigens used to define adipose-derived stromal cells and their functions.

Surface marker	Function	Recommended expression of markers on cell surface	References
CD44	• Transmembrane glycoprotein that expressed on ASCs • Ligand for hyaluronic acid, collagens, osteopontin and matrix metalloproteinases • Functions in hyaluronic acid metabolism, activation and homing of lymphocytes, release of cytokines and cell adhesion	>80%	Sneath *et al.* (1998)[188] Senbanjo *et al.* (2017)[189] Bourin *et al.* (2013)[2]
CD90	• Glycosylphosphatidylinositol-anchored glycoprotein also known as Thy-1 • Highly expressed on undifferentiated ASCs *in vitro* • A decrease in expression implicated in lineage specification and differentiation *in vitro* • CD90 has functions in T-cell activation, fibrosis, cell migration, fibroblast adhesion and wound healing	>80%	Moraes *et al.* (2016)[190] Bourin *et al.* (2013)[2]
CD73	• Ecto-5′-nucleotidase that converts adenosine monophosphate into adenosine • Implicated in the immunosuppressive responses observed in ASCs • CD73 decreases endothelial permeability, thereby preserving barrier functions	>80%	Chen *et al.* (2016)[191] Minor *et al.* (2019)[192] Schneider *et al.* (2019)[193] Bourin *et al.* (2013)[2]
CD105	• Also termed endoglin and is a constitutively phosphorylated transmembrane glycoprotein • Known co-receptor for TGF-β and implicated in cellular proliferation, migration and differentiation • Anti-apoptotic effects in the absence of TGF-β	>80%**	Li *et al.* (2003)[194] Fonsatti and Maio (2004)[195] Levi *et al.* (2011)[196] Bourin *et al.* (2013)[2]
CD36	• Integral membrane glycoprotein present on multiple cell types • Functions in fatty acid transport, lipid metabolism • Interacts with tyrosine kinases to facilitate signal transduction	Variable	Zhao *et al.* (2018)[197] Bourin *et al.* (2013)[2]
CD34	• Transmembrane phosphoglycoprotein protein • Known marker for haematopoietic stem cells • Functions in cell adhesion, proliferation, trafficking and migration of haematopoietic cells	Variable	Healy *et al.* (1995)[198] Nielsen and McNagny (2008) Bourin *et al.* (2013)[2]
CD45	• Receptor-linked protein tyrosine phosphatase expressed on all leukocyte	<2%	Hermiston *et al.* (2003)[199]

	• Functions in lymphocyte development, signalling and function • Essential for histamine degranulation in mast cells after immunoglobulin E cross-linking		Bourin *et al.* (2013)[2]
	ASC: adipose-derived stromal cell; CD: cluster of differentiation; TGF-β: transcription growth factor beta ***Bourin et al. (2013)[2] contrary to this recommendation mention that CD105 expression may be variable between cultures, and suggested that CD13 may be a more suitable alternative either as a substitute marker or an additional marker*		

4.2. Chapter objectives

The objectives of this chapter are to describe the ASC isolation process and to ensure that ASCs used in experiments express surface markers characteristic of ASCs as demonstrated by flow cytometry.

4.3. Materials and Methods

4.3.1. Cell culture and sample information

All ASC experiments were conducted with three independent biological samples (*n=3*). The cells were thawed from previously isolated and cryopreserved ASC samples isolated from donated lipoaspirates after written informed consent was obtained from the donors (Appendix E).

Due to a malfunction of the liquid nitrogen storage tank and the loss of cryopreserved samples, the cultures used to investigate gene expression and protein expression were not the same. Thus, a total of five ASC cultures were immunophenotyped but only three cultures were used to investigate gene expression, and three were used to investigate protein expression (Table 4.2). The lack of continuity between the cultures used to investigate gene expression and protein expression is a limitation of this study, because of the inherent heterogeneity between cultures that may cause variations in the results obtained. However, this was unavoidable and future studies will endeavour to maintain cell culture continuity between assays.

Table 4.2. Adipose-derived stromal cell culture general information

Culture name	Culture source	Procurement	Assays in which cultures were used
A280617-01A	Abdominal	Cryopreserved stock	Gene expression
A150817-01A	Abdominal	Cryopreserved stock	Gene expression
A091019-01A	Abdominal	Isolated during the course of this study	Gene and protein expression
A311019-02T	Thigh	Isolated during the course of this study	Protein expression
A270620-01A	Abdominal	Isolated during the course of this study	Protein expression

All ASC samples were immunophenotyped. The methods used in this study involving the isolation, culture and immunophenotype of ASCs have previously been optimised at the ICMM. No other information other than the culture name was made available for the purposes of this study.

4.3.2. Laboratory information

Cell culture laboratory

Cell culture was done in an Esco Class II Laminar flow bio-safety cabinet (AC2-4Si; Thermo Scientific, Waltham, Massachusetts, United States of America (USA)). All cultures were placed in a water jacketed incubator (Thermo Forma 3111TF, Thermo Fisher Scientific, Waltham, Massachusetts, USA).

Flow cytometry laboratory

Flow cytometric analysis was conducted using two different flow cytometers from Beckman Coulter (Brea, California, USA) namely the Gallios and Cytoflex instruments. Ideally, all analyses should be done on the same instrument to ensure consistency in results. However, because the equipment was replaced half-way through the course of this study, two instruments were used. Optimisation and validation of the new instrument was performed for the marker panel used to characterise ASCs at the ICMM by senior researchers at the ICMM, as all studies conducted at the ICMM that

involves ASCs use the same panel and assay. Sample preparation and gating strategies remained the same regardless of the instrument used.

4.3.3. Monoclonal antibodies used during immunophenotyping

Antibodies and conjugated fluorophores along with the fluorescent detector channels, excitation and emissions and suppliers are summarised in Table 4.3.

Table 4.3. Summary of flow cytometry monoclonal antibodies used in this study.
Monoclonal antibodies and fluorochromes were used to identify ASCs based on a specific panel of cell surface marker expression. Antibody particulars have been summarised below.

Monoclonal antibodies	Conjugated fluorochromes	Fluorescent detector channel (FL; laser (nm); band-pass filter; emission range)	Excitation-max/ emission-max (nm)	Supplier
Mouse anti-human CD 36	APC	FL6 (635; 660/10; 655-665)	650/660	Thermo Fisher Scientific (Waltham, Massachusetts, USA)
Mouse anti-human CD 34	PC5	FL5 (488; 690/50; 665-715)	649/666	Beckman Coulter (Brea, California, USA)
Mouse anti-human CD 44	APC Cy7	FL8 (635; 780/60; 750-810)	650/785	BioLegend (San Diego, California, USA)
Mouse anti-human CD 45	KO	FL10 (405; 525/40; 505-545)	398/528	BD Biosciences (Franklin Lakes, New Jersey, USA)
Mouse anti-human CD 73	BV421	FL9 (405; 450/45; 427.5-472.5)	405/421	eBiosciences (San Diego, California, United States)
Mouse anti-human CD 90	FITC	FL1 (488; 525/40; 505-545)	490/525	BD Biosciences (San Jose, California, USA)
Mouse anti-human CD 105	Phycoerythrin (PE)	FL2 (488; 585/42; 564-606)	565/578	Thermo Fisher Scientific (Waltham, Massachusetts, USA)
CD: cluster of differentiation; APC: allophycocyanin; PC5: Phycoerythrin-Cyanin 5; APC Cy7: allophycocyanin cayanin dye -7 tandem conjugate; KO: Krome Orange; FITC: fluorescein Isothiocyanate; BV421: brilliant violet 421; PE: phycoerythrin; USA: United States of America				

4.3.4. Culture medium supplementation

Growth medium for freshly isolated ASCs was comprised of DMEM (Gibco/Invitrogen™; Carlsbad, California, USA), supplemented with 10% volume/volume (v/v) FBS (Gibco/Invitrogen™; Carlsbad, California, USA), 2% v/v penicillin/streptomycin (200 µg/ml, p/s; Gibco/Invitrogen™; Carlsbad, California, USA) and 0.2% v/v amphotericin B (Fungizone; AmB, 0.5 µg/ml; Gibco/Invitrogen™; Carlsbad, California, USA).

4.3.5. Adipose-derived stromal cell Isolation

Lipoaspirates (25 ml) were aliquoted into 50 ml centrifuge tubes (Falcon™; Corning®; Corning, New York, USA) and topped up with PBS (pH 7.4; Gibco/Invitrogen™; Carlsbad, California, USA) supplemented with 2% (v/v) p/s. The samples were centrifuged at 1660 x *g* for 3 minutes (min) after which the supernatant was aspirated. The washed samples were transferred to new 50 ml tubes and the wash steps repeated twice. A 0.1% weight/volume (w/v) collagenase type I solution (Gibco/Invitrogen™; Carlsbad, California, USA) was prepared in PBS and filtered using a 0.22 µm syringe filter (Sartorius; Göttingen, Germany), attached to a 50 ml syringe (Sartorius, Göttingen, Germany). Lipoaspirate samples were incubated at 37^{o}C in a rotating incubator for approximately 45 min. Incubation time was increased when necessary in order to ensure complete digestion of samples. Samples were centrifuged at 738 x *g* for 5 mins and vigorously shaken to disrupt and mix the pellet, to ensure optimal digestion. The aforementioned step was repeated twice, after which the cell suspension was filtered through 70 µm cell strainers (BD Biosciences, San Jose, California, USA) to remove residual undigested tissue. The collagenase was neutralised by adding growth medium and centrifuged (5 min at 300 x g). Cell pellets were again resuspended and the contents transferred to a single 50 ml tube, topped up to 25 ml with PBS (2% p/s), and centrifuged again. Thereafter the supernatant was aspirated and the pellet was re-suspended in Versalyse™ lysing solution (to lyse any contaminating erythrocytes; Beckman Coulter, Brea, California, USA) for 10 mins at room temperature. The samples were washed in PBS (2% p/s) and centrifuged (300 x *g* for 5 min*)* three times. After the last centrifugation step the supernatant was

aspirated and the pellet resuspended in growth medium. The cells were filtered through a 70 µm cell strainer again to remove any remaining tissue debris. An aliquot of 100 µl SVF was taken for further analysis on the flow cytometer (see 4.3.7. for method and analysis strategy). The SVF was seeded at 50 000 cells/cm^2 in T75 cm^2 flasks (NUNC^{TM}, Roskilde site, Kamstrupvej, Denmark) and incubated for 72 hours at 37ºC/5% CO_2. Thereafter, the cells were washed to remove non-adherent cells by aspirating growth medium, adding 7 ml PBS (2% p/s), swirling the flask gently, aspirating the PBS and then supplementing the culture flask with 7 ml growth medium. The isolation procedure is summarised in Figure 4.3.

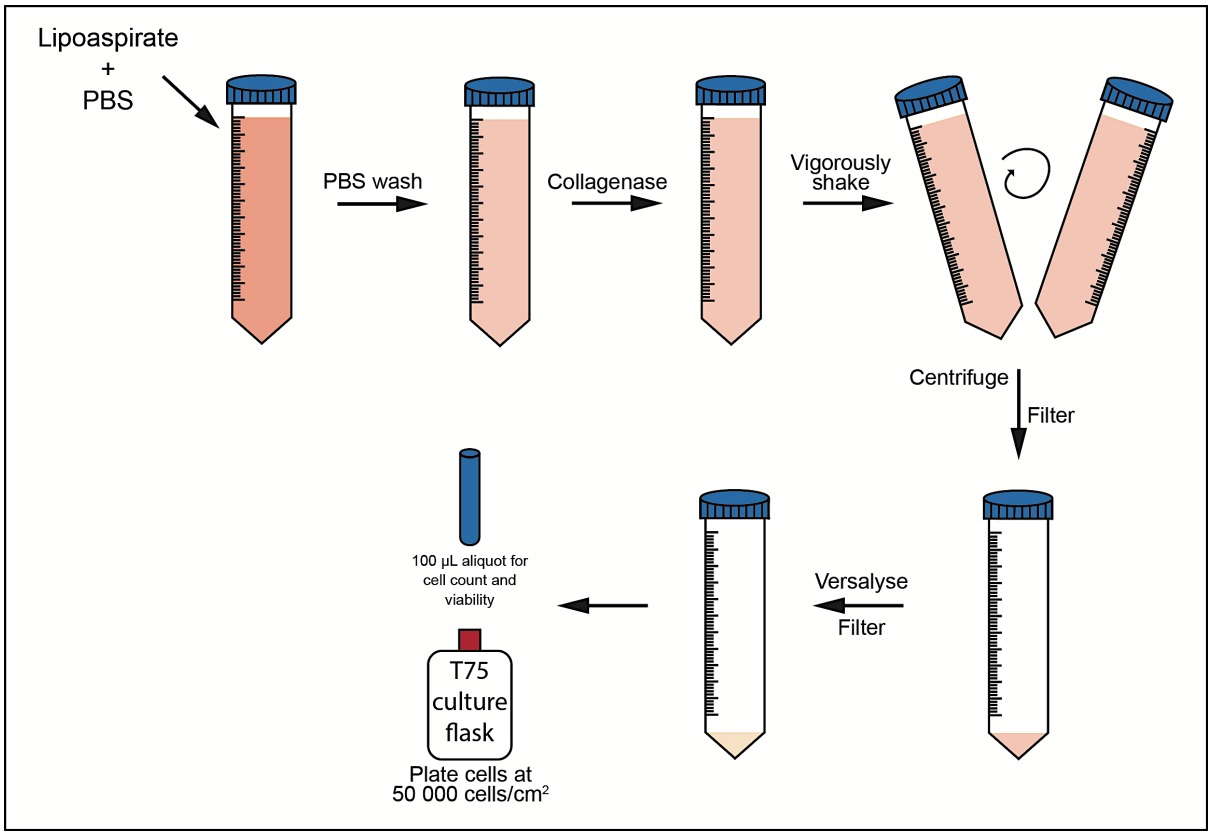

Figure 4.3. Adipose-derived stromal cell isolation.
Lipoaspirates were aliquoted and washed in phosphate buffered solution after which the tissue was digested in collagenase. Following a series of wash, centrifugation and filter steps, the cells were centrifuged to obtain a pellet known as the stromal vascular fraction (SVF). Adipose-derived stromal cells are contained within the pellet, which is then analysed and counted on a flow cytometer and plated for further expansion.

4.3.6. Passaging, maintenance and cryopreservation

Cells were maintained in an incubator at 37°C and 5% CO_2. At 80-90% confluence, ASCs were passaged. Cells expanded in a T75 culture flask were washed with 7 ml pre-warmed PBS (2% p/s). After aspirating the PBS, trypsin (0.25%; 4 ml; Gibco/Invitrogen™, Carlsbad, California, USA) was added to the culture flasks and incubated for 7 min at 37°C/5% CO_2. Thereafter the trypsin was inactivated by the addition of 4 ml growth medium. The cell suspension was transferred to a 50 ml centrifuge tube and centrifuged at 300 x *g* for 5 min, and the supernatant was aspirated. The pellet was then resuspended in 1 ml growth medium. A 100 µl aliquot of the cell suspension was used to count cells on the flow cytometer. Thereafter, cells were seeded at 5000 cells/cm^2 in T75 flasks in 7 ml growth medium for further propagation. Growth medium was replaced bi-weekly.

After passaging, excess cells were cryopreserved at 1 000 000 cells/cryovial in 1 ml cryopreservation medium (90% growth medium and 10% dimethyl sulfoxide (DMSO; Sigma Aldrich Chemie, St Louis, Missouri, USA). Cryovials (Greiner, Bio-One GmbH, Frickenhausen, Germany) were placed in a NALGENE® Mr Frosty™ Cryo 1°C freezing container (Thermo Fisher Scientific, Waltham, Massachusetts, USA) which allowed the cells to cool at 1°C per minute. The container was placed in a -80°C freezer and transferred to liquid nitrogen for long term storage once frozen.

4.3.7. Flow cytometry data acquisition and analysis

Samples were analysed on the Gallios flow cytometer using accompanying Kaluza acquisition software (version 2.1, Beckman Coulter, Beckman Coulter, Brea, California, USA). Data from samples analysed on the Cytoflex flow cytometer was acquired using the CytExpert acquisition and analysis software (version 2.4, Beckman Coulter, Brea, California, USA). All post-acquisition data analysis was done on Kaluza Flow Cytometry Analysis Software (version 2.2, Beckman Coulter, Brea, California, USA). Gating strategies and controls (positive, negative etc) have been summarised in the sections that follow.

4.3.7.1. Cell counts after adipose-derived stromal cell isolation

An aliquot of the SVF suspension (100 µl) was transferred to a flow tube (Beckman Coulter, Brea, California, USA) along with an equal volume of Flow-Count™ fluorospheres (to estimate cell number per µl; Beckman Coulter, Brea, California, USA), 2 µl Vibrant® DyeCycle™ Ruby (to identify nucleated cells in the SVF; VDC; Beckman Coulter, Brea, California, USA) and PBS. Flow-Count™ fluorospheres are multispectral and are therefore detectable in multiple fluorescence channels (FL) including FL1, FL2, FL3 and FL4. In order to visualise Flow-Count™ Fluorospheres, a one-parameter event count versus FL3 histogram (Excitation: 488nm; Emission: 620/30 band-pass (BP)) plot was generated, and visualised using region 'Beads_a' (Figure 4.4A). Additionally, a second two-parameter dot plot (SS versus FL3) was generated and beads were identified as 'Beads_b' (Figure 4.4B). To identify intact counting beads (region 'CAL'), another one-parameter plot measuring FS versus time was gated on region 'Beads_b' (Figure 4.4C). VDC Ruby identified nucleated cells within the SVF and was identified as region 'Nucleated ASCs' on a two-parameter side scatter versus FL7 plot (Figure 4.4D). Flow-Count™ fluorospheres were illustrated as the blue cell population to the far left of the SVF population. Non-nucleated cells were visualised to the immediate left of region 'Nucleated ASCs' while cell clumps were visible to the right.

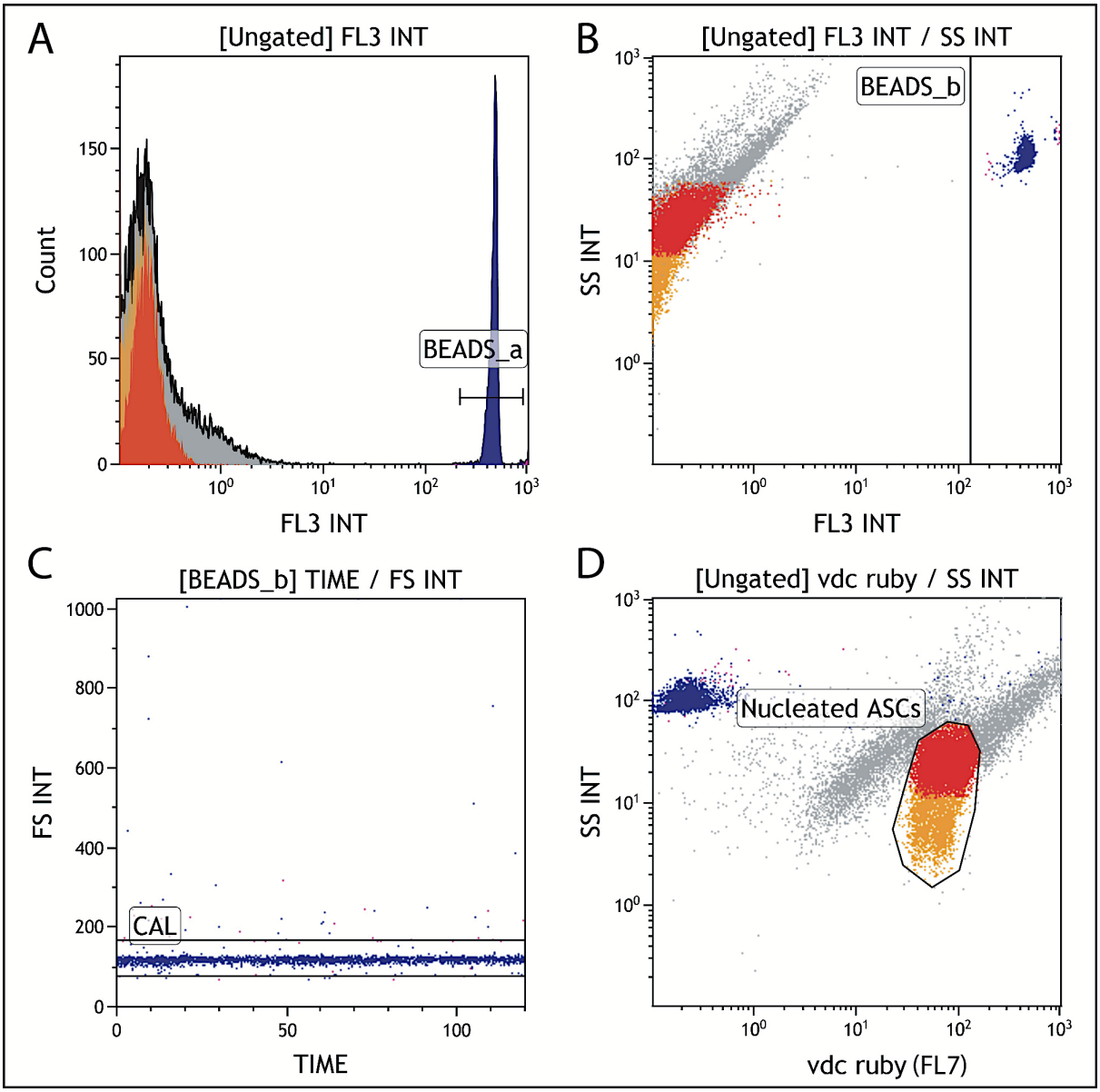

Figure 4.4. Representative images demonstrating the gating strategy used to identify and enumerate nucleated cells within the stromal vascular fraction.
A. Event count versus FL3 identified Flow-Count™ Fluorospheres (region 'Beads_a'). B. Side scatter versus FL3 separated counting beads (region 'Beads_b') from the stromal vascular fraction. C: Forward scatter versus time plot (gated to 'Beads_b') identified intact counting beads (region 'CAL'). D. Nucleated cells (region 'Nucleated ASCs') were identified by a two-parameter side scatter versus FL7 plot.

After absolute cell counts (Figure 4.5, Equation 4.1) and the total number of harvested cells (Figure 4.5, Equation 4.2) had been calculated following flow cytometric analysis, cells were seeded at 5000 cells/cm^2.

Equation 4.1:	Absolute cell count (cells/µl)	=	$\frac{\text{Number of events in region of interest (cells)}}{\text{Number of bead events (beads/µl)}} \times \text{Cal factor}$
Equation 4.2:	Total number of cells harvested	=	Absolute cell count (cells/µl) x Total volume of cell suspension (µl)

Figure 4.5. General equations used to determine cell counts.
Equation 4.1 was used to determine absolute cell count per microliter (cells/µl), while Equation 4.2 was used to determine the total number of cells harvested. Cal factor refers to the number of counting beads/µl obtainable from the Flow-Count™ Fluorospheres product insert. Absolute cell count and total number of cells harvested values were used to determine the number of cells to be seeded for experiments, and the number of cells to be cryopreserved.

4.3.7.2. General cell count regions and gating strategies for passaged cells

Flow-Count™ Fluorospheres were measured on a one-parameter event count versus FL3 plot, and visualised using region 'BEADS' (Figure 4.6A). A forward scatter versus time plot gated to 'BEADS' visualised intact counting beads in region 'CAL' (Figure 4.6B). A Boolean gating strategy ([excl. beads]) was used on a two-parameter, forward scatter (Lin) versus side scatter (Log) plot, to exclude beads from region 'ASCs' in order to enumerate ASCs only (Figure 4.6C). The same strategy was used to enumerate all cell types used in this study (Details pertaining to specific cell types have been discussed in Chapter 5) and cells were enumerated using equations 4.1 and 4.2 (Figure 4.5).

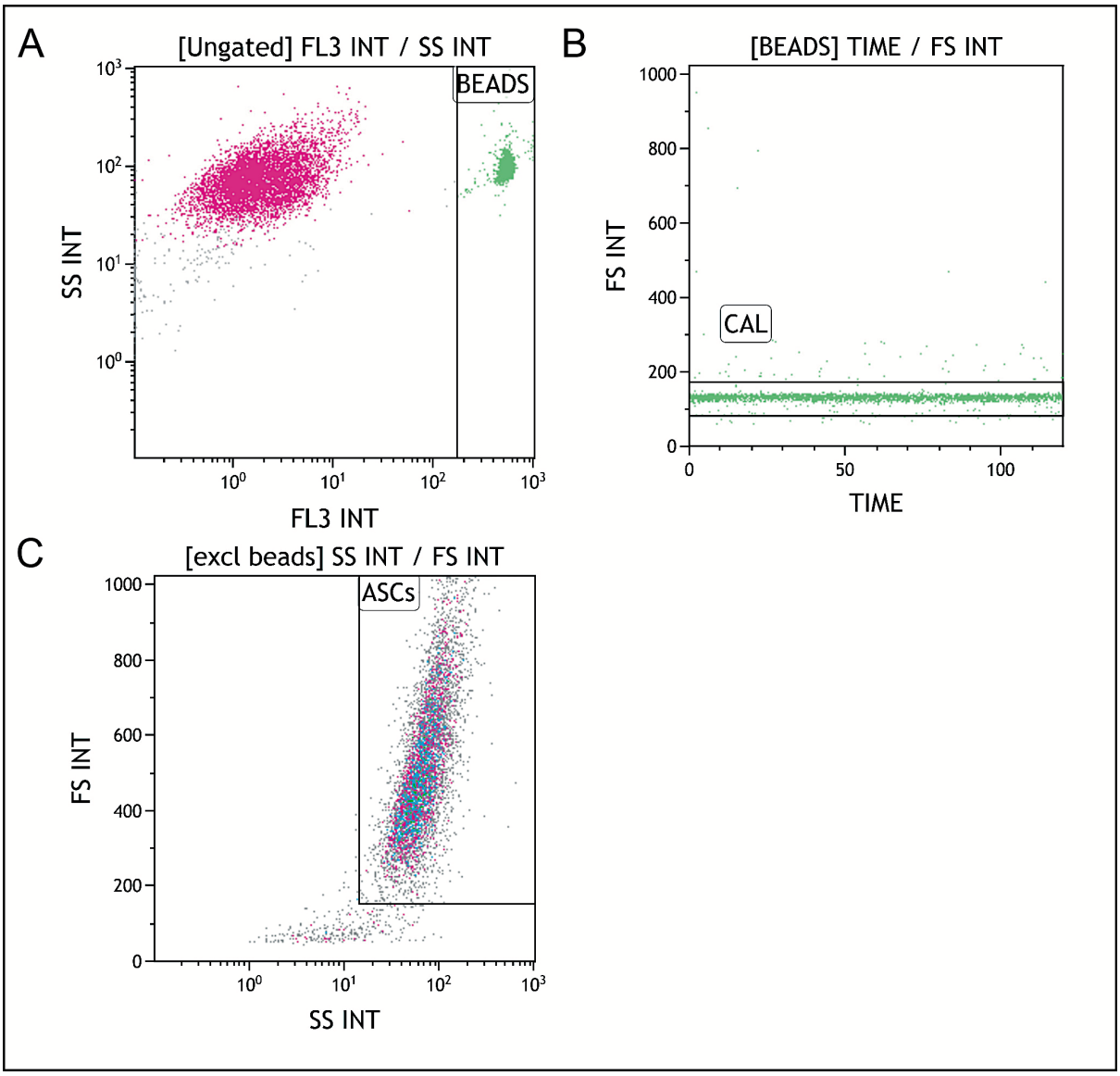

Figure 4.6. Representative images of the gating strategy used to enumerate cells. A. Side scatter versus FL3 measured Flow-Count™ Fluorospheres (region 'BEADS'). B. A one-parameter forward scatter versus time plot visualised intact counting beads as region 'CAL'. C. Forward scatter versus side scatter visualised adipose-derived stromal cells (region 'ASCs').

4.3.7.3. Cell viability

Before ASCs were immunophenotyped, cell viability was determined using 7-AAD. Cell viability was measured to ensure that the cells were not damaged during the isolation process. During apoptosis, cell membrane integrity becomes compromised allowing 7-AAD entry into the nucleus where it binds to DNA.[200] An aliquot of the cell

suspension (100 µl) was transferred to a flow tube, followed by the addition of 5 µl 7- AAD. The flow tube was incubated in the dark for 10 min at room temperature. A two-parameter forward scatter (Lin) versus side scatter (Log) plot was generated and ASCs were identified as region 'ASCs' (Figure 4.7A). In order to determine cell viability, a side scatter versus FL4 plot was generated and gated on 'ASCs', where viable cells were indicated to the left, whilst cells on the right of the gated boundary indicated non-viable cells that were positive for 7-AAD (Figure 4.7B). Cells were considered viable if the measured viability was more than 90%, and used for further experimentation.

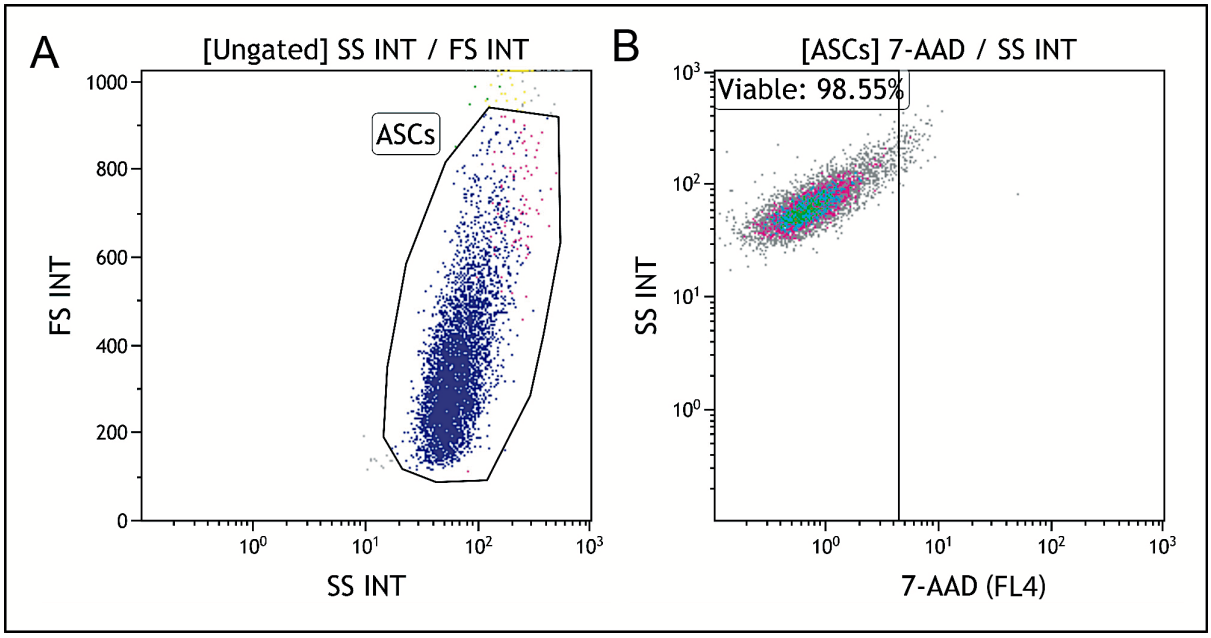

Figure 4.7. Representative image demonstrating the gating strategy used to determine cell viability.
A. Region 'ASCs' identified ASCs on a forward scatter versus side scatter plot. B. Side scatter versus FL4 plot gated on 'ASCs' indicated viable cells.

4.3.7.4. Immunophenotype of adipose derived stromal cells

Phenotypic characterisation is a prerequisite for ASCs used in experimental studies.[69] ASCs were immunophenotyped according to a panel of seven markers ($CD44^{+}CD73^{+}CD90^{+}CD105^{+}$ $CD36^{+}CD34^{variable}CD45^{-}$). Monoclonal antibodies, their conjugated fluorochromes, excitation and emission values and the FL-channels used have been captured in Table 4.3. All ASC samples were immunophenotyped at passage two, with the exception of sample A270620-01A which was

immunophenotyped at passage one. Fluorescence spill over between channels is a common occurrence when using multicolour panels. To correct for this phenomenon, compensation was used to mathematically eliminate spectral overlap between different fluorochromes.[201] In order to calculate compensation and determine immunophenotype, 100 µl aliquots of the cell suspension were independently stained with 5 µl of each antibody. A combination tube of 100 µL of the cell suspension was stained with 5 µl of each antibody to evaluate and adjust the compensation. An unstained control tube with 100 µl cell suspension was included, along with an isotypic control for CD34. All tubes were incubated in the dark for 20 min at room temperature before washing excess antibody from the cells. Thereafter, cells were washed in 500 µl PBS and centrifuged for 5 min x 300 *g* three times. After the final centrifugation, excess PBS was aspirated and the cells were resuspended in 300 µl PBS for analysis on the flow cytometer.

To identify the ASC population (representative region 'A270620'), a two-parameter forward scatter (Lin) versus side scatter (Log) plot was generated. Next, a series of two-parameter plots with four-quadrant regions (all gated to the representative ASC population 'A270620') were generated (Figure 4.8A – 20I).

The four-quadrant regions were set to the unstained samples, where regions 'eg. A- /- ' contained the unstained cell population in red (Figures 4.8B to 4.8E). The stained populations in pink (Figures 4.8F to 4.8I) were visualised in all four regions corresponding to the expression of relative markers (eg. A-/-, A-/+, A+/+ and A+/-). To identify whether ASCs expressed CD90 and CD44, a FL1 (CD90) versus FL8 (CD44) plot was created (Figure 4.8F). CD105 and CD73 were identified by plot FL2 (CD105) versus FL9 (CD73; Figure 4.8G). A FL5 (CD34) versus FL10 (CD45) plot visualised the expression of CD105 an CD45 (Figure 4.8H). CD36 was identified by a FL1 (CD90) versus FL6 (CD36) plot (Figure 4.8I).

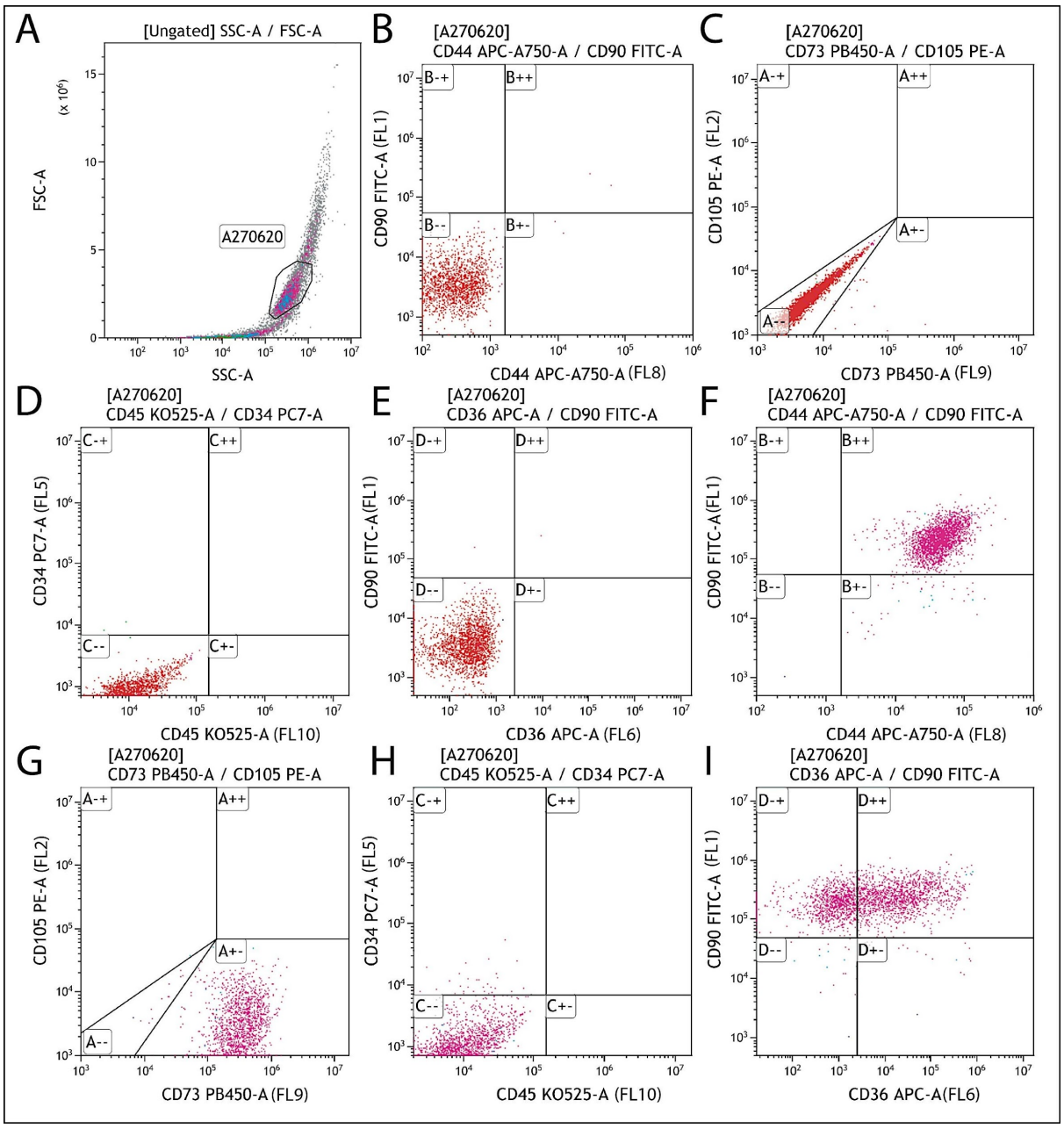

Figure 4.8. Representative schematic of the gating strategies used to immunophenotype adipose-derived stromal cells.
A. Region 'A270620' identified ASCs on a forward scatter (Lin) versus side scatter (Log) plot. Two-parameter plots, all gated on ASC region 'A270620', were subsequently created for analysis. Unstained cells in red were visualised on images B-E in regions '-/-', whilst expression of stained samples (pink) can be viewed on images F-I.

For samples analysed on the Gallios, compensation was automatically calculated using Kaluza Flow Cytometry Analysis Software. Compensation for samples analysed on the Cytoflex was calculated automatically using the CytExpert acquisition and

analysis software. To measure the percentage expression of individual surface markers, single-parameter histogram plots (event count versus FL-channel of target antigen) were created (Figure 4.9). FL-channels of each monoclonal antibody and conjugated fluorochrome are summarised in Table 4.3. Regions were set on the unstained control sample in red to ensure that the region boundaries accurately depicted whether the stained samples were positive for their respective immunophenotypic markers or not Figure 4.9A – 4.9G). The shift in expression between the unstained and stained sample in pink (Figure 4.9H – 4.9N) was measured as a percentage (Figure 4.9).

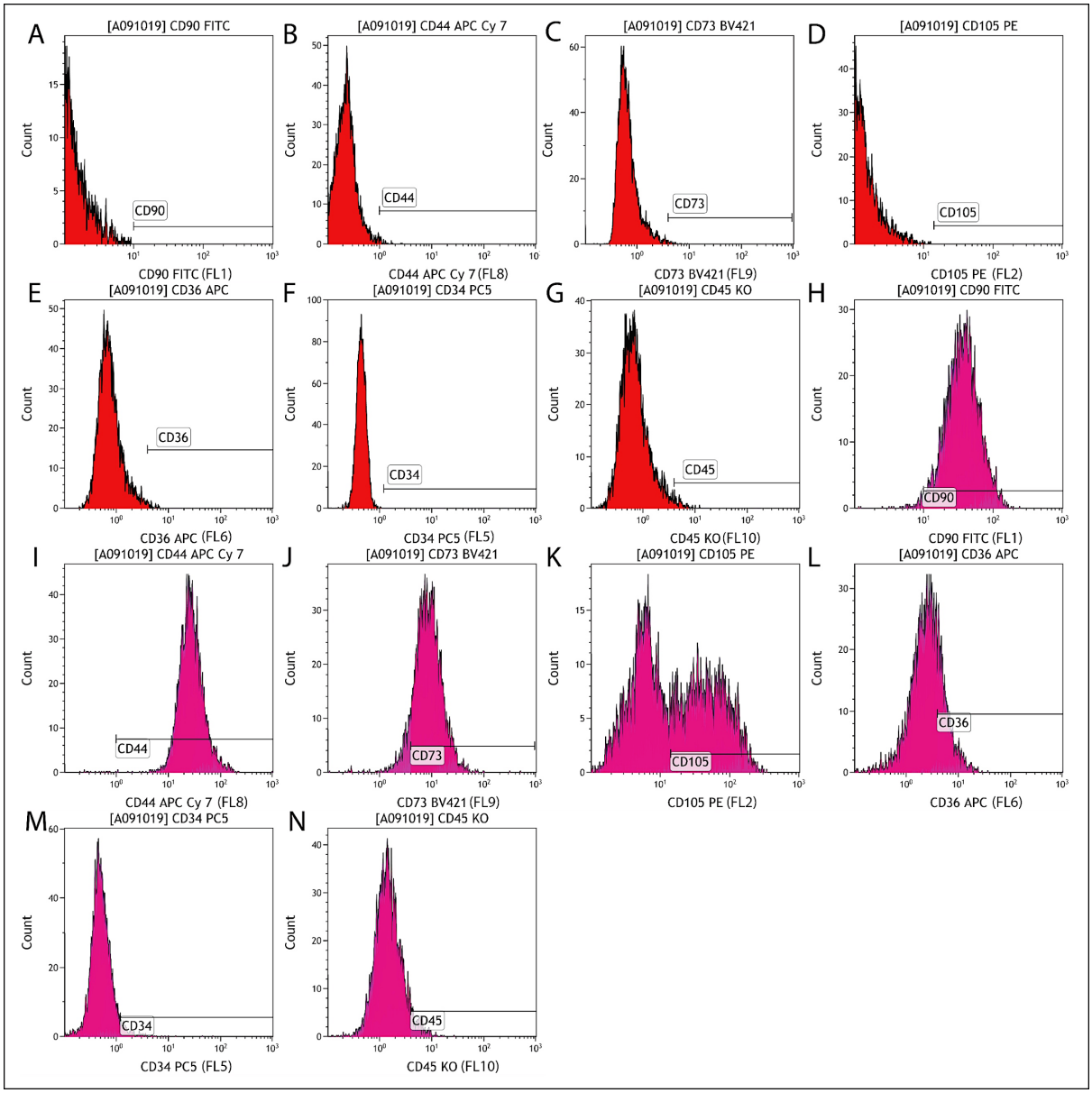

Figure 4.9. Representative illustration of single-parameter plots used to quantify the expression of individual surface antigens.
Event count versus FL-channel was used to measure the expression of markers in the gated ASC population ('A091019'). This strategy was used for all defining surface markers. Cluster of differentiation (CD) 90 was visualised on plots A and H, CD 44 (B and M), CD73 (C and N), CD105 (D and K), CD 36 (E and L), CD34 (F and M) and CD 45 on G and N. Plots A to G illustrate the unstained cells, while plots H to N demonstrate the shift in expression on the stained cells.

Co-expression was determined by generating a tree-plot (Figure 4.10), classifying events into different populations based on gating information and by taking into consideration the data of single-parameter plots.

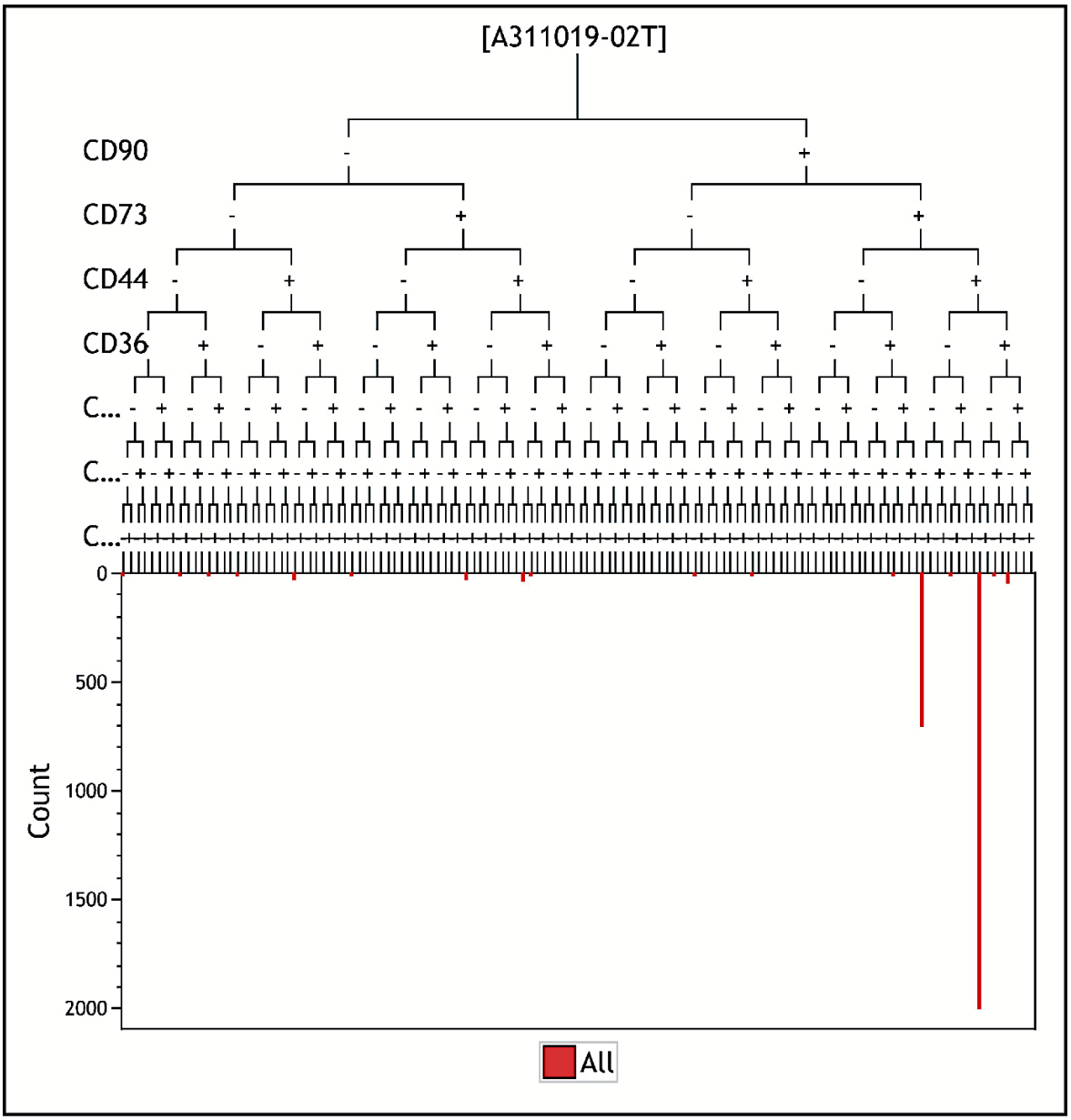

Figure 4.10. Representative illustration of a tree-plot used to determine the co-expression profile of adipose-derived stromal cells.
Branches of the tree illustrate the presence of different co-expression profile permutations.

4.4. Statistical considerations

The number of harvested cells in the SVF was represented as a median with a minimum and maximum range. Means were represented ± the standard deviation.

4.5. Results

Cell number was determined by flow cytometry using Flow-Count™ Fluorospheres (Figure 4.6) and calculated using Equations 4.1 and 4.2 (Figure 4.5). The number of nucleated cells in the SVF varied (Table 4.4). The median number of cells obtained after isolation was 18.4 x 10^7 (range: 60.7 x. 10^6 – 53.2 x 10^7).

Table 4.4. Number of nucleated cells isolated from ASC cultures.
The number of cells harvested was determined by flow cytometry.

Culture name	Number of cells harvested
A280617-01A	53.2 x 10^7
A150817-01A	18.3 x 10^7
A091019-01A	60.7 x 10^6
A311019-02T	22.4 x 10^7
A270620-01A	87.6 x 10^6

Cell viability was determined prior to immunophenotyping ASCs. Average cell viability was 97.85% ± 2.29. ASCs were immunophenotyped by flow cytometry and the expression of individual surface antigens was determined using single-parameter plots (Figure 4.9). CD90 was expressed on 93.29% ± 8.10 of ASCs, CD44 (99.78% ± 0.25) and CD73 (97.07% ± 3.24) was expressed on ASCs. CD105 was present on 11.69% ± 21.13 of cells, CD36 on 64.85% ± 38.08, CD34 on 3.27% ± 2.25 and CD45 on 0.17 ± 0.26 (Figure 4.11).

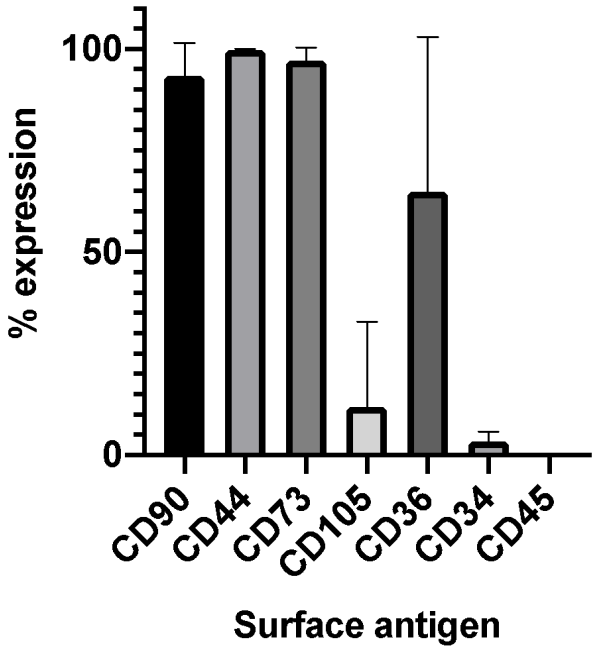

Figure 4.11. Expression of surface antigens on adipose-derived stromal cell cultures. The graph represents the average expression of individual surface antigens (n=5) as a percentage. The standard deviation is represented by error bars.

The co-expression profiles of ASC biological replicates were determined by flow cytometry. Tree plots (Figure 4.10) were generated to identify various co-expression profile permutations. The ASC phenotype was heterogeneous within and between cultures (Figure 4.12A); therefore, ASC populations were identified and recorded if the phenotype was present in more than 1% of the total population. Nine main populations were identified in culture A091019-01A (Figure 4.12B). Within this culture, the two most prominent phenotypes were $CD90^{+}CD73^{+}CD44^{+}CD36^{-}CD34^{-}CD105^{-}CD45^{-}$ (35%) and one similar in expression but positive for CD105 (30%). A150817-01A (Figure 4.12C), was defined by five main populations. In this culture, the most abundant phenotype was $CD90^{+}CD73^{+}CD44^{+}CD36^{+}CD34^{-}CD105^{-}CD45^{-}$ and was expressed on 69% of cells. The dominant phenotype (expressed on 65% of cells) in culture A270620-01A was $CD90^{+}CD73^{+}CD44^{+}CD36^{+}CD34^{-}CD105^{-}CD45^{-}$ (Figure 4.12D). Of the twelve phenotypes in culture A280617-01A (Figure 4.12E), two principal populations were identified as $CD90^{+}CD73^{+}CD44^{+}CD36^{+}CD34^{-}CD105^{-}CD45^{-}$ (33%) and another population, with a similar phenotype, but positive for CD105

(31%). In culture A311019-02T (Figure 4.12F), the foremost phenotype was $CD90^{+}CD73^{+}CD44^{+}CD36^{+}CD34^{-}CD105^{-}CD45^{-}$ (70%).

The most dominant phenotypic profiles within the ASC populations were all positive for CD90, CD44, CD73 and negative for CD45 ($CD90^{+}CD44^{+}CD73^{+}CD45^{-}$). The differences in the co-expression profiles of the most prevalent populations were observed in the markers CD36, CD34 and CD105. These populations were $CD36^{+}CD34^{-}CD105^{-}$ (expressed on 49.02% ± 27.28 of all cells), $CD36^{-}CD34^{-}CD105^{-}$ (19.42% ± 15.07) and $CD36^{+}CD34^{-}CD105^{+}$ (9.83 ± 12.84), $CD36^{+}CD34^{+}CD105^{-}$ (1.81% ± 0.99) and $CD36^{+}CD34^{-}CD105^{-}$ (1.04% ± 0.97) (Figure 4.12G).

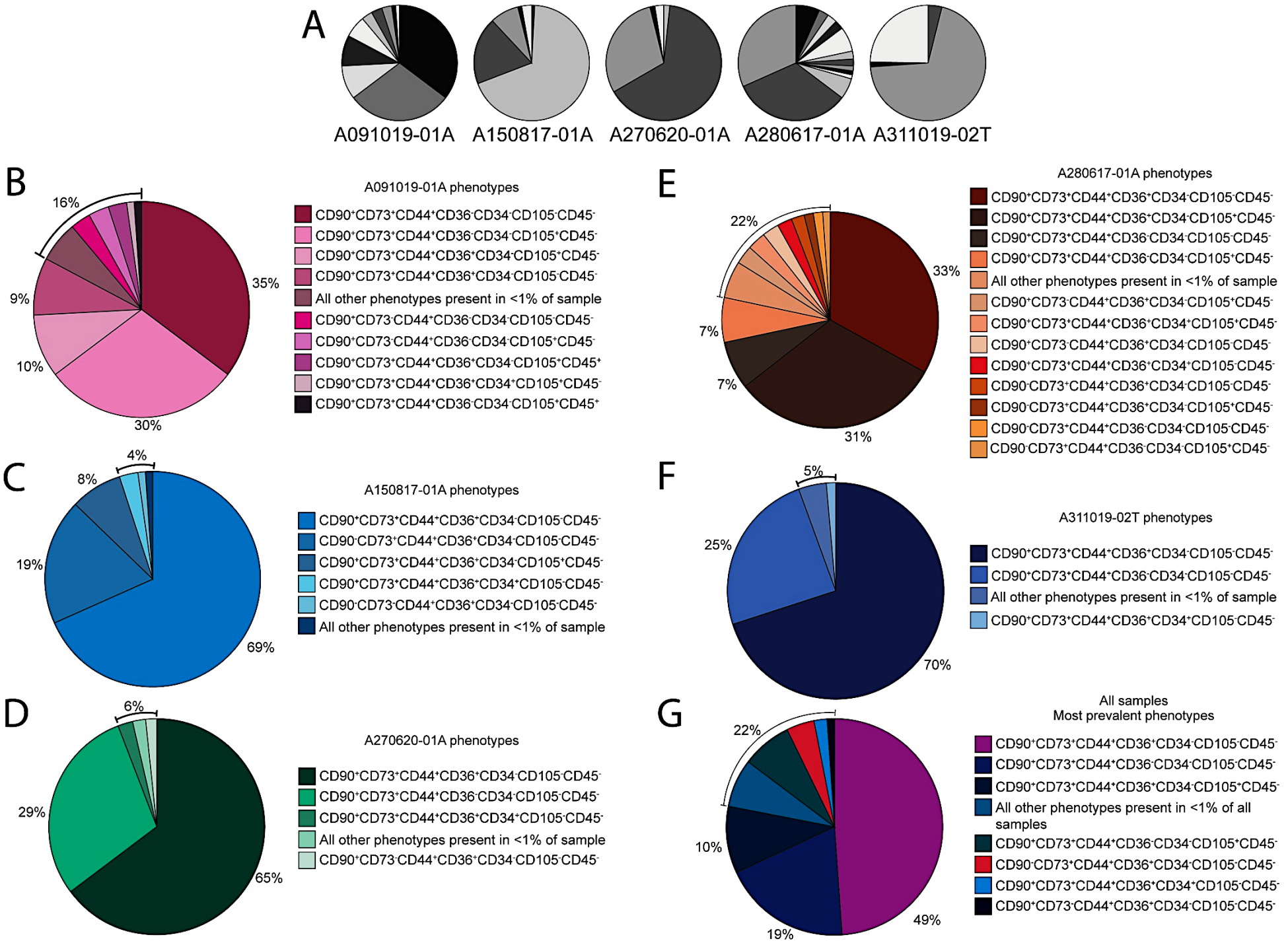
A
A091019-01A
A150817-01A
A270620-01A
A280617-01A
A311019-02T
B
16%
35%
9%
10%
30%
A091019-01A phenotypes
CD90+CD73+CD44+CD36-CD34-CD105-CD45-
CD90+CD73+CD44+CD36-CD34-CD105+CD45-
CD90+CD73+CD44+CD36+CD34-CD105+CD45-
CD90+CD73+CD44+CD36+CD34-CD105-CD45-
All other phenotypes present in <1% of sample
CD90+CD73-CD44+CD36-CD34-CD105-CD45-
CD90+CD73-CD44+CD36-CD34-CD105+CD45-
CD90+CD73+CD44+CD36+CD34-CD105+CD45+
CD90+CD73+CD44+CD36+CD34+CD105+CD45-
CD90+CD73+CD44+CD36-CD34-CD105+CD45+
C
4%
8%
19%
69%
A150817-01A phenotypes
CD90+CD73+CD44+CD36+CD34-CD105-CD45-
CD90-CD73+CD44+CD36+CD34-CD105-CD45-
CD90+CD73+CD44+CD36+CD34-CD105+CD45-
CD90+CD73+CD44+CD36+CD34+CD105-CD45-
CD90-CD73-CD44+CD36+CD34-CD105-CD45-
All other phenotypes present in <1% of sample
D
6%
29%
65%
A270620-01A phenotypes
CD90+CD73+CD44+CD36+CD34-CD105-CD45-
CD90+CD73+CD44+CD36-CD34-CD105-CD45-
CD90+CD73+CD44+CD36+CD34+CD105-CD45-
All other phenotypes present in <1% of sample
CD90+CD73-CD44+CD36+CD34-CD105-CD45-
E
22%
33%
7%
7%
31%
A280617-01A phenotypes
CD90+CD73+CD44+CD36+CD34-CD105-CD45-
CD90+CD73+CD44+CD36+CD34-CD105+CD45-
CD90+CD73+CD44+CD36-CD34-CD105-CD45-
CD90+CD73+CD44+CD36-CD34-CD105+CD45-
All other phenotypes present in <1% of sample
CD90+CD73-CD44+CD36+CD34-CD105+CD45-
CD90+CD73+CD44+CD36+CD34+CD105+CD45-
CD90+CD73-CD44+CD36+CD34-CD105-CD45-
CD90+CD73+CD44+CD36+CD34+CD105-CD45-
CD90-CD73+CD44+CD36+CD34-CD105-CD45-
CD90-CD73+CD44+CD36+CD34-CD105+CD45-
CD90-CD73+CD44+CD36-CD34-CD105-CD45-
CD90-CD73+CD44+CD36-CD34-CD105+CD45-
F
5%
25%
70%
A311019-02T phenotypes
CD90+CD73+CD44+CD36+CD34-CD105-CD45-
CD90+CD73+CD44+CD36-CD34-CD105-CD45-
All other phenotypes present in <1% of sample
CD90+CD73+CD44+CD36+CD34+CD105-CD45-
G
22%
10%
19%
49%
All samples
Most prevalent phenotypes
CD90+CD73+CD44+CD36+CD34-CD105-CD45-
CD90+CD73+CD44+CD36-CD34-CD105-CD45-
CD90+CD73+CD44+CD36+CD34-CD105+CD45-
All other phenotypes present in <1% of all samples
CD90+CD73+CD44+CD36-CD34-CD105+CD45-
CD90-CD73+CD44+CD36+CD34-CD105-CD45-
CD90+CD73+CD44+CD36+CD34+CD105-CD45-
CD90+CD73-CD44+CD36+CD34-CD105-CD45-

Figure 4.12. Pie graph illustrating phenotype heterogeneity within and between adipose-derived stromal cell cultures.
Main ASC phenotypes were labelled individually, while those present on less than 1% of cells were grouped. Relative expression of each phenotype was illustrated as slices in the pie graph and quantified as a percentage. A. Side-by-side visual comparison of phenotypic heterogeneity within each culture, where each pie slice represents a particular phenotype. Nine populations were identified in culture A091019 (B), five in A150817 (C), four in A270620-01A (D), twelve in A280617 (E) and three in A311019 (F). G. The most prominent populations within all cultures are shown, and the average expression was represented on a pie graph, with each phenotype illustrated to the right of the graph.

4.6. Discussion and conclusion

ASCs were immunophenotyped according to the ICMM's panel based on the recommendation by Bourin *et al.* (2013).[2] The ASCs used in this study were highly variable with respect to their immunophenotype and this was evident in large SDs for the data pertaining to CD36 (where CD36 expression was evident on 64.85% ± 38.08 of cells) and CD105 (11.69% ± 21.13). A large SD was also observed in the co-expression profile of the phenotype that was $CD36^{+}CD34^{-}CD105^{+}$ (9.83 ± 12.84). The SD is a measure that indicates the spread of a dataset around its mean. Because the data generated from the samples in this study was limited (n=5 ASC cultures were isolated and characterised in total) and highly variable with respect to immunophenotype expression, it was possible to generate SDs that were larger than the mean. The expression of CD90, CD44 and CD73 was observed in more than 80% of ASCs and CD45 on less than 2%. The exception was CD105, which was variably expressed on 11.69% ± 21.13 of cells. Although CD105 is a preferable marker in the ASC phenotype (should ideally be expressed on more than 80%), it has been noted that its expression is variable.[69,202] In the publication by Bourin and colleagues[2], it was also suggested that CD13 (aminopeptidase N, an ectopeptidase) may be better suited for ASC immunophenotyping due to its higher and more stable expression.[2] The dominant ASC phenotype in this study, which was $CD105^{-}$, is contrary to ASC phenotypes observed in previous studies done at the ICMM using the same isolation procedures. Van Vollenstee *et al.* (2016)[177], Dessels *et al.* (2018)[164] and Durandt *et al.* (2019)[203] all reported ASCs that were consistently $CD105^{+}$ across various culture conditions. To overcome the statistical variability, the sample number should be increased as a future consideration.

During the course of this study, the laboratory experienced persistent fungal contamination. In order to treat it and prevent a resurgence, the polyene AmB (an amphipathic macrolide) was added to the culture medium.[204] Skubis *et al*. (2017)[205] found that treating ASCs with AmB resulted in the downregulation of CD105 and CD73 mRNA. The reason for this remains unclear in the literature as the study done by

Skubis and colleagues is the only one of its kind. This finding may explain the lack of CD105 expression observed in this study. In the present study the expression of CD36 and CD34 was highly variable within and between cultures. In the study by Dessels *et al*. (2018)[164] the ASC phenotype was compared between cultures expanded in FBS and pHPL. The ASC immunophenotype was found to be similar, with the exception of CD34 and CD36 expression. In cultures expanded in FBS, 69.5% of ASCs were $CD34^{-}CD36^{-}$, whilst 50% of those expanded in pHPL were $CD34^{+}CD36^{+}$. In the present study, ASCs were expanded in pHPL and 48.7% ± 30.64 of cells were found to be $CD34^{-}CD36^{-}$, 4.73% ± 5.52 were $CD34^{+}CD36^{+}$ and 46.89% ± 28,54 were $CD34^{-}CD36^{+}$. With respect to the co-expression of CD34 and CD36, the results were similar to those reported by Dessels *et al*. (2018)[164]. The variability in these two markers was also observed by Durandt *et al*. (2019)[203] across multiple passages.

The immunophenotype results indicated that the ASCs used for this study were heterogeneous both within cultures and between cultures with respect to phenotype. This observation was not unexpected, as ASCs are well known to be biologically variable and heterogeneous (discussed in Chapter 2.4). Culture conditions, particularly the addition of the anti-fungal agent AmB, may have contributed to the low expression of the marker CD105. Future studies that endeavour to identify whether this was in fact the cause and the mechanisms through which it may have occurred might be beneficial for future applications, as contamination (although rare if proper aseptic techniques are used) does happen in cell culture. Future studies should also explore non-enzymatic isolation methods more thoroughly in order to adhere to GMP guidelines to further expand on the ability of ASCs to be used therapeutically.

ASCs were thus defined according to the ICMM immunophenotype, with the exception of the expression of CD105, which was variable. However, based on the publication by Bourin *et al.* (2013)[2] it was still acceptable to characterise ASCs as either $CD105^{+}$ or $CD105^{-}$. It may be prudent then to reconsider the immunophenotype investigated

at the ICMM, with respect to CD105, by either adding CD13 as an additional supporting marker or by substituting CD105 with CD13 entirely.

This concludes Chapter 4. The following Chapter 5 contains all the relevant work pertaining to ASC myogenesis.

Chapter 5: Adipose-derived stromal cell myogenic differentiation

This chapter includes all the information pertaining to ASC myogenic induction and concludes with a brief discussion of the findings. The findings contained in this Chapter are further elaborated in the concluding discussion, Chapter 6.

5.1. Introduction

Adipose-derived stromal cell myogenesis has been reported in multiple studies (see Chapter 2, Table 2.4). This process was first described by Zuk *et al*. (2001)[130]. As mentioned in Chapter 2, differentiating ASCs into myocytes is applicable in the field of muscle regeneration and repair. ASCs may be used for wound healing and immunomodulation at sites of tissue damage by differentiating ASCs into muscle cells to facilitate direct replacement of damaged cells, and may be used in combination with bio-scaffolds for muscle regeneration.[120]

Adipose-derived stromal cell myogenesis

ASC myogenesis has successfully been demonstrated *in vitro* using induction medium containing dexamethasone (0.1 µM) and hydrocortisone (50 µM; DH), or 10 µM 5-Aza. 5-Aza has been the favoured method in recent publications, while the former has been used in older publications (see Chapter 2, Table 2.4). The 5-Aza method differs from the one involving DH in three distinct ways. First, the original induction medium described by Zuk and colleagues is made up of DMEM and both FBS and HrS. Secondly, ASCs are both induced and thereafter maintained in the same induction medium.[120,136] The method involving 5-Aza requires cells to be treated with 10 µM 5-Aza in DMEM supplemented with HrS for 24 hr, after which the medium is replaced and the cells maintained in a second medium that is comprised of low glucose DMEM,

FBS, b-FGF and an antimycotic/antimicrobial agent.[159] Thirdly, ASCs induced using DH have been differentiated over 42 days, whilst those induced using 5-Aza have been investigated over a period of 21 days.[120,136,159]

As described in Chapter 2, glucocorticoids stimulate myogenic differentiation by increasing expression of MyoD, MyoG and dysferlin.[149] 5-Aza advances myogenesis by upregulating key myogenic factors such as MyoD and Myf 5 through promoting cell cycle arrest to facilitate the transition between cellular proliferation and fusion, and by demethylating myogenic promoters.[155,156] The main myogenic regulators include Pax 3/7, desmin, MyoD and MyoG. Pax 3/7 are upstream regulatory transcription factors that bind to MyoD promotor regions (along with Six 1/4) to activate its transcription. MyoD in turn enables the transcription of desmin (a sarcomeric structural protein) and MyoG (initiates cellular fusion into myotubes).[87,92,98,107] The first myogenic marker detectable *in vitro* is desmin, followed by Pax 3/7, MyoD and lastly MyoG.[105]

Both of the above-mentioned methods (with the two myogenic differentiation media) were investigated in this study in order to optimise the protocol for ASC myogenesis to be used further in our laboratory.

Investigation of relative myogenic gene expression and kinetics

Relative myogenic gene expression and expression kinetics were investigated with RT-qPCR. This technique has been utilised to investigate ASC myogenesis by other researchers including Gang *et al.* (2004)[136] and Drost *et al.* (2009)[135] (Chapter 2, Table 2.4). The main targets for RT-qPCR in these studies included MyoD, MyoG and MHC.

PCR is a process through which any nucleotide sequence can be amplified into a large number of identical copies. During PCR, a heat-stable polymerase uses single stranded DNA as a template to amplify targeted regions of DNA primed by short

oligonucleotides (primers) in a magnesium-chloride buffer containing deoxynucleoside triphosphates (dNTP).[206] The polymerisation reaction is then iterated by thermal cycling, where an initial high temperature is applied to separate or 'melt' strands of a double helix where after the temperature is lowered to allow primers to anneal to template strands. The heat stable polymerase then incorporates dNTPs complementary to the template strand during the elongation step (Figure 5.1).[206]

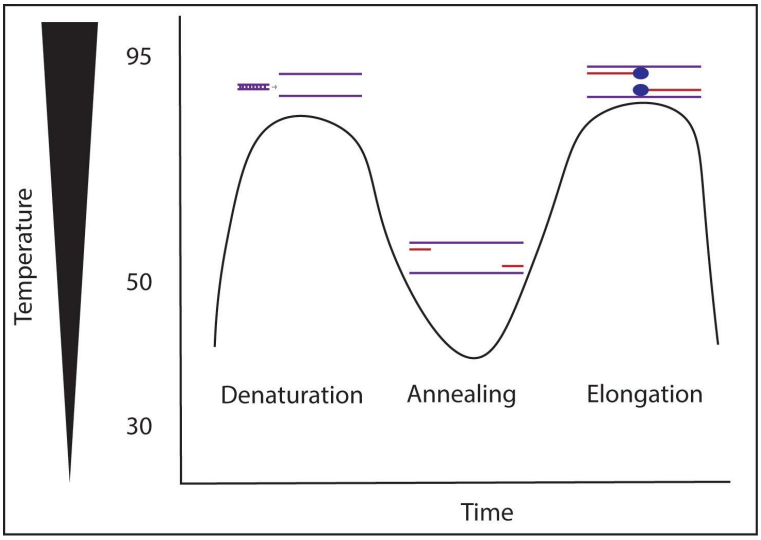

Figure 5.1. Polymerase chain reaction basics.
The PCR reaction is performed by thermal cycling to achieve template denaturation, primer annealing and elongation. A heat stable polymerase incorporates deoxynucleotide triphosphates (adenine, guanine, cytosine and thymine) into the annealed primer sequences using deoxyribonucleic acid as a template.[206] Adapted from Kubista *et al*. The real-time polymerase chain reaction. Mol Aspects Med. 2006;27(2-3):95-125 with permission from Elsevier.

In qPCR, the reaction can be monitored in real-time by measuring the fluorescence of dyes that bind to or intercalate into DNA during polymerisation. The measured fluorescence is thus proportional to the amount of product present in the reaction at any given cycle number.[206] When compared to conventional PCR, qPCR has many advantages including reaction speed, reproducibility and sensitivity. In addition, while conventional PCR is at best semi-quantitative and requires additional steps like gel electrophoresis in order to obtain such information, qPCR is a method that generates quantitative data in real time.[207]

RT-qPCR is widely used to estimate the level of expression of genes of interest. mRNA is isolated and is reverse transcribed into cDNA by the enzyme reverse transcriptase.[208] The reverse transcription step may be prepared by specific primers (decreases background priming) or random and oligo-dT primers (to maximise the number of analysed mRNA molecules).[208] The reproducibility and reliability of a RT-qPCR assay depends on the choice of reference genes and sample preparation. An appropriate reference gene will have stable expression irrespective of experimental conditions. Not all reference genes adhere to this standard, and thus stable expression should be demonstrated prior to the commencement of experiments.[207]

A popular method for detection of amplicons in RT-qPCR involves the use of specifically designed and targeted oligonucleotide primers along with the intercalating dye SYBR® Green I, an asymmetrical cyanine dye with two positive charges which binds strongly to the negatively charged backbone of DNA (Figure 5.2).[209] SYBR Green I emits low levels of background fluorescence when not bound to DNA, but fluoresces strongly upon dsDNA binding. The fluorescent dye binds to the minor groove of the dsDNA amplicons formed after each PCR cycle, and the resulting increase in fluorescence is measured. The threshold cycle (C_T) or crossing point (C_P) indicates the point at which the measured signal exceeds the background signal. If there are high concentrations of the target transcript present, fewer cycles are required to surpass this threshold.[210,211] A disadvantage to this method and its sensitivity is that secondary products may also be detected, and thus an additional melt curve analysis is required at the end of each experiment in order to ascertain primer specificity and product homogeny.[209]

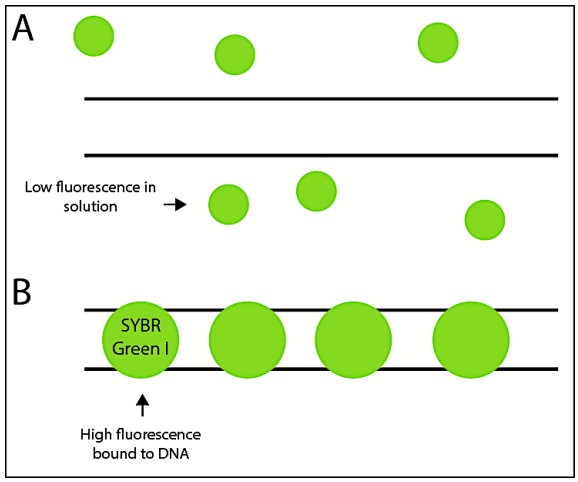

Figure 5.2. SYBR green as an intercalating dye.
SYBR® green I has a low level of detectable fluorescence in solution (A), but once intercalated into double stranded DNA (B) emits a strong, detectable fluorescence signal that may be measured and analysed.[209]

Gene expression may be determined using absolute quantification, where the expression is compared to a previously generated standard curve of known target DNA, or relative quantification, where expression is compared relative to the expression of a reference gene, untreated sample, or calibrator. The relative expression of the gene is then calculated using the comparative C_T method (also known as the $2^{-\Delta\Delta CT}$ method; Figure 5.3 Equation 5.4).[212,213] Two important assumptions of relative quantification are that the efficiency of reverse transcription is 100% and that the efficiency of the target gene amplification is similar to that of the reference gene. An advantage of this method is that it may represent changes in gene expression as a 'fold change'. The disadvantage is that the assumptions made in this method must be met. If they are not met after the PCR has been analysed, the PCR should be further optimised.[212]

In this method, the change in C_T-values between the target and calibrator genes (such as reference genes) for the treated/induced groups is calculated (ΔCT; Figure 5.3 Equation 5.1). Secondly, the difference in C_T-values between the target and reference genes of the untreated/non-induced is calculated (ΔCT; Figure 5.3 Equation 5.2). Lastly, the difference between the two groups determines ΔΔCT (Figure 5.3 Equation 5.3). The value obtained by applying the $2^{-\Delta\Delta CT}$ method essentially depicts the

expression of a target gene relative to one or more reference genes in the induced sample, as compared to the non-induced sample. Depending on the research question that is being investigated, it is also possible to use the same equations where all samples are normalised to a certain time point, instead of a non-induced/untreated sample.

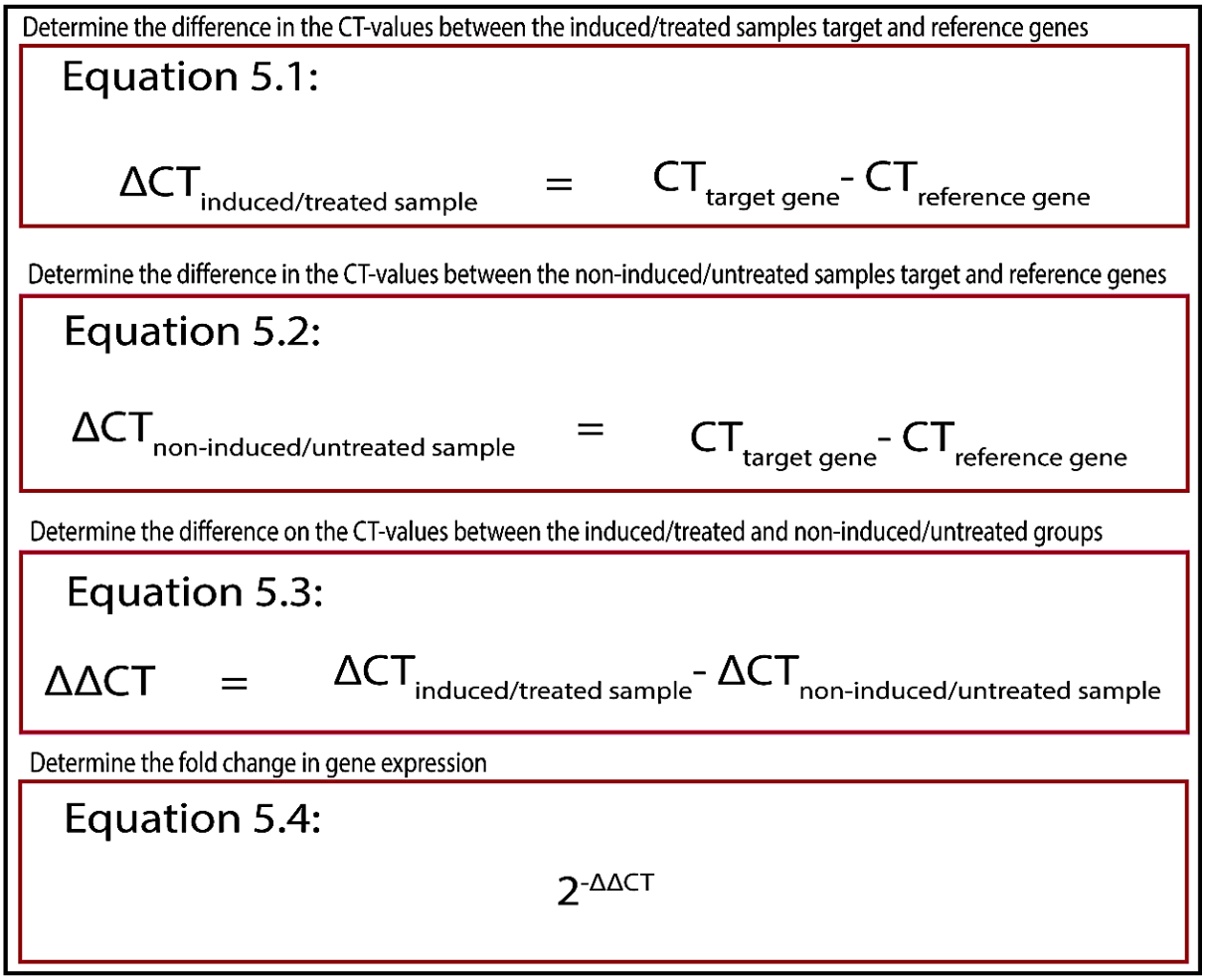

Figure 5.3. Determining the fold-change in gene expression using the comparative CT method.
ΔΔCT (Equation 5.3) is determined by the difference between the ΔCT of the induced/treated samples (Equation 5.1) and the ΔCT of the non-induced/untreated sample (Equation 5.2). The comparative CT method indicates the fold change in relative gene expression and is determined by taking 2 (which represents a theoretical efficiency of 100%) to the power of negative (-) ΔΔCT (Equation 5.4).

The minimum information for publication of quantitative RT-PCR experiments (MIQE) guideline values for RT-qPCR performed in this study are located in Appendix F.[214] A

set of parameters is required to be disclosed with every publication in which qPCR is used as a method. These include information on experimental design, the samples, nucleic acid extraction, reverse transcription, qPCR target information and oligonucleotides, qPCR protocol and validation and data analysis.[214]

The myogenic target genes investigated in this study included MyoD, MyoG and desmin. The reference genes that were used in the RT-qPCR assay were tata binding protein (TBP), β-actin (ACTB) and tyrosine 3-monooxygenase/tryptophan 5-monooxygenase activation protein, zeta (YWHAZ).[215] Myogenic targets, reference genes, and the principle functions of each are laid out in Table 5.1. Stable gene expression was determined prior to experiments, and the results are contained in Appendix G, section G.4.3.

Table 5.1. Target and reference genes used to investigate relative myogenic gene expression.
A summary of the target and reference genes used in this study with their symbols and functions.

Target gene	Abbreviation	Gene function	References
Myogenic differentiation	MyoD	Master regulator for myogenic differentiation	Huri *et al.* (2018)[159]
Desmin	Desmin	Myotube structural protein	
Myogenin	MyoG	Myotube fusion	
Tata binding protein	TBP	Transcription factor for RNA polymerase II	Dessels *et al.* (2019)[215]
β-actin	ACTB	Maintains cytoskeleton structural protein and integrity; cell motility	
Tyrosine 3-monooxygenase/tryptophan 5-monooxygenase activation protein, zeta	YWHAZ	Regulation of signal transduction pathways	

Fluorescence and the fluorescent microscope

Fluorescent microscopy is used to visualise specific targets set against a black background. It may be used to identify structural features of cells and the locations of

components such as organelles and proteins.[216] Fluorescence can be defined as the emission of light at a specific wavelength that occurs within nanoseconds after the absorption of light at a shorter wavelength.[216,217] A fluorophore is a molecule with fluorescent properties. When the ground state of fluorophores becomes excited by photons (light energy) at a specific wavelength, light is emitted at another wavelength and causes it to fluoresce as the fluorophore returns to its ground state.[216,217] The change between the excitation and emission wavelengths is also known as stokes shift. By filtering out the excited light, without blocking the emitted light, it is possible to visualise only the fluorescent object.[217]

The fluorescent microscope comes equipped with specific filter cubes, a dichroic mirror and blocking filters. Traditional filter cubes consist of a dichroic mirror at an angle of 45^{o} and excitation and emission filters. The cube targets light from the light (excitation) source to the sample, and from the sample to the microscope detector.[217] The dichroic mirrors act as the main optical element, and separate the excitation and emission light. Excitation and emission filters ensure that only the appropriate wavelengths of light are transmitted.[217] Fluorescent microscopes allow the visualisation of multiple different fluorophores at the same time, as long as there is little to no overlap in the excitation and emission spectra to prevent light channel bleed-through (observing one fluorescent signal in more than one channel).[216,217] Most conventional fluorescent microscopes are wide-field and require the use of a xenon, mercury or light emitting diode (LED) light source.[218] The disadvantage of using a wide-field microscope is that samples become immersed in light, creating a bleaching phenomenon whereby fluorophores lose fluorescence. As an alternative, the laser scanning confocal microscope (LSM) makes use of lasers as a light source and illuminates only a small, focused areas of the specimen.[218] High-resolution images are achieved by scanning one or multiple focused beams of light which also allows images to be sectioned. A single image is called an optical section.[218]

Immunocytochemistry (ICC) is a method that utilises a fluorescent microscope to visualise the presence of protein targets. ICC was used in this study to qualitatively confirm the presence of myogenic target proteins Pax 3/7, MyoD, MyoG and desmin.

Primary antibodies were targeted to either Pax 3/7, MyoD, MyoG and desmin. Secondary antibodies conjugated to fluorophores were used to visualise the antibody-bound myogenic proteins on the confocal microscope. Indirect conjugation using a primary-secondary antibody protein detection system allows for easy fluorochrome substitution for optimal assay design, and increases signal detection sensitivity.[219] The disadvantages include potential cross-reactivity and higher background noise due to endogenous enzymes or biotin activity, and the attraction of primary and secondary antibodies to endogenous fragment crystallizable (Fc) regions.[220] To obtain optimal images with the least amount of background, both primary and secondary antibodies must be optimised by titration. Optimal images have high fluorescent signal and minimal background staining, and are achieved by titrating both the primary and secondary antibodies on a positive control.[219]

In this study, PHMs were used as a positive control in order to optimise the myogenic ICC protocol. In addition, a C2C12 myoblast cell line was used as a positive control mainly for the identification of morphological features.

5.2. Chapter objectives

Objectives addressed in this chapter were to assess the feasibility of ASC myogenic differentiation *in vitro* using the DH-based and 5-Aza-based induction methods, to determine an optimal differentiation timeline, and to investigate the effect of ASC myogenic induction on cell morphology using light and fluorescence microscopy. The efficacy of two methods of myogenic induction in ASCs was investigated by protein (ICC) and transcriptional analysis (RT-qPCR) of specific myogenic targets. The study attempted to gain an understanding of the kinetics of the genes involved in ASC myogenic differentiation.

5.3. Materials and methods

In this chapter, ASCs were isolated, characterised and cells expanded as previously described in Chapter 4, and were differentiated according to the protocols described below.

5.3.1. Cell culture and sample information

Cell lines used in this study

ASCs, human PHMs and an immortalised murine C2C12 cell line were used in this study. ASCs were obtained as described in Chapter 4. Murine C2C12 myoblasts and PHMs were obtained from Professor. K. Myburgh (Department of Physiology, University of Stellenbosch, Stellenbosch, South Africa) as a kind gift. C2C12s and PHMs were used as a training tool for myogenic morphological features, and PHMs were used to optimise RT-qPCR and ICC experiments.

Adipose-derived stromal cell sample analysis

ASC assays were conducted on three biological repeats (n=3). In the RT-qPCR assays, each biological replicate was run as three technical repeats. For ICC assays, five micrographs were taken at each time point for each condition and biological replicate.

5.3.2. Instrument information

Reverse-transcription real-time polymerase chain reaction instruments

The instruments used in the experiments described in this chapter include the NanoDrop® ND 1000 spectrophotometer (Thermo Fisher Scientific, Waltham,

Massachusetts, USA); a Quantus Fluorometer™ (Promega, Madison, Wisconsin, USA); a 2200 Tapestation from Aligent technologies (Santa Clara, California, United States); the CFX96 real time system and GelDoc™ system from Bio-Rad (Hercules, California, United States); the LightCycler 480 II instrument (Roche, Basel, Switzerland); and the Gene Amp® PCR system 9700 from Applied Biosystems (Life Technologies®/Thermo Fisher Scientific, Carlsbad, California, USA).

Microscope instruments

Micrographs of ASCs, C2C12s and PHMs in culture were taken with the Zeiss PrimoVert inverted light microscope (Carl Zeiss Werke, Göttingen, Germany) using the Zeiss AxioVert A1 digital camera (Carl Zeiss Werke, Göttingen, Germany). Fluorescent images were captured using a Zeiss LSM 800 confocal microscope (Carl Zeiss Werke, Göttingen, Germany). Images were captured using Zen light (Blue edition, version 3.2, Carl Zeiss Werke, Göttingen, Germany) and analysed/edited using Fiji (Image J, version 2.1.0/1.53c; Laboratory for Optical and Computational Instrumentation, University of Wisconsin, Wisconson, USA).

5.3.4. Experimental design and culture plate set up

Myogenic assays were conducted on days zero, three, six, twelve, 24, 30 and 42 for the induction method involving DH and until day 24 for 5-Aza. Time point ‘day zero’ was terminated on the day of myogenic induction (24 hr after cells were initially seeded at 50% confluency), and these cells were not exposed to myogenic induction media. As this was the first-time myogenic studies were conducted at the ICMM, it was elected to adhere to published timelines for differentiation, with minor modifications. Generally, ASC differentiation is investigated every seven days, but because myogenic genes are transiently and sequentially expressed, and because it has not previously been attempted at the ICMM, shorter intervals were investigated at the start of the induction period.

Two plates for each induction medium were prepared for each time point; one plate was used for RNA extraction and RT-qPCR, and the second plate was used for ICC. For RT-qPCR plates, on the day of termination, cells were trypsinised and RNA was extracted and stored at -80^{o}C. cDNA was synthesised after all the RNA was successfully extracted and RT-qPCR was performed (Figure 5.4A). ICC culture plates were set up in a similar fashion; however, each well contained glass coverslips (22mm) that were pre-coated with 0.01% poly-L-Lysine and 12.5 µg/cm^2 type I rat tail collagen (See Appendix G, section G.5 for details pertaining to optimisation). ICC was done on coverslips placed in each well of the 6-well plates at each time point used in myogenic differentiation (Figure 5.4B). Each experimental time-point for every culture included two 6-well plates that investigated the DH- and 5-Aza-based induction methods, along with a non-induced control. Every culture condition was investigated using three coverslips. The staining method involved a primary-secondary antibody system, where the primary antibody was directed to the target protein and the secondary antibody (conjugated to a fluorophore) was directed against the animal in which the primary antibody was made. In this study, primary antibodies were targeted to MyoD, Pax 3/7, desmin and MyoG, and were co-stained according to the schematic shown in Figure 5.3B.

The Zeiss LSM 800 confocal microscope has no filter sets because it is equipped with a continuous filter to accommodate a wide range of wavelengths. It has three lasers namely a 405 nm (UV light) laser, a 488 nm (blue light) laser and a 561 nm (green light) laser. DAPI was visualised using the 405 nm laser, AF 488 using the 488 nm laser and TRITC-phalloidin and AF 555 using the 561 nm laser.

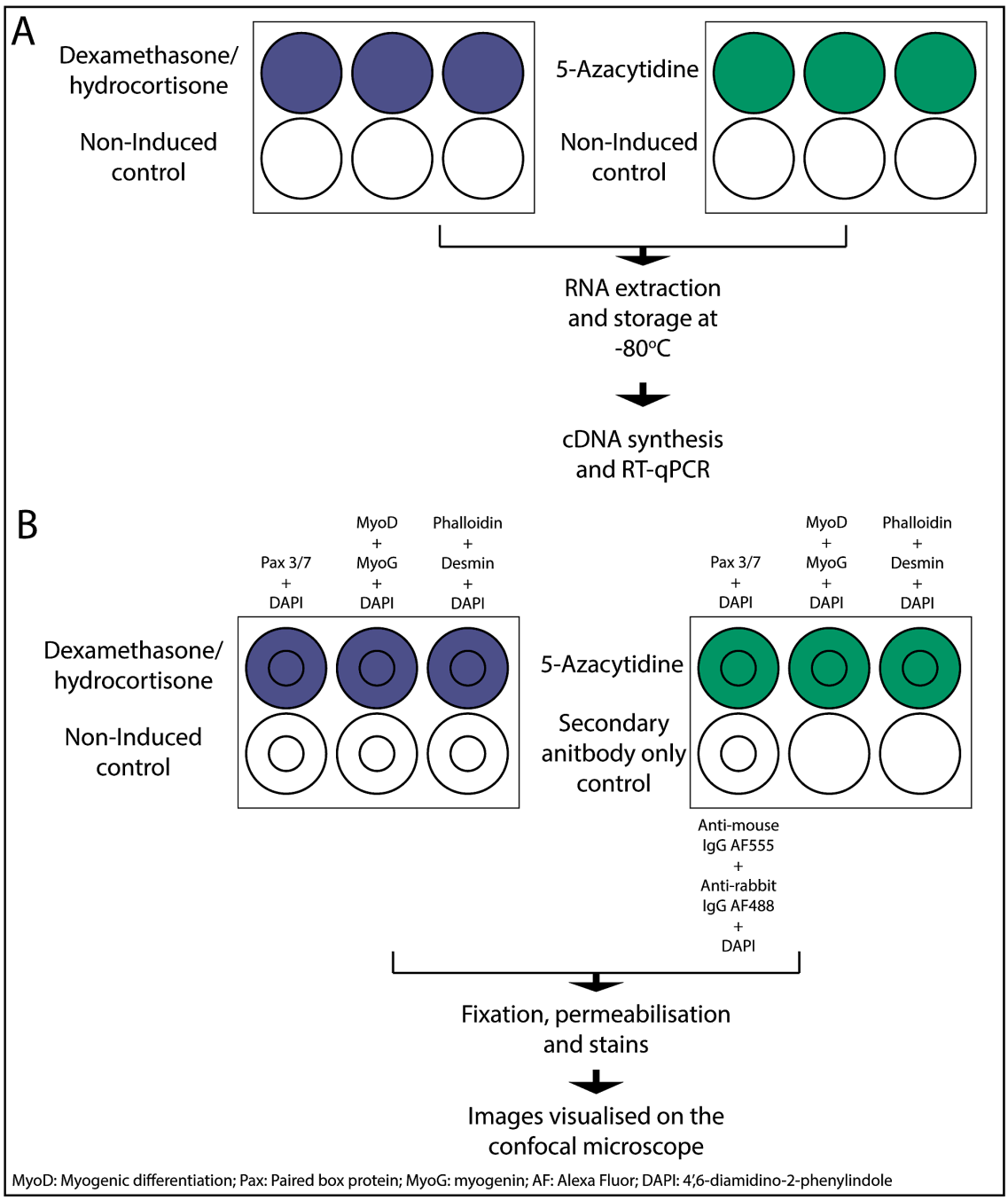

Figure 5.4. Culture plate set up for experimental purposes at every time point.
A. Adipose-derived stromal cells were seeded into two 6-well culture plates (coated with type I collagen) for each induction method and non-induced control. Experiments were terminated, RNA extracted and stored and thereafter cDNA was synthesised for RT-qPCR. B. Adipose-derived stromal cells were seeded into 6-well plates containing cover slips pre-coated with poly-L-lysine and type I rat tail collagen. Experiments were terminated, and cells were fixed, permeabilised and stained according to the schematic above before being viewed on the confocal microscope

5.3.5. Method optimisation

Some methods required extensive optimisation before experiments could be completed; the particulars of this process along with important considerations have been described in Appendix G.

5.3.6. Cell culture and myogenic differentiation

ASCs, PHMs and C2C12s were cultured and differentiated in order to optimise and perform myogenic assays for the purpose of this study.

Culture ware coated with rat tail collagen type I

PHMs and C2C12s are generally propagated and differentiated in culture ware coated with adhesives such as collagen type I to aid in cell adherence to plates. While this is not necessary to expand ASCs, it becomes vital in order to effectively induce myogenic differentiation. In order to save on cost after initial experiments were conducted using ready-made type I collagen purchased from Corning® (Corning, New York, USA), type I collagen was isolated directly from rat tails. This procedure was done by Mr A. Ellero (PhD candidate, Centre for Neuroendocrinology (CNE), Department of Immunology, University of Pretoria) and Dr I. van den Bout (CNE, Department of Physiology, University of Pretoria). Approval from the University of Pretoria Animal Ethics Committee was obtained to isolate collagen from rat tails (approval number: REC107-19).

Culture flasks coated for cell culture and differentiation

Prior to seeding C2C12 and PHM cultures, T75 culture flasks were lined with 5 µg/cm^2 collagen. Collagen stock was diluted in 0.02N acetic acid (Sigma-Aldrich Chemie Darmstadt, Germany) to a working solution of 50 µg/ml (Figure 5.5, Equation 5.5) and 1 ml of the working solution was added to culture ware. Thereafter, culture flasks were placed on an orbital shaker (60 rotations per minute; rpm) overnight and washed twice using PBS (2% p/s) before cells were seeded at 5000 cells/cm^2.

$$\text{Equation 5.5: } V_{collagen}\,(ml) = \frac{V_{solution\ final}\,(ml) \times C_{collagen\ final}\,(mg/ml)}{C_{collagen\ solution}\,(mg/ml)}$$

Figure 5.5. Equation used to make up collagen working solution.
In order to determine the amount of collagen stock solution to be added to 0.02 N acetic acid, the final volume desired ($V_{solution\ final}$) is multiplied by the final desired collagen concentration ($C_{collagen\ final}$), divided by the concentration of the collagen stock solution ($C_{collagen\ solution}$).

Coverslips coated with adhesives for adipose-derived stromal cell differentiation

To ensure that the collagen coating adhered to the glass coverslips, they were thoroughly cleaned and pre-coated with 0.1% poly-L-lysine (Sigma-Aldrich Chemie, Darmstadt, Germany). Glass coverslips (Marienfeld GmbH & Co.KG, Lauda-Königshofen, Germany) were placed in a glass beaker with a solution of 5% (v/v) NaOH (Sigma-Aldrich Chemie, Darmstadt, Germany) and 30% (v/v) ethanol (Sigma-Aldrich Chemie, Darmstadt, Germany) on the orbital shaker overnight, to clean the coverslips of fatty residue and grime. Thereafter the coverslips were washed ten times in double distilled (dd) H_2O and placed in concentrated HCl (12.1 M; Sigma-Aldrich Chemie, Darmstadt, Germany) overnight, to further clean and slightly etch the glass. The concentrated HCl was carefully poured off into a separate glass Schott bottle and the coverslips were washed ten times in ddH_2O before being stored in 70% ethanol until use to ensure cleanliness and sterility. Prior to seeding cells for differentiation experiments, coverslips were placed into 6-well culture plates and left in the class II biosafety cabinet for 24 hr to dry. The coverslips were then washed once in sterile-filtered ddH_2O and left to dry for a further 24 hr after which 1 ml of the undiluted poly-L-lysine solution (0.01% sterile filtered) was added to each well. The culture plates were then placed on an orbital shaker (60 rpm). After 2 hr, the poly-L-lysine was removed and each well containing coverslips was washed ten times with sterile filtered ddH_2O before being left to dry for 72 hr in the biosafety cabinet (poly-L-lysine can be toxic to cells if not dried properly). Thereafter, a solution of 120 µg/ml collagen was prepared and 1 ml of the working solution was added to each well to coat the coverslips with 12.5 µg/cm^2 collagen. The 6-well plates were sealed with parafilm and placed on an orbital shaker (60 rpm) overnight after which the collagen solution was aspirated in the biosafety cabinet and left to dry for an additional 48 hr. One to two hr prior to

seeding cells, each well containing a coverslip was washed twice with ddH_2O before cell-line appropriate CGM was placed in each well.

Cell culture and differentiation media

In this study, complete growth media (CGM), muscle induction media (MIM) and cryopreservation media (Cryo) was specific to each culture and the abbreviations used to refer to each medium along with their composition has been summarised in Table 5.2. Basic fibroblast growth factor (b-FGF) was acquired from Thermo Fisher Scientific (Invitrogen, Waltham, Massachusetts, USA). Horse serum, dexamethasone, hydrocortisone and 5-Aza were acquired from Sigma-Aldrich Chemie (Darmstadt, Germany).

Table 5.2. Cell culture media used in this study, and their compositions.
A comprehensive summary of the various expansion, induction, maintenance and cryopreservation media used in this study, along with their compositions.

	Expansion		Induction		Maintenance		Cryopreservation	
Cell type	Medium abbrev	Medium composition	Medium abbrev	Medium composition	Medium abbrev	Medium composition	Medium abbrev	Medium composition
ASCs	ASC-CGM	DMEM, 5% (v/v**) pHPL, 2% p/s, 0.2% AmB	MIM 1	DMEM, 10% FBS, 5% HrS, 2% p/s and 0.2% AmB; 0.1 µm dexamethasone, 50 µm hydrocortisone			ASC-Cryo	90% ASC-CGM and 10% DMSO
			MIM 2	Low glucose DMEM, 10% FBS, 2% p/s, 0.2% AmB	MIM 2-m	Low glucose DMEM, 10% FBS, 2% p/s, 0.2% AmB, 1 ng/ml b-FGF		
			ASC-NI	DMEM, 10% FBS, 2% p/s and 0.2% AmB; 0.1 µm				
C2C12	C2C12-CGM	DMEM with 20% FBS, 2% p/s, 0.2% AmB	C2C12-MIM	DMEM with 2% FBS, 2% p/s, 0.2% AmB			C2C12-Cryo	20% C2C12-CGM, 70% FBS, 10% DMSO
PHM	PHM-CGM	DMEM, 10% FBS, 2% p/s, 0.2% AmB	PHM-MIM	DMEM with 2% FBS, 2% p/s, 0.2% AmB			PHM-Cryo	90% FBS and 10% DMSO

ASC: adipose-derived stromal cell; C2C12: immortalised murine myoblast cell line; PHM: primary human myoblasts; CGM: complete growth medium; DMEM: Dulbecco's Modified Eagle's Medium; pHPL: pooled human platelet lysates; pen/strep: penicillin/streptomycin; v/v: volume/volume; FBS: fetal bovine serum; HrS: horse serum DMSO: dimethyl sulfoxide; b-FGF: basic fibroblast growth factor; AmB: amphotericin; MIM: muscle induction medium; Cryo: cryopreservation **Abbrev: abbreviation.**
All percentages are indicative of v/v additions.

Cell storage in liquid nitrogen storage, passage, maintenance and cryopreservation

Prior to obtaining cells from liquid nitrogen following storage, a 15 ml centrifuge tube was prepared with 10 ml pre-warmed culture-specific CGM (Table 5.2). Thereafter, the cryovial containing the cells was removed from storage and 1 ml pre-warmed medium was added to the frozen contents of the cryovial. CGM (1ml) was transferred to-and-from the cryovial and 15 ml tube until the contents of the cryovial were completely thawed and transferred to the centrifuge tube. The cells were pelleted by centrifugation at 300 g for 5 min, the supernatant aspirated, and the pellet resuspended in CGM. Thereafter, the entire cell suspension was seeded into a T75 flask and placed in the incubator (37^{o}C, 5% CO_2) to increase cell number. All cells were maintained and passaged as previously described (Chapter 4, section 4.3.6). PHMs and C2C12s were passaged at no more than 70% confluence to avoid spontaneous differentiation which starts to occur at cell confluency. ASCs, PHMS and C2C12 were trypsinized and cryopreserved as previously described in Chapter 4, section 4.3.6). While ASCs were trypsinized for 7 min, C2C12s and PHMs were trypsinized for 4 min only. After passaging, excess cells were cryopreserved at 1x10^6 cells/cryovial in 1 ml culture-specific cryopreservation medium (Table 5.2) and placed in a NALGENE® Mr Frosty™ Cryo 1^{o}C freezing container (Thermo Fisher Scientific, Waltham, Massachusetts, USA) at -80^{o}C until frozen. Thereafter, the cryovials were transferred to liquid nitrogen storage.

Adipose-derived stromal cell myogenic differentiation

ASCs were expanded in ASC-CGM in T75 flasks (Table 5.2) until confluent, and thereafter trypsinized and seeded in 6-well plates lined with 5 µg/cm^2 type I collagen at 5000 cells/cm^2 and incubated at 37^{o}C/5% CO_2 for 24 hr. Thereafter, expansion medium was replaced with MIM 1 or 2 (Table 5.2). The induction process and timelines have been summarised in Figure 5.6. ASCs induced using MIM 1 were induced and maintained in the same medium for 42 days. The induction medium of ASCs induced using MIM 2 was replaced after 24 hr with MIM-2-m for a period of 24 days. The non-

induced ASCs were maintained in ASC-NI. Media were replaced biweekly for the duration of the respective differentiation timelines.

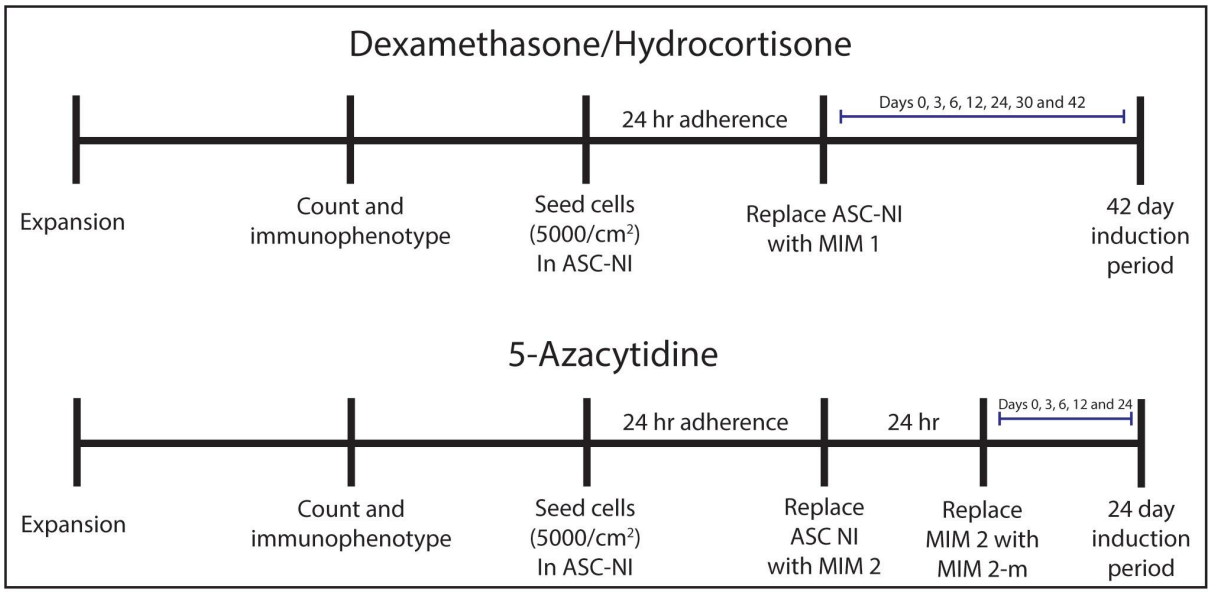

Figure 5.6. Illustration of the myogenic induction timelines used in this study.
This illustration demonstrates the induction process and timelines in the dexamethasone/hydrocortisone (DH) and 5-azacytidine (5-Aza)-based methods. The DH-based method was investigated over 42 days, while the 5-Aza-based method was investigated over 24 days.

Primary human myoblast differentiation

All PHMs were expanded and differentiated in culture flasks lined with 5 µg/cm^2 type I rat tail collagen. PHMs were initially expanded in T75 cm^2 culture flaks to obtain enough cells for experiments, after which they were seeded in 6-well plates (5000 cells/cm^2) for differentiation studies. When PHMs reached ≥ 90% confluency, expansion medium was replaced with PHM-MIM (Figure 5.7). RNA was extracted on days zero, one, three, five and seven. PHM-CGM was replaced twice weekly during expansion and once with PHM-MIM during differentiation.

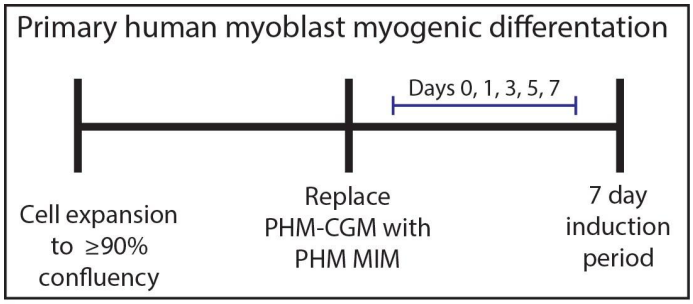

Figure 5.7. Primary human myoblast myogenic induction timeline.
Primary human myoblasts were expanded until reaching ≥ 90% confluency after which expansion medium was replaced with induction medium. PHMs were terminated for myogenic assays on days 0, 1, 3, 5 and 7.

C2C12 murine myoblast differentiation

Similar to PHM differentiation, C2C12s were expanded in culture flasks lined with collagen. C2C12-CGM was replaced with C2C12-MIM upon reaching ≥ 90% confluency. C2C12s were investigated over a period of five days and experiments were terminated on days zero, three and five.

5.3.7. RNA extraction, quantitation and validation

RNA extraction

Total RNA was extracted using either the RNeasy mini or micro plus kits (Qiagen, Hilden, Germany) according to the manufacturer's instructions. Cells were counted prior to RNA extraction as described in Chapter 4. According to the manufacturer's instructions, if the total cell number was < 500 000, the micro kit was used. If the total cell number was > 500 000 cells, the mini kit was used.

Cells were trypsinized and centrifuged to obtain a cell suspension and counted by flow cytometry as described in Chapter 4. To maximise the amount of RNA extracted, cell suspension from the three wells for each condition were pooled. After trypsinisation,

cells were washed three times for 5 min in 1 ml PBS followed by centrifugation to ensure potential contaminants such as phenol red in medium was removed. Before the last wash step, the cell suspension was transferred to a 1.5 ml Eppendorf tube. The supernatant was discarded and the cells resuspended in 350 µl (ASCs) or 600 µl (PHMs) RLT buffer, with β-mercaptoethanol (β-ME, 5 µl per 1 ml RLT buffer; Sigma-Aldrich Chemie, Darmstadt, Germany) added to lyse the cells and eliminate nucleases which could degrade the RNA. The cell suspension was vortexed for one min, centrifuged for 2 min at 21 000 *g*, and vortexed again for 1 min. Thereafter, cells were placed into the genomic DNA (gDNA)-elimination spin column (which uses a silica membrane to selectively bind and retain DNA whilst allowing RNA to pass through the column) and centrifuged for 30 sec at 8000 *g*. The removable column was then discarded, and 70% (v/v) ethanol was added (1:1 with the RLT buffer) to the flow through (the suspension that goes through the column and is collected at the bottom of the tube) and gently mixed by pipetting. The suspension (700 µl, along with any precipitate) was transferred to a RNeasy spin column (containing a membrane that selectively binds to RNA, in order to effectively isolate and purify it on the column membrane), and centrifuged for 15 sec at 8000 *g*. The flow through was discarded, 700 µl RW1 was added to the column and centrifuged for 15 sec at 8000 *g*. The flow through was discarded again, and 500 µl RPE (a mild washing buffer used to remove residual salts left over in the suspension and spin column membrane) was added before being centrifuged for 15 sec at 8000 *g*.

Up to and including the addition of the RPE buffer and centrifugation, the process for both RNeasy micro and mini kits is the same. Minor differences in the protocols after the first addition of RPE buffer to the RNeasy spin column are described below.

Qiagen RNeasy mini plus kit extraction protocol

The flow through was discarded again, and 500 µl RPE was added a second time before being centrifuged for 2 min at 8000 *g*. The flow through was discarded a final time, and the column was placed in a new 2 ml Eppendorf tube. The tube with the spin column was centrifuged for 1 min at 21 000 *g*. Thereafter, the spin column was removed and placed in a sterile, labelled 1.5 ml Eppendorf tube. 40 µl nuclease-free water (supplied by kit) was added onto the membrane of the spin column and left at room temperature for 5 min. Finally, the column was centrifuged for 1 min at 8000 *g* to elute the RNA from the membrane in the RNeasy spin column.

Qiagen RNeasy micro plus kit extraction protocol

Following the first RPE wash and centrifugation step, the flow through was discarded and 500 µl 80% (v/v) ethanol was added to the column and centrifuged for 2 min at 8000 *g*. The flow through was discarded a final time, and the column was placed in a new 2 ml Eppendorf tube. The tube with spin column was centrifuged for 5 min at 21 000 *g* to dry the membrane. Thereafter, the spin column was removed and placed in a sterile, labelled 1.5 ml Eppendorf tube. 14 µl nuclease free water (supplied by kit) was added onto the membrane of the spin column and left at room temperature for 10 min. The spin column was centrifuged a final time for 1 min at 21 000 *g* to elute the RNA.

RNA quantitation and validation

Immediately following RNA extraction, RNA was measured on the NanoDrop® ND 1000 spectrophotometer (Thermo Fisher Scientific, Waltham, Massachusetts, USA) and the concentration, A260/280 nm and A260/230 nm values were recorded before being stored at -80ºC. The A260:A280 ratio is indicative of the RNA purity. A ratio of 1.8-2.1 is indicative of highly purified RNA. The A260:A230 ratio is indicative of other contaminants (such as guanidine isothiocyanate from the kits and phenol red from the media) and is acceptable between 2.0 – 2.2.[221]

Prior to cDNA synthesis, RNA was thawed on ice and integrity was determined. Briefly, a 1 µl aliquot of RNA (concentration between 25 ng/µl and 500 ng/µl) was added to 5 µl RNA Screen tape sample buffer (Aligent technologies, Santa Clara, California, United States). Thereafter, the sample was denatured on a thermal cycler for 3 min at 72^{o}C and placed on ice. The sample was then placed in the 2200 Tape station (Aligent technologies, Santa Clara, California, United States) to determine integrity. RNA integrity was compared to 18S and 28S ribosomal RNA, and an RNA integrity number (Rin)-value between 8 and 10 was considered to be sufficiently pure and viable to proceed.[222]

5.3.8. cDNA synthesis, quantitation and validation.

cDNA synthesis

cDNA was synthesised using the SensiFast^{TM} cDNA synthesis kit (Bioline, London, England) according to the manufacturer's instructions. RNA concentrations were variable, but if the concentration exceeded 1000 ng/µl, working solutions of 500 ng/µl were made. Every cDNA synthesis reaction was accompanied by a no reverse transcriptase (NRT) control sample, to identify if samples and kit buffers contained any gDNA contamination. Thereafter the reaction mixture was prepared as described in Table 5.3.

Table 5.3. cDNA synthesis reaction mixture.
cDNA reactions were made to final reaction volumes according to the manufacturer's instructions.

Reagent or component	cDNA sample tube (µl)	No reverse transcriptase control tube (µl)
5 x TransAmp buffer	4 µl	4 µl
Reverse transcriptase	1 µl	none
RNA	Variable	Variable
Nuclease free water	Variable	Variable
Final reaction volume	20 µl	20 µl

The final reaction mixture was placed in a thermal cycler (Gene Amp® PCR system 9700 from Applied Biosystems, Life Technologies®/Thermo Fisher Scientific, Carlsbad, California, USA) under the following conditions: priming for 10 min at 25°C, RT for 15 min at 42°C, RT inactivation for 5 min at 85°C for 5 min and lastly cooled to 4°C. Thereafter, the cDNA was stored at -20°C until needed.

cDNA quantitation and validation

Following cDNA synthesis, a 1 µl cDNA aliquot was measured on the spectrophotometer and the A260/280 ratio was recorded. An A260/280 ratio of 1.8 - 2.1 indicated pure, intact cDNA.[221]

cDNA was quantified on a Quantus Fluorometer™ (Promega, Madison, Wisconsin, USA) using the Quant-iT™ Picogreen™ dsDNA quantification kit (Thermo Fisher Scientific, Waltham, Massachusetts, USA). Picogreen is a fluorescent dye that binds to dsDNA to form a luminescent complex, which can be used to measure cDNA concentration.[223] The Picogreen assay was done according to the manufacturer's specifications. Working solutions of tris-ethylenediaminetetraacetic acid (Tris-EDTA; TE; 1:20; Sigma-Aldrich Chemie, Darmstadt, Germany) and Picogreen (1:200) were freshly prepared. A dsDNA standard (2 µg/ml) calibrator tube was prepared and 1 µl added to a tube containing TE buffer and Picogreen to a final volume of 200 µl. A blank tube was prepared by adding 100 µl TE buffer and 100 µl Picogreen to a 0.5 ml tube. The instrument was calibrated by running the prepared blank to remove background resulting from TE and unbound Picogreen, followed by the dsDNA standard to calibrate the measurement tool. Quantitation tubes were prepared by adding 99 µl of the former and 100 µl of the latter to 0.5 ml Eppendorf tubes (kept in the dark). cDNA samples were quantified by adding 1 µl of each sample to quantitation tubes. The tubes were then incubated for 5 min in the dark before being measured with the fluorometer and concentrations recorded.

5.3.9. Preparing primer stocks

Lyophilised primers were dissolved in concentrated TE buffer (10mM Tris pH 8.0, 1mM EDTA) as directed by manufacturer's instructions, to a stock solution of 100 µM. Working solutions of 10 µM were prepared with molecular grade water and stored at -20°C until required. The primers (MyoD, desmin and MyoG; sequences not previously published) that were used to confirm skeletal myogenesis along with the reference genes (YWHAZ, ACTB and TBP)[215] were purchased from Integrated DNA Technologies (IDT, Coralville, Iowa USA) and are summarised in Table 5.4.

Table 5.4. Primer pairs and sequences.
MyoD, Des and MyoG were the main myogenic target genes, and YWHAZ, ACTB and TBP were used as reference genes.

Target/ reference gene	Forward primer sequence	Reverse primer sequence	Amplicon length (bp)	Accession number	Reference
MyoD	CACAACGGACGACTTCTA	CTCTTCGGGTTTCAGGAG	112	NM_002478.5	Primer sequences previously designed at the ICMM that have not been published
MyoG	GGCGTGTAAGGTGTGTAA	CAGGGTGCTTCTCTTCAG	124	NM_002479.6	
Desmin	GGTCTCTTACTTTCCTTTCC	TCTCTTCTCCAGCATCTC	135	NM_001382713.1	
YWHAZ	TGACATTGGGTAGCATTAAC	GCACCTGACAAATAGAAAGA	126	NM_001172085	Dessels *et al.* (2019)[215]
ACTB	CCAGCACAATGAAGATCAA	CTCGTCATACTCCTGCTT	128	NM_001101.4	
TBP	GAGTTAAGAGTGTTGATGTAGG	CCTGGGACTGGAAAGTAA	130	NM_001135699.1	

5.3.10. Reverse-transcriptase real time polymerase chain reaction

Sample preparation and reaction programming

RT-qPCR was performed on the LightCycler 480 II (Roche, Basel, Switzerland) using 96-well plates (Roche, Basel, Switzerland) and LightCycler® 480 SYBR Green I Master Mix (Roche, Basel, Switzerland). The reactions were performed in triplicate in a final volume of 10 µl. The reaction mix was prepared as described in Table 5.5. Working solutions of 2 ng/µl cDNA were prepared and 4 ng of the appropriate cDNA was added to each reaction.

Table 5.5. qPCR master mix preparation.
Reactions were prepared according to the manufacturer's specifications.

Reagent	Stock solution	Working solution	Reaction volume (µl)
dH_2O			2.2
SYBR green master mix	2 x	1 x	5
Forward primer	10 µM	400 nM	0.4
Reverse primer	10 µM	400 nM	0.4
Amount of final master mix to be added to each well			8
Amount of cDNA to be added		2 ng/µl	2
Total well volume			10

The programming for the qPCR reaction, including cycle times and temperatures for denaturation and amplification as well as reaction ramp rate is summarised in Table 5.6.

Table 5.6. LightCycler 480 II qPCR reaction programming.
qPCR was done by cycling temperatures to denature and amplify DNA.

Stage of reaction	Condition
Denaturation	95ºC for 5 min
Amplification (45 cycles)	95ºC for 30 sec
	62ºC for 30 sec
	72ºC for 30 sec
Melt curve	95ºC for 30 sec
	40ºC for 30 sec
Ramp rate	0.1ºC/sec

Data was analysed using the LightCycler® 480 Software (Version 1.5.1; Roche, Basel, Switzerland).

Plate design and relevant controls

Every 96-well plate included the relevant samples to be investigated for a specific target gene, three reference genes (ACTB, TBP and YWHAZ) and no-template controls (NTC) for each primer pair. A positive control for the relevant target gene

(either MyoD, Des or MyoG) was included on the plates. The cDNA for the positive controls was synthesised from RNA extracted from PHMs on the day of their induction. All reactions were performed in triplicate.

5.3.11. Immunocytochemistry

Antibody and fluorescent staining solutions were pre-prepared and diluted in the blocking solution (to prevent non-specific binding of primary and secondary antibodies). Mouse anti-human MyoD (1:200; Thermo Fisher Scientific, Carlsbad, California, USA) and rabbit anti-human MyoG (1:400; Abcam, Cambridge, United Kingdom) were co-stained on the same coverslip, while mouse anti-human Pax 3/7 (1:100; Santa Cruz Biotechnologies, Dallas, Texas, USA) and desmin (1:500; Cell Signaling, Danvers, Massachusetts, USA) were stained individually. MyoD and Pax 3/7 were counterstained with anti-mouse IgG conjugated to AF 555 (1:400; Abcam, Cambridge, United Kingdom), while MyoG and desmin were counterstained with anti-rabbit IgG conjugated to AF 488 (1:400; Abcam, Cambridge, United Kingdom). Cover slips stained with desmin were co-stained with TRITC-phalloidin (1:400; Sigma-Aldrich Chemie, Darmstadt, Germany). Each plate included a negative control (combination of secondary-antibodies only). All coverslips were counterstained with DAPI to visualise nuclei (1:1000; Thermo Fisher Scientific, Carlsbad, California, USA). Actin fibers were visualised with TRITC-phalloidin.

Antibody staining (primary and secondary) was done in a staining chamber. The staining chamber consisted of a large petri dish with a labelled grid placed at the bottom. Each block in the grid corresponded to a particular antibody target. The inside of the chamber was lined with parafilm, onto which a drop of antibody solution was placed. The lid of the petri dish was covered in foil to ensure a dark environment on the inside of the chamber. Each chamber was labelled according to its culture. This was to ensure even staining across the coverslip and reduce the volume of antibody needed to stain a coverslip (Figure 5.8).

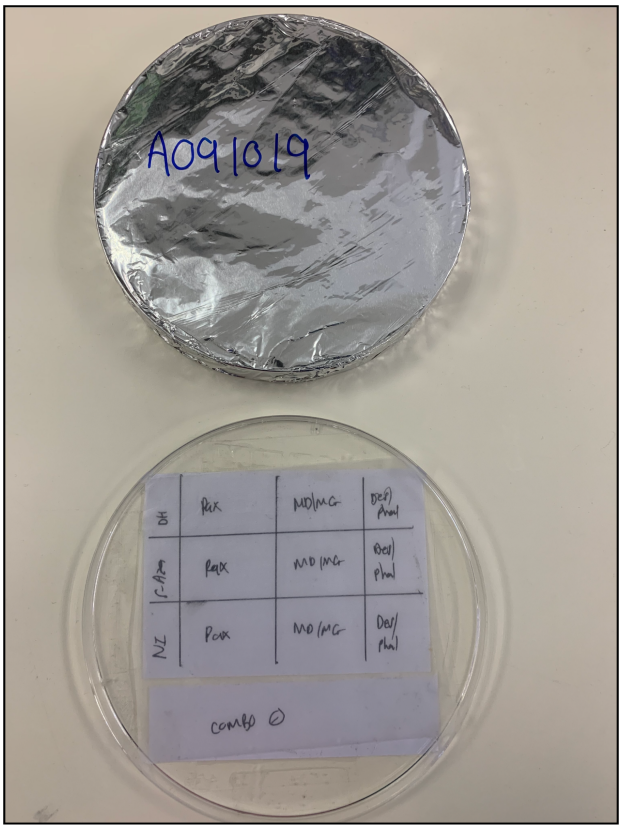

Figure 5.8. Photograph of the staining chamber used in the course this study for immunocytochemistry.
Antibody staining (primary and secondary) was performed in a staining chamber which consisted of a large petri dish with a labelled grid attached to the bottom and lined with fresh parafilm.

The ICC protocol encompassed five main steps and included fixation, permeabilization, blocking, antibody and fluorescent staining and finally mounting. All time-related steps during fixation, permeabilization and the rinse steps with PBS were done on an orbital shaker at 60 rpm (which ensures an even distribution of solution in the well).

Preparation of paraformaldehyde

In order to prepare 500 ml paraformaldehyde (PFA; 4%, pH 6.9 – 7.2; Sigma-Aldrich Chemie, Darmstadt, Germany), 350 ml PBS was added to a Schott bottle on a magnetic stirrer (with heating capabilities) and placed in a well-ventilated fume hood. The PBS was then heated to 60°C before 20 g PFA was added to the solution.

Thereafter, 1M NaOH was added drop-wise to the Schott bottle until the PFA powder dissolved and the solution became clear. The solution was topped up with PBS to a final volume of 500 ml. The pH was adjusted with concentrated HCl until it was within the range of pH 6.9 – 7.2. The 4% PFA solution was filtered through filter paper (to remove particle residue), aliquoted into 50 ml tubes and stored at -20^{o}C once the solution has cooled.

Cell fixation, permeabilization and blocking.

Medium was aspirated from wells destined for ICC. Cells were fixed inside the wells of the 6-well plate with 1 ml 4% PFA for 15 min. Thereafter, the fixative was aspirated and the wells thoroughly washed thrice with PBS. Cells were then permeabilised with 1ml 0.2% Triton X-100 for 5 min. The solution was aspirated and the wells washed with PBS three times. Cells were placed for 1 hr at room temperature using 1 ml blocking solution made up of 5% bovine serum albumin (BSA; Biowest, Nuaillé, France) and 0.3 M glycine (Sigma-Aldrich Chemie, Darmstadt, Germany) in PBS, per well. The BSA was included to prevent non-specific binding of antibodies and the glycine was included to block any free aldehyde groups that may have formed from using PFA (an aldehyde-based fixative) which could potentially increase background fluorescence by binding to secondary antibodies.[224] The blocking solution was aspirated and cells were washed thrice with PBS.

Primary and secondary antibody stains

Primary antibody solution (60 µl drops) was placed onto the parafilm corresponding to the appropriate block on the grid within the staining chamber (Figure 5.9A). The appropriate coverslips were then carefully removed from their wells and placed cell-side down onto the corresponding drop of primary antibody solution (Figure 5.9B). Thereafter, the sides of the staining chamber were lined with damp tissue paper to prevent the coverslips from drying out (Figure 5.9C). The lid was placed onto the

staining chamber, and the entire chamber was kept at 4°C overnight to allow the primary antibodies to bind to their respective targets.

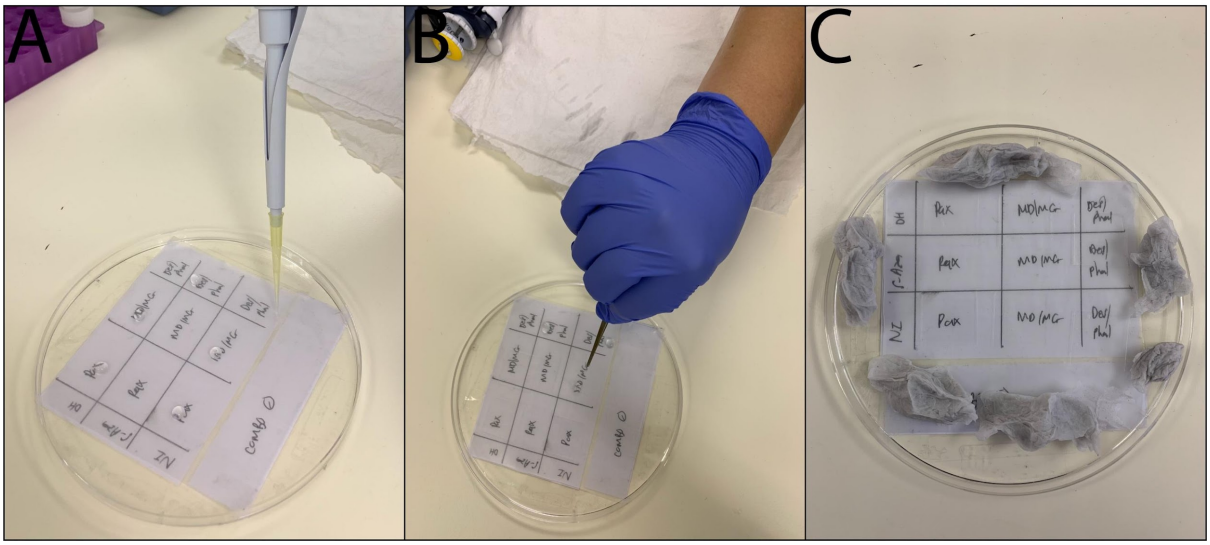

Figure 5.9. The antibody and fluorescent staining procedure in the staining chamber. A. Droplets of the antibody solution is placed within the appropriate block on the grid. B. Coverslips are placed cell-side down onto the droplet. C. Wet tissue paper is placed along the sides of the chamber.

The staining chamber was then removed from the fridge and the coverslips were carefully transferred from the chamber (cell-side up) back into their respective wells in the 6-well plates. To ensure all unbound primary antibody had been removed, the coverslips were washed inside the wells with 2 ml PBS thrice for 5 min. After the wash, the same process was repeated with the secondary antibody solutions. Drops of the appropriate secondary antibody solution were placed on the appropriate block in the grid of the staining chamber, the coverslips were carefully transferred onto the droplet (cell-side down). Thereafter, the lid was placed onto the chamber and the chamber was placed in the dark for 60 min, to allow secondary antibodies to bind to their targets. The coverslips were transferred back into their respective wells (cell-side up) and washed thrice for 5 min with PBS.

Fluorescent counterstains to visualise actin fibers and nuclei

Following the secondary antibody stain, the coverslips on which actin fibers needed to be visualised were stained using the staining chamber with TRITC-phalloidin (1:400) for 15 min, before being washed 3 x 5 min with PBS. Thereafter, all coverslips were counter-stained with 1 ml DAPI (1:1000) inside the wells of the 6-well plates for 5 min in the dark, and washed three times with PBS (for 5 min).

Coverslips mounted onto microscope slides

Coverslips were mounted onto labelled microscope slides (Paul Marienfeld GmbH & Co.KG, Lauda-Königshofen, Germany) using Fluoromount^{TM} (Sigma-Aldrich Chemie, Darmstadt, Germany), an aqueous mounting solution. A drop of the mounting fluid was placed onto the microscope slide and the coverslip was carefully transferred cell-side down onto the drop. The slides were then placed in a container to dry overnight at room temperature, and thereafter stored at 4^{o}C in the dark, until imaged on the confocal microscope.

5.3.12. Calculation of the fusion index

The fusion index is a numerical value calculated based on the detection of myogenic features such as multinucleation and tube formation using ICC (Figure 5.10 Equation 5.6).

$$\text{Equation 5.6: } \underset{(\%)}{\text{Fusion Index}} = \frac{\text{Number of myotube nuclei } (\geq 3 \text{ nuclei})}{\text{Total number of nuclei}} \times 100$$

Figure 5.10. Calculation of the fusion index.
The fusion index (%) is calculated by taking the number of nuclei within myotubes and dividing this by the total number of nuclei in the field of vision and multiplying the number by 100 to get a percentage value.

The fusion index is a semi-quantitative value, and involves counting nuclei within myotubes manually or using software such as Image J (Laboratory for Optical and

Computational Instrumentation, University of Wisconsin, Wisconson, USA). The limitation of using this value to estimate fusion, resides in the fact that software can often count multiple nuclei as one, miss nuclei at the boundaries of the image, and cannot separate nuclei that appear to lie on top of each other. Similarly, manually counting myotubes may result in the counter making subtle counting mistakes. It is, however, widely used to evaluate muscle fusion *in vitro*.[139,225] The fusion index was determined using at least five fields of vision at every time-point during the differentiation of C2C12s, PHMs and ASCs.

5.4. Statistical considerations

Due to the small sample size (n=3) the data was assumed to be non-parametric. Descriptive statistics were included where applicable. The Mann-Whitney U test (used to compare two means) was used to compare means between induced and non-induced samples and between induction methods. The Kruskal-Wallis test (to compare three or more means) followed by Dunn's post hoc test for multiple comparisons was used to compare means between the days for each condition. The conservative Dunn's post-hoc test for multiple comparisons was used because it does not assume that the data adheres to any particular distribution. The significance level was set as $\alpha = 0.05$, and a *p*-value of < 0.05 was considered statistically significant. Means were reported ± SEM.

5.5. Results

5.5.1. Relative gene expression

The mRNA expression of the myogenic genes MyoD, desmin and MyoG was determined by RT-qPCR. The relative mRNA expression was determined according to the comparative C_T-method, effectively representing gene expression as a relative fold-change.[212] The data was analysed in two ways: i) as the target gene (desmin) normalised to reference genes (the mean C_T-value between YWHAZ, TBP and ACTB) in the induced samples, relative to the non-induced sample ($2^{-\Delta\Delta CT}$, where $\Delta\Delta CT = \Delta CT_{Induced\ sample} - \Delta CT_{non\text{-}induced\ sample}$); and (ii) as the target gene normalised to reference genes in both the induced and non-induced samples, relative to day zero ($2^{-\Delta\Delta CT}$, where $\Delta\Delta CT = \Delta CT_{Induced/non\ induced\ samples} - \Delta CT_{day\ zero}$). The latter results were included because amplification of desmin was also observed in the non-induced samples, thus making day zero a baseline to which the relative expression of desmin in both the induced and non-induced conditions could be compared. This method allowed the relative gene expression to also be interpreted as 'a change in the fold expression due to a particular treatment or induction method' ($2^{-\Delta\Delta CT}$).[212] The change in the fold expression of desmin was indicated on bar graphs with the x-axis set at 1, to indicate whether the expression of desmin increased ($2^{-\Delta\Delta CT} > 1$) or decreased ($2^{-\Delta\Delta CT} < 1$) as compared to either the non-induced samples or day zero.

Over the induction period, no amplification of MyoG or MyoD was observed at any time point between day zero and day 24, for either the DH-, 5-Aza- or non-induced conditions. Thus, only desmin was analysed. Furthermore, due to the amplification of some NRTs, days 30 and 42 were excluded from analysis in the DH-induced samples. All samples were thus analysed up until day 24 only.

The expression of desmin in the induced samples relative to the non-induced sample

Relative to the non-induced sample, the fold-change in the expression of desmin in samples induced using the DH induction method indicated a slight decrease on days three ($2^{-\Delta\Delta CT}$ = 0.24 ± 0.15), six (0.20 ± 0.11), twelve (0.66 ± 0.41) and 24 (0.19 ± 0.06). In samples induced using the 5-Aza induction method, desmin expression decreased on days three ($2^{-\Delta\Delta CT}$ = 0.21 ± 0.07); 6 (0.32 ± 0.21) and 24 (0.65 ± 0.25) while slightly increasing by 1.3 ± 0.58-fold on day twelve (Figure 5.11).

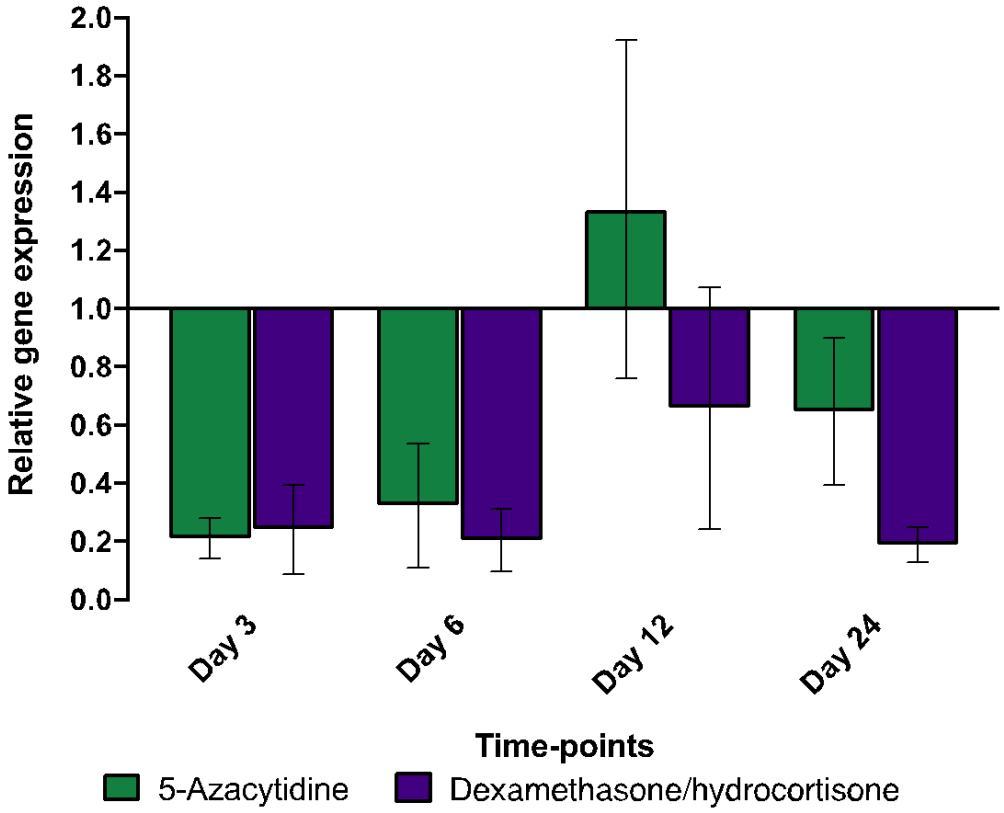

Figure 5.11. Expression of desmin in the samples induced using the dexamethasone/hydrocortisone (DH) and 5-azacytidine (5-Aza) methods, relative to the non-induced sample.
The relative expression (as determined using the comparative C_T-method) of desmin in the DH and 5-Aza induction methods is shown over a period of 24 days. In both the DH and 5-Aza methods, desmin showed a decreased trend in expression at all time-points, except for day 12, where the 5-Aza based method indicated a slight increase. The x-axis is shown to intersect with the y-axis at 1. Bars below the x-axis indicated where the expression of desmin decreased as a fold-change relative to the non-induced sample, while the bar above the x-axis indicated an increase. No data was significant, and thus it was not indicated. Bars represent the mean ± standard error of the mean. The sample size is represented by n=3.

When comparing the expression of desmin in the DH- and 5-Aza-induced samples, relative to the non-induced sample, no statistically significant change in gene expression was noted on days three (*p*-value*: 0.7000*), six (*p*-value*: 0.7000)*, twelve (*p*-value*: 0.4000*) or 24 (*p*-value*: 0.2000*).

The change in the mean expression of desmin between time points within the samples induced using the DH induction method was analysed using the Kruskal-Wallis followed by Dunn's post-hoc statistical tests. No statistically significant changes in gene expression were noted between days three and six (*p-value > 0.9999*), days three and twelve (*p-value > 0.9999*), days three and 24 (*p-value > 0.9999*), days six and twelve (*p-value > 0.9999*), days six and 24 (*p-value > 0.9999*) and days twelve and 24 (*p-value > 0.9999*). In the samples induced using the 5-Aza induction method, no statistically significant change in the mean expression of desmin was found between days three and six (*p-value > 0.9999*), days three and twelve (*p-value > 0.1887*), days three and 24 (*p-value > 0.8462*), days six and twelve (*p-value > 0.3255*), days six and 24 (*p-value > 0.9999*) and days twelve and 24 (*p-value > 0.9999*).

The expression of desmin in the induced and non-induced samples relative to day zero

Relative to day zero (Figure 5.12), samples induced using the DH induction method showed that desmin was downregulated on days three ($2^{-\Delta\Delta CT}$ = 0.87 ± 0.49), six (0.63 ± 0.29), twelve (1.55 ± 1.22) and 24 (0.34 ± 0.07). In samples induced using the 5-Aza induction method, desmin was upregulated on days three (1.008 ± 0.65-fold), six (1.36 ± 1.00), and twelve (6.23 ± 5.57), and was downregulated on day 24 (0.69 ± 0.24). Desmin was upregulated in the non-induced samples on days three (6.25 ± 4.51-fold), six (8.75 ± 7.09), twelve (7.12 ± 6.18) and 24 (1.54 ± 0.83).

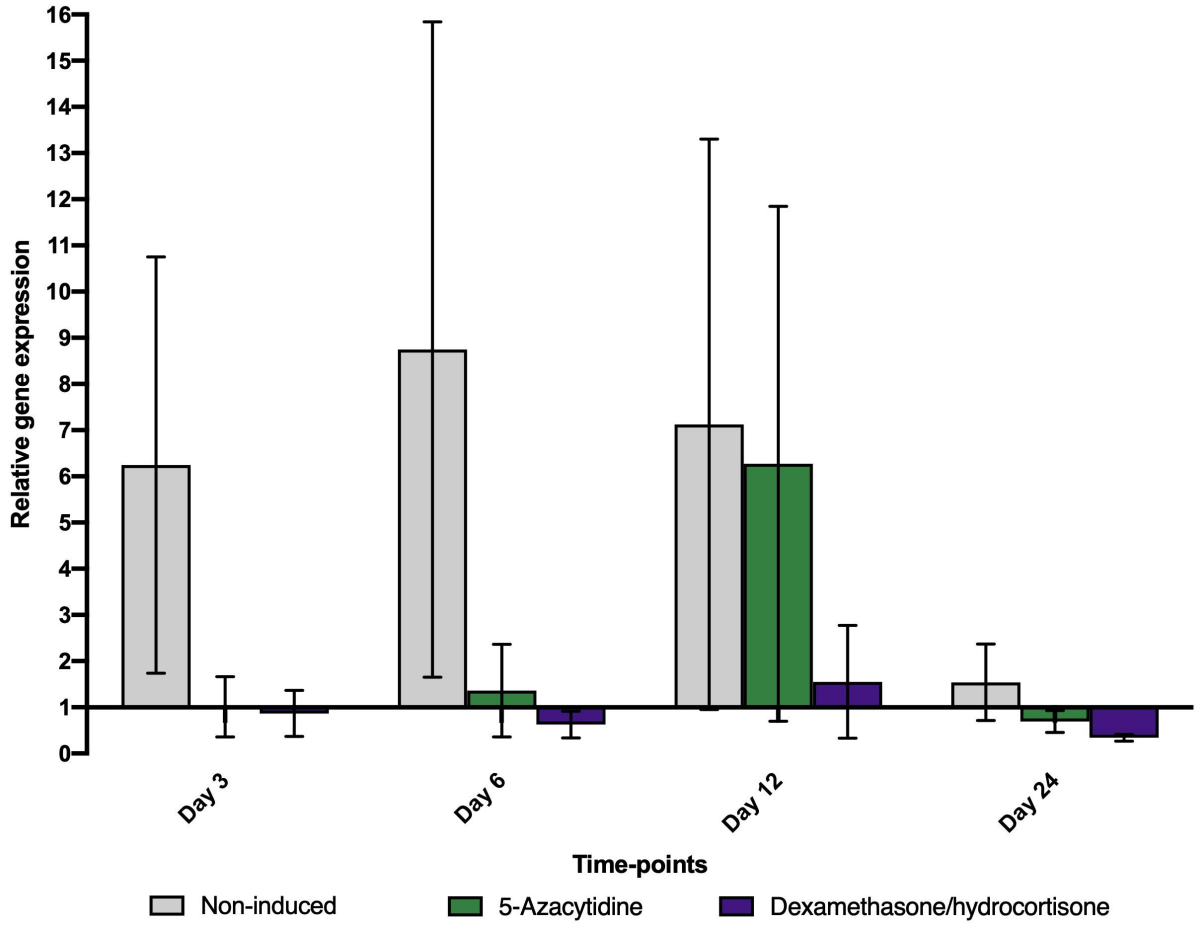

Figure 5.12. Expression of desmin in the induced and non-induced samples relative to day zero.
The relative expression (as determined using the comparative C_T-method) of desmin in the induced samples (dexamethasone/hydrocortisone and 5-azacytidine induction methods) as well as the non-induced samples, is shown over a period of 24 days. Bars represent the mean ± standard error of the mean. The sample size is represented by n=3. The x-axis is shown to intersect with the y-axis at 1 so that bars below the x-axis represent where the expression of desmin decreases as a fold-change relative to day zero, while the bar above the x-axis indicates an increase.

The relative expression of desmin in the DH-, 5-Aza- and non-induced samples was also examined relative to day zero. When comparing the relative expression of desmin between the DH-induced samples compared to the non-induced sample, relative to day zero, no statistically significant change in gene expression was noted on days three (*p-value 0.2000*), six (*p-value 0.2000*), twelve (*p-value >0.9999*) and 24 (*p-value 0.4000*). There was no statistically significant change in desmin expression when comparing 5-Aza -induced samples to non-induced samples, relative to day zero, on

days three (*p-value 0.2000*), six (*p-value 0.4000*), twelve (*p-value >0.9999*) and 24 (*p-value >0.9999*).

The change in the mean expression of desmin between time points within the samples induced using DH was analysed using the Kruskal-Wallis followed by Dunn's post-hoc statistical tests. No statistical significance was found in the expression of desmin between days three and six (*p-value > 0.9999*), days three and twelve (*p-value > 0.9999*), days three and 24 (*p-value > 0.9999*), days six and twelve (*p-value > 0.9999*), days six and 24 (*p-value > 0.9999*) and days 12 and 24 (*p-value > 0.9999*) within the samples induced using the DH induction method. No statistical significance was evident between days three and six (*p-value > 0.9999*), days three and twelve (*p-value > 0.9999*), days three and 24 (*p-value > 0.9999*), days six and twelve (*p-value > 0.9999*), days six and 24 (*p-value > 0.9999*) and days twelve and 24 (*p-value > 0.9999*) within the samples induced using 5-Aza. No significant change in desmin expression was noted between days three and six (*p-value > 0.9999*), days three and twelve (*p-value > 0.9999*), days three and 24 (*p-value > 0.9999*), days six and twelve (*p-value > 0.9999*) and days six and 24 (*p-value > 0.9999*) in the non-induced samples.

In summary, no amplification of MyoD or MyoG was observed and thus could not be analysed (see Figure G.3 for the amplification plots of the positive controls). There was no significant change in the expression of desmin in any condition, relative to both the non-induced sample and day zero and thus, no conclusions could be drawn from this data.

5.5.2. Qualitative assessment of myogenic morphological features

Murine C2C12 myoblasts

Qualitative assessments were performed using brightfield and fluorescence microscopy. C2C12s and PHMs were used as positive controls for myogenic morphology (tube-like cells that are multinucleated). Brightfield micrographs of C2C12s showed notable tube-like cell formation on days three and five post-induction, with visible multinucleation (Figure 5.13). C2C12 cells exhibited notable autofluorescence in brightfield images around myotubes and made it difficult to balance the contrast without losing resolution and the visibility of some morphological features.

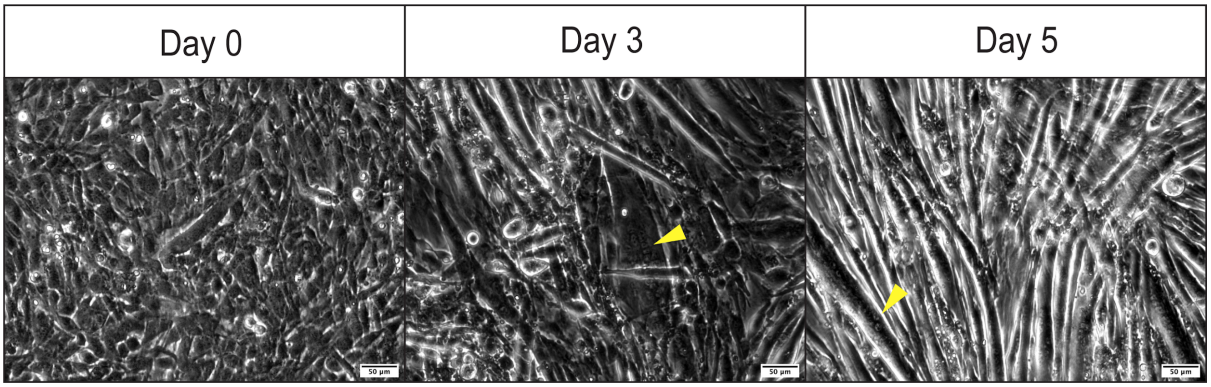

Figure 5.13. Representative brightfield micrographs of differentiating murine C2C12 myoblasts over 5 days.
C2C12s were induced on day 0, where cells appeared to be confluent. Yellow arrows indicate examples of myotubes. Images were taken at 200x magnification, and the scale bar is indicative of 50 µm.

Fluorescent images of C2C12 myoblasts further demonstrated myotubes with visible multinucleation. Myotube boundaries were clearly visible when staining actin filaments with TRITC-phalloidin (Figure 5.14).

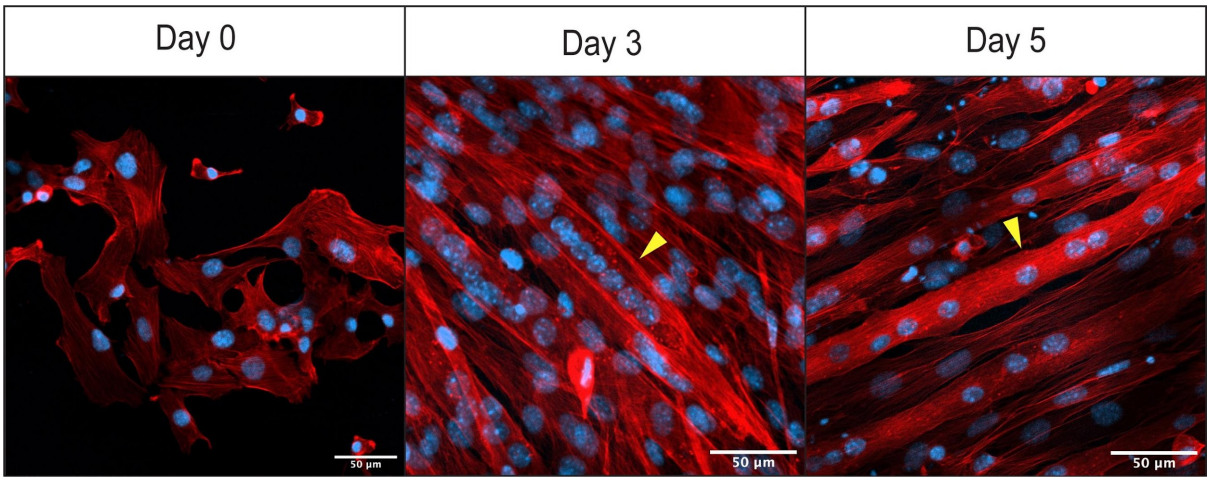

Figure 5.14. Representative fluorescent confocal micrographs of differentiating murine C2C12 myoblasts.
Yellow arrows indicated visible multinucleated myotubes. Actin filaments were visualised with TRITC-phalloidin (red) and nuclei with 4′,6-diamidino-2-phenylindole (DAPI, blue). Images were taken at 200x magnification using the 20x objective. Scale bar = 50 µm.

Primary human myoblasts

In addition to serving as a positive control for myogenic morphology, PHMs were also used to optimise the staining of myogenic targets using ICC. PHMs were differentiated over seven days. Brightfield images of differentiating PHMs indicated some multinucleated myotubes on the day of induction (day zero) with the number of visible myotubes increasing over time on days three, five and seven (Figure 5.15).

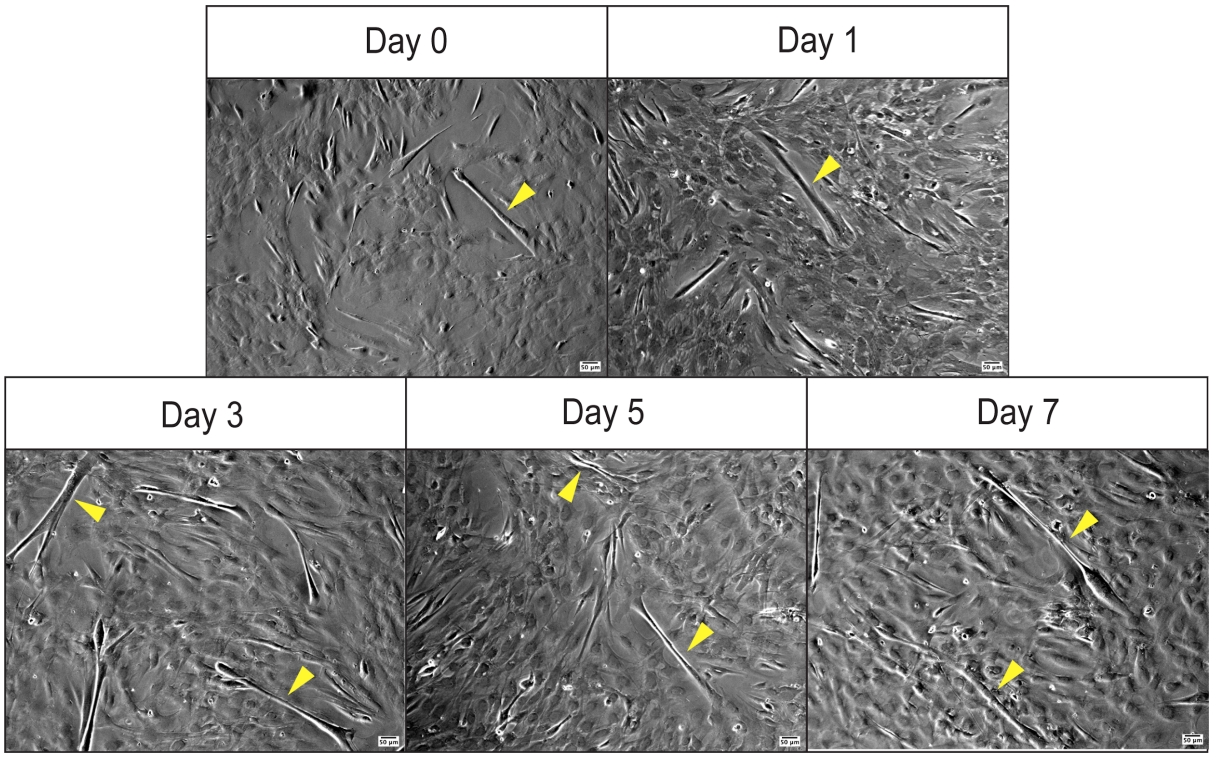

Figure 5.15. Representative brightfield micrographs of differentiating primary human myoblasts.
Yellow arrows indicated visible myotubes. Images were taken at 100x magnification. The scale bar was set as 50 µm.

The staining procedures for the myogenic target proteins Pax 3/7, MyoD, MyoG and desmin was optimised on PHMs, the positive control for myogenic protein targets in this study. PHMs were stained for target proteins on days zero, one, three, five and seven. The intermediate filament desmin was co-visualised with actin fibers, and indicated both differentiating and differentiated cells (Figure 5.16). Desmin was vividly expressed in differentiating myocytes and in differentiated myotubes as meandering fibers that encircle the nuclei. Desmin fibers appeared to converge from either one or both cellular poles.

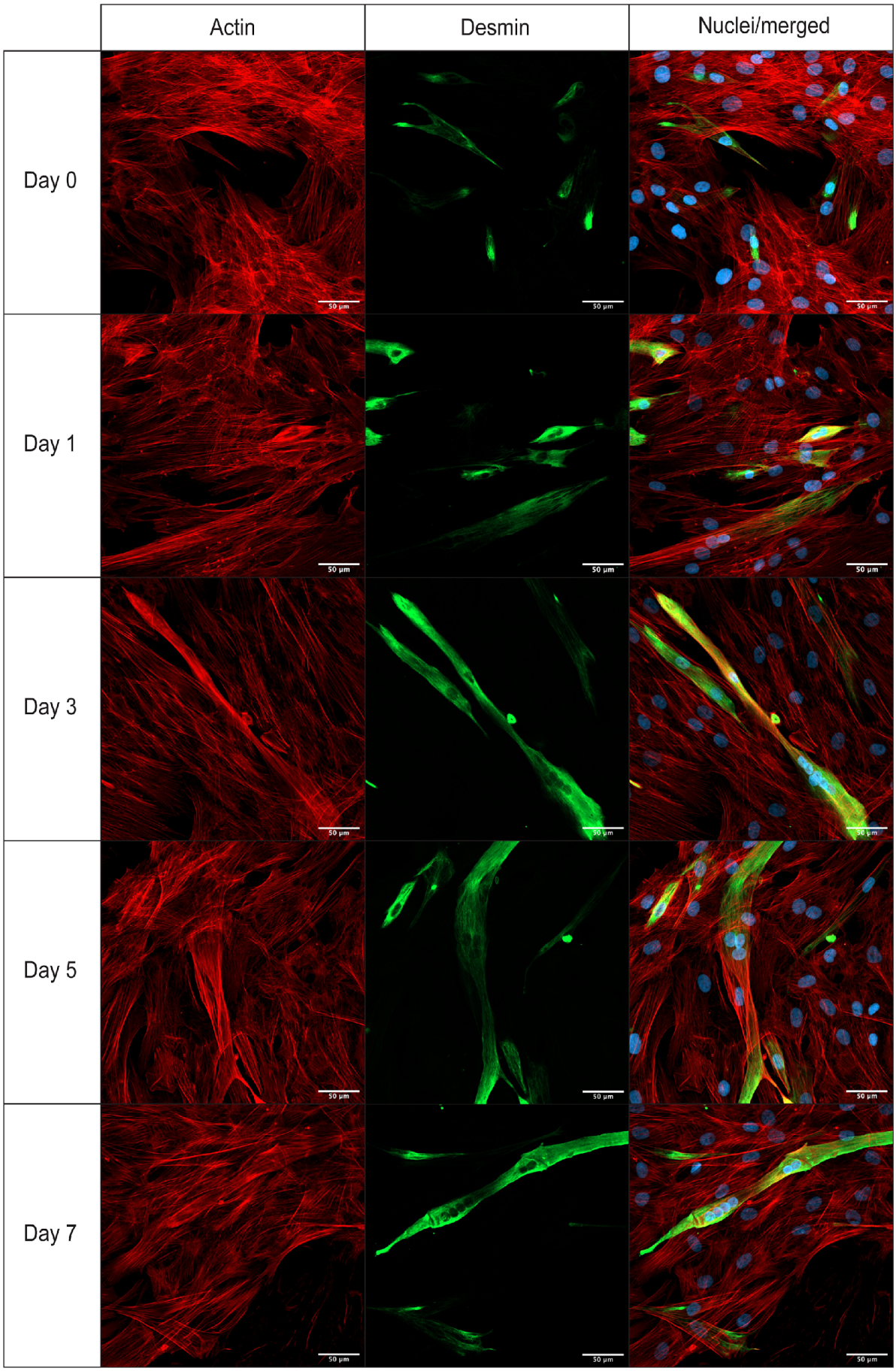
Actin
Desmin
Nuclei/merged
Day 0
Day 1
Day 3
Day 5
Day 7
50 µm

Figure 5.16. Representative micrographs of differentiating primary human myoblasts with visualised actin filaments and desmin.
Primary human myoblasts were stained with TRITC-phalloidin (red) to visualise actin filaments, and rabbit anti-human desmin conjugated to anti-rabbit IgG labelled with Alexa Fluor (AF) 488 to visualise desmin (green). Nuclei (blue) were stained using DAPI. Images were taken on days 0, 1, 3, 5 and 7 using a 20x objective (200 x magnification). The scale bar was set to 50 µm.

Pax 3/7 was detected on days zero, one, three, five and seven. However, it was most detectable on days zero and one with the number of positive nuclei becoming gradually harder to find on days three, five and seven. Additionally, more background was visible on days five (Figure 5.17) and seven, indicating that the signal-to-noise ratio was likely decreasing (Figure 5.17).

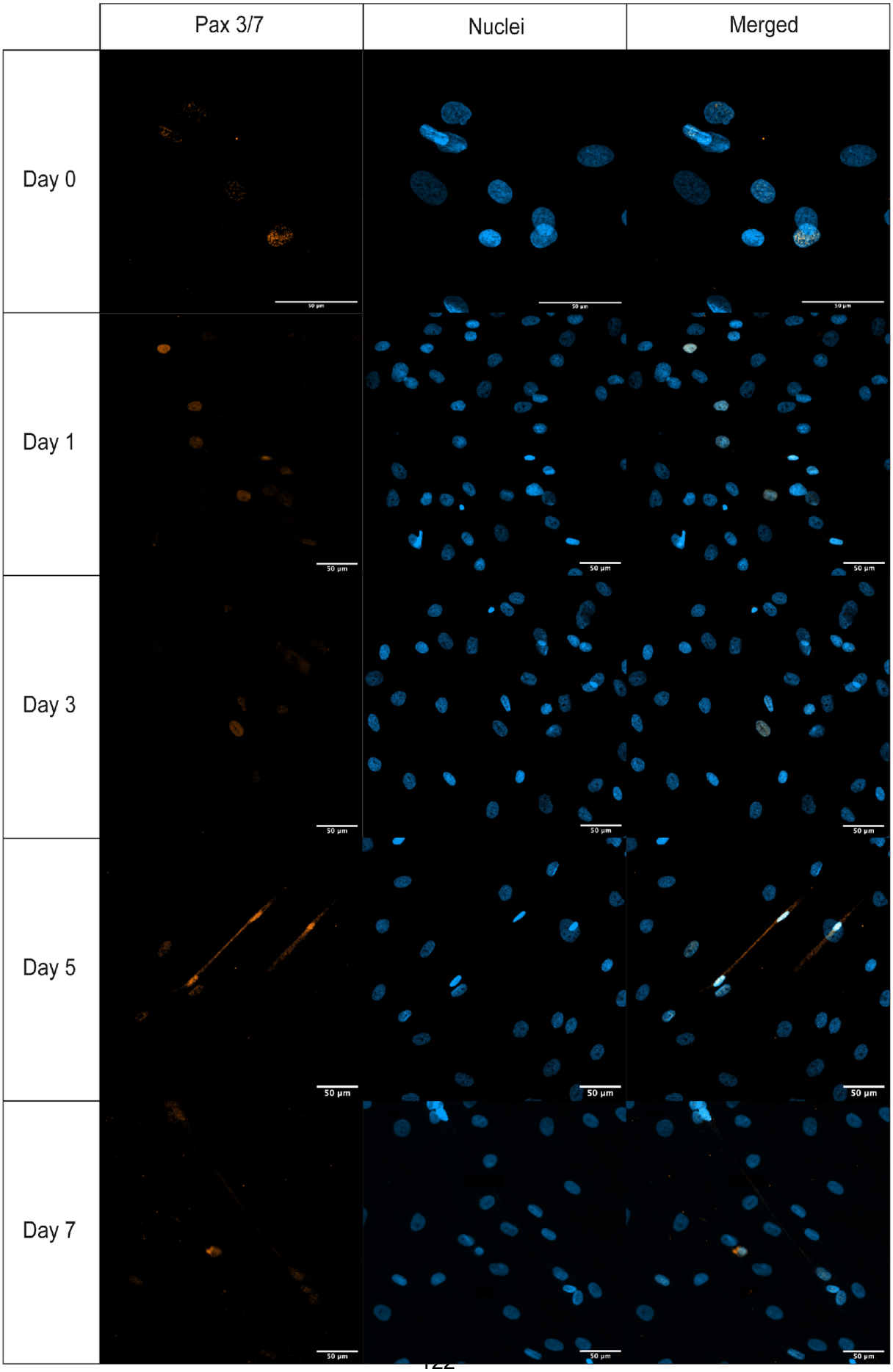
Pax 3/7
Nuclei
Merged
Day 0
Day 1
Day 3
Day 5
Day 7
50 µm

Figure 5.17. Representative micrographs visualising paired box proteins 3 and 7 in differentiating primary human myoblasts.
Paired box proteins (Pax) 3/7 were visualised using anti-mouse IgG conjugated to Alexa Fluor (AF) 555 (orange). Nuclei (blue) were visualised with DAPI. Day 0 micrographs were imaged using the 40x objective (400x magnification), and days 1, 3, 5 and 7 were imaged on the 20x objective (200x magnification). Scale bar = 50 μm.

MyoD and MyoG were detected on days zero, one, three, five and seven. MyoD was abundantly visible on days zero, one and three and became progressively less so on days five and seven (Figure 5.18). As with Pax 3/7, a fluorescent background became more apparent on days five (Figure 5.25) and seven, possibly indicating a waning signal-to-noise ratio and inferred a possible decrease in the expression of MyoD. Additionally, MyoD and MyoG co-expression was evident in multiple nuclei at every time point.

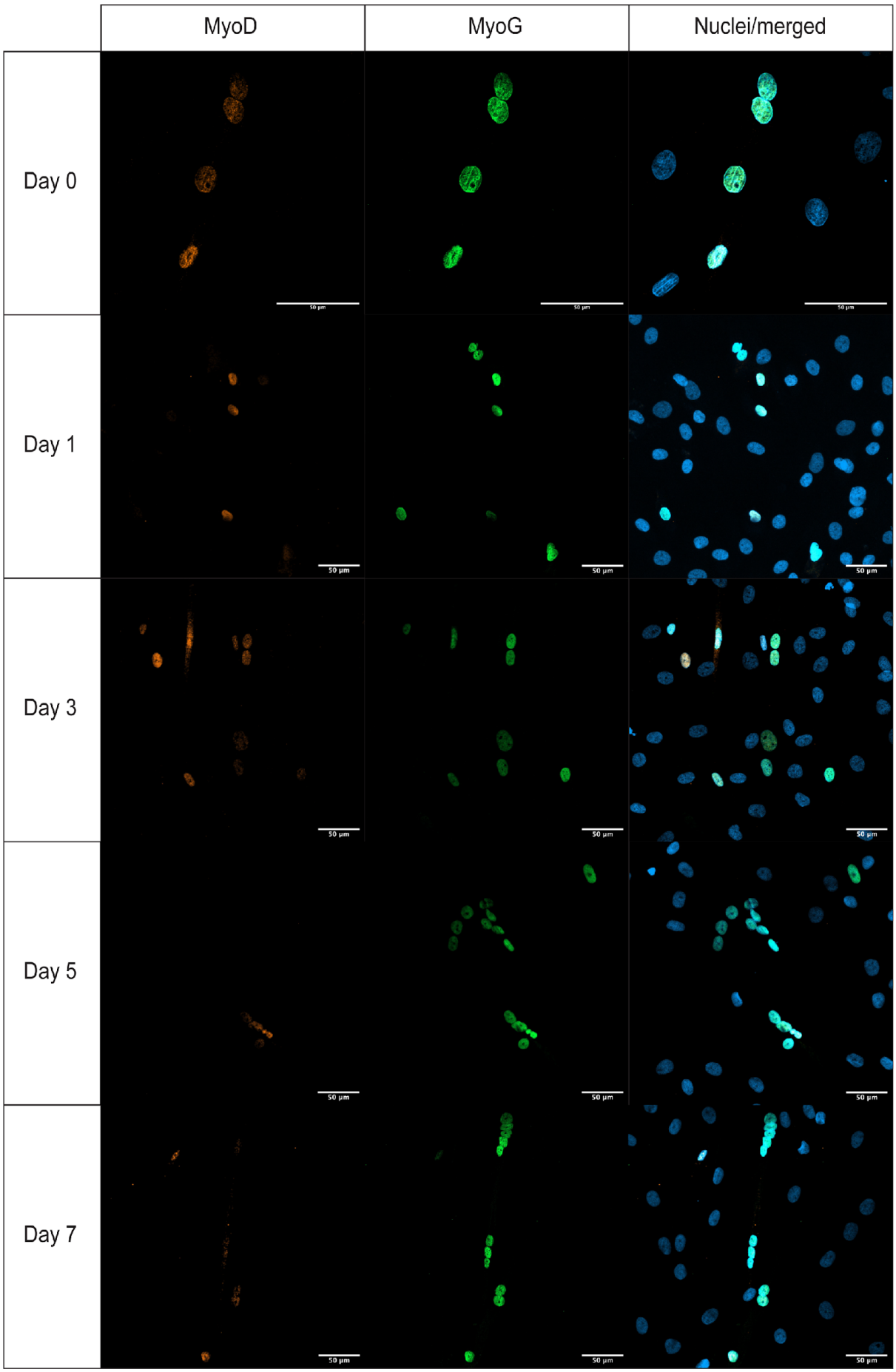
MyoD
MyoG
Nuclei/merged
Day 0
Day 1
Day 3
Day 5
Day 7
50 µm

Figure 5.18. Representative micrographs visualising the transcription factors myogenic differentiation and myogenin in differentiating primary human myoblasts.
Primary human myoblasts were differentiated over a period of 7 days. Myogenic differentiation (MyoD) was visualised using anti-mouse IgG conjugated to Alexa Fluor (AF) 555 (orange). Myogenin (MyoG) was visualised using anti-rabbit IgG conjugated to AF 488 (green). Nuclei (blue) were visualised with DAPI. Micrographs taken on day zero were done using a 40x objective (400x magnification), and those taken on days 1, 3, 5 and 7 with the 20x objective (200x magnification). Scale bar = 50 µm.

Adipose-derived stromal cells

Brightfield microscopy images of ASCs revealed no visible myotube formation at any time point in ASCs induced using either DH or 5-Aza based methods. No myotubes were visible in the non-induced cells (Figure 5.19). ASCs induced with 5-Aza appeared distinctly more elongated post-induction, and were less confluent at every time point when compared to ASCs induced using DH. Additionally, in the 5-Aza induced samples, few cells appeared to have the same three-dimensional tube-like shape with surrounding auto-fluorescence as with the myotubes seen in differentiated C2C12s and PHMs on day twelve post-induction. This was not observed in the DH samples. Interestingly, visible lipid droplet and possible adipocyte formation was observed on days 24, 30 and 42 in ASCs induced using DH, while none was observed in cells induced using 5-Aza. Non-induced ASCs had no notable features over 42 days in culture aside from being overly confluent with cells changing their elongated, spindle shape to a more compact morphology.

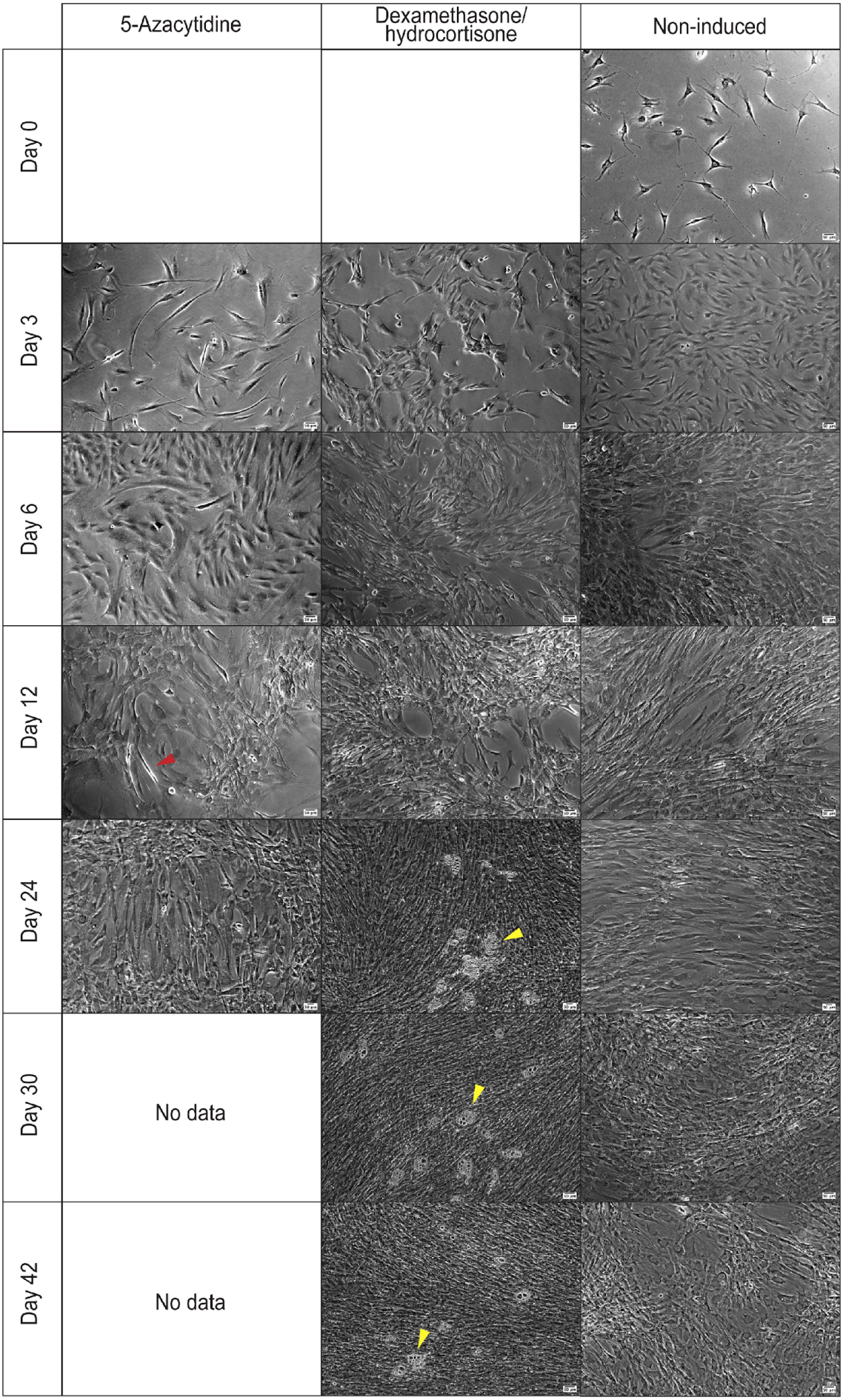
5-Azacytidine
Dexamethasone/ hydrocortisone
Non-induced
Day 0
Day 3
Day 6
Day 12
Day 24
Day 30
Day 42
No data
No data

Figure 5.19. Representative brightfield micrographs of differentiating adipose-derived stromal cells.
Adipose-derived stromal cells were induced using either dexamethasone/hydrocortisone (DH) or 5-azacytidine (5-Aza). A non-induced control was included. The red arrow indicated a tube-like structure in ASCs induced using 5-Aza on day 12. Yellow arrows indicated visible lipid droplet formation in ASCs induced using DH on days 24, 30 and 42. Images were taken at 100x magnification. The scale bar was set as 50 µm.

ASCs expressing desmin were detected at all time points for both the 5-Aza and DH-induced cells (Figure 5.20). Although it is important to note that the micrographs in Figure 5.20 include representative images where desmin staining was visible in ASCs, it does not reflect the frequency at which it was present when images were taken at random fields of vision. Few cells actually expressed desmin when entire coverslips were examined.

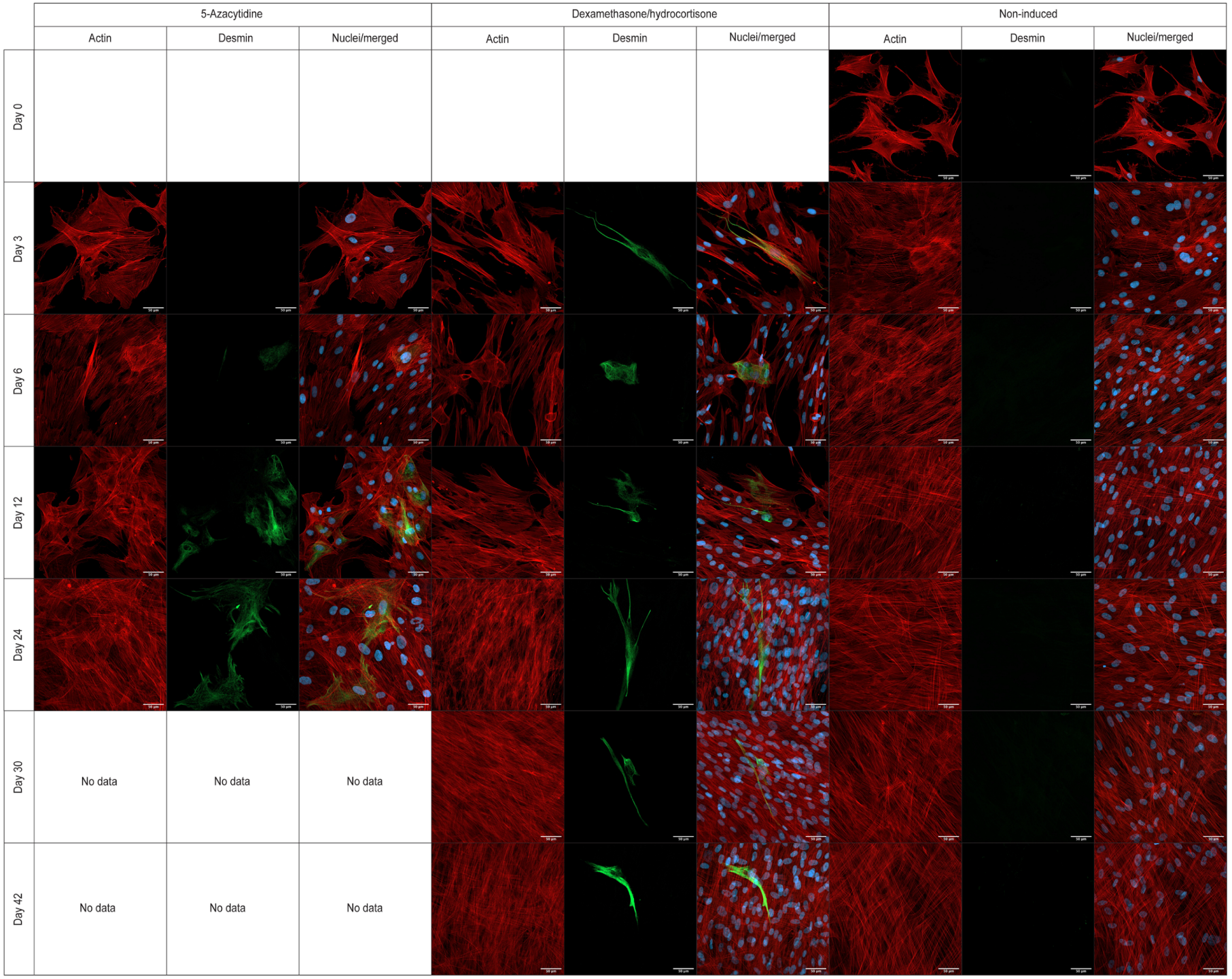
5-Azacytidine
Dexamethasone/hydrocortisone
Non-induced
Actin
Desmin
Nuclei/merged
Day 0
Day 3
Day 6
Day 12
Day 24
Day 30
Day 42
No data
No data
No data
No data
No data
No data

Figure 5.20. Representative micrographs showing actin filaments and desmin in differentiating adipose-derived stromal cells.
Adipose-derived stromal cells (ASC) were differentiated over 24 days when ASCs were induced using 5-azacytidine and 42 days when induced with DH. Actin filaments were visualised using TRITC-phalloidin (red). Desmin was stained using anti-rabbit IgG conjugated to AF 488 (green) and nuclei (blue) were stained with 4′,6-Diamidino-2-phenylindole (DAPI). Micrographs taken with the 20x objective (200x magnification). Scale bar = 50 µm.

Pax 3/7 was detected in ASCs on days six, twelve and 24 post-induction with 5-Aza and days twelve, 24 and 30 post-induction with DH and in non-induced cells. No Pax 3/7-positive cells were visible on day 42 post-induction with DH or in the non-induced cells (Figure 5.21). The absence of the marker was likely due to a decrease in the expression of Pax 3/7.

No MyoD or MyoG was visible in differentiating ASCs at any time point (Figure 5.22).

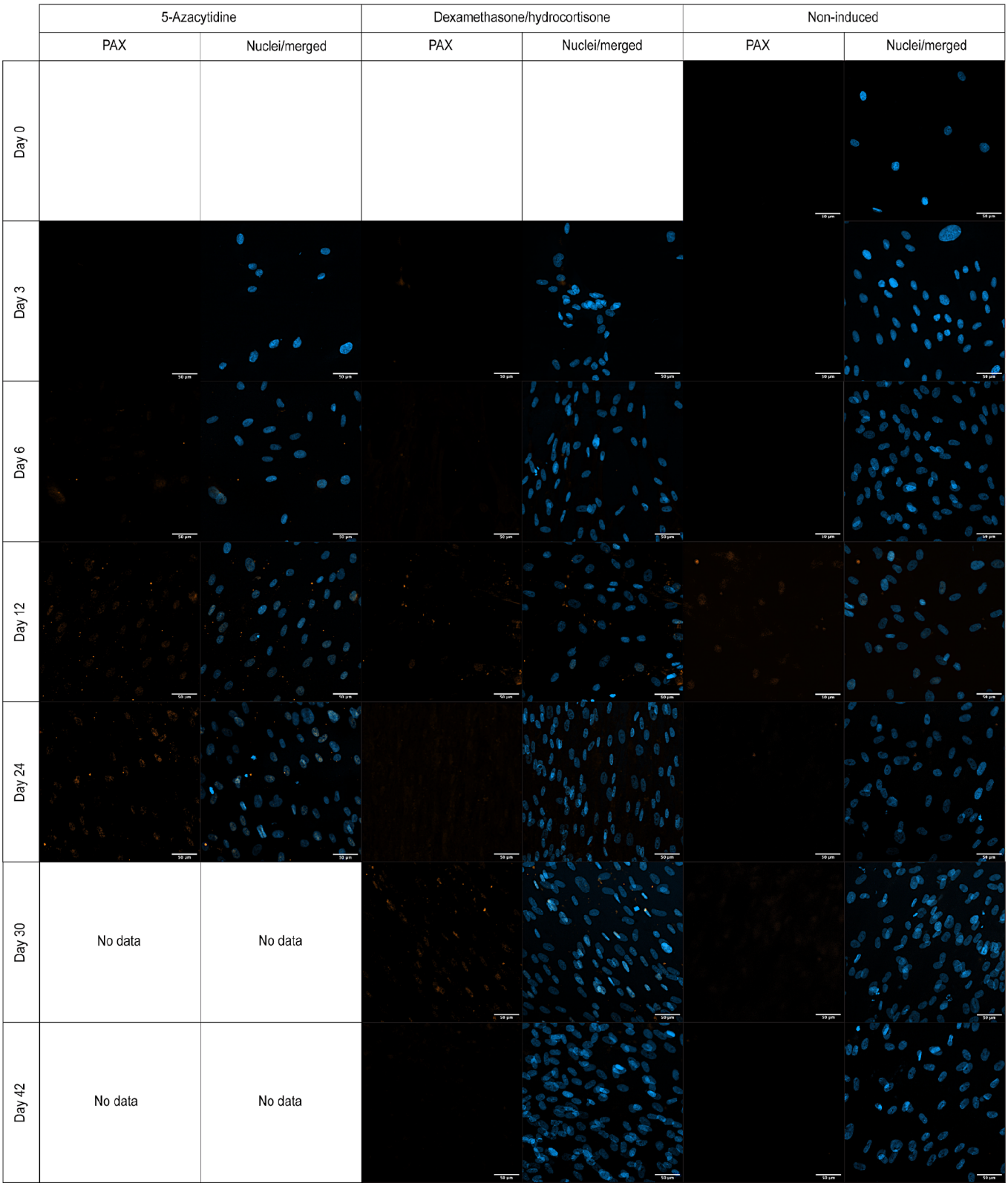

Figure 5.21. Representative images visualising the paired box proteins 3/7 in differentiating adipose-derived stromal cells.
ASCs induced using 5-azacytidine were examined over 24 days, while those induced using dexamethasone/hydrocortisone, as well as the non-induced control cells were investigated over 42 days. Paired box proteins (Pax) 3/7 were visualised in cells using anti-mouse IgG conjugated to Alexa Fluor (AF) 555 (orange). Nuclei were stained blue with DAPI. Micrographs were imaged with the 20x objective (200x magnification). Scale bar was set to 50 µm

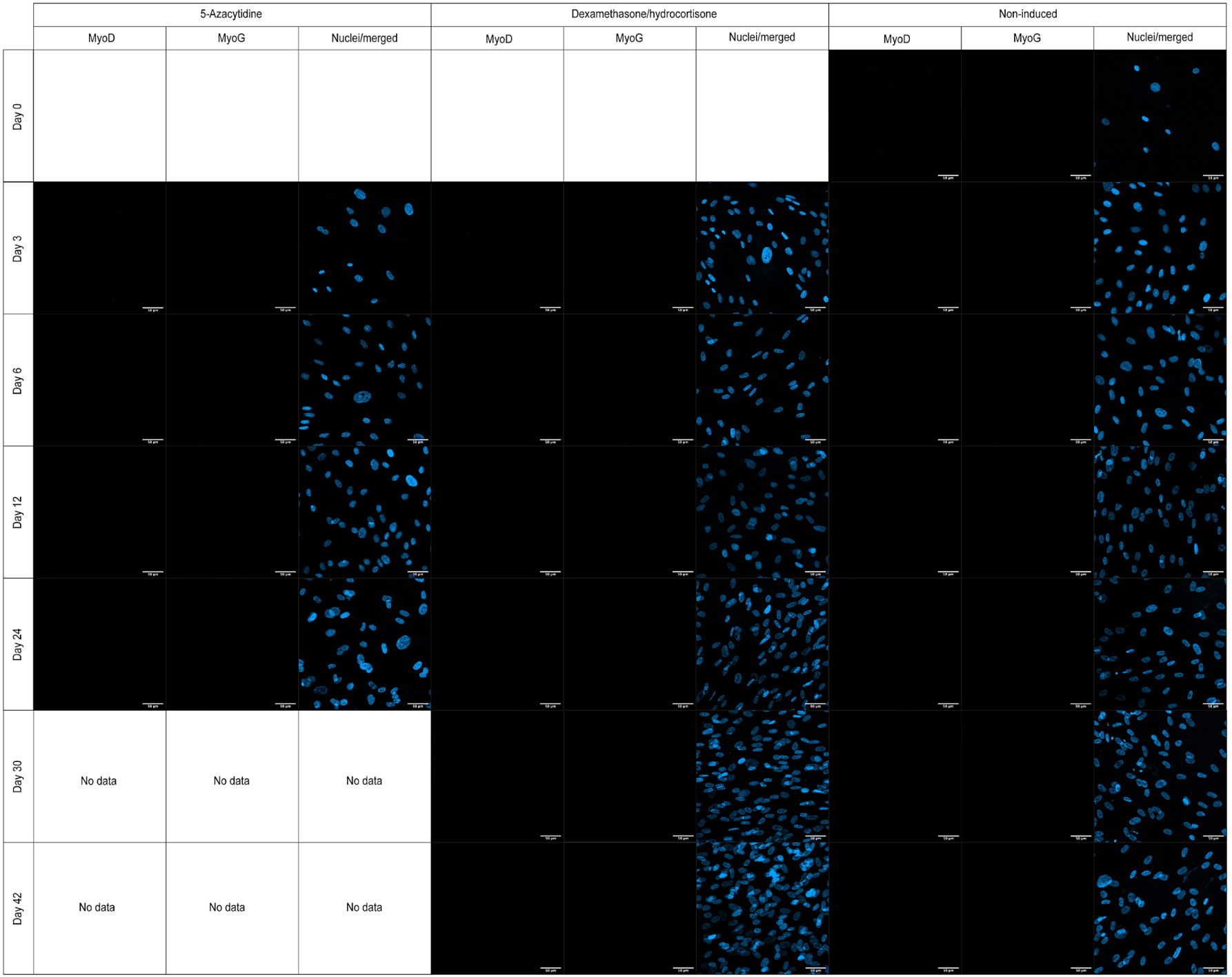
5-Azacytidine
Dexamethasone/hydrocortisone
Non-induced
MyoD
MyoG
Nuclei/merged
MyoD
MyoG
Nuclei/merged
MyoD
MyoG
Nuclei/merged
Day 0
Day 3
Day 6
Day 12
Day 24
Day 30
Day 42
No data
No data
No data
No data
No data
No data

Figure 5.22. Representative images showing the transcription factors myogenic differentiation and myogenin in differentiating adipose-derived stromal cells.
Myogenic differentiation (MyoD) was stained orange using anti-mouse IgG conjugated to Alexa Fluor (AF) 555. Myogenin (MyoG) was stained green using anti-rabbit IgG conjugated to AF 488. Nuclei (blue) were stained with 4′,6-Diamidino-2-phenylindole (DAPI). Micrographs taken at 200x magnification with the 20x objective. Scale bar was set as 50 µm.

Fusion index

The fusion index was calculated according to Equation 5.6. The fusion index for C2C12s (Figure 5.23A) was determined to be 1.36% ± 3.03 on day zero, 55.70% ± 23.10 on day three and 76.22% ± 8.45 on day five. There was a significant increase in myotube fusion in C2C12s on day five (p-value < 0.0100) post-induction. The fusion index for PHMs (Figure 5.23B) was determined for day zero (0%), day one (20.67% ± 12.93) on day three (29.49% ± 11.72), day five (32.96% ± 11.51) and day seven (23.03% ± 12.86). There was a significant increase in myotube fusion on days three (p-value < 0.0500) and five (p-value < 0.0100). The fusion index for ASCs was 0% at all time points, as no multinucleated myotubes were visible on the confocal fluorescence images.

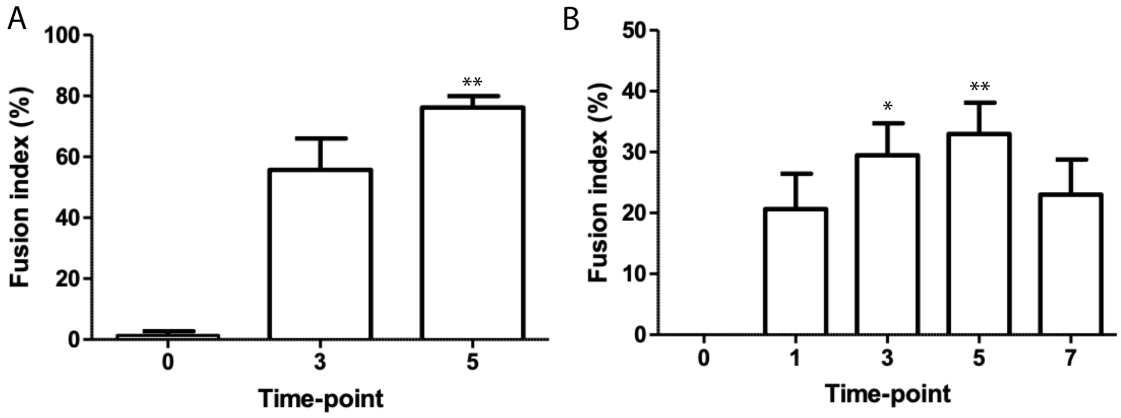

Figure 5.23. Fusion indices as determined for C2C12 myoblast and primary human myoblast differentiation.
A. C2C12 myoblasts were differentiated over a period of 5 days. There was a significant increase in C2C12 fusion on day 5. B. Primary human myoblasts were differentiated over a period of 7 days. Primary human myoblast fusion increased significantly on days 3 and 5 post-induction. Significance was demonstrated as an asterisk (*), where p-value < 0.05*, p-value < 0.0100** and p-value < 0.001***. Bars represent the mean ± standard error of the mean. The sample size is represented by n=5 (technical replicates).

C2C12s and PHMs were both used as positive controls in this study for myogenesis, and were demonstrated to differentiate into multinucleated myotubes.

5.6. Discussion and conclusion

The expression of myogenic target proteins Pax 3/7, MyoD, MyoG and desmin were qualitatively confirmed on the positive control, PHMs, to show that the primary and secondary antibodies stained their protein targets specifically and effectively. All protein targets were detected in PHMs differentiated over seven days, with Pax 3/7 and MyoD appearing to visually decrease towards day five and seven. MyoG was visible at all time points and was co-expressed with MyoD, as MyoD induces the expression of MyoG (discussed in Chapter 2, section 2.7).[98] The presence of MyoG indicated that the transcriptional programming reached a point of no return in muscle differentiation whereby myoblasts exits the cell cycle and fuse with other MyoG-positive cells to form myotubes.[88,100]

PHMs expressing desmin appeared to increase steadily over seven days with larger desmin-positive cells and multinucleated myotubes becoming visible. Thus, PHMs expressed myogenic factors, and differentiated in a manner similar to what has been reported in other studies involving PHM differentiation.[226-229] The fusion index was used to evaluate myoblast fusion which was 0% at the end of the differentiation timeline in ASCs, as there were no myotubes visible. C2C12 myoblasts had the highest fusion index (79%), followed by PHMs (23%) at the end of their respective differentiation timelines.

In this study, we attempted to differentiate ASCs into a myogenic lineage using the DH and 5-Aza-induction methods, and this was compared to a non-induced control. RT-qPCR was used to quantitatively assess the expression of desmin, MyoD and MyoG mRNA over time (Table 5.7).[230] As MyoD and MyoG were not detected by RT-

qPCR at any time point, this data was not analysed further. Desmin was amplified in all three biological replicates in every condition, at every time point. However, no statistically significant changes in gene expression were noted when comparing the DH and 5-Aza induction methods relative to either the non-induced sample or day zero, at any time point. Relative to the non-induced conditions the fold increase in the expression of desmin for both methods was negligible (less than 2-fold). However, in the samples induced using 5-Aza, desmin expression steadily increased up until Day twelve, to 6.27-fold before decreasing again on day 24. Interestingly, the highest relative expression was recorded in the non-induced samples, where the trend indicated desmin expression was highest on day three (6.25-fold), day six (8.75-fold), Day twelve (7.12-fold) and 1.54-fold on day 24.

The reasons for the changes in the levels of expression are not known. More samples would need to be investigated to elucidate what the implications may be.

Table 5.7. Summary of RT-qPCR trends observed in the fold-expression of myogenic factors after adipose-derived stromal cell induction.
Green arrows represent an increase/decrease in the fold-change in expression in ASCs induced with 5-azacytidine; purple arrows represent ASCs induced with dexamethasone/hydrocortisone and orange represent the non-induced sample. Coloured dots represent no change from baseline, black dots represent no amplification of the target.

Relative to the non-induced sample					
	Day 0	Day 3	Day 6	Day 12	Day 24
MyoD	●●●	●●●	●●●	●●●	●●●
MyoG	●●●	●●●	●●●	●●●	●●●
Desmin	●●	↓ ↓	↓ ↓	↑ ↓	↓ ↓
Relative to day zero					
	Day 0	Day 3	Day 6	Day 12	Day 24
MyoD	●●●	●●●	●●●	●●●	●●●
MyoG	●●●	●●●	●●●	●●●	●●●
Desmin	●●●	↓ ↓ ↑	↑ ↓ ↑	↑ ↑ ↑	↓ ↓ ↑

The expression of desmin has been shown to steadily increase over time in ASCs that have been induced into a myogenic lineage by previous studies.[133] Trends in 5-Aza-induced ASC differentiation in this study adhered to some characteristics of previously published data with respect to desmin expression, namely that desmin expression was upregulated on day six relative to day zero and on day twelve relative to both day zero and to non-induced samples.[133,158] This observation does not provide any conclusive evidence that 5-Aza is a more efficient inducer of differentiation, as no statistically significant difference was observed, but does point to a trend that could be better understood with a larger sample size. No further comments could be made on the expression kinetics of myogenic genes in this study, with respect to ASCs induced using either induction method.

The proteins MyoD and MyoG were not detected during ASC myogenesis at any time point or under any culture condition. However, both Pax 3/7 and desmin were confirmed using ICC. Desmin is one of the first detectable markers of myogenesis, as is Pax 3/7 (Chapter 2, Figure 2.9). Pax 3 and 7 are considered master regulators of early myogenesis, and regulate the expression of MyoD (the master regulator that commits cells to the myogenic transcriptional program).[78] MyoD then induces the expression of MyoG.[90] The expression of desmin on the other hand appears to be regulated by two up-stream E-box sequences that have binding affinity for both Myf 5 and MyoD. Desmin is upregulated before these two factors and maintains its expression.[106]

It is possible that MyoD was not detected by ICC because it was below the limit of detection. MyoG was not detected with ICC possibly since it is a moderate to late marker for myogenic differentiation, and the ASCs did not progress that far down the myogenic pathway. The results obtained from ICC with respect to the expression of desmin seemed to support the results obtained from RT-qPCR in the sense that desmin mRNA was detected in every sample at every time point. However, the ICC results did not support the data generated by analysing the relative gene expression of desmin in the non-induced sample when normalised to day zero. In this case, the non-induced sample actually showed the highest fold-increase in the expression of desmin and yet the protein was not visible on the fluorescent images. This is possible, as it has been shown that mRNA transcription does not necessarily correlate with protein expression.[231-233] A recent study by Wolmarans *et al.* (2021)[234] identified a contractile cell subpopulation, with markers consistent with those expressed by pericytes and vascular smooth muscle cells within the heterogeneous ASC population. This is likely to be the reason why cells that expressed desmin mRNA were present in the non-induced sample. This then raises the question as to whether the cells that displayed some myogenic differentiation were truly ASCs and not simply vascular smooth muscle cells that were present during the initial ASC isolation and in subsequent cell populations that were used in the course of this study.

With respect to relative gene expression analysis in this study, all *p*-values were greater than 0.05. In some cases, SEMs were relatively large in proportion to the sample means. What this indicated was that the sample size was too small to overcome the biological variation between samples with regard to providing statistically meaningful results. The combination of these two factors meant that statistically, no conclusion could be made as to which of the myogenic differentiation media was most effective at inducing myogenesis with respect to the non-induced and day zero controls. In order to make such a conclusion in the future, the solution might be for future studies to increase the sample size from three biological replicates to at least five or more. Addressing inter-sample variation might be more difficult, as ASCs are primary cells with an inherent heterogeneity. A solution might be to sort cells prior to conducting differentiation studies, and for cells to be excluded based on markers expressed on other cell populations such as CD56 (skeletal muscle cell precursor), CD146 (a pericyte marker) or α-smooth muscle actin (smooth muscle cells).[235-237]

In this study, ICC micrographs were only qualitatively assessed. However, in order to gain maximal data from fluorescence images, these might also be semi or quantitatively assessed depending on the application.[238] However, to do this, micrographs need to be visualised under the same conditions and software settings. In this study, it was not possible to generate fluorescence images using the same software settings. This was due to several complications that included slight changes to laser power, gain and aperture in order to visualise every element as clearly as possible. While doing this may result in clearer images, it limits the analysis of these images to qualitative investigation. To try and work around this, other solutions were explored but these also had inherent limitations, and ultimately could not be used (Table 5.8).

Table 5.8. Methods that could potentially have been used to quantitatively assess fluorescence images.
Several methods were considered in order to assess images quantitatively, but were met with several limitations that have been listed below.

Image data analysis method	Limitations
Determining the % of cells positive for specific markers relative to the total number of cells	● The frequency of cells positive for markers such as desmin captured within different fields of view was exceptionally low. Thus, if the analysis was based on 5 images that all included positive cells (as was the case in this study) the results would not accurately represent the entire data set ● Artefacts of cell culture may influence this result because: ○ ASCs are heterogenous primary cells with differing proliferation rates and differentiation capabilities. Therefore, some coverslips may have more cells, and subsequently more marker-positive cells ○ Slight errors in seeding cells may cause some coverslips to start with more or less cells ○ Uneven adhesive coating of the coverslips may cause cells to adhere better in some sections and lift in others, resulting in a different number of cells
Determining the absolute number of cells per coverslip that are positive for a specific marker	● Artefacts of cell culture (as above) ● The coverslips will be subjected to long exposure times in order to detect positive cells, which may cause the fluorescence to quench, and some low-signal targets to be lost. ● The counter may simply miss positive cells whilst going through the coverslip ● The total number of nuclei per coverslip would need to be determined (and it was not done in this study), in order to correct for and normalise culturing artefacts
Measuring fluorescence intensity	● Laser power and gain were constantly adjusted in this study, which meant that no image could be compared in terms of fluorescence intensity

	● Tetramethylrhodamine (TRITC)-phalloidin (usually imaged on the 561 nm laser of the confocal microscope) was slightly detectable in the 488 nm laser channel. This could be corrected for by simply reducing the gain, laser power and adjusting contrast settings but it could not remove the background fluorescent signal from the metadata. Thus, any values obtained from fluorescent intensity would have included the fluorescence from the TRITC-phalloidin.
Normalising histograms	● Histograms generated using the metadata of every image could have been normalised to all be within the same range to make the intensities relative to each other and make them comparable ● This would generate relative pixel values within each image in terms of their 'brightness' ● This method was limited because it assumes that the distribution of light intensity values for each image would follow a normal distribution. This in turn could be influenced by various staining or morphological irregularities such as the formation of lipid droplets, the fluorescence of cell debris or contaminating dust or clumps that could spike or cause irregular fluorescence (outlier pixel values) ● Time and labour intensive to do whilst also requiring a specialised skill set (computational photography)

According to the ASC myogenesis modelling studies published by Huri *et al*. (2014)[158] and Deshpande and Spector (2017)[160] (Chapter 2, Figure 2.10), ASCs that adopt the myogenic program will first express Pax 3/7 (stage zero and one), then desmin (stage two, three, four and five), while MyoD becomes expressed during stage three of differentiation, and MyoG during stage four and five. Based on the presence of both desmin and Pax 3/7, ASCs in this study thus only differentiated as far as stage two. Trends in desmin expression indicated that day twelve post-induction may signal a change in the myogenic transcriptional programming. Desmin was increased on this day for the 5-Aza-based induction method relative to the non-induced sample. Similarly, relative to day zero, desmin expression appeared to peak with both induction methods as well the non-induced methods on day twelve However, as previously discussed, the lack of statistical significance does not provide any conclusive evidence, and future studies should further investigate the trend that was observed in this study. For myogenic differentiation to progress *in vitro,* Huri and collogues[158] as well as Deshpande and Spector (2017)[160] suggested that both MyoD and later MyoG needs to accumulate above a certain threshold (the definition of which remains unclear from the literature). It is then possible to infer based on their research, that MyoD did not reach the necessary threshold to further propagate myogenic differentiation in the ASCs induced to differentiate in this study.

ASCs were expanded in pHPL, differentiated using two previously published myogenic induction methods, and assessed quantitatively using RT-qPCR and qualitatively using ICC. Only the muscle-specific intermediate filament desmin was confirmed using RT-qPCR and ICC, while the presence of both desmin and Pax 3/7 was confirmed using ICC. This indicated that ASC myogenesis only progressed as far as stage two. No conclusions could be drawn from the results obtained in this study due to high inter-sample variability and low sample number.

This concludes chapter 5. The following Chapter 6 concludes the dissertation.

Chapter 6: Concluding remarks and future perspectives

Chapter 6 includes an in-depth discussion of particulars highlighted in the previous chapters. This chapter concludes the dissertation with all conclusions, limitations and future perspectives discussed.

The multipotent properties of ASCs have made them attractive for cell-based therapies and regenerative medicine. ASCs can classically, upon exposure to various combinations of chemical compounds, differentiate into adipogenic, osteogenic and chondrogenic cell types. Myogenesis of human ASCs has previously been demonstrated by few researchers (Chapter 2, Table 2.3) using dexamethasone/hydrocortisone or 5-Aza differentiation media, and as such there is little literature to draw from. The aim of this study was to optimise the myogenic differentiation of ASCs. ASCs were isolated from adipose tissue, immunophenotyped, expanded and induced to differentiate over either 24 days (5-Aza-based method) or 42 days (dexamethasone/hydrocortisone-based method). Only the two previously published methods were considered, and not the individual constituents. The subsequent myogenic differentiation was then assessed using RT-qPCR and ICC.

Cells used in experiments were investigated using flow cytometry to ensure that they expressed surface markers characteristic of ASCs. The immunophenotype of ASCs used in this study was $CD90^{+}CD73^{+}CD44^{+}CD36^{+}CD34^{variable}CD105^{+}CD45^{-}$. The largely negative expression of CD105 observed in the ASCs of this study did not compare to studies done previously at the ICMM.[164,177,203] As previously discussed in Chapter 4 (section 4.6), the main variable considered with respect to this finding was the addition of AmB. Briefly, ASCs may have been affected due to the AmB added to the expansion and induction media to prevent fungal contamination of the cells. A study by Skubis *et al*. (2017)[205] reported downregulation in the expression of CD105 in ASCs treated with AmB.

Different liposuction methods were also considered. However, studies have shown that while different liposuction techniques may influence ASC yield, they do not influence viability, proliferation, or differentiation capacity.[239-241] What was not investigated in this study was whether the downregulation of CD105 observed in the majority of cells, affected differentiation. Incidentally, a study by Jin *et al.* (2009)[242] suggested that the downregulation of CD 105 is associated with multilineage differentiation. However, no studies have been done with respect to the expression of any phenotypic marker and ASC myogenic potential. This represents a research area that future studies could potentially explore, as a study from Anderson *et al.* (2013)[243] involving MSCs from other sources has suggested that $CD105^-$ MSCs may have higher adipogenic and osteogenic potential than $CD105^+$ MSCs. If CD105 can affect the potential of MSCs to differentiate into the classical lineages, then it may also affect the non-classical myogenic lineage, but that hypothesis has yet to be investigated.

Myogenesis was successfully achieved using the positive controls (C2C12 and PHMs). The PHMs expressed all myogenic markers over the 7-day differentiation period, and this allowed myogenic assays to be optimised (Appendix G). The fusion index indicated efficient differentiation was taking place in both cultures, with C2C12s achieving the highest fusion followed by the PHMs. Both cell lines had clear multinucleated myotube formation, as shown by brightfield and fluorescent micrographs. In contrast, the ASCs did not effectively differentiate into a myogenic lineage. RT-qPCR and ICC results indicated that the ASCs in this study did not express MyoD or MyoG at any time point or under any induction condition. Desmin was the only myogenic target that was detected using both RT-qPCR and ICC, while Pax 3/7 was observed from day six by ICC using both induction methods (Chapter 5, Table 5.11). The findings in this study with respect to the expression of MyoD and MyoG were contrary to what has been reported in previous studies on human ASC myogenesis for both induction methods, while desmin was the only marker expressed similarly.[130,131,133,135,136,158,159,244] Most studies reported the presence of MyoD, MyoG and desmin within one week of induction when induced using the dexamethasone/hydrocortisone-based method.[130,131,136]

In this study, MyoD and MyoG were not detected, while desmin and Pax 3/7 were confirmed in the first week after differentiation. In other studies where ASCs were induced using the 5-Aza-based method, the presence of Pax 3/7 was confirmed in the first week of differentiation and became less frequently detected in cells thereafter. MyoD was confirmed after two weeks and desmin within one.[133,135,158,159,244] The results indicate that the PHMs differentiated to at least stage 6 (multinucleated myotubes were visible) whilst ASCs only reached stage two according to the models (Chapter 2, Figure 2.10) described by Huri *et al*. (2014)[158] and Deshpande and Spector (2017).[160]

Literature in which human ASCs have been differentiated into a myogenic lineage is scarce. The studies that reported this process in human cells are summarised in Chapter 2, Table 2.3. In addition, the techniques, induction media and myogenic markers investigated differ, making robust comparisons between studies challenging. The lack of standardisation and challenges in experimental reproducibility in this study as well as the literature, speak to well-known limitations associated with ASCs (discussed in Chapter 2). These limitations have yet to be addressed, and future studies on ASC myogenesis should endeavour to bring more standardisation with respect to different assays used, reference gene selection in RT-qPCR, and target molecules which need to consistently be included and differentiation culture procedures. However, methods recently outlined by Huri *et al.* (2018)[159] provide a potential basis for standardisation of ASC myogenesis, but this has yet to be applied routinely.

Part of the objectives of this study were to initiate a GMP-compliant protocol by expanding ASCs in pHPL, a human alternative to FBS. Although exploring human alternatives was not the focus of this study, previous studies in our laboratory have shown it to be an effective medium supplement for expansion.[164] Additionally, studies have not provided conclusive evidence that it significantly affects ASC differentiation.[170-172] However, these studies focused on classical lineages and not

myogenesis. With the limited differentiation observed in this study, it cannot be excluded that expanding ASCs in pHPL did not potentially affect their myogenic differentiation ability. Dessels *et al.* (2019)[245] reported significant differences in the transcriptome of ASCs expanded in medium supplemented with pHPL as compared to those expanded in medium containing FBS. Specifically, these differences were observed in genes involved in the cell cycle, division, and proliferation, while ASCs propagated in FBS displayed an upregulation in genes involved in the formation of extracellular matrix.[245] Even though myogenic differentiation occurred in medium supplemented with FBS and HrS, it is not clear whether the transcriptomic differences brought about during the expansion phase persist even after induction. This is especially relevant when considering the expression of myogenic regulators such as MyoD, which are closely linked to the cell cycle (discussed in Chapter 2).[96] This represents another research area future studies could investigate in terms of medium supplementation and lineage-specific effects. Future studies involving ASC myogenesis should first focus on ASC differentiation using media supplemented with FBS only during the expansion phase, and without the addition of AmB in order to elucidate whether the aforementioned two variables might affect myogenic differentiation.

In Chapter 2, MSC heterogeneity was described in terms of tissues of origin and differentiation capacity. BM-MSCs are known to have higher osteogenic and chondrogenic potential than ASCs.[246] ASCs display more efficient adipogenic differentiation potential than BM-MSCs.[247] In single-cell and bulk-RNA studies, Zhou *et al.* (2019)[248] demonstrated that ASCs have lower transcriptomic heterogeneity when compared to BM-MSCs. The idea that cells can be genetically 'primed' to differentiate into a particular lineage by the conditions in their microenvironment is not new. Xie *et al.* (2013)[249] demonstrated that equine ASCs and BM-MSCs had similar tri-lineage differentiation potential. However, adipogenic genes were upregulated to a greater degree and more rapidly in ASCs whilst osteogenic genes were highly upregulated BM-MSCs. Furthermore, Monaco *et al.* (2012)[250] showed that ASCs had superior lipid metabolism to BM-MSCs and demonstrated that ASCs expressed significantly lower

osteopontin than BM-MSCs. Their results confirmed findings from Vishnubalaji *et al.* (2012)[251] and demonstrated that ASCs may differentiate into an adipogenic lineage with more proclivity than BM-MSCs. Xu *et al.* (2017)[55] further demonstrated that the methylation status of lineage specific promoters differed between sources. Adipogenic promoters were hypomethylated in ASCs, while osteogenic promoters were methylated and vice versa in BM-MSCs.[55]

While these studies have mostly focused on comparisons between ASCs and BM-MSCs with respect to classical lineages, one study did investigate myogenic potential between different MSC sources. Meligy *et al.* (2012)[134] investigated the myogenic potential of rat-derived ASCs, BM-MSCs and muscle-derived (MD)-MSCs using the 5-Aza-based induction method. MD-MSCs were shown to have the highest myogenic potential, followed by BM-MSCs and lastly ASCs. Results from these studies further strengthen the argument that MSCs may already be genetically primed to a specific lineage depending on their location of origin. Lineage priming could therefore be a potential reason for the poor differentiation of ASCs into muscle observed in this study. Tissue source should therefore be considered for future myogenic differentiation studies.

Interestingly, lipid droplets were observed from day twelve in ASCs induced with dexamethasone/hydrocortisone, indicating that adipogenesis was taking place. This may be explained by firstly considering that ASCs were isolated from lipoaspirates and more readily differentiate into an adipogenic lineage. Secondly, dexamethasone is a primary chemical component in adipogenic induction and upregulates adipogenic factors such as PPARγ and C/EBPα and β.[122] Thirdly, the SVF is a heterogeneous population of cells and pre-adipocytes may have been seeded along with the ASC cell population.[252] Adipogenesis happens spontaneously upon confluency,[253] and the appearance of lipid droplets coincided with ASC confluency post-induction in this study. Additionally, Seo *et al.* (2018) co-cultured adipocytes and C2C12s and demonstrated that adipogenesis, via an autocrine pathway involving interleukin (IL)-6,

inhibited C2C12 myogenic differentiation. This suggests that myogenic differentiation may have been impaired in the ASCs induced using the dexamethasone/hydrocortisone-based induction method. Future studies should aim to explore the interplay between the different lineages using methods such as high through-put screening (eg. micro-arrays or single cell RNA-sequencing) to understand the complex dynamics of ASC differentiation, which to date are still not well understood.[254]

Myogenesis is a complex process involving multiple transcription factors. Post-natal myogenesis is facilitated by Pax 7^{+}/$MyoD^{-}$ satellite cells, the native population of adult stem cells in skeletal muscle. Upon exercise or trauma-induced injury, satellite cells are activated to repair muscle injury before returning to a quiescent state.[255] Injury creates an inflammatory environment, where neutrophils and macrophages gather to mitigate the injury. Cytokines from macrophages (e.g. tumour necrosis factor – alpha (TNF-α)) recruit and activate surrounding satellite cells.[256] Satellite cells have a perpetually active Myf 5 locus, indicating their readiness to differentiate down the myogenic pathway.[257] Upon recruitment and activation, Pax 7 becomes downregulated and MyoD upregulated to subsequently propagate the myogenic differentiation pathway (discussed in detail in Chapter 2).[257] What is crucial to note is that satellite cells *in vivo* are activated partly in response to mechanical influences (exercise or trauma-induced stretching or tearing). The same may be said for myogenesis *in vitro*, where studies have shown that myogenesis may be significantly enhanced under dynamic conditions, using uni-axial strain or mechanical stretching.[258] Huri *et al*. (2013, 2014, 2018)[133,158,159] demonstrated unequivocally that mechanical induction is essential to promote myogenesis to terminal stages (stages 5 and 6) in ASCs. Huri and colleagues found that the expression between myogenic markers Pax 3/7, MyoD and desmin was significantly higher in ASCs induced using both chemical and mechanical methods.[133,158,159] Additionally, the expression of Pax 3/7, MyoD and desmin was detected earlier than observed under static conditions. Additionally, MHC (a terminal marker for myogenic differentiation not investigated in the present study)

was upregulated and confirmed using ICC in ASCs induced under dynamic conditions, which was not detected under static conditions.[133,158,159]

ASCs induced under dynamic conditions had visible multinucleated myotube formation and cellular alignment, whilst ASCs under static conditions had a random distribution and significantly fewer multinucleated cells.[133] A recent study by Ergene *et al.* (2020)[259] further confirmed the findings by Huri and colleagues. ASCs were seeded onto three-dimensional scaffolds, induced using 5-Aza under dynamic conditions, and subsequent differentiation compared to cultures induced under static conditions. Only those induced under dynamic conditions expressed MyoD, MyoG, desmin and MHC. The results from these studies demonstrate that mimicking the *in vivo* physiological and structural environment is an essential component in efficient ASC myogenic differentiation. Huri *et al.* (2013)[133] also confirmed that mechanical induction alone cannot induce myogenesis, and that the combination of chemical and mechanical induction is necessary. In this study, ASCs were induced under static conditions using chemical induction only. Absence of mechanical input is likely the second contributing factor to the low levels of myogenesis observed in this study. Future studies should endeavour to implement the mechanical component in order to effectively study ASC myogenesis *in vitro*.

This study aimed to optimise the myogenic differentiation of ASCs but did not succeed beyond stage two of myogenesis. However, it did succeed in optimising methods that may be used for the evaluation of *in vitro* myogenesis in the future, with minor adjustments and limitations using positive controls. Future studies might consider adjusting the ASC immunophenotypic panel to either substitute CD105 or add an additional marker such as CD13 (a multifunctional aminopeptidase), which according to Bourin *et al.* (2013)[69] is more consistently expressed on MSCs than CD105 (shown to have variable expression).[260] Wolmarans *et al.* (2021).[234] previously demonstrated the heterogeneity of cells plated from the SVF, which included smooth muscle cells. Sorting ASCs from the SVF using fluorescence-activated cell sorting (FACS) could be used to begin with pure populations of ASCs, excluding contaminating cell types already expected to express myogenic markers.

In this study, RT-qPCR of cDNA obtained from bulk-isolated RNA was performed. Bulk RNA sequencing measures average gene expression levels from the entire population of cells; tissue complexity and cell heterogeneity may interfere with detecting differential gene expression.[261] Although computational and statistical software and algorithms exist to mitigate the variability that may be present in bulk RNA, they have some limiting assumptions. They require prior knowledge of the expression kinetics of the genes of interest in the specific cell type, cell population compositions and a list of pre-selected and verified reference genes.[261] While the latter was employed in this study, it does not rectify the averaging artefacts that comes with using bulk-RNA. Two ways to mitigate these limitations in future studies may be to introduce additional technical replicates in the RNA isolation process instead of pooling RNA from multiple wells, or to use single cell analysis. Additionally, in order to gain an understanding of the efficiency of myogenic differentiation and protein expression kinetics, future studies may opt to include flow cytometry to capture data at a single cell level. The presence of myogenic target proteins was assessed qualitatively using ICC because of changes to software parameters during imaging which made semi-quantitative data collection impossible. Future studies should endeavour to take images using the same software parameters in order to obtain semi-quantitative data.

No conclusion could be drawn with regard to selection of the best myogenic induction medium as none of the data generated for this study revealed statistically significant differences. Biological variance and a small sample size may have contributed to the statistical insignificance observed in this study. Future studies should include a larger sample size to improve on statistical power and to better compensate for the inherent biological variance present in primary cells. In this study, ASCs were isolated, characterised according to a standardised panel, induced to differentiate into a myogenic lineage using two different methods and that differentiation assessed using various methods. ASCs were expanded in pHPL to introduce some GMP-compliance in the protocol. The main aim of this study was to optimise and establish the methods pertaining to ASC myogenic differentiation using two previously published induction methods. As ASCs did not differentiate into a myogenic lineage, this aim could not be

fully met. However, the accompanying assays were sufficiently optimised, with multiple areas highlighted where improvements can be made for future studies. The myogenic potential of ASCs are undeniable, but requires very specific chemical and mechanical conditions to effectively induce myogenesis *in vitro* and should be incorporated in future studies of this nature.

This concludes Chapter 6, and the dissertation.

Appendices

Appendix A: University of Pretoria approval from the Research Ethics Committee

UNIVERSITEIT VAN PRETORIA
UNIVERSITY OF PRETORIA
YUNIBESITHI YA PRETORIA

Faculty of Health Sciences

Institution: The Research Ethics Committee, Faculty Health Sciences, University of Pretoria complies with ICH-GCP guidelines and has US Federal wide Assurance.

- FWA 00002567, Approved dd 22 May 2002 and Expires 03/20/2022.
- IORG #: IORG0001762 OMB No. 0990-0279 Approved for use through February 28, 2022 and Expires: 03/04/2023.

22 January 2021

Approval Certificate
Annual Renewal

Ethics Reference No.: 468/2018
Title: In vitro adipose derived stromal cell myogenic differentiation.

Dear Miss S Grobbelaar

The **Annual Renewal** as supported by documents received between 2021-01-05 and 2021-01-20 for your research, was approved by the Faculty of Health Sciences Research Ethics Committee on 2021-01-20 as resolved by its quorate meeting.

Please note the following about your ethics approval:

- Renewal of ethics approval is valid for 1 year, subsequent annual renewal will become due on 2022-01-22.
- Please remember to use your protocol number (468/2018) on any documents or correspondence with the Research Ethics Committee regarding your research.
- Please note that the Research Ethics Committee may ask further questions, seek additional information, require further modification, monitor the conduct of your research, or suspend or withdraw ethics approval.

Ethics approval is subject to the following:

- The ethics approval is conditional on the research being conducted as stipulated by the details of all documents submitted to the Committee. In the event that a further need arises to change who the investigators are, the methods or any other aspect, such changes must be submitted as an Amendment for approval by the Committee.

We wish you the best with your research.

Yours sincerely

Dr R Sommers
MBChB MMed (Int) MPharmMed PhD
Deputy Chairperson of the Faculty of Health Sciences Research Ethics Committee, University of Pretoria

The Faculty of Health Sciences Research Ethics Committee complies with the SA National Act 61 of 2003 as it pertains to health research and the United States Code of Federal Regulations Title 45 and 46. This committee abides by the ethical norms and principles for research, established by the Declaration of Helsinki, the South African Medical Research Council Guidelines as well as the Guidelines for Ethical Research: Principles Structures and Processes. Second Edition 2015 (Department of Health)

Research Ethics Committee
Room 4-60, Level 4, Tswelopele Building
University of Pretoria, Private Bag x323
Gezina 0031, South Africa
Tel +27 (0)12 356 3084
Email: deepeka.behari@up.ac.za
www.up.ac.za

Fakulteit Gesondheidswetenskappe
Lefapha la Disaense tša Maphelo

Appendix B: University of Pretoria approval from the Animal Ethics Committee

Appendix C: SANBS ethical approval for the use of pHPL

Appendix D: University of Pretoria ethical approval for the use of freshly isolated ASCs

The amendment included approval for the use of freshly isolated ASCs for this project, as well as others at the ICMM.

UNIVERSITEIT VAN PRETORIA
UNIVERSITY OF PRETORIA
YUNIBESITHI YA PRETORIA

Faculty of Health Sciences

Institution: The Research Ethics Committee, Faculty Health Sciences, University of Pretoria complies with ICH-GCP guidelines and has US Federal wide Assurance.

- FWA 00002567, Approved dd 22 May 2002 and Expires 03/20/2022.
- IORG #: IORG0001762 OMB No. 0990-0279 Approved for use through February 28, 2022 and Expires: 03/04/2023.

16 March 2020

Approval Certificate
Amendment

Ethics Reference No.: 424/2018
Title: Human alternatives to foetal bovine serum for the expansion of human adipose-derived stem cells

Dear Ms AR Gerber

The **Amendment** as supported by documents received between 2020-02-26 and 2020-03-11 for your research, was approved by the Faculty of Health Sciences Research Ethics Committee on its quorate meeting of 2020-03-11.

Please note the following about your ethics approval:

- Please remember to use your protocol number (424/2018) on any documents or correspondence with the Research Ethics Committee regarding your research.
- Please note that the Research Ethics Committee may ask further questions, seek additional information, require further modification, monitor the conduct of your research, or suspend or withdraw ethics approval.

Ethics approval is subject to the following:

- The ethics approval is conditional on the research being conducted as stipulated by the details of all documents submitted to the Committee. In the event that a further need arises to change who the investigators are, the methods or any other aspect, such changes must be submitted as an Amendment for approval by the Committee.

We wish you the best with your research.

Yours sincerely

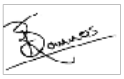

Dr R Sommers
MBChB MMed (Int) MPharmMed PhD
Deputy Chairperson of the Faculty of Health Sciences Research Ethics Committee, University of Pretoria

The Faculty of Health Sciences Research Ethics Committee complies with the SA National Act 61 of 2003 as it pertains to health research and the United States Code of Federal Regulations Title 45 and 46. This committee abides by the ethical norms and principles for research, established by the Declaration of Helsinki, the South African Medical Research Council Guidelines as well as the Guidelines for Ethical Research: Principles Structures and Processes, Second Edition 2015 (Department of Health).

Research Ethics Committee
Room 4-60, Level 4, Tswelopele Building
University of Pretoria, Private Bag x323
Gezina 0031, South Africa
Tel: +27 (0)12 356 3084
Email: deepeka.behari@up.ac.za
www.up.ac.za

Fakulteit Gesondheidswetenskappe
Lefapha la Disaense tša Maphelo

Appendix E: Informed consent document presented to patients when ASCs are collected for isolation

Dear Patient/Participant: _____

INTRODUCTION

You are invited to participate in a research study that is being carried out by the Department of Immunology at the University of Pretoria. This information leaflet is to help you to decide if you would like to participate. Before you agree to take part in this study you should fully understand what is involved. If you have any questions, which are not fully explained in this leaflet, do not hesitate to ask the investigator. You should not agree to take part unless you are completely happy about all the procedures involved. Your personal health will not be compromised by the procedures. These procedures have already been discussed with your doctor beforehand.

THE PURPOSE OF THE STUDY

Researchers at the University of Pretoria would like to investigate the healing properties of adult stem cells for possible future application in regenerative medicine. Regenerative medicine refers to experimental (current status) medicine where researchers try to replace, improve or restore the function of cells that do not function optimally in the body. Adult stem cells are present in various tissues in the body, including fat (adipose) tissue. These adult stem cells could potentially be used to cure patients with various kinds of injuries or diseases. In order to use these cells to cure humans in the future, researchers must first study their characteristics, behaviour, growth and interactions with other cells and/or organisms in the body. This is done by isolating these cells from the fat (adipose) tissue and perform experiments in the laboratory (tissue culture) and/or using experimental animal models.
These adult stem cells can also be used to investigate the process of fat formation. Scientists are able to mimic the formation of fat cells using adult stem cells isolated from fat (adipose) tissue. Obesity is becoming an increasing problem worldwide and in order to find solutions to combat obesity it is important to understand the biological processes involved in the formation of fat. It is also important to understand the interactions of infectious organisms, like HIV and *Mycobacterium tuberculosis* (organism that cause tuberculosis in humans), with stem cells in order to provide safe treatment options in the future. It is therefore important that researchers also investigate the interactions between these infectious organisms and stem cells by performing experiments in the laboratory as well as using experimental animal models. Investigations will be performed on cellular (intact cells) and molecular (investigating the effect on various treatments/exposures to the genetic footprint of cells) levels. For molecular studies we will need to isolate genetic material (DNA and RNA) from your cells.

Many of the experiments that researchers perform require the isolation of genetic material, also known as DNA and RNA, from cells. Genetic material contains information about the cell that only can be revealed if researchers perform specialized tests on the genetic material. These tests are often needed in order to completely understand the characteristics of cells. Genetic information also allows researchers to look into what effect infectious agents, such as *Mycobacterium tuberculosis* (cause tuberculosis in humans) and HIV, might have on these cells. In addition, molecular biology tests (tests that make use of DNA or RNA) are often the most sensitive tests available to detect if cells are infected with bacteria (such as *Mycobacterium tuberculosis)* and/or viruses (such as HIV).

No unethical procedures will be used when collecting the samples and performing the experiments.

ADIPOSE TISSUE COLLECTION

During various normal plastic surgery operations, adipose tissue (fat) will be excised (cut out) or aspirated (sucked out), and discarded. This adipose tissue, does not serve a purpose to the patient's body anymore, but could serve as a valuable source of stem cells for researchers in the field of regenerative medicine. No additional fat will be collected for the study. Only the fat that the doctor planned to aspirate/cut away during the procedures discussed with you during the consultation visits will be collected.

There will be no added risks or discomfort with the collection of the adipose tissue other than normally associated with the specific procedure the patient will experience during normal operative procedures.

CONFIDENTIALITY

Each participant's sample will be assigned a specific code and this code will be used from there on in all research studies. Certain information, including race, ethnicity, gender and medical history, may be important for scientific reasons. This information will be linked to the sample code and not to your identity. Research reports and articles in scientific journals will not include any information that may identify you.

In some isolated cases it might however be important for the doctors or researchers involved in the study to convey medical information to medical personnel or appropriate Research Ethics committees. In such a case, you by signing this document, give permission to the investigator to release your medical records to regulatory health authorities or an appropriate Research Ethics committee. If necessary, these medical professionals will discuss the results with your doctor and everyone will act in your best interest.

ETHICAL APPROVAL

The protocol involved for this study was submitted to the Research Ethics Committee. This study has received written approval from the Research Ethics Committee of the Faculty of Health Sciences at the University of Pretoria. The study is structured in accordance with the Declaration of Helsinki, which deals with the recommendations of guiding doctors in biomedical research involving humans.
You are also welcome to contact the Faculty of Health Sciences Ethics Committee at the University of Pretoria if you have any concerns or questions. Their contact details are:

The Research Ethics Office:
Tel: 012 - 354 1330 or 012 - 354 1677
Fax: 012 - 354 1367

RIGHTS OF THE PARTICIPANT

Your participation in this study is entirely voluntary and you can refuse to participate or withdraw consent at any time without stating any reason. Your withdrawal will not affect your access to medical care or the quality of medical care that you will receive. Your participation or withdrawal from the study would not affect you in any way.

FINANCIAL GAIN OR LOSS

There will be no financial gain or loss to you, should you participate or withdraw from the study. This research could potentially lead to future profitable treatments. However, you will not have access to these profits. There will be no additional financial costs for you to participate in the study.

The participant has no legal remedy and will not share in any financial gain that may be derived from the study

INFORMATION AND CONTACT PERSON

If at any time you would like to find out more information or have any questions regarding the study, please do not hesitate to contact the researchers.

Dr. C. Durandt: 012 -319 2101

Prof. M.S. Pepper: 012 420 3845 or 012 420 5317

PERSONAL/MEDICAL INFORMATION

The information below may be important for scientific reasons. This information will be linked to the sample code and not to your identity.

Gender: _____

Ethnicity: _____

Date of Birth: _____

Weight: _____

Height: _____

Waste Circumference: _____

Do you smoke? YES NO

Are you suffering from:

Diabetes YES NO

Cardiovascular disease YES NO

Hypertension YES NO

INFORMED CONSENT

WHAT IS EXPECTED?

I confirm that the person asking my consent to take part in this study has told me about the nature, process, risks, discomforts and benefits of the study. I have also received, read and understood the above written information regarding the study. I am aware that the results of the study, including personal details, will be anonymously processed into research reports. I am participating willingly. I have had time to ask questions and have no objection to participate in the study. I understand that there is no penalty should I wish to discontinue with the study and my withdrawal will not affect my access to medical care or the quality of medical care I will receive.

I also understand that certain laboratory tests may require the isolation of genetic material, also known as DNA and RNA and give herewith permission that the researchers may extract RNA/DNA from cells isolated from the adipose tissue.

YES	NO

I hereby give the researchers permission to perform routine HIV, hepatitis B and hepatitis C tests on the adipose tissue donated. Testing for these infectious agents is important for our work as we only like to work with tissue that is negative for these infections. If the researchers detect HIV or hepatitis B or C in the sample, the codified sample details will be sent to _____, who will notify you. If you do not wish us to test your tissue for HIV or hepatitis B or hepatitis C, or if you do not wish to know the results of these tests, we will not be able to include you in the study. In the case on an HIV positive result, you will be counselled and treated by qualified medical personnel.

YES	NO

I have received a copy of this informed consent agreement.

Participant full names (print):_____

Participant signature: _____Date: _____

Investigator full names (print):_____

Investigator signature:_____Date:_____

Witness full names (print):_____

Witness signature:_____Date:_____

Witness full names (print):_____

Witness signature:_____Date:_____

Appendix F: Minimum Information for Publication of Quantitative Real-Time PCR Experiments

F.1. Introduction

The MIQE guidelines described by Bustin *et al.* (2009)[214] aimed to target the reliability, reproducibility, integrity and transparency of research and experimental procedures. It describes the minimum amount of information that is necessary to be included with manuscripts for publication, to evaluate data generated using qPCR. It allows reviewers and the scientific community to assess the validity of the assays and protocols used.[214] The guidelines were established to address the publication of inconsistent, misleading and irreproducible results.[262] The information required by the MIQE guidelines to be included as supplementary information to manuscripts and publications include: experimental design, sample information, nucleic extraction particulars, reverse transcription, qPCR target information, qPCR oligonucleotide particulars, qPCR protocol, qPCR validation and data analysis. This study aimed to adhere to the MIQE guidelines as was possible. All information labelled by the MIQE guidelines as 'essential' has been included in this document.

F.2. Experimental design

For experimental design particulars, please refer to Chapter 5, section 5.3.4 and 5.3.9.

F.2.1. Definition of experimental and control groups and numbers within each group

Three ASC biological replicates were used in the course of this study, and each replicate was run in three technical repeats for every time point and culture and induction condition. These included the 5-Aza- and dexamethasone/hydrocortisone-based induction methods, as well as a non-induced control. PHMs were used to optimise myogenic target gene annealing temperatures and melt curves (to

demonstrate specific binding). Additionally, PHMs were included on every qPCR plate as a positive control for each target gene in three technical replicates.

F.3. Sample

F.3.1. Description

RNA was extracted from both ASCs and PHMs. In the ASCs, RNA was extracted from samples induced using the 5-Aza and dexamethasone/hydrocortisone-based induction methods as well as from non-induced cells (control). RNA was extracted at the following time points: days 0, 3, 6, 12 and 24 (5-Aza-based induction methods) and additional days 30 and 42 for the dexamethasone/hydrocortisone-based induction method and the non-induced ASCs.

F.3.2. Microdissection or macrodissection

The samples were not subjected to micro- or macrodissection.

F.3.3. Processing

For sample processing please refer to Chapter 5, sections 5.3.6, 5.3.7, 5.3.8 and 5.3.9.

F.3.4. If frozen – how and how quickly?

Sample cryopreservation has been described in Chapter 5, section 5.3.6, 5.3.7 and 5.3.8.

F.3.5. If fixed – how and how quickly?

Samples were not fixed.

F.3.6. Storage

RNA extraction was performed immediately after trypsinisation (0.25% Trypsin/EDTA). The extracted RNA was then stored at -80ºC until cDNA could be synthesised. cDNA was stored at -20ºC until it was used for RT-qPCR.

F.4. Nucleic Acid Extraction

Total RNA was extracted according to the method described in Chapter 5, section 5.3.7.

F.4.1. DNase or RNase treatment

No DNase or RNase treatment was performed.

F.4.2. Contamination assessment

NRT controls generated during the cDNA synthesis process was used to assess gDNA contamination. The reference gene YWHAZ was used in the reaction master mix to identify potential gDNA contamination (Figure F1).

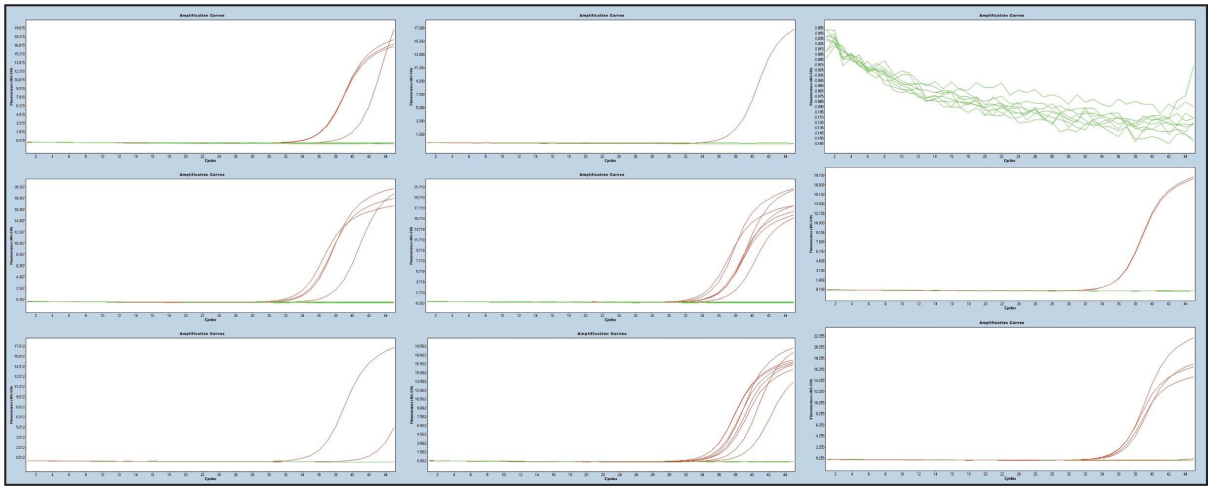

Figure F1: Amplification plots for no reverse transcriptase controls.

The reference gene tyrosine 3-monooxygenase/tryptophan 5-monooxygenase activation protein, zeta (YWHAZ) was used to detect genomic deoxyribonucleic acid (gDNA) contamination using 2 ng/µl of template. Some no reverse transcriptase (NRT) control samples were amplified at 35 or more cycles, indicating gDNA was present.

Most gDNA contamination was present at C_T-values of ≥ 35, thus any qPCR results that were amplified above 35 cycles were excluded from analysis. In samples where the NRT amplified in at least two technical replicates at cycle numbers below 35 were excluded from analysis.

F.4.3. Nucleic acid quantification, purity and integrity

Refer to Chapter 5, section 5.3.7 for sample preparations and instruments used. Refer to Table F1 for the concentrations and integrity values for all the RNA extracted in this study.

Table F1. Total ribonucleic acid extraction concentrations and integrity values.

Total ribonucleic acid extracted from adipose-derived stromal cells in this study, and measured first using the Nanodrop® ND 1000 spectrophotometer and the Aligent Tapestation® 2200.

	NanoDrop® ND 1000 spectrophotometer				Tapestation® 2200		
Culture	**Time point (day)**	**Sample**	**260/280**	**230/260**	**ng/µl**	**Rin value**	**ng/µl**
A150817	0	Day zero 1	2,06	0,8	213,4	9,6	212
		Day zero 2	2,03	0.39	185,25		
	1	DH	2,05	1,6	231,4		
		5-Aza	2,08	0,58	127,05		
		Not induced 1	2,06	1,51	163,29		
		2	2,06	0,86	171,57		
	3	DH	2,04	1,58	287,3	10	74,4
		5-Aza	2,07	1,18	214,91	9,6	207
		Not induced	2,06	0,9	318,39	9,9	279
	6	DH	2,05	0,68	350,16	9,9	248
		5-Aza	2,07	2,1	914,53	9,9	384
		Not induced	2,06	1,64	332,5	10	308
	9	DH	2,05	1,55	334,7		
		5-Aza	2,09	1,77	846,63		
		Not induced	2,07	0,82	246,09		
	12	DH	2,06	0,75	227,16	9,6	415
		5-Aza	2,05	1,44	304,03	9,4	299
		Not induced	2,06	0,67	73,03	9,4	53,4
	18	DH	2,06	1,67	344,79		
		5-Aza	2,08	2,2	1094,08		
		Not induced	2,05	1,61	333,62		
	24	DH	2,07	2,02	632,6	9,6	612

		5-Aza 1	2,02	1,73	432,55	9,7	279
		2	2,04	0,92	281,76		
		Not induced 1	2,06	0,99	215,55	9,7	114
		2	2,1	0,49	72,78		
	30	DH	2,05	1,66	321,58	9,8	372
		5-Aza	2,09	1,75	531,18		
		Not induced 1	2,09	0,87	152,47	9,8	78,4
		2	2,16	0,26	44,96		
	36	DH	2,06	0,73	207,98		
		Not induced	2,03	2,1	374,64		
	42	DH	2,05	1,44	322,76	9,7	224
		Not induced	2,06	1,02	257,84	10	169
A280617	0	Day zero	2,06	0,26	52,97	9,8	64
	1	DH	2,05	1,42	196,9		
		5-Aza	2,03	0,77	57,36		
		Not induced	2,05	0,93	103,4		
	3	DH	2,04	1,35	267,52	9,9	428
		5-Aza	2,06	0,74	196,04	10	302
		Not induced	2,05	1,08	214,22	10	302
	6	Dex/Hydro	2,03	0,56	101,97	10	127
		5-Aza	2,08	0,58	68,43	10	83,4
		Not induced	1,96	0,41	31,91	10	38,1
	9	DH	2,09	1,77	228,42		
		5-Aza	2,1	0,46	81,42		
		Not induced	2,23	0,25	30,23		
	12	DH	2,08	1,34	71,45	10	99
		5-Aza	1,79	0,17	10,65	9,9	25,9
		Not induced	2,5	0,05	5,49	10	28,2
	18	DH	2,07	0,66	110,64		

		5-Aza	2,07	0,73	82,1		
		Not induced	2,03	0,4	32		
	24	DH	2,06	1,61	262,7	9,9	406
		5-Aza	2,04	0,26	20,87	9,8	38,2
		Not induced	2,07	0,85	144,67	9,9	215
	30	DH	2,04	1,09	179,82	10	269
		5-Aza	2,04	1,12	302,14		
		Not induced	1,92	0,26	25,03	10	29,7
	36	DH	2,09	0,76	163,11		
		Not induced	2,02	0,25	15,59		
	42	DH	2,14	1,41	117,68	10	101
		Not induced	2,2	0,68	18,69	10	14,6
A091019	0	Day zero	2,05	0,63	83,41		
			2,04	1,93	361,2	9,8	398
	1	DH	2,07	1,75	231,59		
		5-Aza	2,07	1,19	66,7		
		Not induced	2,04	1,81	352,58		
	3	DH	2,09	1,78	852,31	10	212
		5-Aza	2,06	1,7	163,16	9,9	189
		Not induced	2,04	1,22	294,81	9,9	339
	6	DH	2,09	1,9	1114,47	9,9	569
		5-Aza	2,06	1,79	238,84	10	305
		Not induced	2,09	2,03	775,65	10	194
	9	DH	2,02	1,62	426,66		
		5-Aza	2,05	1,82	329,22		
		Not induced	2,07	1,82	114,81		
	12	DH	2,07	2,18	921,81	9,9	462
		5-Aza	2,06	2,2	763,63	10	452
		Not induced	2,07	1,74	152,51	10	204

	18	DH	2,07	2,22	1002,23		
		5-Aza	2,08	2,17	625,08		
		Not induced	2,07	1,9	105,77		
	24	DH	2,1	2,18	1124,42	9,9	468
		5-Aza	2,06	2,16	387,57	9,8	593
		Not induced	2,03	0,46	23,61	10	25,3
	30	DH	2,08	2,22	1047,9	9,9	287
		5-Aza	2,09	1,75	764,68		
		Not induced	2,07	0,2	74,47	9,9	76,2
	36	DH	2,07	2,22	878,4		
		Not induced	2,02	1,72	61,29		
	42	DH	2,06	2,18	1665,03	9,9	362
		Not induced	2,07	1,55	58,77	10	71,2
5-Aza: 5-azacytidine; DH: dexamethasone/hydrocortisone							

RNA integrity values were generated before cDNA was synthesised, using the Tapestation® 2200 from Aligent Technologies (Santa Clara, California, USA; Figure F.2).

F.4.5. Inhibition testing

No inhibition testing was performed.

F5. Reverse Transcription

Please refer to Chapter 5, section 5.3.8 for the particulars surrounding the reverse transcription step. The SensiFast™ cDNA synthesis kit (Bioline, London, England) was used to reverse transcribe mRNA into cDNA. The kit provides no information other than the following quoted product excerpt: *"one unit catalyses the incorporation of 1 nmol of dTTP into acid- soluble material in 10 min at 370C in 50nM Tris-HCL, pH8.6, 40nm KCl, 1mM MnSO4, 1 mM DTT, and 0.5 mM [3H]TTP, using 200 µM oligo(dT)12-18-primed poly(A)n as template."*

F.5.1. cDNA Quantification & Purity Check

Refer to Chapter 5, section 5.3.8, and Appendix G (method optimisation) for all the particulars surrounding cDNA synthesis, measurement and purity. The NanoDrop® ND 1000 spectrophotometer was used to determine the A260/A280 ratio for cDNA. cDNA A260/A280 ratios ranged between 1.75 – 1.91.

F.5.2. Quantitation cycle (Cq) values with and without reverse transcriptase (RT)

NRTs were produced for every sample and the reference gene YWHAZ was used to detect gDNA contamination, with a template concentration of 2 ng/µl. The results obtained have been summarised in Table F.3, whilst Figure F.1 visually represents the results.

Table F.3: No reverse transcriptase control cycle numbers.

Every sample had a corresponding no reverse transcriptase control.

A091019		A150817		A280617	
Sample NRT	**C_P value**	**Sample NRT**	**C_P value**	**Sample NRT**	**C_P value**
D0 NRT	35.72	D0 NRT	ND	D0 NRT	34.04
D0 NRT	35.86	D0 NRT	ND	D0 NRT	36.13
D0 NRT	ND	D0 NRT	ND	D0 NRT	ND
D3 DH NRT	ND	D3 DH NRT	ND	D3 DH NRT	37.08
D3 DH NRT	ND	D3 DH NRT	ND	D3 DH NRT	ND
D3 DH NRT	37.33	D3 DH NRT	ND	D3 DH NRT	ND
D6 DH NRT	ND	D3 5AZA NRT	ND	D6 DH NRT	ND
D6 DH NRT	36.28	D3 5AZA NRT	37.58	D6 DH NRT	34.73
D6 DH NRT	35.66	D3 5AZA NRT	36.13	D6 DH NRT	ND
D3 5AZA NRT	35.65	D3 NI NRT	ND	D3 5AZA NRT	35.70
D3 5AZA NRT	35.88	D3 NI NRT	ND	D3 5AZA NRT	35.61
D3 5AZA NRT	ND	D3 NI NRT	35.48	D3 5AZA NRT	ND
D6 5AZA NRT	35.83	D6 DH NRT	35.97	D6 5AZA NRT	ND
D6 5AZA NRT	40.00	D6 DH NRT	35.85	D6 5AZA NRT	ND
D6 5AZA NRT	ND	D6 DH NRT	ND	D6 5AZA NRT	ND
D3 NI NRT	ND	D6 5AZA NRT	ND	D3 NI NRT	ND
D3 NI NRT	ND	D6 5AZA NRT	34.76	D3 NI NRT	35.87
D3 NI NRT	35.67	D6 5AZA NRT	34.76	D3 NI NRT	ND
D6 NI NRT	ND	D6 NI NRT	ND	D6 NI NRT	ND
D6 NI NRT	ND	D6 NI NRT	39.57	D6 NI NRT	ND
D6 NI NRT	36.73	D6 NI NRT	ND	D6 NI NRT	ND
D12 DH NRT	35.79	D12 DH NRT	40.00	D12 DH NRT	ND
D12 DH NRT	ND	D12 DH NRT	ND	D12 DH NRT	37.59
D12 DH NRT	ND	D12 DH NRT	35.83	D12 DH NRT	ND
D12 5AZA NRT	ND	D12 5 AZA NRT	ND	D12 5AZA NRT	ND
D12 5AZA NRT	ND	D12 5 AZA NRT	ND	D12 5AZA NRT	ND
D12 5AZA NRT	ND	D12 5 AZA NRT	ND	D12 5AZA NRT	ND
D24 5AZA NRT	ND	D24 5 AZA NRT	ND	D24 5AZA NRT	ND
D24 5AZA NRT	40.00	D24 5 AZA NRT	40.00	D24 5AZA NRT	ND
D24 5AZA NRT	ND	D24 5 AZA NRT	34.93	D24 5AZA NRT	ND

D12 NI NRT	ND	D12 NI NRT	ND	D12 NI NRT	ND
D12 NI NRT	35.82	D12 NI NRT	ND	D12 NI NRT	ND
D12 NI NRT	ND	D12 NI NRT	ND	D12 NI NRT	ND
D24 NI NRT	ND	D24 NI NRT	ND	D24 NI NRT	34.21
D24 NI NRT	ND	D24 NI NRT	ND	D24 NI NRT	34.59
D24 NI NRT	ND	D24 NI NRT	ND	D24 NI NRT	33.45
D24 DH NRT	ND	D34 DH NRT	ND	D24 DH NRT	ND
D24 DH NRT	ND	D34 DH NRT	ND	D24 DH NRT	ND
D24 DH NRT	ND	D34 DH NRT	40.00	D24 DH NRT	ND
D30 DH NRT	ND	D30 DH NRT	ND	D30 DH NRT	ND
D30 DH NRT	35.89	D30 DH NRT	ND	D30 DH NRT	ND
D30 DH NRT	ND	D30 DH NRT	ND	D30 DH NRT	ND
D30 NI NRT	ND	D30 NRT	ND	D30 NI NRT	ND
D30 NI NRT	35.99	D30 NRT	ND	D30 NI NRT	ND
D30 NI NRT	ND	D30 NRT	ND	D30 NI NRT	ND
D42 DH NRT	35.68	D42 DH NRT	ND	D42 DH NRT	ND
D42 DH NRT	36.19	D42 DH NRT	35.67	D42 DH NRT	ND
D42 DH NRT	ND	D42 DH NRT	ND	D42 DH NRT	ND
D42 NI NRT	35.54	D42 NI NRT	ND	D42 NI NRT	ND
D42 NI NRT	ND	D42 NI NRT	ND	D42 NI NRT	ND
D42 NI NRT	40.00	D42 NI NRT	35.65	D42 NI NRT	ND

C_p: Crossing point; DH: dexamethasone/hydrocortisone; 5-Aza: 5-azacytidine; NI: non-induced; NRT: no reverse transcriptase; ND: not detected; D: day

F.5.3. cDNA storage

The cDNA was stored at -20 0C until used in RT-qPCR experiments.

F.6. qPCR Target Information

The accession numbers and amplicon lengths for the target and reference genes have been listed in Chapter 5, Table 5.4.

F.6.1. In silico specificity screen and primer locations

The specificity of the primers was assessed *in silico* using NCBI Primer BLAST® tool. Images of primer locations were generated using the same tool (Figure F2).

Figure F2: *In silico* primer blasts and locations.

The NCBI Primer BLAST® tool was used to assess the binding specificity of the myogenic target genes myogenic differentiation (MyoD), myogenin (MyoG) and desmin and to visualise their locations.

A.6.3 Splice variants targeted

No splice variants were targeted.

F.7. qPCR Oligonucleotides

Primer sequences for target and reference genes have been summarised in Chapter 5, Table 5.4.

F.7.1. Location and identity of any modifications

There were no modifications.

F.7.2. Manufacturer of oligonucleotides

Oligonucleotides were manufactured by Integrated DNA Technologies (IDT; Coralville, IA, USA).

F.8. RT-qPCR Protocol

RT-qPCR was performed as described in Chapter 5, section 5.3.10.

F.8.1. Polymerase identity & concentration

The LightCycler® 480 SYBR Green I Master Mix was used in this study. The polymerase in the master mix is FastStart™ Taq DNA polymerase (Roche, Basel, Switzerland), and the concentration was not indicated.

F.8.2. Buffer/kit identity and manufacturer

The LightCycler® 480 SYBR Green I Master Mix (Roche, Basel, Switzerland; Catalogue number: 04887352001) was used.

F.8.3. Additives

No additives were used.

F.8.4. Manufacturer of plates/tubes and catalogue numbers

LightCycler® 480 Multiwell Plate 96 white plates (Roche, Basel, Switzerland; Catalogue 17 number: 04729692001) were used.

F.8.5. Manufacturer of qPCR instrument

The LightCycler 480 II instrument was manufactured by Roche (Basel, Switzerland).

A.9. qPCR Validation

A.9.1. Specificity

Melt curves were generated to assess the specificity of primer binding to their targets, and have been described in Appendix G (method optimisation).

A.9.2. No template controls

No template controls were included for every target- and reference gene on every plate (Figure F3).

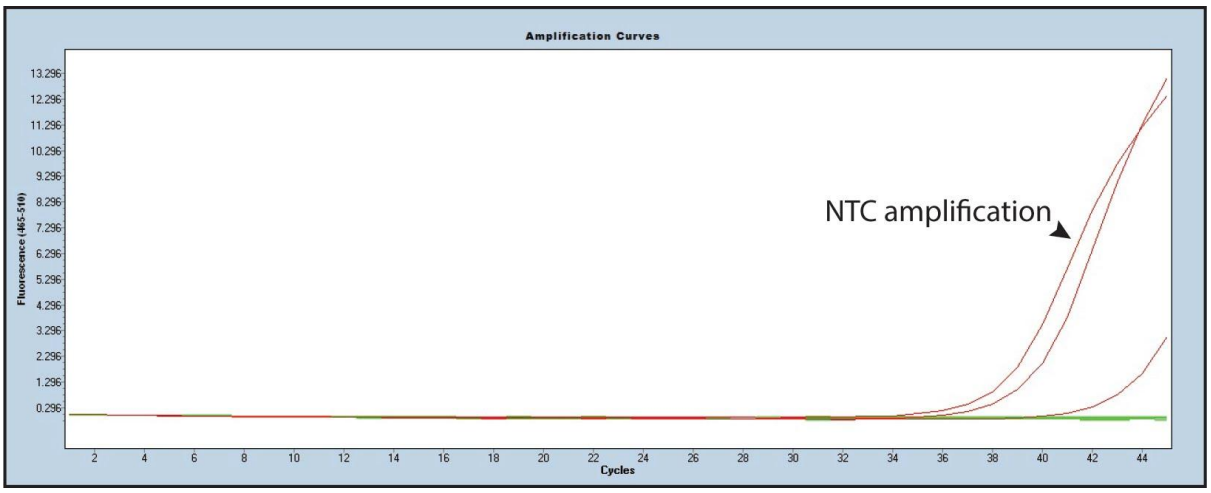

Figure F3: Representative no template control amplification plots.

No template controls were included on every plate for every gene on the plate.

There was some amplification in NTCs that was likely due to spot contamination from handling and plating errors. Thus, if amplification was detected in at least two technical replicates, the sample was excluded form analysis.

F.9.3. Standard curves

As relative quantification for gene expression was used in this study, standard curves were not generated and an amplification efficiency of 2.0 was assumed.

F.9.4. Evidence for limit of detection

Limit of detection was not performed.

F.9.5. If multiplex, efficiency and LOD for each assay

Multiplexing was not performed.

F.10. Data Analysis

F.10.1. qPCR analysis program

The LightCycler® Software (Version 1.5.1; Roche, Basel, Switzerland) was used to analyse data.

F.10.2. Quantitation cycle (Cq) method determination

The second derivative maximum method was used to determine the C_q-values (LightCycler® Software and algorithms).

F.10.3. Outlier identification and disposition

Outlier tests could not be performed because of a small sample size (n=3).

F.10.4. Results of no template controls (NTCs)

The C_q-values for the NTCs were zero, with few samples indicating spot contamination was present. If at least two technical replicates amplified, the sample was excluded from analysis.

F.10.5. Justification of number and choice of reference genes

Three reference genes were used in this study: TBP, ACTB and YWHAZ. These genes have been used, optimised, validated and investigated at the ICMM which suggested that they were appropriate to use.[215]

F.10.6. Normalisation method

The induced samples were normalised using the comparative C_T method (Chapter 5, Figure 5.3, Equations 5.1 – 5.4).

F.10.7. Number of biological replicates

Three ASC biological replicates were investigated.

F.10.8. Number and stage (RT or qPCR) of technical replicates

Three technical repeats were included on the qPCR plate using cDNA form the same sample.

F.10.9. Repeatability (intra-assay variation)

A SD of < 1 between the technical replicates was considered repeatable.

F.10.10. Statistics

See Chapter 3, and Chapter 5, section 5.4.

Appendix G: Method optimisation

G.1. RNA extraction

Initially, RNA extractions using the Qiagen RNeasy mini plus kit yielded low concentrations of RNA especially when isolating RNA from PHMs. The cause was determined to be inefficient lysing of the cells.

The manufacturer's instructions specified that after adding 350 µl RLT buffer (included with the kit), the cells should be vortexed for 1 min before being transferred to the gDNA elimination column. RNA yield was greatly improved after increasing the amount RLT buffer from 350 µl to 600 µl, and by modifying the lysis step according to the manufacturer's suggestions to include (in addition to the initial 1 min vortex step), 2 min centrifugation on maximum speed and a second 1 min vortex step.

G.2. The A260/A230 ratio

The A260/A230 ratio after RNA extraction was below the required range for nearly all RNA extractions, indicating that other contaminants may have been present in the sample. This was likely due to residual guanidine thiocyanate, which is present in the lysis buffer. Qiagen is aware of this fault with their kits, but have indicated that guanidine thiocyanate contamination of up to 100 mM in RNA samples will not compromise the reliability of downstream applications.[263] The low A260/230 ratios found in this study was thus accepted to be insignificant, and experiments were continued.

G.3. cDNA quantification

cDNA may be quantified using either a spectrophotometer or fluorometer. Initially, cDNA was quantified using the spectrophotometer but cDNA concentrations were found to be higher than expected. The cDNA synthesis kit manufacturer's instructions specify that RNA is reverse transcribed into cDNA in a 1:1 ratio if the efficiency of the conversion was 100%. Essentially, this means that if 1000 ng total RNA is added to the reaction, 1000 ng total cDNA should be synthesised in a final volume of 20 µl. This would equate to a cDNA concentration of 50 ng/µl. cDNA measured using the spectrophotometer did not reflect concentrations accurately as opposed to those measured on the fluorometer (likely due to residual oligonucleotides and other components that remained from the cDNA synthesis buffer mixtures). This was confirmed using RNA isolated form PHMs at passage 11. cDNA was synthesised in triplicate and measured using both the spectrophotometer (after synthesis) and the fluorometer (using the Picogreen™ dsDNA quantification assay; Table G.1).

Table G.1. cDNA concentrations when measured with a spectrophotometer and a fluorometer.

cDNA was synthesised from RNA isolated from primary human myoblasts.

		Spectrophotometer		Fluorometer
Sample ID	**Expected ng/µl***	**260/280**	**Nanodrop (ng/uL)**	**Concentration (ng/uL)**
PHM P11 R1	56.7	1.80	1073.95	5.9
PHM P11 R2	56.7	1.81	1077.76	8.5
PHM P11 R3	56.7	1.80	1069.47	8.5

PHM: primary human myoblasts; P: passage; R: repeat
*If the mRNA to cDNA conversion was 1:1 (or 100%)

G.4. Primer optimisation and validation

G.4.1. In silico primer validation

All primer pairs were previously designed at the ICMM. The reference gene primer pairs have been thoroughly validated and previously optimised for use in the laboratory for ASC-related experiments.[215] Myogenic target gene primers pairs were optimised and validated for use in this study. The NCBI Primer-Blast® tool was used to validate primer specificity *in silico.* The MyoD, Des and MyoG primer pairs were all found to have no off-target specificity (Figure G.1).

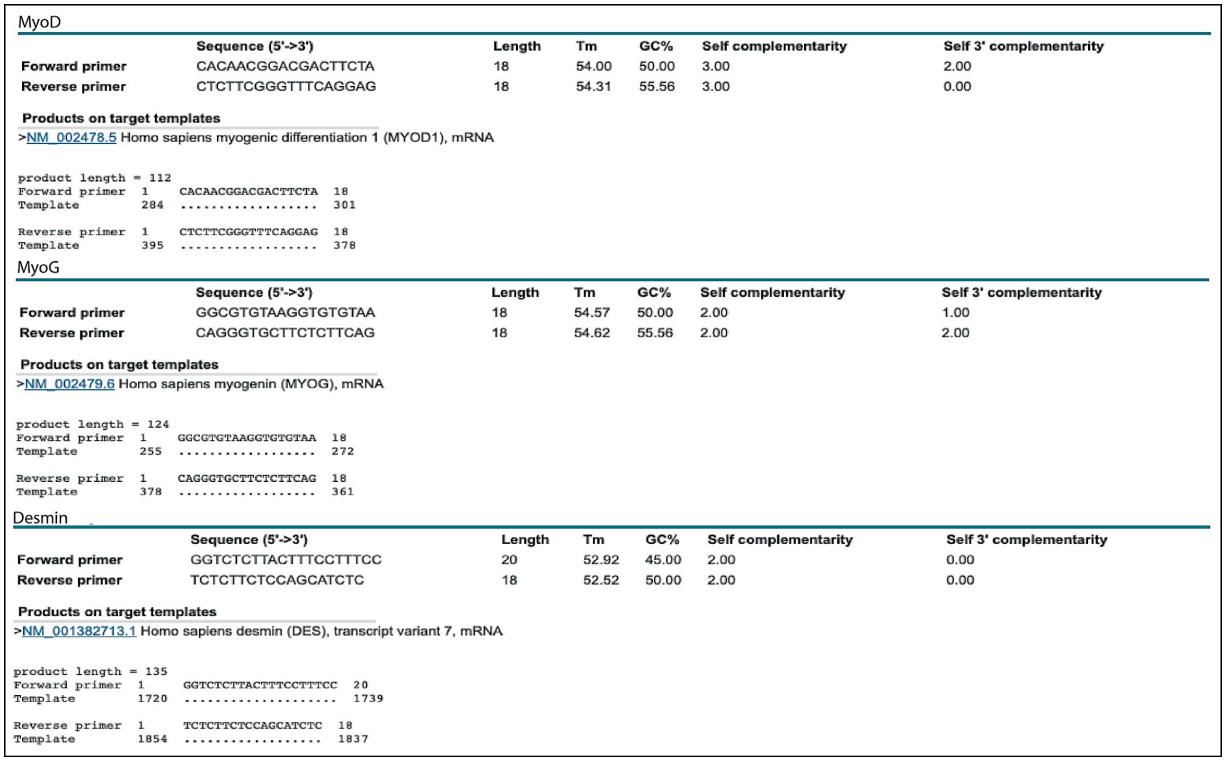

MyoD

	Sequence (5'->3')	Length	Tm	GC%	Self complementarity	Self 3' complementarity
Forward primer	CACAACGGACGACTTCTA	18	54.00	50.00	3.00	2.00
Reverse primer	CTCTTCGGGTTTCAGGAG	18	54.31	55.56	3.00	0.00

Products on target templates

>NM_002478.5 Homo sapiens myogenic differentiation 1 (MYOD1), mRNA

```
product length = 112
Forward primer  1    CACAACGGACGACTTCTA  18
Template        284  ..................  301

Reverse primer  1    CTCTTCGGGTTTCAGGAG  18
Template        395  ..................  378
```

MyoG

	Sequence (5'->3')	Length	Tm	GC%	Self complementarity	Self 3' complementarity
Forward primer	GGCGTGTAAGGTGTGTAA	18	54.57	50.00	2.00	1.00
Reverse primer	CAGGGTGCTTCTCTTCAG	18	54.62	55.56	2.00	2.00

Products on target templates

>NM_002479.6 Homo sapiens myogenin (MYOG), mRNA

```
product length = 124
Forward primer  1    GGCGTGTAAGGTGTGTAA  18
Template        255  ..................  272

Reverse primer  1    CAGGGTGCTTCTCTTCAG  18
Template        378  ..................  361
```

Desmin

	Sequence (5'->3')	Length	Tm	GC%	Self complementarity	Self 3' complementarity
Forward primer	GGTCTCTTACTTTCCTTTCC	20	52.92	45.00	2.00	0.00
Reverse primer	TCTCTTCTCCAGCATCTC	18	52.52	50.00	2.00	0.00

Products on target templates

>NM_001382713.1 Homo sapiens desmin (DES), transcript variant 7, mRNA

```
product length = 135
Forward primer  1     GGTCTCTTACTTTCCTTTCC  20
Template        1720  ....................  1739

Reverse primer  1     TCTCTTCTCCAGCATCTC  18
Template        1854  ..................  1837
```

Figure G.1. NCBI Primer Blast tool.

MyoD, MyoG and desmin primer pairs were validated using the NCBI Primer-Blast® tool to determine primer specificity.

G.4.2. Primer melting temperature optimisation

Primer melting temperatures (Tm) were optimised on gDNA using the gradient temperature feature on the CFX96 real-time PCR instrument from BioRad (Hercules, California, United States). gDNA was crudely extracted from ASCs using the Kapa express extract kit (Sigma-Aldrich Chemie Darmstadt, Germany). Briefly, 1 x 10^6 ASCs were centrifuged and medium aspirated. Thereafter, the cells were resuspended in a reaction mix containing 88 µl PCR-grade water, 10 µl 10x KAPA Express Extract Buffer, and 2 µl Kapa Express Extract Enzyme (reagents supplied by the kit with a unique buffer and proteases for a crude extraction of DNA). The lysis was performed in a thermal cycler in two steps, namely lysis (75^{o}C for 10 min) and enzyme activation (95^{o}C for 5 min). The gDNA extract was quantified on the spectrophotometer (A260/280 = 1.34; A260/230 = 0,66).

A 50 ng/µl working solution of the gDNA extract was made by diluting in PCR grade water. Then, 25 µl of PCR reaction mix was prepared in a 200 µl PCR tube (preparation summarised in Table G.2).

Table G.2. Gradient polymerase chain reaction master mix preparation. Reactions were prepared according to the manufacturer's specifications.

Reagent	Reaction volume (µl)
Taq ready mix	12.5
Forward primer	0.75
Reverse primer	0.75
PCR grade water	10
gDNA (50 ng/µl)	1
Total reaction volume	25

Each row in CFX96 PCR instrument represented a different melting temperature. The temperatures in the gradient were 51.4^{o}C, 52.1^{o}C, 53.7^{o}C, 55.3^{o}C, 57.7^{o}C and 59.7^{o}C. The reaction programming is described in Table G.3.

Table G.3: CFX96 real-time PCR instrument reaction programming.

PCR was achieved by cycling temperatures to denature and amplify DNA.

PCR step	Conditions	Number of cycles
Denaturation	94°C for 2 min	1
Denaturation	94°C for 30 sec	30
Annealing	Gradient-dependent temperature 30 sec	
Extension	72°C for 30 sec	
Final elongation	72°C for 10 min	1
Hold	Indefinite	1

Reaction mixes for each primer pair were prepared for every melting temperature. Additionally, an 80 ml, 2% (w/v) agarose gel was prepared with 4 µl added ethidium bromide (1µg/ml, for visualisation; Sigma-Aldrich Chemie, Darmstadt, Germany). Following the PCR reaction, each sample was mixed with 6x loading dye (1 µl loading dye per 5 µl sample; Sigma-Aldrich Chemie, Darmstadt, Germany) and 10 µl of the sample was loaded into each well of the gel. DNA ladder lanes were loaded with the same volume of FastRuler™ Low-range DNA ladder (Thermo Fisher Scientific, Waltham, Massachusetts, USA). Agarose gel electrophoresis was done at 90 V for 50 min. Thereafter, the gel was analysed using a GelDoc™ instrument Bio-Rad (Hercules, California, USA). The optimal Tm for the MyoD and MyoG primer pairs were determined to be ~ 59.7°C and ~ 57.7°C respectively, and 59.7°C for the desmin primer pair. These numbers were rounded to the closest decimal, as 58°C and 60°C (Figure G.2). The visualised bands for MyoD and desmin were not clear following gel electrophoresis, presenting another limitation. Ideally all bands should be clearly visible, and future experiments may increase the DNA concentration used, use shorter UV exposure times and increase run time to ensure better resolution.

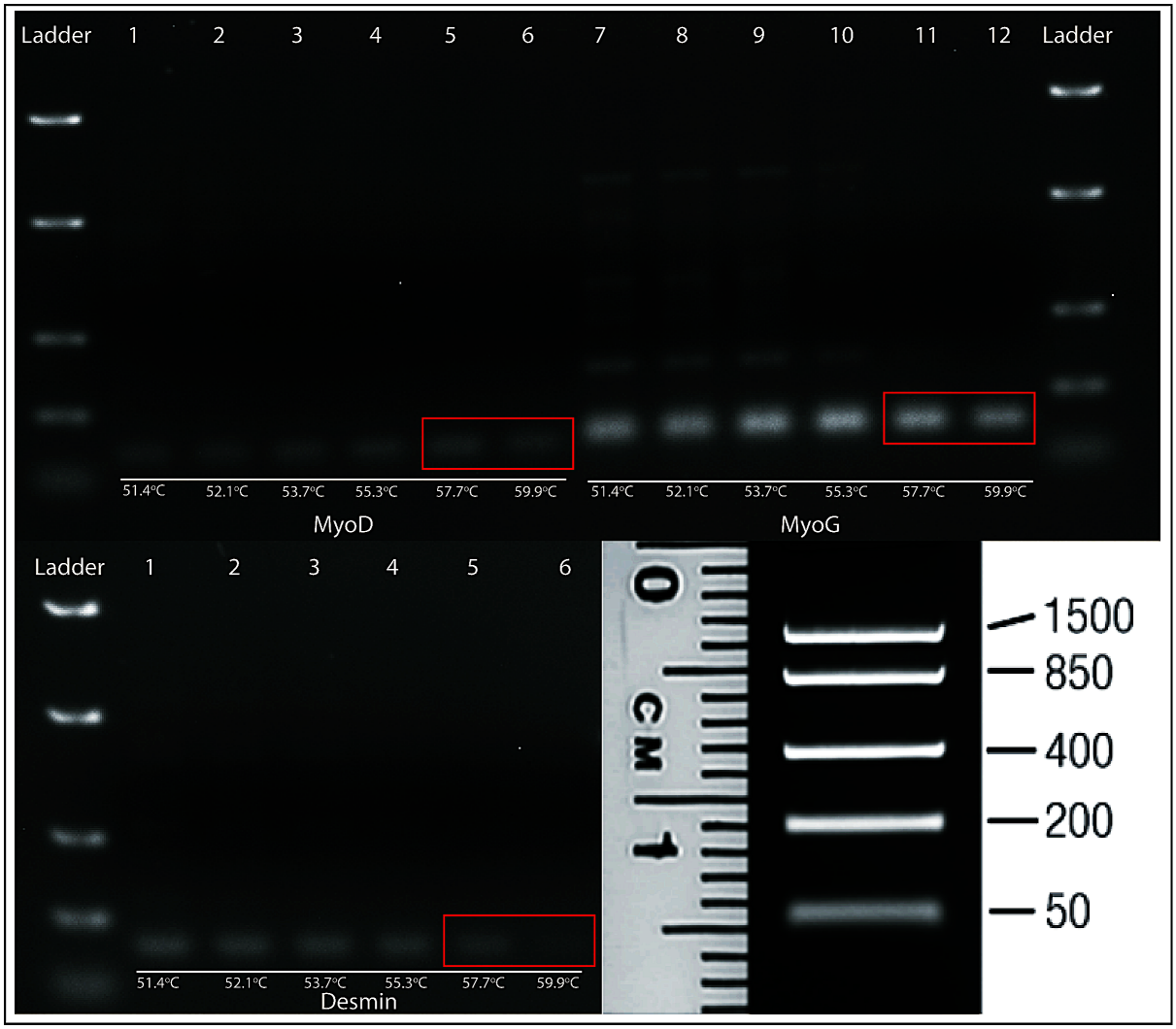

Figure G.2. Optimal primer melting temperatures.

FastRuler™ Low-range DNA ladder was loaded in lanes labelled 'Ladder'. Lane number and corresponding temperatures have been defined to the right of the figure. The primer pairs MyoD, MyoG and desmin are labelled below their corresponding lanes. The investigated melting temperatures have been labelled below their corresponding lane in white. In the top gel, MyoD samples were loaded in lanes 1 – 6 and MyoG samples in lanes 7-12. In the bottom gel, desmin samples were loaded in lanes 1 – 6. Optimal melting temperatures are indicated in red boxes.

Myogenic and reference primer annealing specificity and Tm was then further validated on the LightCycler 480 II. This was done on RNA isolated from PHMs at each experimental time point, using a melting temperature of 60°C (this temperature was used to ensure adequate amplification of both the target genes and the reference genes, which has previously been optimised to 62°C) and the reaction conditions stipulated in Chapter 5, Table 5.6.

Melt curves were done after every qPCR run and was integrated as part of the reaction's standard programming. Based on the melt curves generated, all primer pairs including those for YWHAZ (Figure G.3B), TBP (Figure G.3C), MyoD (Figure G.3D), MyoG (Figure G.3E) and desmin (Figure G.3F) generated single peaks indicating that specific targets were generated. However, the exception was reference gene ACTB, where the melt curve indicated two peaks (Figure G.3A). This particular reference gene and its primer pairs have previously been used and validated at the ICMM.[215]

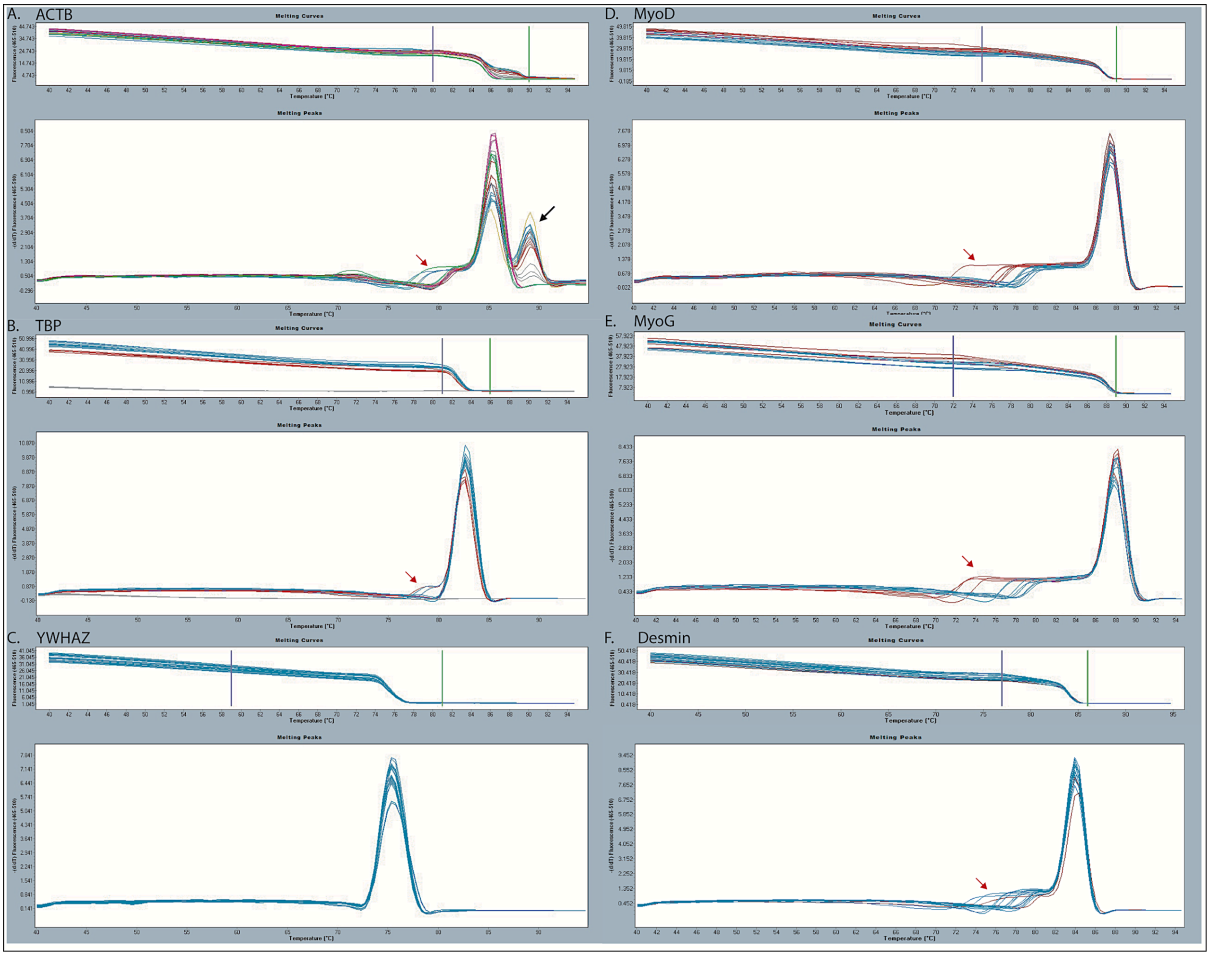

Figure G.3. Melt curves generated for reference and target genes.

Single peaks on a melt curve indicated specific gene targets were amplified, and showed that primer annealing was specific to the desired targets for TBP (B), YWHAZ (C), MyoD (D), MyoG (E) and desmin (F). Two peaks were observed in the melt curve for ACTB (A; indicated by a black arrow).

The double peaks are thus likely a result of gDNA contamination in the primer stock, as was indicated by NTC amplification (Figure G.4) and represents a limitation in this experiment. As ACTB targets were detected at a lower C_P-value than the contamination in the primer stock and for the purpose of this study, ACTB was still included as a reference gene.

Another observation indicated on all melt curves except for YWHAZ (Figure G.3B) was the formation of 'shoulders' (Figure G.3; indicated by red arrows), likely caused by

imperfect primer binding, as primer dimers tend to form perfect peaks at lower primer melting temperatures. These 'shoulders' may have been caused by either the Tm or ramp rate. While the formation of shoulders does not affect the outcome of the experiments significantly, future studies may increase the Tm and/or ramp rate to decrease their formation and smooth out the melt curve.[264]

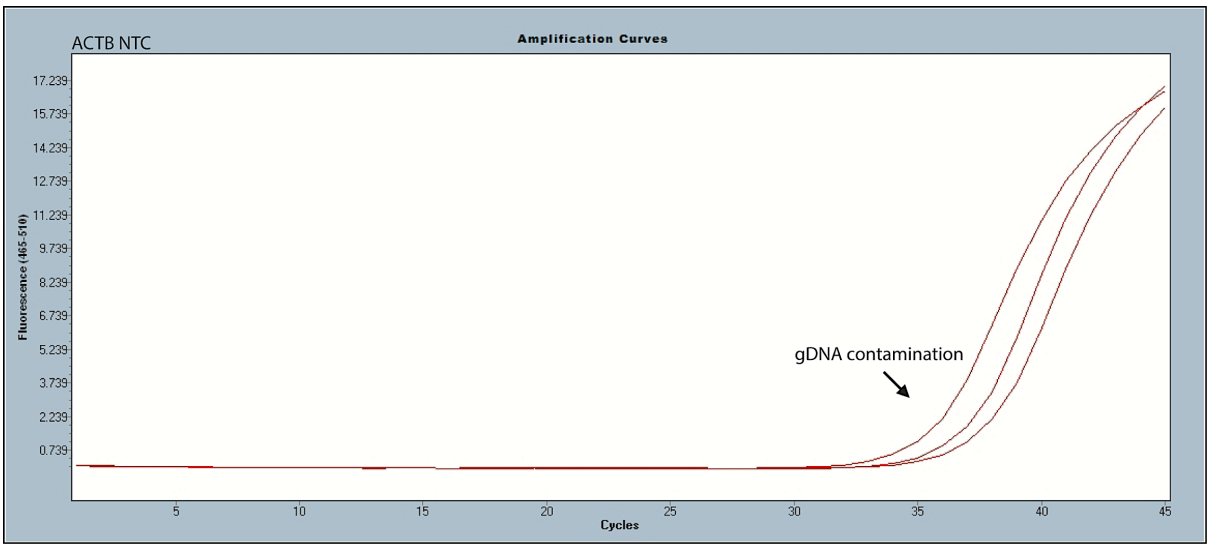

Figure G.4. Image of the amplification graph generated from the no template control for beta-actin.

Amplification was observed in the no template controls for beta-actin (ACTB), indicating that the primer stock solution was likely contaminated by genomic DNA (gDNA).

In summary, primers were shown to be specific for their target genes at a Tm of 60°C as determined through optimisation. The ACTB primer stock was shown to be contaminated. Future studies may further optimise reaction conditions and increase the Tm and/or ramp rate in order to decrease the possibility of imperfect primer binding occurring (Figure G.3). Additionally, analysis should be done immediately following the reaction to ensure stock contamination can be addressed.

G.4.3. Stable expression of reference genes

At the ICMM, Dessels *et al.* (2019)[215] previously investigated the stable expression of 11 reference genes under adipogenic differentiating conditions. The results of that study showed that ACTB, YWHAZ and TBP were amongst the most stably expressed genes in ASCs under induced and non-induced conditions over a period of time, and

thus were selected as reference genes for this study. However, since the study by Dessels and colleagues investigated stable expression under adipogenic conditions alone, the same needed to be demonstrated again under myogenic conditions. In order to demonstrate stable expression of reference genes ACTB, YWHAZ and TBP, qPCR was performed on ASC cDNA from one biological replicate under all culture conditions and across all time points. Every sample was run in triplicate technical repeats and data was analysed using the statistical package NormFinder (v0.953) in Microsoft Excel.

Ideally, this should have been done on at least 3 biological replicates. However, the amount of isolated RNA and thus synthesised cDNA were significant limiting factors. This represented another limitation to the qPCR data generated in this chapter, as the variability inherently present between biological replicates were not considered. Any future experiments should ensure that an adequate amount of RNA is isolated and cDNA synthesised. Furthermore, this experiment should be repeated using the cDNA of least three biological replicates under all culture conditions over time. Additionally, only three reference genes were considered in this study. Investigating other potential reference genes may reveal more suitable candidates and could be another focus point in future studies involving ASC myogenesis.

Analysis using NormFinder revealed that all three reference genes were stably expressed under all induction- and culture conditions, and across all time points. A larger stability index value indicates variable expression of a reference gene, while a small index value indicates stable expression. The most stably expressed was YWHAZ followed by ACTB and TBP (Table G.4).

Table G.4. Stable expression of reference genes.

Stable expression of reference genes YWHAZ, ACTB and TBP were determined using NormFinder.

Gene name	Stability rank	Stability value
YWHAZ	1	0,105
ACTB	2	0,108
TBP	3	0,124

In summary, YWHAZ, ACTB and TBP were demonstrated to be stably expressed in ASCs under myogenic-induced and non-induced conditions over time. These reference genes were thus used for all subsequent qPCR experiments.

G.4.4. RT-qPCR data analysis

For both the induced and non-induced samples, each reaction was performed in triplicate and the SD of the C_T-values were determined. If the sample values obtained between triplicate wells had a SD of less than 0.5, the sample was included in analysis. Those with an SD above 0.5, and where a replicate well (outlier) could not be removed, were excluded. Ideally, these samples should have been repeated, but because the amount of extracted RNA and by extension synthesised cDNA were significantly limited, this was not possible. Amplification observed in some NTC and NRC controls indicate gDNA contamination of a few samples (Appendix F). However, all contamination amplification was detected after 35 cycles, and thus any samples that showed amplification at a C_T-value of 35 and above were not considered for analysis. Because of this, days 30 and 42 in the DH samples were excluded from this study and all induction conditions were analysed up until day 24 only. The comparative C_T-method indicates values as fold change from the baseline (which is equal to 1). Upregulation of genes were noted when the corresponding $2^{-\Delta\Delta CT}$ value was higher than 1, and was considered downregulated when the value was less than 1.

G.5. Optimising coating coverslips with type I collagen

Collagen Type I is a natural adhesive used in cell culture where cell attachment to the flask alone proves challenging. C2C12s and PHMs were expanded and differentiated on culture flasks lined with collagen. Using collagen type I as a coating for ASC cell culture and myogenic differentiation has been done before.[159,265] Whilst ASCs did not need collagen-coated culture flasks during the expansion phase, as they are naturally adherent cells, it was necessary to add the coating when seeding for differentiation experiments. When inducing ASCs on coverslips that were coated with 5 µg/cm^2 type I collagen, the cells lifted and became unviable. The reason why the cells lift post-induction or why the collagen coating on the glass failed remained unclear and could not be elucidated from the literature.

In order to address this, two types of coverslips were tested and included, namely plastic polymer coverslips (Ibidi GmbH, Gräfelfing, Germany) and glass coverslips. Additionally, it was decided to try pre-coating the coverslips with poly-L-lysine (a small natural homopolymer used to coat culture substrates that effectively binds to glass) and to increase the collagen coating concentration from 5 µg/cm^2 to 12.5 µg/cm^2 after consulting with a technical specialist from Corning (New York, USA). Both types of coverslips were pre-coated with poly-L-lysine before being coated with collagen type I (section 5.3.5.1). ASCs were seeded onto the coverslips inside a 6-well plate at 5000 cells/cm^2 and left for 24 hr to adhere. Medium was replaced with MIM 1 and 2 and after 24 hr the cells were viewed under the microscope. Cells remained adhered to glass coverslips most effectively, while lifting from the polymer coverslips (Figure G.5).

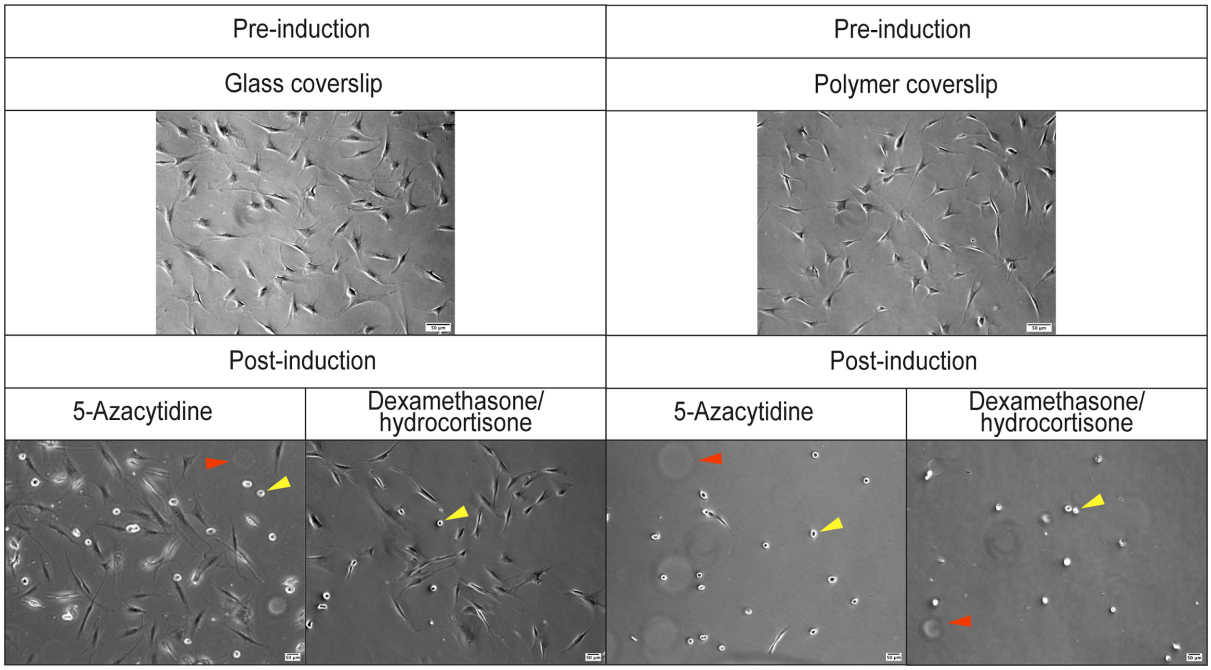

Figure G.5: Micrographs demonstrating adipose-derived stromal cell adherence following coverslip coating procedures.

Adipose-derived stromal cells (ASC) were seeded onto glass and plastic polymer coverslips coated with 0.01% Poly-L-lysine and 12.5 µg/cm^2 collagen. Red arrows indicate floating cell debris in another focal plane. Yellow arrows indicate non-adherent or lifting cells. Pre-induction images were taken at 200x magnification, and post-induction images at 100x magnification. Scale bar = 50 µm.

G.6. Determining optimal antibody and fluorescent stain dilutions and co-stain combinations for immunocytochemistry

Optimal primary antibody and phalloidin dilutions were determined using antibodies diluted at various concentrations (starting with the manufacturer's recommendation). Secondary antibody dilutions remained constant at 1:400 (as per manufacturer's instructions). Antibodies for ICC were optimised on PHMs, whilst actin staining using phalloidin was optimised on undifferentiated ASCs. DAPI was diluted to 1:1000 and stained for 5 min as per the manufacturer's instructions. MyoD (mouse anti-human) was co-stained with MyoG (rabbit anti-human) and desmin (rabbit anti-human) was co-stained with TRITC-phalloidin. Ideally, all antibodies should be optimised on the same cell culture, but because a positive control for myogenic proteins were needed

PHMs were used to optimise antibody stains. Because actin is present is ASCs, it could be used to optimise actin staining.

G.6.1. Phalloidin optimisation

Phalloidin staining was optimised using a checkerboard experiment. The incubation times that were investigated were 10 and 15 min and the dilutions included 1:200, 1:300 and 1:400. Phalloidin was found to stain most effective at a dilution of 1:400 with an incubation time of 15 min (Figure G.6).

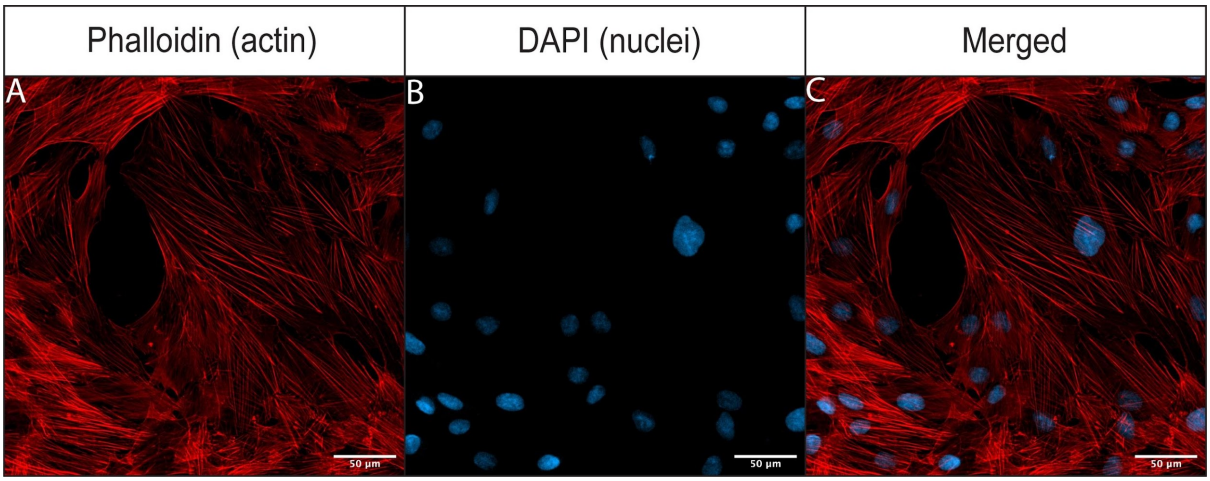

Figure G.6. Optimal phalloidin dilution for immunocytochemistry.

Confocal micrographs of adipose-derived stromal cells stained with tetramethylrhodamine (TRITC)-phalloidin (A. 1:400) for 15 min, and DAPI (B. 1:1000) for 5 min. Images were merged to show the phalloidin-DAPI co-stain (C). TRITC-phalloidin was visualised using the 561 nm laser, and DAPI the 405 nm laser. Confocal images were visualised using the 20x objective (200x magnification), and the scale bar was set to 50 µm.

G.6.2. Primary and secondary antibody optimisation

Before deciding on co-stains and prior to optimising primary antibodies, it was first determined whether there were any non-specific interactions evident in the samples when stained with only the secondary antibodies, anti-mouse IgG conjugated to AF 555 and anti-rabbit IgG conjugated to AF 488. No non-specific binding or interactions were observed (Figure G.7). In Figure G.7 it is important to note that the colour

contrast (Figure 5.15A and B) was boosted to the point where background became visible to demonstrate that there were no non-specific interactions.

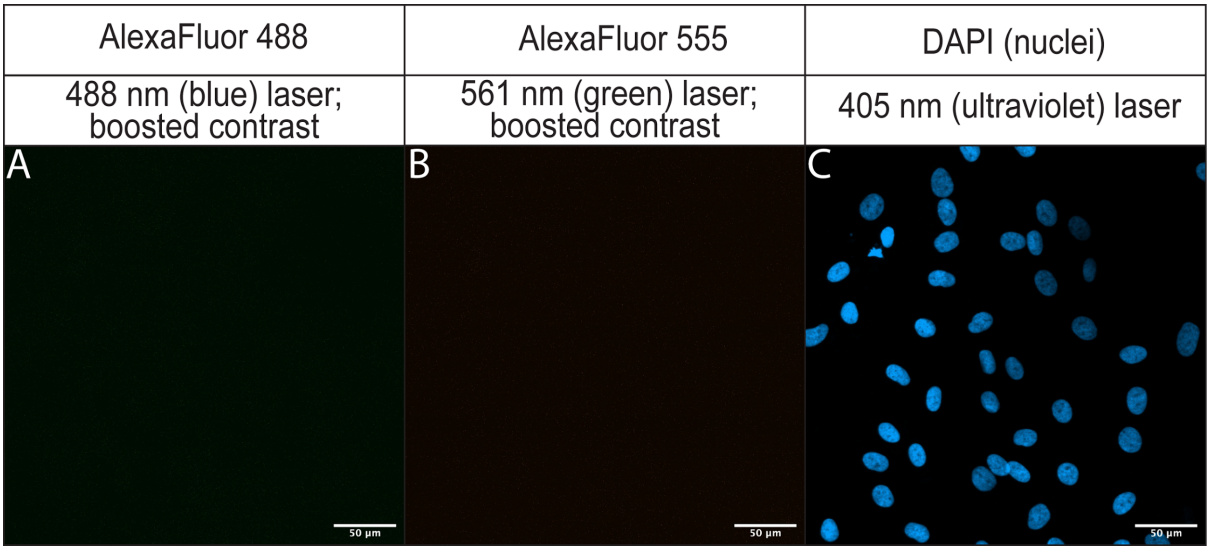

Figure G.7: Secondary antibody only controls.

Samples were stained with the secondary antibodies anti-rabbit IgG conjugated to Alexa Fluor (AF) 488 (A) and anti-mouse IgG conjugated to AF 555 (B). 4′,6-Diamidino-2-phenylindole (C, DAPI) stained nuclei and demonstrated the presence of cells. AF 488 was visualised using the 488nm laser, AF 555 using the 561 nm laser and DAPI with the 405 nm laser. Micrographs were captured using the 20x objective (200x magnification), and the scale bar was set to 50 µm.

In cases where excitation and emission spectra slightly overlap, it is possible to detect fluorescence in more than one laser channel. As MyoD and MyoG are both nuclear TFs, it was essential to demonstrate that the fluorescent signals of these two fluorophores were visible in only one laser channel. This was done to avoid interpreting results that indicated both myogenic targets stained positive in one nucleus when it was in fact only one target with a fluorescent signal visible in more than one laser channel. In order to demonstrate this, primary and secondary antibody stains for both MyoD and MyoG were done on PHMs on day five post-induction. Thereafter, each antibody-fluorophore complex was imaged using both the 488 nm (blue light) and the 561nm (green light) lasers. The MyoD/anti-mouse IgG - AF 555 complex was visible in the green laser channel only and the MyoG/anti-rabbit iGG - AF 488 complex was

only visible when excited with the blue laser. This demonstrated that MyoD and MyoG could be stained concurrently and that the results were accurate (Figure G.8).

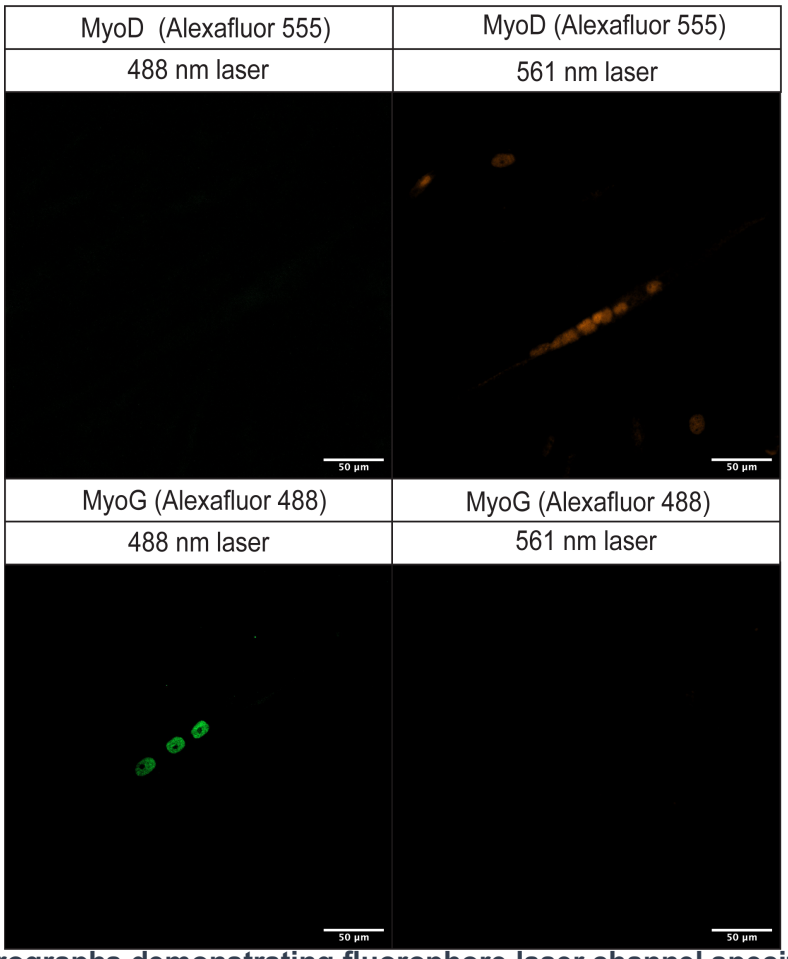

Figure G.8. Micrographs demonstrating fluorophore laser channel specificity.

Primary human myoblasts on day five post-induction were stained with myogenic differentiation 1 (MyoD) and myogenin (MyoG) and their respective secondary antibodies. The targets were visualised in both the 488 nm and 561 nm channels. Images were captured using the 20x objective (200x magnification), and the scale bar was set to 50 µm.

Optimal primary antibody dilutions were determined after titrating antibodies from the dilutions recommended in the manufacturer's instructions and was determined for MyoD (1:200), MyoG (1:400), Pax 3/7 (1:100) and desmin (1:500). The dilutions were then subsequently used to label target proteins on PHMs (the positive control for myogenic protein targets in this study) to demonstrate that the dilutions effectively stained the appropriate myogenic targets (Figure G.9).

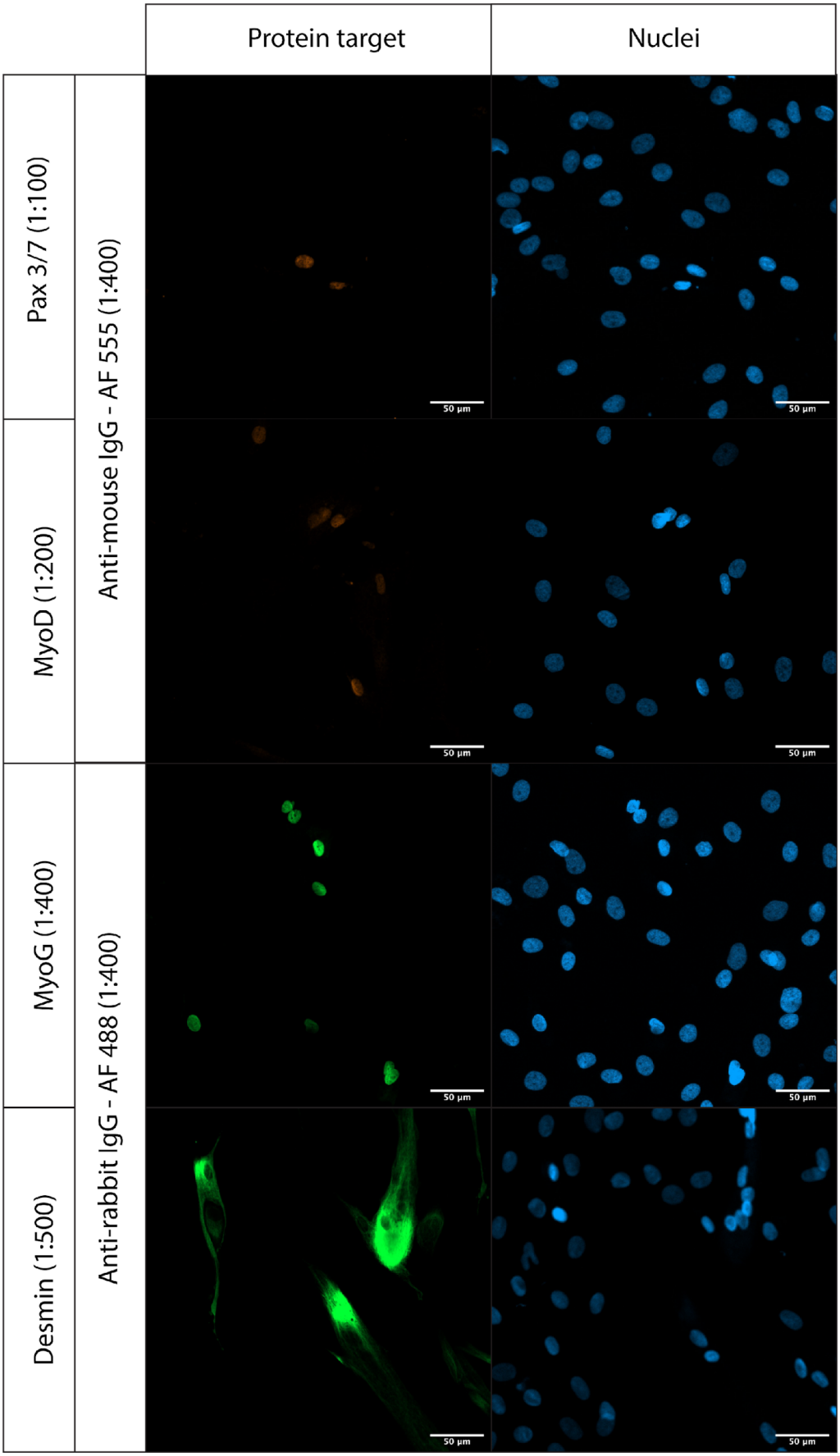
Protein target
Nuclei
Pax 3/7 (1:100)
MyoD (1:200)
MyoG (1:400)
Desmin (1:500)
Anti-mouse IgG - AF 555 (1:400)
Anti-rabbit IgG - AF 488 (1:400)
50 µm

Figure G.9. Final dilutions used to visualise myogenic target proteins in primary human myoblasts.

Primary human myoblasts were stained with mouse anti-human paired box protein (Pax) 3/7, mouse anti-human myogenic differentiation (MyoD), rabbit anti-human myogenin (MyoG) and rabbit anti-human desmin. Pax 3/7 and MyoD were counterstained with anti-mouse immunoglobulin G (IgG) conjugated to Alexa Fluor (AF) 555 (orange) and MyoG and desmin with anti-rabbit IgG conjugated to AF 488 (green). Nuclei (blue) were stained using 4′,6-Diamidino-2-phenylindole (DAPI). Images were taken using a 20x objective (200 x magnification) with the scale bar set as 50 µm.

Background fluorescence was noted when Pax 3/7 and -MyoD were counterstained with anti-mouse IgG conjugated to AF 555. The reason for this was likely due to a low signal-to-noise ratio, a well-known flaw in confocal microscopy due to various factors including specimen type, microscope pinhole size, laser power and fluorophore bleaching (due to laser exposure).[266] If the microscope pinhole diameter is increased, more light floods the field of view. This may improve the visibility of the object in view, but will also increase background noise and autofluorescence while also diminishing the fluorophores signals in that entire area. Increasing laser power may also boost the signal and improve the visibility and focus of the target, but results in fluorophore saturation.[266] When the confocal microscope 'scans' an image to capture it, it also hovers briefly at every frame which also influences the amount of time that fluorophores are exposed to a particular laser light. It is also important to consider that an image is rarely captured once, especially when a sample has been stained for multiple protein targets and fluorophores.[266] Future studies should consider using an amplification system, such as the avidin-biotin amplification system to enhance the fluorescent signal of Pax 3/7 and MyoD.[267] Alternatively, secondary antibodies conjugated to other fluorophores with stronger signals could be investigated and paired with target proteins that are weakly expressed and therefore difficult to detect.

References

1. Natürliche schöpfungsgeschichte von dr. Ernst häckel, professor in jena. Berlin bei georg reimer. 1868 s. 568. Archiv der Pharmazie. 1869;189(3):282-283.
2. Haeckel E. Anthropogenie, 1st edn (leipzig: Wilhelmengelmann). 1874.
3. Haeckel E. Anthropogenie-3rd edn. Wilhelm Engelmann, Leipzig. 1877.
4. Velten L, Haas SF, Raffel S, Blaszkiewicz S, Islam S, Hennig BP*, et al.* Human haematopoietic stem cell lineage commitment is a continuous process. Nat Cell Biol. 2017;19(4):271-281.
5. Baker CL, Pera MF. Capturing totipotent stem cells. Cell Stem Cell. 2018;22(1):25-34.
6. Singh VK, Saini A, Kalsan M, Kumar N, Chandra R. Describing the stem cell potency: The various methods of functional assessment and in silico diagnostics. Front Cell Dev Biol. 2016;4:134-134.
7. Kallmeyer K, André-Lévigne D, Baquié M, Krause KH, Pepper MS, Pittet-Cuénod B*, et al.* Fate of systemically and locally administered adipose-derived mesenchymal stromal cells and their effect on wound healing. Stem Cells Transl Med. 2020;9(1):131-144.
8. Raju R, Chau D, Cho DS, Park Y, Verfaillie CM, Hu W-S. Cell expansion during directed differentiation of stem cells toward the hepatic lineage. Stem Cells Dev. 2017;26(4).
9. Sheng G. The developmental basis of mesenchymal stem/stromal cells (mscs). BMC Dev Biol. 2015;15:44-44.
10. Takahashi K, Tanabe K, Ohnuki M, Narita M, Ichisaka T, Tomoda K*, et al.* Induction of pluripotent stem cells from adult human fibroblasts by defined factors. Cell. 2007;131(5):861-872.
11. Xu L, Zhang K, Wang J. Exploring the mechanisms of differentiation, dedifferentiation, reprogramming and transdifferentiation. PLoS One. 2014;9(8):e105216.
12. Takahashi K, Yamanaka S. Induction of pluripotent stem cells from mouse embryonic and adult fibroblast cultures by defined factors. Cell. 2006;126(4):663-676.
13. Baedke J. The epigenetic landscape in the course of time: Conrad hal waddington's methodological impact on the life sciences. Stud Hist Philos Sci A. 2013;44(4, Part B):756-773.
14. Pubmed.Gov [internet]. [cited march 2020]. Available from: Https://pubmed.Ncbi.Nlm.Nih.Gov/?Term=%28mesenchymal+stem+cell%29+and+%28mesenchymal+stromal+cell%29&sort=.
15. Pittenger MF, Discher DE, Péault BM, Phinney DG, Hare JM, Caplan AI. Mesenchymal stem cell perspective: Cell biology to clinical progress. NPJ Regen Med. 2019;4:22-22.
16. Tiziana S, Gianfranco P, Umberto G. Clinical trials with mesenchymal stem cells: An update. Cell Transplant. 2016;25(5):829-848.

17. Zhao J, Wang J, Dang J, Zhu W, Chen Y, Zhang X*, et al.* A preclinical study—systemic evaluation of safety on mesenchymal stem cells derived from human gingiva tissue. Stem Cell Res Ther. 2019;10(1):165.
18. Elgaz S, Kuçi Z, Kuçi S, Bönig H, Bader P. Clinical use of mesenchymal stromal cells in the treatment of acute graft-versus-host disease. Transfus Med Hemother. 2019;46(1):27-34.
19. Tigenix and takeda announce alofisel® (darvadstrocel) receives approval to treat complex perianal fistulas in crohn's disease in europe. [updated: 23 march 2018; cited 30 march 2020]. Available from: Https://www.Takeda.Com/newsroom/newsreleases/2018/tigenix-and-takeda-announce-alofisel-receives-approval-in-europe/
20. Caplan AI. Mesenchymal stem cells: Time to change the name! Stem Cells Transl Med. 2017;6(6):1445-1451.
21. Caplan AI. Mesenchymal stem cells. J Orthop Res. 1991;9(5):641-650.
22. Friedenstein A, Chailakhjan R, Lalykina K. The development of fibroblast colonies in monolayer cultures of guinea-pig bone marrow and spleen cells. Cell Proliferat. 1970;3(4):393-403.
23. Friedenstein AJ, Chailakhyan RK, Latsinik NV, Panasyuk AF, Keiliss-Borok IV. Stromal cells responsible for transferring the microenvironment of the hemopoietic tissues: Cloning in vitro and retransplantation in vivo. Transplantation. 1974;17(4):331-340.
24. Yu-Show F, Chia-Hui L, Kuo-An C, Chang-Ching Y, Tung-Lin C, Tsui-Ling K*, et al.* Xenograft of human umbilical mesenchymal stem cells from wharton's jelly differentiating into osteocytes and reducing osteoclast activity reverses osteoporosis in ovariectomized rats. Cell Transplant. 2018;27(1):194-208.
25. Kassis I, Zangi L, Rivkin R, Levdansky L, Samuel S, Marx G*, et al.* Isolation of mesenchymal stem cells from g-csf-mobilized human peripheral blood using fibrin microbeads. Bone Marrow Transplant. 2006;37(10):967-976.
26. Huang GT, Gronthos S, Shi S. Mesenchymal stem cells derived from dental tissues vs. Those from other sources: Their biology and role in regenerative medicine. J Dent Res. 2009;88(9):792-806.
27. Jia Z, Liang Y, Xu X, Li X, Liu Q, Ou Y*, et al.* Isolation and characterization of human mesenchymal stem cells derived from synovial fluid by magnetic-activated cell sorting (macs). Cell Biol Int. 2018;42(3):262-271.
28. Maziarz RT, Arthurs J, Horwitz E. Institutional profile: The international society for cellular therapy: Evolving to meet the demands of the regenerative medicine industry. Regen Med. 2011;6(2):163-166.
29. Horwitz EM, Le Blanc K, Dominici M, Mueller I, Slaper-Cortenbach I, Marini FC*, et al.* Clarification of the nomenclature for msc: The international society for cellular therapy position statement. Cytotherapy. 2005;7(5):393-395.
30. de Windt Tommy S, Vonk Lucienne A, Saris Daniel BF. Response to: Mesenchymal stem cells: Time to change the name! Stem Cells Transl Med. 2017;6(8):1747-1748.
31. Dominici M, Le Blanc K, Mueller I, Slaper-Cortenbach I, Marini F, Krause D*, et al.* Minimal criteria for defining multipotent mesenchymal stromal cells. The international society for cellular therapy position statement. Cytotherapy. 2006;8(4):315-317.

32. Simmons PJ, Torok-Storb B. Identification of stromal cell precursors in human bone marrow by a novel monoclonal antibody, stro-1. Blood. 1991;78(1):55-62.
33. Mabuchi Y, Morikawa S, Harada S, Niibe K, Suzuki S, Renault-Mihara F*, et al.* Lngfr(+)thy-1(+)vcam-1(hi+) cells reveal functionally distinct subpopulations in mesenchymal stem cells. Stem Cell Rep.1(2):152-165.
34. Gang EJ, Bosnakovski D, Figueiredo CA, Visser JW, Perlingeiro RC. Ssea-4 identifies mesenchymal stem cells from bone marrow. Blood. 2007;109(4):1743-1751.
35. Battula VL, Treml S, Bareiss PM, Gieseke F, Roelofs H, de Zwart P*, et al.* Isolation of functionally distinct mesenchymal stem cell subsets using antibodies against cd56, cd271, and mesenchymal stem cell antigen-1. Haematologica. 2009;94(2):173-184.
36. Ponnaiyan D, Jegadeesan V. Comparison of phenotype and differentiation marker gene expression profiles in human dental pulp and bone marrow mesenchymal stem cells. Eur J Dent. 2014;8(3):307-313.
37. BüHring H-JR, Battula VL, Treml S, Schewe B, Kanz L, Vogel W. Novel markers for the prospective isolation of human msc. Ann NY Acad Sci. 2007;1106(01):262-271.
38. Álvarez-Viejo M, Menéndez-Menéndez Y, Otero-Hernández J. Cd271 as a marker to identify mesenchymal stem cells from diverse sources before culture. World J Stem Cells. 2015;7(2):470-476.
39. Ong WK, Tan CS, Chan KL, Goesantoso GG, Chan XH, Chan E*, et al.* Identification of specific cell-surface markers of adipose-derived stem cells from subcutaneous and visceral fat depots. Stem Cell Rep. 2014;2(2):171-179.
40. Qian H, Le Blanc K, Sigvardsson M. Primary mesenchymal stem and progenitor cells from bone marrow lack expression of cd44 protein. J Biol Chem. 2012;287(31):25795-25807.
41. Fotia C, Massa A, Boriani F, Baldini N, Granchi D. Hypoxia enhances proliferation and stemness of human adipose-derived mesenchymal stem cells. Cytotechnology. 2015;67(6):1073-1084.
42. Cano E, Gebala V, Gerhardt H. Pericytes or mesenchymal stem cells: Is that the question? Cell Stem Cell. 2017;20(3):296-297.
43. Attwell D, Mishra A, Hall CN, O'Farrell FM, Dalkara T. What is a pericyte? J Cereb Blood Flow Metab. 2016;36(2):451-455.
44. Birbrair A, Borges IdT, Gilson Sena IF, Almeida GrG, da Silva Meirelles L, Gonçalves R*, et al.* How plastic are pericytes? Stem Cells Dev. 2017;26(14).
45. Crisan M, Yap S, Casteilla L, Chen C-W, Corselli M, Park TS*, et al.* A perivascular origin for mesenchymal stem cells in multiple human organs. Cell Stem Cell. 2008;3(3):301-313.
46. Dellavalle A, Sampaolesi M, Tonlorenzi R, Tagliafico E, Sacchetti B, Perani L*, et al.* Pericytes of human skeletal muscle are myogenic precursors distinct from satellite cells. Nat Cell Biol. 2007;9(3):255-267.
47. Chen WCW, Baily JE, Corselli M, Díaz ME, Sun B, Xiang G*, et al.* Human myocardial pericytes: Multipotent mesodermal precursors exhibiting cardiac specificity. Stem Cells. 2015;33(2):557-573.
48. Krautler NJ, Kana V, Kranich J, Tian Y, Perera D, Lemm D*, et al.* Follicular dendritic cells emerge from ubiquitous perivascular precursors. Cell. 2012;150(1):194-206.

49. Guimaraes-Camboa N, Cattaneo P, Sun Y, Moore-Morris T, Gu Y, Dalton ND*, et al.* Pericytes of multiple organs do not behave as mesenchymal stem cells in vivo. Cell Stem Cell. 2017;20(3):345-359.e345.
50. McLeod CM, Mauck RL. On the origin and impact of mesenchymal stem cell heterogeneity: New insights and emerging tools for single cell analysis. Eur Cell Mater [Internet]. 2017; 34:[217-231 pp.].
51. Chang YJ, Shih DT, Tseng CP, Hsieh TB, Lee DC, Hwang SM. Disparate mesenchyme-lineage tendencies in mesenchymal stem cells from human bone marrow and umbilical cord blood. Stem Cells. 2006;24(3):679-685.
52. Choudhery MS, Badowski M, Muise A, Pierce J, Harris DT. Donor age negatively impacts adipose tissue-derived mesenchymal stem cell expansion and differentiation. J Transl Med. 2014;12(1):8.
53. Ferrer-Lorente R, Bejar MT, Tous M, Vilahur G, Badimon L. Systems biology approach to identify alterations in the stem cell reservoir of subcutaneous adipose tissue in a rat model of diabetes: Effects on differentiation potential and function. Diabetologia. 2014;57(1):246-256.
54. Wang J, Liao L, Wang S, Tan J. Cell therapy with autologous mesenchymal stem cells-how the disease process impacts clinical considerations. Cytotherapy. 2013;15(8):893-904.
55. Xu L, Liu Y, Sun Y, Wang B, Xiong Y, Lin W*, et al.* Tissue source determines the differentiation potentials of mesenchymal stem cells: A comparative study of human mesenchymal stem cells from bone marrow and adipose tissue. Stem Cell Res Ther. 2017;8(1):275.
56. Lu LL, Liu YJ, Yang SG, Zhao QJ, Wang X, Gong W*, et al.* Isolation and characterization of human umbilical cord mesenchymal stem cells with hematopoiesis-supportive function and other potentials. Haematologica. 2006;91(8):1017-1026.
57. Peng L, Jia Z, Yin X, Zhang X, Liu Y, Chen P*, et al.* Comparative analysis of mesenchymal stem cells from bone marrow, cartilage, and adipose tissue. Stem Cells Dev. 2008;17(4):761-773.
58. Selich A, Daudert J, Hass R, Philipp F, von Kaisenberg C, Paul G*, et al.* Massive clonal selection and transiently contributing clones during expansion of mesenchymal stem cell cultures revealed by lentiviral rgb-barcode technology. Stem Cells Transl Med. 2016;5(5):591-601.
59. Méhes E, Biri-Kovács B, Isai DG, Gulyás M, Nyitray L, Czirók A. Matrigel patterning reflects multicellular contractility. PLoS Comput Biol. 2019;15(10):e1007431.
60. Francescone RA, 3rd, Faibish M, Shao R. A matrigel-based tube formation assay to assess the vasculogenic activity of tumor cells. J Vis Exp. 2011(55):3040.
61. Paredes B, Santana A, Arribas MI, Vicente-Salar N, de Aza PN, Roche E*, et al.* Phenotypic differences during the osteogenic differentiation of single cell-derived clones isolated from human lipoaspirates. J Tissue Eng Regen Med. 2011;5(8):589-599.
62. Kuçi Z, Seiberth J, Latifi-Pupovci H, Wehner S, Stein S, Grez M*, et al.* Clonal analysis of multipotent stromal cells derived from cd271+ bone marrow mononuclear cells: Functional heterogeneity and different mechanisms of allosuppression. Haematologica. 2013;98(10):1609-1616.

63. Okamoto T, Aoyama T, Nakayama T, Nakamata T, Hosaka T, Nishijo K*, et al.* Clonal heterogeneity in differentiation potential of immortalized human mesenchymal stem cells. Biochem Biophys Res Commun. 2002;295(2):354-361.
64. Russell KC, Phinney DG, Lacey MR, Barrilleaux BL, Meyertholen KE, O'Connor KC. In vitro high-capacity assay to quantify the clonal heterogeneity in trilineage potential of mesenchymal stem cells reveals a complex hierarchy of lineage commitment. Stem Cells. 2010;28(4):788-798.
65. Selich A, Ha T-C, Morgan M, Falk CS, von Kaisenberg C, Schambach A*, et al.* Cytokine selection of msc clones with different functionality. Stem Cell Rep. 2019;13(2):262-273.
66. Jo CH, Lee YG, Shin WH, Kim H, Chai JW, Jeong EC*, et al.* Intra-articular injection of mesenchymal stem cells for the treatment of osteoarthritis of the knee: A proof-of-concept clinical trial. Stem Cells. 2014;32(5):1254-1266.
67. Hjortholm N, Jaddini E, Hałaburda K, Snarski E. Strategies of pain reduction during the bone marrow biopsy. Ann Hematol. 2013;92(2):145-149.
68. Schneider S, Unger M, van Griensven M, Balmayor ER. Adipose-derived mesenchymal stem cells from liposuction and resected fat are feasible sources for regenerative medicine. Eur J Med Res. 2017;22(1):17.
69. Bourin P, Bunnell BA, Casteilla L, Dominici M, Katz AJ, March KL*, et al.* Stromal cells from the adipose tissue-derived stromal vascular fraction and culture expanded adipose tissue-derived stromal/stem cells: A joint statement of the international federation for adipose therapeutics and science (ifats) and the international society for cellular therapy (isct). Cytotherapy. 2013;15(6):641-648.
70. L. LR, Jan F. Functional and clinical significance of skeletal muscle architecture. Muscle Nerve. 2000;23(11):1647-1666.
71. Frontera WR, Ochala J. Skeletal muscle: A brief review of structure and function. Behav Genet. 2015;45(2):183-195.
72. Le Verche V, Sunshine SS, Hammers D, Sweeney HL, Paushkin S. Skeletal muscle in spinal muscular atrophy as an opportunity for therapeutic intervention. Spinal muscle atrophy: Academic Press; 2017. p. 341-356.
73. Mukund K, Subramaniam S. Skeletal muscle: A review of molecular structure and function, in health and disease. Wiley Interdiscip Rev Syst Biol Med. 2020;12(1):e1462.
74. González-Morales N, Holenka TK, Schöck F, Kadrmas JL. Filamin actin-binding and titin-binding fulfill distinct functions in z-disc cohesion. PLoS Genet. 2017;13(7):e1006880.
75. Luther PK. The vertebrate muscle z-disc: Sarcomere anchor for structure and signalling. Muscle Res Cell Motil. 2009;30(5):171-185.
76. Pappas CT, Bhattacharya N, Cooper JA, Gregorio CC. Nebulin interacts with capz and regulates thin filament architecture within the z-disc. Mol Biol Cell. 2008;19(5):1837-1847.
77. Marzuca-Nassr GN, Vitzel KF, Mancilla-Solorza E, Marquez JL. Sarcomere structure: The importance of desmin protein in muscle atrophy. J Morphol. 2018;36(2):576-583.
78. Bentzinger CF, Wang YX, Rudnicki MA. Building muscle: Molecular regulation of myogenesis. Cold Spring Harb Perspect Biol. 2012;4(2):a008342.

79. Chang CN, Kioussi C. Location, location, location: Signals in muscle specification. J Dev Biol. 2018;6(2).
80. Relaix F, Rocancourt D, Mansouri A, Buckingham M. A pax3/pax7-dependent population of skeletal muscle progenitor cells. Nature. 2005;435(7044):948-953.
81. Chal J, Pourquié O. Making muscle: Skeletal myogenesis in vivo and in vitro. Development. 2017;144(12):2104-2122.
82. Weintraub H, Davis R, Tapscott S, Thayer M, Krause M, Benezra R*, et al.* The myod gene family: Nodal point during specification of the muscle cell lineage. Science. 1991;251(4995):761-766.
83. Conerly ML, Yao Z, Zhong JW, Groudine M, Tapscott SJ. Distinct activities of myf5 and myod indicate separate roles in skeletal muscle lineage specification and differentiation. Dev Cell. 2016;36(4):375-385.
84. Hutcheson DA, Zhao J, Merrell A, Haldar M, Kardon G. Embryonic and fetal limb myogenic cells are derived from developmentally distinct progenitors and have different requirements for beta-catenin. Genes Dev. 2009;23(8):997-1013.
85. Maqbool T, Jagla K. Genetic control of muscle development: Learning from drosophila. J Muscle Res Cell Motil. 2007;28(7-8):397-407.
86. Kawakami K, Sato S, Ozaki H, Ikeda K. Six family genes-structure and function as transcription factors and their roles in development. Bioessays. 2000;22(7):616-626.
87. Grifone R, Demignon J, Houbron C, Souil E, Niro C, Seller MJ*, et al.* Six1 and six4 homeoproteins are required for pax3 and mrf expression during myogenesis in the mouse embryo. Development. 2005;132(9):2235-2249.
88. Buckingham M, Rigby PW. Gene regulatory networks and transcriptional mechanisms that control myogenesis. Dev Cell. 2014;28(3):225-238.
89. Giordani J, Bajard L, Demignon J, Daubas P, Buckingham M, Maire P. Six proteins regulate the activation of myf5 expression in embryonic mouse limbs. Proc Natl Acad Sci. 2007;104(27):11310-11315.
90. Maroto M, Reshef R, Münsterberg AE, Koester S, Goulding M, Lassar AB. Ectopic pax-3 activates myod and myf-5 expression in embryonic mesoderm and neural tissue. Cell. 1997;89(1):139-148.
91. Londhe P, Davie JK. Sequential association of myogenic regulatory factors and e proteins at muscle-specific genes. Skelet Muscle. 2011;1(1):14.
92. Hu P, Geles KG, Paik JH, DePinho RA, Tjian R. Codependent activators direct myoblast-specific myod transcription. Dev Cell. 2008;15(4):534-546.
93. Yao J, Fetter RD, Hu P, Betzig E, Tjian R. Subnuclear segregation of genes and core promoter factors in myogenesis. Genes Dev. 2011;25(6):569-580.
94. Kitzmann M, Carnac G, Vandromme M, Primig M, Lamb NJ, Fernandez A. The muscle regulatory factors myod and myf-5 undergo distinct cell cycle-specific expression in muscle cells. J Cell Biol. 1998;142(6):1447-1459.
95. Simone C, Stiegler P, Bagella L, Pucci B, Bellan C, De Falco G*, et al.* Activation of myod-dependent transcription by cdk9/cyclin t2. Oncogene. 2002;21(26):4137-4148.
96. Kitzmann M, Fernandez A. Crosstalk between cell cycle regulators and the myogenic factor myod in skeletal myoblasts. Cell Mol Life Sci. 2001;58(4):571-579.

97. Tapscott SJ. The circuitry of a master switch: Myod and the regulation of skeletal muscle gene transcription. Development. 2005;132(12):2685-2695.
98. Deato MDE, Marr MT, Sottero T, Inouye C, Hu P, Tjian R. Myod targets taf3/trf3 to activate myogenin transcription. Mol Cell. 2008;32(1):96-105.
99. Liu QC, Zha XH, Faralli H, Yin H, Louis-Jeune C, Perdiguero E*, et al.* Comparative expression profiling identifies differential roles for myogenin and p38α mapk signaling in myogenesis. J Mol Cell Biol. 2012;4(6):386-397.
100. Higashioka K, Koizumi N, Sakurai H, Sotozono C, Sato T. Myogenic differentiation from myogenin-mutated human ips cells by crispr/cas9. Stem Cells Int. 2017;2017:9210494.
101. Hernández-Hernández JM, García-González EG, Brun CE, Rudnicki MA. The myogenic regulatory factors, determinants of muscle development, cell identity and regeneration. Semin Cell Dev Biol. 2017;72:10-18.
102. Moretti I, Ciciliot S, Dyar KA, Abraham R, Murgia M, Agatea L*, et al.* Mrf4 negatively regulates adult skeletal muscle growth by repressing mef2 activity. Nat Commun. 2016;7:12397.
103. Kassar-Duchossoy L, Gayraud-Morel B, Gomès D, Rocancourt D, Buckingham M, Shinin V*, et al.* Mrf4 determines skeletal muscle identity in myf5:Myod double-mutant mice. Nature. 2004;431:466.
104. Andrés V, Walsh K. Myogenin expression, cell cycle withdrawal, and phenotypic differentiation are temporally separable events that precede cell fusion upon myogenesis. J Cell Biol. 1996;132(4):657-666.
105. Creuzet S, Lescaudron L, Li Z, Fontaine-Pérus J. Myod, myogenin, and desmin-nls-lacz transgene emphasize the distinct patterns of satellite cell activation in growth and regeneration. Exp Cell Res. 1998;243(2):241-253.
106. Li H, Capetanaki Y. Regulation of the mouse desmin gene: Transactivated by myod, myogenin, mrf4 and myf5. Nucleic Acids Res. 1993;21(2):335-343.
107. Li H, Capetanaki Y. An e box in the desmin promoter cooperates with the e box and mef-2 sites of a distal enhancer to direct muscle-specific transcription. Embo j. 1994;13(15):3580-3589.
108. McCall GE, Haddad F, Roy RR, Zhong H, Edgerton VR, Baldwin KM. Transcriptional regulation of the myosin heavy chain iib gene in inactive rat soleus. Muscle Nerve. 2009;40(3):411-419.
109. Swoap SJ. In vivo analysis of the myosin heavy chain iib promoter region. Am J Physiol. 1998;274(3):C681-687.
110. Tedesco FS, Dellavalle A, Diaz-Manera J, Messina G, Cossu G. Repairing skeletal muscle: Regenerative potential of skeletal muscle stem cells. J Clin Invest. 2010;120(1):11-19.
111. Gharaibeh B, Chun-Lansinger Y, Hagen T, Ingham SJ, Wright V, Fu F*, et al.* Biological approaches to improve skeletal muscle healing after injury and disease. Birth Defects Res C Embryo Today. 2012;96(1):82-94.
112. McCullagh KJA, Perlingeiro RCR. Coaxing stem cells for skeletal muscle repair. Adv Drug Deliv Rev. 2015;84:198-207.
113. Peçanha R, Bagno LdLeS, Ribeiro MB, Robottom Ferreira AB, Moraes MOr, Zapata-Sudo G*, et al.* Adipose-derived stem-cell treatment of skeletal muscle injury. J Bone Joint Surg Am. 2012;94(7):609-617.
114. Merritt EK, Cannon MV, Hammers DW, Le LN, Gokhale R, Sarathy A*, et al.* Repair of traumatic skeletal muscle injury with bone-marrow-derived

mesenchymal stem cells seeded on extracellular matrix. Tissue Eng. 2010;16(9):2871-2881.
115. Sun C, Serra C, Lee G, Wagner KR. Stem cell-based therapies for duchenne muscular dystrophy. Exp Neurol. 2020;323:113086.
116. De Bari C, Dell'Accio F, Vandenabeele F, Vermeesch JR, Raymackers JM, Luyten FP. Skeletal muscle repair by adult human mesenchymal stem cells from synovial membrane. J Cell Biol. 2003;160(6):909-918.
117. Klimczak A, Zimna A, Malcher A, Kozlowska U, Futoma K, Czarnota J*, et al.* Co-transplantation of bone marrow-mscs and myogenic stem/progenitor cells from adult donors improves muscle function of patients with duchenne muscular dystrophy. Cells. 2020;9(5).
118. Bouglé A, Rocheteau P, Briand D, Hardy D, Verdonk F, Tremolada C*, et al.* Beneficial role of adipose-derived mesenchymal stem cells from microfragmented fat in a murine model of duchenne muscular dystrophy. Muscle Nerve. 2019;60(3):328-335.
119. Qiu X, Liu S, Zhang H, Zhu B, Su Y, Zheng C*, et al.* Mesenchymal stem cells and extracellular matrix scaffold promote muscle regeneration by synergistically regulating macrophage polarization toward the m2 phenotype. Stem Cell Res Ther. 2018;9(1):88.
120. Pumberger M, Qazi TH, Ehrentraut MC, Textor M, Kueper J, Stoltenburg-Didinger G*, et al.* Synthetic niche to modulate regenerative potential of mscs and enhance skeletal muscle regeneration. Biomaterials. 2016;99:95-108.
121. Ambele MA, Dessels C, Durandt C, Pepper MS. Genome-wide analysis of gene expression during adipogenesis in human adipose-derived stromal cells reveals novel patterns of gene expression during adipocyte differentiation. Stem Cell Res. 2016;16(3):725-734.
122. Guo L, Li X, Tang QQ. Transcriptional regulation of adipocyte differentiation: A central role for ccaat/enhancer-binding protein (c/ebp) β. J Biol Chem. 2015;290(2):755-761.
123. Stromps J-P, Paul NE, Rath B, Nourbakhsh M, Bernhagen J, Pallua N. Chondrogenic differentiation of human adipose-derived stem cells: A new path in articular cartilage defect management? BioMed Res Int. 2014;2014:740926-740926.
124. Wang W, Rigueur D, Lyons KM. Tgfβ signaling in cartilage development and maintenance. Birth Defects Res C Embryo Today. 2014;102(1):37-51.
125. Marshall CD, Brett EA, Moore AL, Wan DC, Longaker MT. In vitro and in vivo osteogenic differentiation of human adipose-derived stromal cells. Methods Mol Biol. 2019;1891:9-18.
126. Nishimura I, Hisanaga R, Sato T, Arano T, Nomoto S, Ikada Y*, et al.* Effect of osteogenic differentiation medium on proliferation and differentiation of human mesenchymal stem cells in three-dimensional culture with radial flow bioreactor. Regen Ther. 2015;2:24-31.
127. Chung CH, Golub EE, Forbes E, Tokuoka T, Shapiro IM. Mechanism of action of beta-glycerophosphate on bone cell mineralization. Calcif Tissue Int. 1992;51(4):305-311.
128. Prockop DJ, Kivirikko KI. Collagens: Molecular biology, diseases, and potentials for therapy. Annu Rev Biochem. 1995;64:403-434.

129. Hamidouche Z, Haÿ E, Vaudin P, Charbord P, Schüle R, Marie PJ*, et al.* Fhl2 mediates dexamethasone-induced mesenchymal cell differentiation into osteoblasts by activating wnt/beta-catenin signaling-dependent runx2 expression. Faseb j. 2008;22(11):3813-3822.
130. Zuk PA, Zhu M, Mizuno H, Huang J, Futrell JW, Katz AJ*, et al.* Multilineage cells from human adipose tissue: Implications for cell-based therapies. Tissue Eng. 2001;7(2):211-228.
131. Mizuno H, Zuk PA, Zhu M, Lorenz HP, Benhaim P, Hedrick MH. Myogenic differentiation by human processed lipoaspirate cells. Plast Reconstr Surg. 2002;109(1):199-209; discussion 210-191.
132. Aboalola D, Han VKM. Different effects of insulin-like growth factor-1 and insulin-like growth factor-2 on myogenic differentiation of human mesenchymal stem cells. Stem Cells Int. 2017;2017(2):1-15.
133. Yilgor Huri P, Cook CA, Hutton DL, Goh BC, Gimble JM, DiGirolamo DJ*, et al.* Biophysical cues enhance myogenesis of human adipose derived stem/stromal cells. Biochem Biophys Res Commun. 2013;438(1):180-185.
134. Meligy FY, Shigemura K, Behnsawy HM, Fujisawa M, Kawabata M, Shirakawa T. The efficiency of in vitro isolation and myogenic differentiation of mscs derived from adipose connective tissue, bone marrow, and skeletal muscle tissue. In Vitro Cell Dev Biol Anim. 2012;48(4):203-215.
135. Drost AC, Weng S, Feil G, Schafer J, Baumann S, Kanz L*, et al.* In vitro myogenic differentiation of human bone marrow-derived mesenchymal stem cells as a potential treatment for urethral sphincter muscle repair. Ann NY Acad Sci. 2009;1176:135-143.
136. Gang EJ, Jeong JA, Hong SH, Hwang SH, Kim SW, Yang IH*, et al.* Skeletal myogenic differentiation of mesenchymal stem cells isolated from human umbilical cord blood. Stem Cells. 2004;22(4):617-624.
137. Sung MS, Mun J-Y, Kwon O, Kwon K-S, Oh D-B. Efficient myogenic differentiation of human adipose-derived stem cells by the transduction of engineered myod protein. Biochem Biophys Res Commun. 2013;437(1):156-161.
138. Lawson MA, Purslow PP. Differentiation of myoblasts in serum-free media: Effects of modified media are cell line-specific. Cell Tissue Res. 2000;167(2-3):130-137.
139. Venter C, Niesler CU. Cellular alignment and fusion: Quantifying the effect of macrophages and fibroblasts on myoblast terminal differentiation. Exp Cell Res. 2018;370(2):542-550.
140. Yaffe D, Saxel ORA. Serial passaging and differentiation of myogenic cells isolated from dystrophic mouse muscle. Nature. 1977;270(5639):725-727.
141. Franke J, Abs V, Zizzadoro C, Abraham G. Comparative study of the effects of fetal bovine serum versus horse serum on growth and differentiation of primary equine bronchial fibroblasts. BMC Vet Res. 2014;10:119-119.
142. Mullen PA. Ii. Serum constituents. Equine Vet J. 1969;1(5):190-194.
143. Lawson MA, Purslow PP. Differentiation of myoblasts in serum-free media: Effects of modified media are cell line-specific. Cell Tissue Res. 2000;167(2-3):130-137.

144. Oakley RH, Cidlowski JA. The biology of the glucocorticoid receptor: New signaling mechanisms in health and disease. J Allergy Clin Immunol. 2013;132(5):1033-1044.
145. Surjit M, Ganti KP, Mukherji A, Ye T, Hua G, Metzger D*, et al.* Widespread negative response elements mediate direct repression by agonist-liganded glucocorticoid receptor. Cell. 2011;145(2):224-241.
146. Braun TP, Marks DL. The regulation of muscle mass by endogenous glucocorticoids. Front Physiol. 2015;6:12.
147. Kuo T, Harris CA, Wang J-C. Metabolic functions of glucocorticoid receptor in skeletal muscle. Mol Cell Endocrinol. 2013;380(1-2):79-88.
148. Larson AA, Syverud BC, Florida SE, Rodriguez BL, Pantelic MN, Larkin LM. Effects of dexamethasone dose and timing on tissue-engineered skeletal muscle units. Cell Tissue Res. 2018;205(4):197-207.
149. Belanto JJ, Diaz-Perez SV, Magyar CE, Maxwell MM, Yilmaz Y, Topp K*, et al.* Dexamethasone induces dysferlin in myoblasts and enhances their myogenic differentiation. Neuromuscul Disord. 2010;20(2):111-121.
150. Han D-S, Yang W-S, Kao T-W. Dexamethasone treatment at the myoblast stage enhanced c2c12 myocyte differentiation. Int J Med Sci. 2017;14(5):434-443.
151. Zalin RJ. The role of hormones and prostanoids in the in vitro proliferation and differentiation of human myoblasts. Exp Cell Res. 1987;172(2):265-281.
152. Stresemann C, Lyko F. Modes of action of the DNA methyltransferase inhibitors azacytidine and decitabine. Int J Cancer. 2008;123(1):8-13.
153. Kribelbauer JF, Lu X-J, Rohs R, Mann RS, Bussemaker HJ. Toward a mechanistic understanding of DNA methylation readout by transcription factors. J Mol Biol. 2020;432(6):1801-1815.
154. Noer A, Sørensen AL, Boquest AC, Collas P. Stable cpg hypomethylation of adipogenic promoters in freshly isolated, cultured, and differentiated mesenchymal stem cells from adipose tissue. Mol Biol Cell. 2006;17(8):3543-3556.
155. Vera-Pérez B, Arribas MI, Vicente-Salar N, Reig JA, Roche E. DNA methylation profile of different clones of human adipose stem cells does not allow to predict their differentiation potential. J Histotechnol. 2019;42(4):183-192.
156. Montesano A, Luzi L, Senesi P, Terruzzi I. Modulation of cell cycle progression by 5-azacytidine is associated with early myogenesis induction in murine myoblasts. Int J Biol Sci. 2013;9(4):391-402.
157. Kaur K, Yang J, Eisenberg CA, Eisenberg LM. 5-azacytidine promotes the transdifferentiation of cardiac cells to skeletal myocytes. Cell Reprogram. 2014;16(5):324-330.
158. Huri PY, Wang A, Spector AA, Grayson WL. Multistage adipose-derived stem cell myogenesis: An experimental and modeling study. Cell Mol Bioeng. 2014;7(4):497-509.
159. Huri PY, Morrissette-McAlmon J, Grayson WL. Myogenic differentiation of ascs using biochemical and biophysical induction. Methods Mol Biol. 2018;1773:123-135.
160. Deshpande RS, Spector AA. Modeling stem cell myogenic differentiation. Sci Rep. 2017;7(1).

161. Mason C, Dunnill P. A brief definition of regenerative medicine. Regen Med. 2008;3(1):1-5.
162. Gimble JM, Katz AJ, Bunnell BA. Adipose-derived stem cells for regenerative medicine. Circ Res. 2007;100(9):1249-1260.
163. Viganò M, Budelli S, Lavazza C, Montemurro T, Montelatici E, de Cesare S*, et al.* Tips and tricks for validation of quality control analytical methods in good manufacturing practice mesenchymal stromal cell production. Stem Cells Int. 2018;2018:3038565.
164. Dessels C, Durandt C, Pepper MS. Comparison of human platelet lysate alternatives using expired and freshly isolated platelet concentrates for adipose-derived stromal cell expansion. Platelets. 2018:1-12.
165. Camilleri ET, Gustafson MP, Dudakovic A, Riester SM, Garces CG, Paradise CR*, et al.* Identification and validation of multiple cell surface markers of clinical-grade adipose-derived mesenchymal stromal cells as novel release criteria for good manufacturing practice-compliant production. Stem Cell Res Ther. 2016;7(1):107.
166. Dessels c. Expansion of human adipose-derived stem cells: Human alternatives to foetal bovine serum [dissertation]. Pretoria, south africa: University of pretoria, 2016. .
167. Kølle S-FT, Fischer-Nielsen A, Mathiasen AB, Elberg JJ, Oliveri RS, Glovinski PV*, et al.* Enrichment of autologous fat grafts with ex-vivo expanded adipose tissue-derived stem cells for graft survival: A randomised placebo-controlled trial. Lancet. 2013;382(9898):1113-1120.
168. Dhurat R, Sukesh M. Principles and methods of preparation of platelet-rich plasma: A review and author's perspective. J Cutan Aesthet Surg. 2014;7(4):189-197.
169. Schallmoser K, Strunk D. Generation of a pool of human platelet lysate and efficient use in cell culture. Basic cell culture protocols: Springer; 2013. p. 349-362.
170. Cowper M, Frazier T, Wu X, Curley L, Ma MH, Mohuiddin OA*, et al.* Human platelet lysate as a functional substitute for fetal bovine serum in the culture of human adipose derived stromal/stem cells. Cells. 2019;8(7):724.
171. Mojica-Henshaw MP, jacobson P, Morris J, Kelley L, Pierce J, Boyer M*, et al.* Serum-converted platelet lysate can substitute for fetal bovine serum in human mesenchymal stromal cell cultures. Cytotherapy. 2013;15(12):1458-1468.
172. Shansky YD, Sergeeva NS, Sviridova IK, Karalkin PA, Kirsanova VA, Akhmedova SA*, et al.* Human platelet lysate sustains the osteogenic/adipogenic differentiation potential of adipose-derived mesenchymal stromal cells and maintains their DNA integrity in vitro. Cell Tissue Res. 2019;207(3-4):149-164.
173. van Vollenstee FA, Dessels C, Kallmeyer K, de Villiers D, Potgieter M, Durandt C*, et al.* Isolation and characterization of adipose-derived stromal cells. Stem cell processing: Springer International Publishing; 2016. p. 131-161.
174. Durandt C, van Vollenstee FA, Dessels C, Kallmeyer K, de Villiers D, Murdoch C*, et al.* Novel flow cytometric approach for the detection of adipocyte subpopulations during adipogenesis. J Lipid Res. 2016;57(4):729-742.

175. de Villiers D, Potgieter M, Ambele MA, Adam L, Durandt C, Pepper MS. The role of reactive oxygen species in adipogenic differentiation. Springer US. p. 1-20.
176. Ambele MA, Pepper MS. Identification of transcription factors potentially involved in human adipogenesis in vitro. Mol Genet Genomic Med. 2017;5(3):210-222.
177. van Vollenstee FA, Jackson C, Hoffmann D, Potgieter M, Durandt C, Pepper MS. Human adipose derived mesenchymal stromal cells transduced with gfp lentiviral vectors: Assessment of immunophenotype and differentiation capacity in vitro. Cytotechnology. 2016;68(5):2049-2060.
178. Dzobo K, Turnley T, Wishart A, Rowe A, Kallmeyer K, van Vollenstee FA*, et al.* Fibroblast-derived extracellular matrix induces chondrogenic differentiation in human adipose-derived mesenchymal stromal/stem cells in vitro. Int J Mol Sci. 2016;17(8).
179. De Francesco F, Mannucci S, Conti G, Dai Prè E, Sbarbati A, Riccio M. A non-enzymatic method to obtain a fat tissue derivative highly enriched in adipose stem cells (ascs) from human lipoaspirates: Preliminary results. Int J Mol Sci. 2018;19(7):2061.
180. Chaput B, Bertheuil N, Escubes M, Grolleau JL, Garrido I, Laloze J*, et al.* Mechanically isolated stromal vascular fraction provides a valid and useful collagenase-free alternative technique: A comparative study. Plast Reconstr Surg. 2016;138(4):807-819.
181. Raposio E, Caruana G, Bonomini S, Libondi G. A novel and effective strategy for the isolation of adipose-derived stem cells: Minimally manipulated adipose-derived stem cells for more rapid and safe stem cell therapy. Plast Reconstr Surg. 2014;133(6):1406-1409.
182. Bajek A, Gurtowska N, Gackowska L, Kubiszewska I, Bodnar M, Marszałek A*, et al.* Does the liposuction method influence the phenotypic characteristic of human adipose-derived stem cells? Biosci Rep. 2015;35(3).
183. Busser H, De Bruyn C, Urbain F, Najar M, Pieters K, Raicevic G*, et al.* Isolation of adipose-derived stromal cells without enzymatic treatment: Expansion, phenotypical, and functional characterization. Stem Cells Dev. 2014;23(19):2390-2400.
184. Fuoco NL, de Oliveira RG, Marcelino MY, Stessuk T, Sakalem ME, Medina DAL*, et al.* Efficient isolation and proliferation of human adipose-derived mesenchymal stromal cells in xeno-free conditions. Mol Biol Rep. 2020;47(4):2475-2486.
185. McCoy JP. Basic principles of flow cytometry. Hematol Oncol Clin North Am. 2002;16(2):229-243.
186. Ohnuma K, Yomo T, Asashima M, Kaneko K. Sorting of cells of the same size, shape, and cell cycle stage for a single cell level assay without staining. BMC Cell Biol. 2006;7(1):25.
187. Adan A, Alizada G, Kiraz Y, Baran Y, Nalbant A. Flow cytometry: Basic principles and applications. Crit Rev Biotechnol. 2017;37(2):163-176.
188. Sneath RJ, Mangham DC. The normal structure and function of cd44 and its role in neoplasia. Mol Pathol. 1998;51(4):191-200.

189. Senbanjo LT, Chellaiah MA. Cd44: A multifunctional cell surface adhesion receptor is a regulator of progression and metastasis of cancer cells. Front Cell Dev Biol. 2017;5(18).
190. Moraes DA, Sibov TT, Pavon LF, Alvim PQ, Bonadio RS, Da Silva JR*, et al.* A reduction in cd90 (thy-1) expression results in increased differentiation of mesenchymal stromal cells. Stem Cell Res Ther. 2016;7(1):97-97.
191. Chen X, Shao H, Zhi Y, Xiao Q, Su C, Dong L*, et al.* Cd73 pathway contributes to the immunosuppressive ability of mesenchymal stem cells in intraocular autoimmune responses. Stem Cells Dev. 2016;25(4):337-346.
192. Minor M, Alcedo KP, Battaglia RA, Snider NT. Cell type- and tissue-specific functions of ecto-5′-nucleotidase (cd73). Am J Physiol Cell Physiol. 2019;317(6):C1079-C1092.
193. Schneider E, Rissiek A, Winzer R, Puig B, Rissiek B, Haag F*, et al.* Generation and function of non-cell-bound cd73 in inflammation. Front Immunol. 2019;10(1729).
194. Li C, Issa R, Kumar P, Hampson IN, Lopez-Novoa JM, Bernabeu C*, et al.* Cd105 prevents apoptosis in hypoxic endothelial cells. J Cell Sci. 2003;116(Pt 13):2677-2685.
195. Fonsatti E, Maio M. Highlights on endoglin (cd105): From basic findings towards clinical applications in human cancer. J Transl Med. 2004;2(1):18.
196. Levi B, Wan DC, Glotzbach JP, Hyun J, Januszyk M, Montoro D*, et al.* Cd105 protein depletion enhances human adipose-derived stromal cell osteogenesis through reduction of transforming growth factor β1 (tgf-β1) signaling. J Biol Chem. 2011;286(45):39497-39509.
197. Zhao L, Varghese Z, Moorhead JF, Chen Y, Ruan XZ. Cd36 and lipid metabolism in the evolution of atherosclerosis. Br Med Bull. 2018;126(1):101-112.
198. Healy L, May G, Gale K, Grosveld F, Greaves M, Enver T. The stem cell antigen cd34 functions as a regulator of hemopoietic cell adhesion. Proc Natl Acad Sci. 1995;92(26):12240-12244.
199. Hermiston ML, Xu Z, Weiss A. Cd45: A critical regulator of signaling thresholds in immune cells. Annu Rev Immunol. 2003;21(1):107-137.
200. Zembruski NCL, Stache V, Haefeli WE, Weiss J. 7-aminoactinomycin d for apoptosis staining in flow cytometry. Anal Biochem. 2012;429(1):79-81.
201. Baumgarth N, Roederer M. A practical approach to multicolor flow cytometry for immunophenotyping. J Immunol Methods. 2000;243(1-2):77-97.
202. Cleary MA, Narcisi R, Focke K, van der Linden R, Brama PAJ, van Osch GJVM. Expression of cd105 on expanded mesenchymal stem cells does not predict their chondrogenic potential. Osteoarthritis Cartilage. 2016;24(5):868-872.
203. Durandt C, Dessels C, da Silva C, Murdoch C, Pepper MS. The effect of early rounds of ex vivo expansion and cryopreservation on the adipogenic differentiation capacity of adipose-derived stromal/stem cells. Sci Rep. 2019;9(1):15943.
204. Mesa-Arango AC, Scorzoni L, Zaragoza O. It only takes one to do many jobs: Amphotericin b as antifungal and immunomodulatory drug. Front Microbiol. 2012;3:286-286.

205. Skubis A, Gola J, Sikora B, Hybiak J, Paul-Samojedny M, Mazurek U*, et al.* Impact of antibiotics on the proliferation and differentiation of human adipose-derived mesenchymal stem cells. Int J Mol Sci. 2017;18(12).
206. Kubista M, Andrade JM, Bengtsson M, Forootan A, Jonák J, Lind K*, et al.* The real-time polymerase chain reaction. Mol Aspects Med. 2006;27(2-3):95-125.
207. Klein D. Quantification using real-time pcr technology: Applications and limitations. Trends Mol Med. 2002;8(6):257-260.
208. Bustin SA. Absolute quantification of mrna using real-time reverse transcription polymerase chain reaction assays. J Mol Endocrinol. 2000;25(2):169-193.
209. Navarro E, Serrano-Heras G, Castaño MJ, Solera J. Real-time pcr detection chemistry. Clinica Chimica Acta. 2015;439:231-250.
210. Cao H, Shockey JM. Comparison of taqman and sybr green qpcr methods for quantitative gene expression in tung tree tissues. J Agric Food Chem. 2012;60(50):12296-12303.
211. VanGuilder HD, Vrana KE, Freeman WM. Twenty-five years of quantitative pcr for gene expression analysis. Biotechniques. 2008;44(5):619-626.
212. Schmittgen TD, Livak KJ. Analyzing real-time pcr data by the comparative ct method. Nat Protoc. 2008;3(6):1101-1108.
213. Livak KJ, Schmittgen TD. Analysis of relative gene expression data using real-time quantitative pcr and the 2−δδct method. Methods. 2001;25(4):402-408.
214. Bustin SA, Benes V, Garson JA, Hellemans J, Huggett J, Kubista M*, et al.* The miqe guidelines: Minimum information for publication of quantitative real-time pcr experiments. Clin Chem. 2009;55(4):611-622.
215. Dessels C, Pepper MS. Reference gene expression in adipose-derived stromal cells undergoing adipogenic differentiation. Tissue Eng. 2019;25(6):353-366.
216. Lichtman JW, Conchello J-A. Fluorescence microscopy. Nat Methods. 2005;2(12):910-919.
217. Sanderson MJ, Smith I, Parker I, Bootman MD. Fluorescence microscopy. Cold Spring Harb Protoc. 2014;2014(10):pdb.top071795.
218. Paddock SW. Principles and practices of laser scanning confocal microscopy. Mol Biotechnol. 2000;16(2):127-149.
219. Hoffman GE, Murphy KJ, Sita LV. The importance of titrating antibodies for immunocytochemical methods. Curr Protoc Neurosci. 2016;76:2.12.11-12.12.37.
220. Buchwalow I, Samoilova V, Boecker W, Tiemann M. Non-specific binding of antibodies in immunohistochemistry: Fallacies and facts. Sci Rep. 2011;1(1):28.
221. Wilfinger WW, Mackey K, Chomczynski P. Effect of ph and ionic strength on the spectrophotometric assessment of nucleic acid purity. Biotechniques. 1997;22(3):474-476, 478-481.
222. Schroeder A, Mueller O, Stocker S, Salowsky R, Leiber M, Gassmann M*, et al.* The rin: An rna integrity number for assigning integrity values to rna measurements. BMC Mol Biol. 2006;7(1):3.
223. Dragan AI, Casas-Finet JR, Bishop ES, Strouse RJ, Schenerman MA, Geddes CD. Characterization of picogreen interaction with dsdna and the origin of its fluorescence enhancement upon binding. Biophys J. 2010;99(9):3010-3019.

224. Rosas-Arellano A, Villalobos-González JB, Palma-Tirado L, Beltrán FA, Cárabez-Trejo A, Missirlis F*, et al.* A simple solution for antibody signal enhancement in immunofluorescence and triple immunogold assays. Histochem Cell Biol. 2016;146(4):421-430.
225. McColl R, Nkosi M, Snyman C, Niesler C. Analysis and quantification of in vitro myoblast fusion using the ladd multiple stain. Biotechniques. 2016;61(6):323-326.
226. Megeney LA, Rudnicki MA. Determination versus differentiation and the myod family of transcription factors. Biochem Cell Biol. 1995;73(9-10):723-732.
227. Brzóska E, Przewoźniak M, Grabowska I, Jańczyk-Ilach K, Moraczewski J. Pax3 and pax7 expression during myoblast differentiation in vitro and fast and slow muscle regeneration in vivo. Cell Biol Int. 2009;33(4):483-492.
228. Cai A, Hardt M, Schneider P, Schmid R, Lange C, Dippold D*, et al.* Myogenic differentiation of primary myoblasts and mesenchymal stromal cells under serum-free conditions on pcl-collagen i-nanoscaffolds. BMC Biotechnol. 2018;18(1):75.
229. van der Ven PFM, Schaart G, Jap PHK, Sengers RCA, Stadhouders AM, Ramaekers FCS. Differentiation of human skeletal muscle cells in culture: Maturation as indicated by titin and desmin striation. Cell Tissue Res. 1992;270(1):189-198.
230. Sarcar S, Tulalamba W, Rincon MY, Tipanee J, Pham HQ, Evens H*, et al.* Next-generation muscle-directed gene therapy by in silico vector design. Nat Commun. 2019;10(1):492.
231. Koussounadis A, Langdon SP, Um IH, Harrison DJ, Smith VA. Relationship between differentially expressed mrna and mrna-protein correlations in a xenograft model system. Sci Rep. 2015;5(1):10775.
232. Gry M, Rimini R, Strömberg S, Asplund A, Pontén F, Uhlén M*, et al.* Correlations between rna and protein expression profiles in 23 human cell lines. BMC Genom. 2009;10(1):365.
233. Gray SM, Xin Y, Ross EC, Chazotte BM, Capozzi ME, El K*, et al.* Discordance between glp-1r gene and protein expression in mouse pancreatic islet cells. Int J Biol Chem. 2020;295(33):11529-11541.
234. Wolmarans E, Mellet J, Durandt C, Joubert F, Pepper MS. Single-cell transcriptome analysis of human adipose-derived stromal cells identifies a contractile cell subpopulation. Stem Cells Int. 2021;2021:5595172.
235. Uezumi A, Nakatani M, Ikemoto-Uezumi M, Yamamoto N, Morita M, Yamaguchi A*, et al.* Cell-surface protein profiling identifies distinctive markers of progenitor cells in human skeletal muscle. Stem Cell Rep. 2016;7(2):263-278.
236. Chen J, Luo Y, Huang H, Wu S, Feng J, Zhang J*, et al.* Cd146 is essential for pdgfrβ-induced pericyte recruitment. Protein Cell. 2018;9(8):743-747.
237. Liu M, Gomez D. Smooth muscle cell phenotypic diversity. Arterioscler Thromb Vasc Biol. 2019;39(9):1715-1723.
238. Caicedo JC, Cooper S, Heigwer F, Warchal S, Qiu P, Molnar C*, et al.* Data-analysis strategies for image-based cell profiling. Nat Methods. 2017;14(9):849-863.
239. Jurgens WJFM, Oedayrajsingh-Varma MJ, Helder MN, Zandiehdoulabi B, Schouten TE, Kuik DJ*, et al.* Effect of tissue-harvesting site on yield of stem

cells derived from adipose tissue: Implications for cell-based therapies. Cell Tissue Res. 2008;332(3):415-426.
240. Kocan B, Maziarz A, Tabarkiewicz J, Ochiya T, Banaś-Ząbczyk A. Trophic activity and phenotype of adipose tissue-derived mesenchymal stem cells as a background of their regenerative potential. Stem Cells Int. 2017;2017:1653254-1653254.
241. Travnickova M, Pajorova J, Zarubova J, Krocilova N, Molitor M, Bacakova L. The influence of negative pressure and of the harvesting site on the characteristics of human adipose tissue-derived stromal cells from lipoaspirates. Stem Cells Int. 2020;2020:1016231.
242. Jin HJ, Park SK, Oh W, Yang YS, Kim SW, Choi SJ. Down-regulation of cd105 is associated with multi-lineage differentiation in human umbilical cord blood-derived mesenchymal stem cells. Biochem Biophys Res Commun. 2009;381(4):676-681.
243. Anderson P, Carrillo-Gálvez AB, García-Pérez A, Cobo M, Martín F. Cd105 (endoglin)-negative murine mesenchymal stromal cells define a new multipotent subpopulation with distinct differentiation and immunomodulatory capacities. PLoS One. 2013;8(10):e76979.
244. Zhang D, Yan K, Zhou J, Xu T, Xu M, Lin J*, et al.* Myogenic differentiation of human amniotic mesenchymal cells and its tissue repair capacity on volumetric muscle loss. J Tissue Eng. 2019;10:2041731419887100.
245. Dessels C, Ambele MA, Pepper MS. The effect of medium supplementation and serial passaging on the transcriptome of human adipose-derived stromal cells expanded in vitro. Stem Cell Res Ther. 2019;10(1):253.
246. Liao H-T, Chen C-T. Osteogenic potential: Comparison between bone marrow and adipose-derived mesenchymal stem cells. World J Stem Cells. 2014;6(3):288-295.
247. Mohamed-Ahmed S, Fristad I, Lie SA, Suliman S, Mustafa K, Vindenes H*, et al.* Adipose-derived and bone marrow mesenchymal stem cells: A donor-matched comparison. Stem Cell Res Ther. 2018;9(1):168.
248. Zhou W, Lin J, Zhao K, Jin K, He Q, Hu Y*, et al.* Single-cell profiles and clinically useful properties of human mesenchymal stem cells of adipose and bone marrow origin. Am J Sports Med. 2019;47(7):1722-1733.
249. Xie L, Zhang N, Marsano A, Vunjak-Novakovic G, Zhang Y, Lopez MJ. In vitro mesenchymal trilineage differentiation and extracellular matrix production by adipose and bone marrow derived adult equine multipotent stromal cells on a collagen scaffold. Stem Cell Rev Rep. 2013;9(6):858-872.
250. Monaco E, Bionaz M, Rodriguez-Zas S, Hurley WL, Wheeler MB. Transcriptomics comparison between porcine adipose and bone marrow mesenchymal stem cells during in vitro osteogenic and adipogenic differentiation. PLoS One. 2012;7(3):e32481.
251. Vishnubalaji R, Al-Nbaheen M, Kadalmani B, Aldahmash A, Ramesh T. Comparative investigation of the differentiation capability of bone-marrow- and adipose-derived mesenchymal stem cells by qualitative and quantitative analysis. Cell Tissue Res. 2012;347(2):419-427.
252. Church CD, Berry R, Rodeheffer MS. Isolation and study of adipocyte precursors. Methods Enzymol. 2014;537:31-46.

253. Yang D, Li N, Zhang G. Spontaneous adipogenic differentiation potential of adipose-derived stem cells decreased with increasing cell passages. Mol Med Rep. 2018;17(4):6109-6115.
254. Robert AW, Marcon BH, Dallagiovanna B, Shigunov P. Adipogenesis, osteogenesis, and chondrogenesis of human mesenchymal stem/stromal cells: A comparative transcriptome approach. Front Cell Dev Biol. 2020;8(561).
255. Ding S, Wang F, Liu Y, Li S, Zhou G, Hu P. Characterization and isolation of highly purified porcine satellite cells. Cell Death Dis. 2017;3(1):17003.
256. Garg K, Corona BT, Walters TJ. Therapeutic strategies for preventing skeletal muscle fibrosis after injury. Front Pharmacol. 2015;6:87-87.
257. Asfour HA, Allouh MZ, Said RS. Myogenic regulatory factors: The orchestrators of myogenesis after 30 years of discovery. Exp Biol Med. 2018;243(2):118-128.
258. Wang Y, Song J, Liu X, Liu J, Zhang Q, Yan X*, et al.* Multiple effects of mechanical stretch on myogenic progenitor cells. Stem Cells Dev. 2020;29(6):336-352.
259. Ergene E, Sezlev Bilecen D, Kaya B, Yilgor Huri P, Hasirci V. 3d cellular alignment and biomimetic mechanical stimulation enhance human adipose-derived stem cell myogenesis. Biomed Mater. 2020;15(5):055017.
260. Rahman MM, Subramani J, Ghosh M, Denninger JK, Takeda K, Fong GH*, et al.* Cd13 promotes mesenchymal stem cell-mediated regeneration of ischemic muscle. Front Physiol. 2014;4:402.
261. Dong M, Thennavan A, Urrutia E, Li Y, Perou CM, Zou F*, et al.* Scdc: Bulk gene expression deconvolution by multiple single-cell rna sequencing references. Brief Bioinform. 2020;22(1):416-427.
262. Bustin SA. Why the need for qpcr publication guidelines? The case for miqe. Methods. 2010;50(4):217-226.
263. Qiagen.Com [internet]. Effects of low a260/a230 ratios in rna preparations on downstream applications [cited january 2021]. Available from: Https://www.Qiagen.Com/us/resources/faq?Id=c59936fb-4f1e-4191-9c16-ff083cb24574&lang=en
264. Ruijter JM, Ruiz-Villalba A, van den Hoff AJJ, Gunst QD, Wittwer CT, van den Hoff MJB. Removal of artifact bias from qpcr results using DNA melting curve analysis. The FASEB Journal. 2019;33(12):14542-14555.
265. Somaiah C, Kumar A, Mawrie D, Sharma A, Patil SD, Bhattacharyya J*, et al.* Collagen promotes higher adhesion, survival and proliferation of mesenchymal stem cells. PLOS ONE. 2015;10(12):e0145068.
266. Sheppard CJ, Gan X, Gu M, Roy M. Signal-to-noise ratio in confocal microscopes. Handbook of biological confocal microscopy: Springer; 2006. p. 442-452.
267. Speel E, Schutte B, Ramaekers F, Hopman A. The effect of avidin-biotin interactions in detection systems for in situ hybridization. J Histochem Cytchem. 1992;40(1):135-141.